SYNTHESIS AND CHARACTERIZATION OF NOVEL RARE EARTH PHOSPHATES AND RIETVELD STRUCTURAL ANALYSIS OF RARE EARTH ORTHOBORATES

A THESIS SUBMITTED TO
THE GRADUATE SCHOOL OF NATURAL AND APPLIED SCIENCES
OF
MIDDLE EAST TECHNICAL UNIVERSITY

BY

SEMİH SEYYİDOĞLU

IN PARTIAL FULFILLMENT OF THE REQUIREMENTS
FOR
THE DEGREE OF DOCTOR OF PHILOSOPHY
IN
CHEMISTRY

SEPTEMBER 2009

Approval of the thesis:

SYNTHESIS AND CHARACTERIZATION OF NOVEL RARE EARTH PHOSPHATES AND RIETVELD STRUCTURAL ANALYSIS OF RARE EARTH ORTHOBORATES

submitted by **SEMİH SEYYİDOĞLU** in partial fulfillment of the requirements for the degree of **Doctor of Philosophy in Department of Chemistry, Middle East Technical University** by,

Prof. Dr. Canan Özgen _____
Dean, Graduate School of **Natural and Applied Sciences**

Prof. Dr. Ahmet M. Önal _____
Head of Department, **Chemistry Dept.**

Assoc. Prof. Dr. Ayşen Yılmaz _____
Supervisor, **Chemistry Dept., METU**

Prof. Dr. Macit Özenbaş _____
Co-Supervisor, **Metallurgical and Mat. Eng. Dept., METU**

Examining Committee Members:

Prof. Dr. Saim Özkar _____
Chemistry Dept., METU

Assoc. Prof. Dr. Ayşen Yılmaz _____
Chemistry Dept., METU

Prof. Dr. Ali Usanmaz _____
Chemistry Dept., METU

Prof. Dr. Ceyhan Kayran _____
Chemistry Dept., METU

Prof. Dr. Leyla Tatar Yıldırım _____
Physical Engineering Dept., Hacettepe University

Date: _____

I hereby declare that all information in this document has been obtained and presented in accordance with academic rules and ethical conduct. I also declare that, as required by these rules and conduct, I have fully cited and referenced all material and results that are not original to this work.

Name, Last name: SEMİH SEYYİDOĞLU

Signature :

ABSTRACT

SYNTHESIS AND CHARACTERIZATION OF NOVEL RARE EARTH PHOSPHATES AND RIETVELD STRUCTURAL ANALYSIS OF RARE EARTH ORTHOBORATES

Seyyidoğlu, Semih

Ph.D., Department of Chemistry

Supervisor: Assoc.Prof.Dr. Ayşen Yılmaz

Co-Supervisor: Prof.Dr. Macit Özenbaş

September 2009, 209 pages

This thesis covers the synthesis and the characterization of sodium lanthanide oxide phosphates, rare earth added strontium pyrophosphates and the Rietveld structural analysis of rare earth orthoborates. Solid state and microwave-assisted synthesis method was employed for the synthesis of desired materials. The formation of the produced phases was confirmed by X-ray Diffraction (XRD), Infrared FT-IR, Raman, Scanning Electron Microscopy (SEM) methods. By using Rietveld Refinement method, structural analysis of rare earth orthoborates were done and three dimensional crystal structures were found.

In the first part of the thesis, some new sodium lanthanide oxide phosphates were synthesized by solid state reaction method from Ln_2O_3 (where Ln= La, Nd, Sm, Gd, Dy, Ho, Er, Yb), Na_2CO_3, $NH_4H_2PO_4$ at 1100 ^oC. Na_2LaOPO_4, Na_2NdOPO_4, and Na_2SmOPO_4 produced with the space group is *Pmm2*. With the help of the same procedure new orthorhombic Na_2DyOPO_4, Na_2HoOPO_4, Na_2ErOPO_4, and Na_2YbOPO_4 were synthesized for the first time in the literature at 1100 ^oC with the same space group *Pmm2*.

In the second part of the thesis, $Sr_2P_2O_7$ - ZrP_2O_7 solid solution was obtained by the solid state reaction and they were characterized for the first time in literature and subjected to thermoluminescence measurements showing $Sr_2P_2O_7$ has glow curve around 100 ^oC. Then CuO and some rare earth oxides (Y_2O_3, La_2O_3, CeO_2, Pr_6O_{11}, Nd_2O_3, Sm_2O_3, Eu_2O_3, Gd_2O_3, Tb_2O_3, Dy_2O_3, Ho_2O_3, Er_2O_3, Tm_2O_3, Yb_2O_3, Lu_2O_3) 0.5-15% (by weight) were added to pure $Sr_2P_2O_7$. After structural determinations by XRD, thermoluminescence studies showed two glow peaks of Pr, Ho, and Nd along with Cu-added samples, one of them is always at around 90 ^oC and the other TL-thermoluminescence- peak around 180, 275, and 285 ^oC, respectively. This study showed that rare earth added $Sr_2P_2O_7$ materials can be promising material for dosimetric applications.

In the third part of this work, time saving microwave-assisted synthesis method was applied to produce pure $LnBO_3$ (Ln=La, Nd, Dy, Ho) by using urea and sucrose as a microwave active organic additive. For $LaBO_3$ and $NdBO_3$, space group found as *Pnma* and for $DyBO_3$ and $HoBO_3$ powders crystallized in hexagonal unit cell with *P-6c2* space group. All microwave-assisted products have particle sizes lower than 1 μm.

In the final part of this study, pure $LnBO_3$ (Ln=Y, La, Nd, Sm, Eu, Gd, Dy, Ho, Er, Tm, Yb, Lu) powder samples were produced by using solid state reactions of Ln_2O_3 and H_3BO_3 (ratio=1:2) heated at 900 ^oC for 10 hours and 1000 ^oC for 5 hours. The crystallographic studies conducted with rietveld structural refinement and unit cell parameters, background functions, profile parameters, zero shift, atomic positions, and unisotropic thermal parameters were refined. $LaBO_3$ and $NdBO_3$ were solved based on *Pnma* orthorhombic structure while the crystal structure of YBO_3, $DyBO_3$ and $HoBO_3$ were monoclinic *C2/c*. $SmBO_3$ showed triclinic *P-1* structure.

Keywords: XRD, Rietveld, Thermoluminescence, borates, phosphates, pyrophosphates, rare-earths, FT-IR, Raman, SEM.

ÖZ

YENİ NADİR TOPRAK ELELEMENTİ FOSFATLARININ SENTEZ VE KARAKTERİZASYONU VE NADİR TOPRAK ELEMENTİ ORTOBORATLARININ RİETVELD YAPISAL ANALİZİ

Seyyidoğlu, Semih

Doktora, Kimya Bölümü

Tez Yöneticisi: Doç.Dr. Ayşen Yılmaz

Ortak Tez Yöneticisi: Prof. Dr.Macit Özenbaş

Eylül 2009, 209 sayfa

Bu çalışma, sodyum lantanit oksit fosfatların, nadir toprak elementi katkılanmış stronsiyum pirofosfatların sentez ve karakterizasyonu ile nadir toprak elementi ortoboratların Rietveld yapısal analizini kapsamaktadır. Hedeflenen malzemelerin sentezi için katı-hal ve mikrodalga-destekli sentez yöntemleri uygulandı. Sentezlenen bileşiklerin karakterizasyonu X-Işınları Toz Kırınımı (XRD), Infrared FT-IR, Raman, Taramalı Elektron Mikroskopu (SEM) yöntemleri kullanılarak yürütüldü. Rietveld Arıtım Yöntemi kullanılarak nadir toprak elementi ortoboratlarının yapısal analizi yapılmış ve üç boyutlu şekilleri saptanabildi.

Bu tezin ilk kısmında, bazı yeni sodyum lantanit oksit fosfatları Ln_2O_3 (Ln= La, Nd, Sm, Gd, Dy, Ho, Er, Yb), Na_2CO_3, $NH_4H_2PO_4$ bileşiklerinin 1100 ^oC'de katı hal tepkimesiyle sentezlendi. Na_2LaOPO_4, Na_2NdOPO_4, ve Na_2SmOPO_4 bileşikleri *Pmm2* uzay grubuyla üretildi. Aynı prosedürle Na_2DyOPO_4, Na_2HoOPO_4, Na_2ErOPO_4, and Na_2YbOPO_4 bileşikleri de literatürde ilk defa *Pmm2* uzay grubunda sentezlendi.

Tezin ikinci kısmında, literatürde ilk defa $Sr_2P_2O_7$-ZrP_2O_7 katı çözeltisi katı kal yöntemiyle elde edildi ve karakterize edilip termolüminesans çalışmalarında kullanıldı. Bu çalışmalarda $Sr_2P_2O_7$ bileşiğinin 100 ^oC civarında ışıma piki olduğu görüldü. Daha sonra saf $Sr_2P_2O_7$ bileşiğine CuO ve % 0.5-15 oranları (ağırlıkça) arasında bazı nadir toprak elementi oksitleri (Y_2O_3, La_2O_3, CeO_2, Pr_6O_{11}, Nd_2O_3, Sm_2O_3, Eu_2O_3, Gd_2O_3, Tb_2O_3, Dy_2O_3, Ho_2O_3, Er_2O_3, Tm_2O_3, Yb_2O_3, Lu_2O_3) eklendi. XRD ile yapılan yapısal belirlemelerden sonra, termolüminesans çalışmaları, Cu ile birlikte $Sr_2P_2O_7$ bileşiğine eklenen Pr, Ho, Nd bileşiklerinde iki ışıma piki olduğunu ve bu piklerden birinin her zaman 90 ^oC civarında ve diğerinin sırayla 180, 275, 285 ^oC derecelerde olduğunu ispatladı. Sonuç olarak bu malzemeler dozimetrik uygulamalarda kullanılabilecek malzeme adayıdır.

Bu çalışmanın üçüncü kısmında, üre ve sukrozun yakıt olarak kullanıldığı zamandan kazanç sağlayan mikrodalga-yardımlı sentez yöntemi saf $LnBO_3$ (Ln=La, Nd, Dy, Ho) üretmek için uygulandı. $LaBO_3$ ve $NdBO_3$, bileşikleri için uzay grubu Pnma olarak bulunmuştur. $DyBO_3$ and $HoBO_3$ toz bileşikleri hekzagonal birim hücre içinde *P-6c2* uzay grubuyla kristallenmiştir. Microdalga-yardımıyla üretilen tüm ürünlerin parçacık boyutunun 1 μm'nin altında olduğu gözlemlendi.

Bu çalışmanın son bölümünde, saf $LnBO_3$ (Ln=Y, La, Nd, Sm, Eu, Gd, Dy, Ho, Er, Tm, Yb, Lu) toz numuneleri Ln_2O_3 ve H_3BO_3 (oran=1:2) bileşiklerinin 900 ^oC'de 10 saat ve 1000 ^oC'de 5 saat ısıtılmasıyla üretildi. Lantanit ortoboratların kristallografik çalışmaları Rietveld yapısal arıtımıyla yapıldı ve birim hücre parametreleri, taban fonksiyonları, profil parametreleri, sıfır kayması, atomik pozisyonlar ve isotropik olmayan termal parametreler arıtılmıştır. YBO_3, $DyBO_3$ ve $HoBO_3$ bileşiklerinin kristal yapıları monoklinik *C2/c* sistemden oluşurken, $LaBO_3$ ve $NdBO_3$ bileşikleri Pnma ortorombik yapı esas alınarak çözüldü. $SmBO_3$ bileşiği triklinik *P-1* yapıdadır.

Anahtar Kelimeler: XRD, Rietveld, Termolüminesans, boratlar, fosfatlar, pirofosfatlar, nadir toprak elementleri, FT-IR, Raman, SEM.

TO MY WIFE CEREN, TO OUR DAUGHTER DEFNE
AND TO MY FAMILY

ACKNOWLEDGEMENTS

The author wishes to express his deepest gratitude to his supervisor Assoc.Prof.Dr. Ayşen Yılmaz and co-supervisor Prof.Dr. Macit Özenbaş for giving the author the opportunity to conduct Ph.D. studies under their supervision. Sincere appreciaton is especially for their guidance, comments, constructive critism, encouragement, patience and insight throughout the research as well as leading the author to work independently.

It is great pleasure to thank my supervisor Assoc.Prof.Dr. Ayşen Yılmaz for her valuable guidance, support, advices for the completion of this work. She provided an academic environment of intellectual enrichment, advice and stimulation to excel and the lesson I learned under her guidance will serve me well in the future. I thank her very much for everything.

I would also like to thank the examining committee member Prof. Dr. Gülhan Özbayoğlu for her suggestions and comments during this study. I also wish to thank Prof.Dr. Ceyhan Kayran for her moral support and encouragement all the time.

I would like to express my thanks to Prof. Dr. Necmeddin Yazıcı for providing research facilities in Physical Engineering Department in Gaziantep University and extend my sincerest thanks for his great help in the thermoluminescence measurements, valuable comments and suggestions.

I would like to thank to Prof. Dr. Leyla Tatar Yıldırım and Assoc. Prof. Dr. Filiz Betül Kaynak from Hacettepe University and Prof.Dr. Orhan Büyükgüngör from Ondokuz Mayıs University for introducing the field of single crystal work and for their valuable discussion and friendship.

I wish to thank also Prof. Dr. Onuralp Yücel and Dr. Bora Derin from Adnan Tekin Ceramic Research Center of Istanbul Technical University for XRD measurements.

The author would like to thank to Prof. Dr. Barbara Albert for providing research opportunities in her laboratory at Eduard-Zintl Institüt am Technische Universität Darmstadt, sparing time for discussions and fabulous comments. Special thanks are to Dr. Katrin Hoffmann, for fresh, energetic and enthuastic way of approaching rietveld issues, invaluable help in refinement area to thesis, and a very friendly approach other than a supervisor. I wish to express my sincere thanks Gerd Bruhn for his help and patience in FTIR measurements. I also want to thank to Frederic Stober for his help during my Darmstadt visit.

Special thanks are to Michael W. Pitcher, for fresh, energetic, and enthusiastic way of approaching to issues, invaluable help to my research, and a very friendly approach.

The author would like to thank to ICDD (International Centre for Diffraction Data) for giving me scholarship to attend Advanced XRD Clinics Education. I would like to thank TUBITAK (107T181) for financial support to go to USA.

I am very grateful to my best friend Dr. Senem Kıralp Kayahan for her irreplaceable friendship, understanding, endless patience, continual support and being with me whenever I need and also her acquaintance at lunch.

I would like to give my special thanks to Prof. Dr. Levent K. Toppare for his inspiring discussions and wisdom for academia and life.

I wish to express my sincere thanks to Mehmet Kayhan and Tolga Depci for their help during the experiments and for their friendship. I wish to express my sincere thanks to Asli Tuba Taşkın for her help in academic search after I moved.

Colleagues from the neighboring groups, Görkem Günbaş, Yusuf Nur, Mehmet Zahmakıran, Asuman Durmuş, Nur Banu Öztaş, Abidin Balan, Simge Tarkuç, Aysel Kızıltay, Timur Karadağ and Yusuf Aktaş are kindly appreciated for sharing the depressing and cold environment of the D-block in the department. Appreciation is expented to colleques in the Department of Chemistry, Middle East Technical University.

Words fail to express my eternal gratitude to my parents Fatma Bengi and Ömer Faruk Seyyidoğlu and my brother Emin Ferhan Seyyidoğlu, for giving me the intellectual and emotional guidance that made me who I am, and for their never-ending support, encouragement along with understanding for my frequent absences. This thesis could not have come to an end without their encouragement and tolerance.

Finally, my special thanks goes to my wife Ceren Obakan Seyyidoğlu for her continuous support, love and patience to my long working hours, absence at weekends, sometimes weeks and for not leaving me alone in my stressful days. Without her none of this work could be accomplished.

I would like to thank METU for funding my thesis with the project number of BAP-01-03-DPT-03K-120920/09, BAP-2006-07-02-00-01, BAP - 2005-07-02-00-53, TUBITAK 107T181, TUBITAK 107M447.

TABLE OF CONTENTS

LIST OF TABLES

TABLES

LIST OF FIGURES

FIGURES

LIST OF ABBREVIATIONS

ABBREVIATIONS

CELREF	Cell Refinement Computer Program
CSD	Cambridge Structural Database
EDX	Energy Dispersive X-ray Fluorescence
FTIR	Fourier-Transform Infrared
FWHM	Full-Width Half Maximum
ICDD	International Centre for Diffraction Data
ICSD	Inorganic Crystal Structure Database
KTP	Potassium titanium oxide phosphate
LMCT	Ligand-to-Metal-Charge-Transfer
Ln	Lanthanide
LT	Low Temperature
GSAS	General Structure Analysis System
HT	High Temperature
MW	Microwave
NIST	National Institute of Standards and Technology
NMR	Nuclear Magnetic Resonance
NRCC	Natinal Research Council of Canada
PDF	Powder Diffraction File
R_p	Residual Profile
RTP	Rubidium titanium oxide phosphate
R_{wp}	Weighed residual profile
SEM	Scanning Electron Microscope
TL	Thermoluminescence
U_{iso}	Isotropic thermal displacement factor
UV-LED	Ultraviolet-Light Emitting Diodes
XRD	X-Ray Diffraction

CHAPTER 1

INTRODUCTION

1.1. Phosphates

For several reasons related to potential applications such as ionic conductivity or superconductivity, nonlinear optical properties, ferroelectricity, magnetism, laser properties, catalytic activity, etc., metal oxide phosphate compounds are still currently being investigated, i.e., $KTiOPO_4$ (KTP) (Miyamoto et al. 1995), $NbOPO_4$ (Moreno-Real et al.1998), $BiCoPO_5$ (Ketatni et al. 1999), $VOPO_4.3H_2O$ (Griesel et al. 2004), , $Pb_2BiO_2PO_4$ (Mizrahi et al. 1997), $Bi_{\sim 6.2}Cu_{\sim 6.2}O_8(PO_4)_5$ (Ketatni et al. 2003). Among these metal oxide phosphates, potassium titanium oxide phosphate $KTiOPO_4$ (KTP) crystals exhibit excellent nonlinear optical properties in the visible range, because of their high nonlinear coefficients and wide acceptance of temperature and angular fluctuations (Miyamoto et al. 1995). High thermal stability, good mechanical characteristics, transparency over a large wavelength range, large nonlinear optical coefficients, high damage threshold, and broad angular acceptance of KTP have made it the standard material for several industrial and medical applications (Bhaumik et al. 2002).

The structure of $Li_{(1-2x)}Ni_xTiOPO_4$ was resolved by Manoun et al. (2005) and they represented that the structure of the compositions $0 \leq x \leq 0.25$ is based on a three-dimensional framework constructed of chains of alternating TiO_6 octahedra and PO_4 tetrahedra, with the lithium and nickel atoms in cavities of the framework as shown in the Figure 1.1. KTP has an orthorhombic structure and belongs to the acentric point group *mm2* (space group $Pna2_1$). Its structure consists of PO_4 tetrahedra and TiO_6 octahedra with potassium in larger voids. Ti-O bonds are short which are believed to be the prime cause of the nonlinear properties of $KTiOPO_4$.

This family of compounds is generalized as $ABOXO_4$ where A may be K (Bhaumik et al. 2002), Rb, Ni (Jazouli et al. 1998), B may be Ti, Nb (Chani et al. 1997, Koseva et al. 2003, Moorthy et al. 1998), Nd (Sole et al. 1996), Sn, Mg (Chani et al. 1996), or a combination of two of these ions; X may be P, As (Chani et al. 1999).

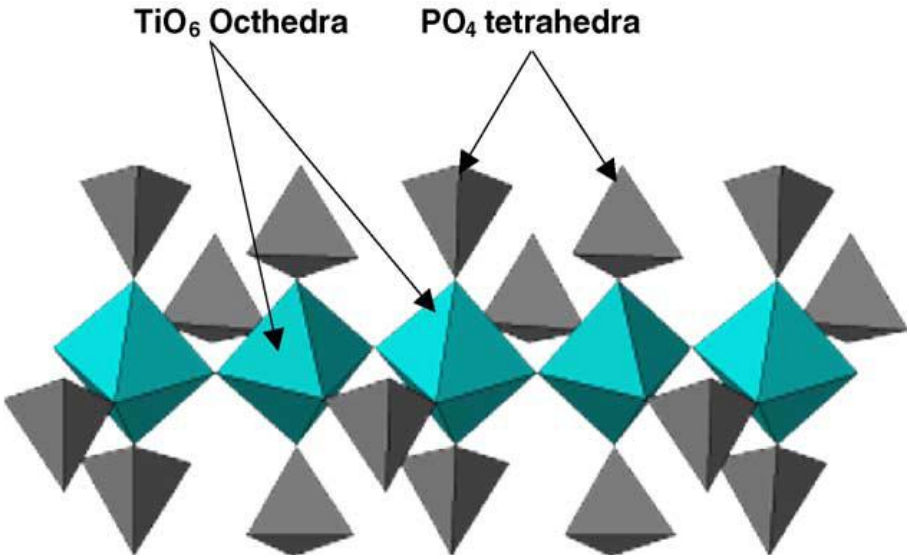

Figure 1.1. The structure of $Li_{(1-2x)}Ni_xTiOPO_4$ represented by Ti-O-Ti-O- chains (Manoun et al. 2005).

In the paper published by Carjaval et al. (2001, 2002), the effect of Er- and Yb- doping on the Nb:KTP crystals were investigated. As these materials seem promising materials for future research, KTP (Hu et al. 2003, Wang et al. 2002), many isostructural compounds are studied by large number of researchers. In the work done by Zhang et al. (2004), an effective blue coherent laser was obtained using Ce:KTP crystals. Kling et al. (2004) and Zaldo (1999) coworkers studied photoluminescence properties of Er- and Nd- implanted KTP and RTP crystals and the optical absorption of Nd^{3+} in KTP single crystals and in those co-doped with Al, Na and W have been studied (Zaldo et al. 2000, Zaldo et al. 1998). In addition to these, many research group worked on the mechanical (Stus et al. 2004), and optical

properties of KTP, RTP and Nb:KTP (Roth et al. 2004, Roth et al. 2001, Liu et al. 2000, Zhang et al. 2000).

As lanthanide phosphates ($Ln PO_4$) have a wide range of potential applications for optical materials, including laser, phosphors, and more recently, anti UV-materials either in the form of powders, coatings or dense sintered parts, they have become of growing interest during the past few years and numerous researchers have been devoted to these compounds recently (Hirai et al. 2004, Schwarz et al. 1998, Kloss et al. 1997, Schwarz et al. 1997). Champion's group has reported the synthesis, characterization (Lucas et al. 2004a) and thermal (Lucas et al. 2004b) behaviour of $Ln PO_4.H_2O$ while Onada (Onada et al. 2002) and coworkers have synthesized $Ln PO_4.H_2O$ by using lanthanides where Ln= La, Ce, Nd; and oxide, carbonate, chloride, nitrate, sulphate, oxalate and fluoride as an anion.

While lots of reports present in the literature dealing with the synthesis, characterization and the properties of KTP and related materials, there are only few reports regarding the preparation of lanthanide oxide phosphates, some of which possesses KTP-type structure. A research performed by Kizilyalli' research group showed the precence of two orthorhombic lanthanide oxide phosphates i.e., Na_2GdOPO_4 (Gönen et al. 2000) and Na_2LaOPO_4 (Uztetik-Amour et al. 1995). However no attempt for the syntheses of other sodium lanthanide oxide phosphates has yet been reported in the literature.

1.2. Pyrophosphate

Pyrophosphates are technologically important materials due to their applications as ceramic, catalysts, ion exchange and optical materials. Because of their potential applications, many researchers synthesized either single crystal or powder pyrophosphates. The pyrophosphates were found in literature containing different formula group. Among these, one is $M^{IV}P_2O_7$ (M^{IV} is tetravalent), and the other is $M^{II}{}_2P_2O_7$ (M^{II} is divalent), and $M^{I}M^{III}P_2O_7$ (mixed valance).

The cubic ZrP_2O_7 is one of the most known pyrophosphate in $M^{IV}P_2O_7$ type. Symmetry characterization of cubic ZrP_2O_7 was studied by Withers et al. (2001) and Khorsvani et al. (1996) investigated unusual P-O-P bond angles in cubic ZrP_2O_7. The phosphate tetrahedra connected to zirconium octahedra in ZrP_2O_7 structure was represented by Khosrovani et al. (1996) and given in Figure 1.2. The crystal structure of novel cubic pyrophosphate WP_2O_7 was reported in Lisnyak et al. (2000). Phase transition studies of pseudocubic SnP_2O_7 was published by Gover, Withers and coworkers (Gover et al. 2002).

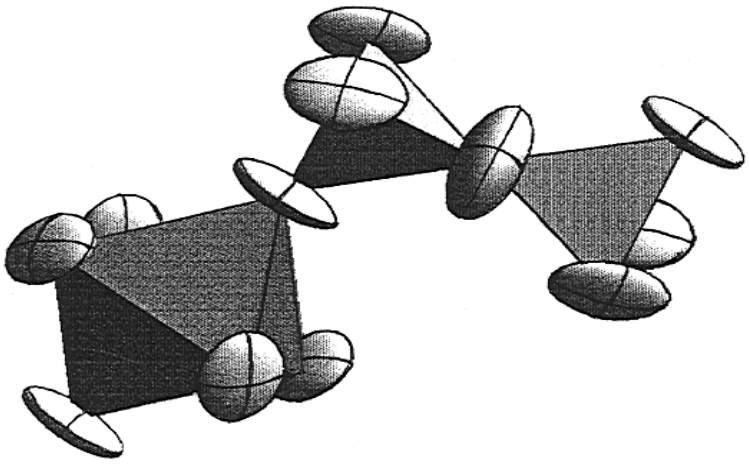

Figure 1.2. The phosphate tetrahedral and a zirconium octahedron for ZrP_2O_7 structure (Khorosvani et al. 1996).

In the second formula group, the $[P_2O_7]^{4-}$ group containing divalent metals are given. Triclinic tin (II) pyrophosphate $Sn_2P_2O_7$ single crystals were obtained in argon flow in Shpanchenko's group (Chernaya et al. 2005). Another divalent metal containing triclinic pyrophosphate was obtained by Guler and Kurtulus (2005). They have followed microwave-assisted route to synthesize $Pb_2P_2O_7$. Besides these divalent metal containing pyrophosphates, Smaalen's group synthesized orthorhombic vanadyl pyrophosphate $(VO)_2P_2O_7$ by heating $VO(PO_4).0.5H_2O$ under argon atmosphere (Smaalen et al. 2005).

The mixed valance metal containing group is the largest member of pyrophosphates. Kızılyallı et al. (1993) synthesized orthorhombic $NaGdP_2O_7$ by using solid state reaction and orthorhombic $HGdP_2O_7$ (Kızılyallı 1987) by precipitation methods. Similarly, tetragonal $NaDyP_2O_7$ (Tie et al. 1997), orthorhombic $NaLaP_2O_7$ (Ferid et al. 2004a), monoclinic $NaEuP_2O_7$ (Ferid et al. 2004b), and orthorhombic KYP_2O_7 (Hamady et al. 1994) were obtained by many researchers. Single crystals of $K_2SrP_2O_7$ (Trunov et al. 1990), $Rb_2SrP_2O_7$ and $CsSrP_2O_7$ were synthesized by Trunov et al. (1991) . They synthesized monoclinic $LiMoP_2O_7$ (Ledain et al. 1996) single-crystals by controlled cooling. Same procedure was applied and triclinic $PbFe_2(P_2O_7)_2$, monoclinic $BaFe_2(P_2O_7)_2$, and $CuFe_2(P_2O_7)_2$ were produced by Boutfessi et al. (1996a, 1996b). Another kind of diphosphate materials with the general formula $RbLnP_2O_7$ (where Ln= Dy, Ho, Y Er, Tm, Yb) (Khay et al. 2001a), $CsLnP_2O_7$ (where Ln= Gd, Tb, Dy, Ho, Y Er, Tm, Yb) (Khay et al. 2001b), and α-$Ca_2P_2O_7$, $CaCuP_2O_7$, $SrCuP_2O_7$, $SrCdP_2O_7$, $BaMgP_2O_7$ (Idrissi et al. 2004) have been deal of many studies. Hydrothermal synthesis of monoclinic $Na_2CrP_2O_7.0.5H_2O$ was achieved by Stock et al. (2000). A new, dicationic, and acidic orthorhombic $KHMgP_2O_7$ was obtained by Assaaoudi et al. (2005). A series of compounds $(M^a_{0.5}M^b_{0.5})P_2O_7$, M^aM^b= AlTa, FeTa, GaTa, InNb, YNb, NdTa, and BiTa that are close structural relatives of cubic ZrP_2O_7 were prepared by Varga et al. (2005).

There were very few publications in literature about the properties of zirconium and strontium pyrophosphates. Emission spectra of ZrP_2O_7 activated with Eu^{3+} and Tb^{3+} were investigated by Pelova and Grigorov (1997) and dielectric properites of ZrP_2O_7 was investigated by Kim and Yim (1999). Besides these, zirconium pyrophosphates are used as catalyst in n-butane oxidative dehydration (Marcu et al. 2002) and used as a new packing material for high performance liquid chromatography (Inoue and Ohtaki 1993). Prasad and coworkers investigated preparation and ammoxidation functionality of zirconium phosphate-supported V_2O_5 catalysts (Srilakshimi et al. 2006).

Also, crystal structure and phase transitions of strontium zirconium diorthophosphate, $SrZr(PO_4)_2$, was published recently (Fukuda et al. 2004) while europium-ion doped strontium pyrophosphate and its photoluminescence work was done by Natarajan et al. (2004). Semiconductive properties of Ti and Zr pyrophosphate catalysts were studied by Marcu et al. (2002). Amezawa's work (2005) was based on high temperature protonic conduction in $Sr_2P_2O_7$ - $LaPO_4$ system.

Luminescent applications of pyrophosphates are subject of many research groups. The allotropic forms and photoluminescent properties of europium-doped calcium pyrophosphates were described by Doat et al.(2005) while Schipper et al. (1994) examined luminescence of hafnium pyrophosphate which emit in the UV spectral range. Recently, the crystal structure and luminescence spectra of new potassium erbium pyrophosphate dihydrate $ErKP_2O_7.2H_2O$ were published by Assaaoudi et al. (2006). Ce-doped luminescence of first lutetium diphosphate $NH_4LuP_2O_7$ was shown by Li et al. (2005).

Thermoluminescence properties of pure and doped strontium pyrophosphates were demonstrated by various scientific research groups because the rare earth activated inorganic phosphors are widely used in a variety of applications, such as lamp industry, color display, radiation dosimetry and X-ray imaging (Natarajan et al. 2004). The emission of Eu^{2+} ions varies from blue to red depending on the host lattice due to crystal-field effects. Eu^{2+} activated strontium pyrophosphate is considered to be a potential candidate for use in lamps for photo-therapy of hyper bilirubinemia (infant jaundice), since its emission is at 420 nm with negligible contribution from ultra-violet radiation; and hence, will be safe for treating infants. In fact, Eu^{2+} and Mn^{2+} co-doped $Sr_2P_2O_7$ has been suggested as one of the potential phosphors, to be used in the phosphor mixture for obtaining white light emission from UV - LED devices (Srivastava 2003). The solid solution of ZrP_2O_7-$Sr_2P_2O_7$ was synthesized and the thermoluminescence properties of these solid solutions were examined (Seyyidoglu et al. 2007).

1.2.1. Thermoluminescence

It is possible to define the phenomenon of thermoluminescence (TL) in several different ways, one of which is emission of light when a material is heated. Yet, in the details of the mechanism the definition gets a bit more complicated. Mahesh et al. (1989) described the thermoluminescent phosphors as materials that keep the energy given by a pre-excitation by an appropriate type of radiation, ultraviolet, nuclear or cosmic waves, within itself. Then, when the luminescent object is subjected to heat up to a certain temperature which triggers the release of energy, it is possible to observe emission of this energy as visible light. Thermoluminescent materials are used in radiation dosimetry (clinical, radiotherapy, personnel) (Cuong et al. 2004) and are functional in archeological and geological dating.

Thermoluminescent materials find wide spread use in industry in two different areas which are further divided into subgroups. First major area of thermoluminescence is the "radiation dosimetry". Radiation dosimetry is the measurement and/or calculation of the absorbed dose from an exposure to ionizing radiation in tissue and in matter. Secondly, thermoluminescence properties of materials are beneficial in dating of archeological and geological samples that includes complications compared to radiation dosimetry (Chen and Mckeever 1997, Mahesh et al. 1989, Pradhan 1981).

1.3. Borates

Boron, which is semi-metallic element with an atomic number of 5, does not occur in nature as free element due to its unstable nature in elemental form. There are more than 230 borate minerals (Kistler et al. 1994). Commercial boron mineral deposits are distributed globally in the following areas depending on the appropriate combination of the volcanic activity and the climate for example in South West USA Mojave Desert, Turkey and South America Andean Belt.

The world's largest borate reserves occur in Turkey in Western Anatolia, South of the Marmara Sea within an area rougly 300 km east-west by 150 km North-south. The main borate districts in Turkey are Bigadiç, Kestelek, Sultançayırı, Emet and Kırka (Kistler and Helvacı, 1994). Turkey is the largest producer of natural borates in the world. The only producer of the borates in Turkey is the government owned ETİ Mine Works. The other countries in the world who produce boron are United States, Russia, Kazakhstan, Argentina, China, Peru and Chile.

Table 1.1. World Boron Reserves (Roskill, 2002)

Country	**Total Reserve (Million Tons)**	**%**
Turkey	563	64
USA	80	9
Russia	100	11
China	36	4
Chile	41	4
Bolivia	15	2
Peru	22	3
Argentina	9	1
Kazakhstan	15	2
TOTAL	**885**	**100**

Turkey is the world's major source of colemanite. Ulexite is found mainly in Turkey, Andes of South America and China. The total world reserves are 885 million tons (Grand total including proven, probable and possible reserves) on B_2O_3 basis with the following shares given in Table 1.1. (Roskill, 2002).

Borates and borate derivatives find an unusually large range of uses today. The principal application area of borates is the glass industry which is accounting for an estaimated 43% of the total world borate consumption (Roskill, 2002). Detergent and the enamel, frit, glaze areas follow the glass industry. The other usage areas of

the boron compounds are in agricultural purposes, fertilizers, wood preservation, flame reterdants, abbrasives, herbicides, pharmaceuticals, nuclear applications, metallurgical fluxing, photography, textile finishing, armour protection, advanced composites, abrasives, cutting edges, nuclear weapons, catalysts, electronic components, purifying chemicals, cleaning chemicals, hydrogen cells (Roskill, 2002).

1.3.1. The Crystal Structure of Borates

The crystal chemistry of borates and the structural systems of its basis differ from those for silicates, phosphates, sulfates, carbonates, nitrates since anionic groups in the borate class can be both B-tetrahedra and B-triangles (Belokoneva 2005). Investigation of the phase diagrams of borate systems has resulted in the synthesis of about 600 anhydrous borates, borosilicates and their structural derivatives (Leonyuk et al. 1983). Most of these borates melt incongruently and borate melts have a high viscosity because of their tendency to form various complex polyanions of different composition and configuration.

In recent years more and more research has been concentrated on borate crystals since the possibility of wide isomorphous substitutions one can consider these borates as polyfunctional materials with device potential. Generally, the structure of anhydrous borates is characterized by a variety of discrete and condensed BO_3 and BO_4 anions. Predominant structures among borates, especially binary and more complex borate groups are isolated BO_3 triangles (about 65%) (Leonyuk 1997).

Yuan and Xue (2007) have worked on the classification and the algebraic description of crystal chemistry of borates are given by topological type of fundemental building blocks. The 70-year history of borate structure determinations has illustrated the unique chemistry of borates, characterized by the following distinguishing features (Becker, 2001; Filatov & Bubnova, 2000; Touboul et al., 2003):

(i) In borate crystal structures, the B atoms can have both three [$B\varphi_3$] and four [$B\varphi_4$] coordinations to oxygen or hydroxyl groups ($\varphi = O^{2-}$, OH^-),
(ii) Both $B\varphi_3$ triangles and $B\varphi_4$ tetrahedra can be connected to each other.
(iii) FBBs can polymerize into complex borate polyanions such as those with infinite chains, layers and network anions.

1.3.2. Rare Earth Orthoborates

Many compounds containing rare-earths are good candidates for applications in laser and luminescence materials, but the emission is often quenched by doping ion interactions over a critical concentration. The quenching phenomenon is reduced when active ions are separated by the large anions such as PO_4, WO_4. Specially, rare-earth borate compounds present a great structural complexity because boron atoms can form planar or nonplanar BO_3 groups, where three oxygen atoms form sp^2 hybrids, and also tetrahedral BO_4 groups, where four oxygen atoms form sp^3 hybrids (Chinn and Hong 1976).

During the past few years, much interest has been devoted to the study of yttrium and lanthanide orthoborates because of their high UV transparency and exceptional optical damage threshold, that make them attractive for numerous applications. In the last couple of years considerable effort has been given to improve the performance of these materials (Veenis and Bril, 1978). So, improving the performance, as well as any sensible interpretation of the luminescent properties, requires a well-defined crystal structure of these compounds (Ren et al. 1999).

Various methodes have been developed to prepare high-quality $LnBO_3$:Eu phosphors, such as solid-state reaction (Lemanceau et al. 1999, Zhang et al. 2008), coprecipitation method (Lemanceau et al. 1999, Kim et al. 2002), combustion synthesis (Tukia et al. 2005), ultrasonic spray pyrolysis (Kim et al. 2000), sol-gel technique (Boyer et al. 2001, Boyer et al. 1999, Zhu et al. 2008) and sol-gel pyrolysis process (Wei et al. 2002a, Wei et al. 2002b).

In Klassen's (Klassen et al., 2005) research, lutetium and yttrium borates doped with europium, terbium, gadolinium, etc., have been produced by dissolving initial oxides and nitrates in ammonium nitrate melt and thermal decomposition of the solvent. Three methods were employed to prepare the red phosphor $(Y,Gd)BO_3$; coprecipitation-combustion method, salt assisted combustion method and emulsion method by Cui et al. (2008). Powder samples of $YBO_3:Eu^{3+}$ were prepared using either the conventional solid-state reaction, or soft routes such as wet process or sol–gel method starting with alkoxides precursors by Boyer et al. (2003).

A number of studies have been devoted on hydrothermal synthesis of $LnBO_3$, and $LnBO_3$ nanoparticles or $LnBO_3$ with specific morphologies were obtained (Li et al. 2006, Jiang et al. 2004a, Kim and Kang 2005, Jiang et al. 2003, Jiang et al. 2004b, Zhang and Lin 2004, Yang et al. 2008). For example, Jiang et al. (2003) have prepared YBO_3:Eu nanoparticles (particle size; 20 nm) by a hydrothermal method in the presence of urea. Jiang et al. (2004b) have reported the formation of donut-like assembly of YBO_3:Eu crystals by the hydrothermal method under an alkaline condition. $Y_{1-x}BO_3:Nd_x$ nanoparticles prepared by mild hydrothermal synthesis and found to be isostructural with YBO_3 crystal (PDF#16-277) by Wang et al. (2004a). Wang et al. (2006) also synthesized Vaterite-type $Y_{1-x}Tb_xBO_3$ phosphors using hydrothermal synthesis method. Zhang and Lin (2004) have reported that YBO_3:Eu crystals with flower-and hedgehog fungus-like structures synthesized by the hydrothermal method under acidic conditions.

Beside the luminescent properties, the different material properties of rare eath orthoborates have been also examined by several groups. Amezawa et al. (2004) have reported the high temperature protonic conduction in 1 mol %Sr doped $LaBO_3$. Laser absorbance studies of samarium borate was investigated by Huili et al. (2007). The nanosize lanthanide borates were also investigated. Lanthanum borate nanowires have been fabricated by reacting lanthanum oxide and boron with carbon nanotubes at 1100 ^oC (Lin et al. 2007).

Lanthanide orthoborate, $LnBO_3$, is compositionally the simplest of the compounds in the Ln_2O_3-B_2O_3 systems. Yet, the crystal structure determination has been far more complicated. Although numerous efforts have been given to the structure determination, there are still considerable controversies left. Levin et al (1961) have investigated their polymorphism and reported on the regions of stability of the different structures in relation with borates preparation temperature and the ionic radius of the rare earth compounds. They showed that the structures of the rare earth borates are related to the three crystalline forms of $CaCO_3$, aragonite, vaterite, and calcite, depending on the rare earth. The orthoborates of the light rare earths (La to Nd) exhibit the aragonite-type structure and those of the heavy rare earths (Sm to Yb) possess the vaterite-type structure.

Many of aragonite type rare earth borates reported for $LaBO_3$ (Nakatsuda et al. 2006, Gornuyova 2003, Tukia et al. 2005), $NdBO_3$ (Müller-Bunz et al. 2003, Gornuyova 2003, Laureiro et al. 1990), $CeBO_3$ (Goubin et al. 2004). Aragonite type rare earth orthoborates ($PrBO_3$, $SmBO_3$, $EuBO_3$) were also synthesized by Meyer (1969) and Laureiro et al. (1991). The crystal structure of aragonite type $LaBO_3$ were explained first time by Abdulaev et al. where he investigated space-group setting as Pmcn (1976). The aragonite- and calcite-type orthoborates contain triangular BO_3^{3-} groups confirmed by both X-ray diffraction and spectroscopic studies (Levin et al. 1961, Antic-Fidancev et al. 1992, Bohlhoff et al. 1971).

In Gornuyova's PhD Thesis (2003), the projection of the structure of $LaBO_3$ (Aragonite-Type) paralel to [010] and the coordination polyhedra of La-Atom in the structure of $LaBO_3$ (Aragonite type) were well defined and shown in Figure 1.3. and Figure 1.4., respectively. In Figure 1.3., it is obviously seen that trigonal planar [BO_3] surrounds nine coordinated La atoms. As shown in Figure 1.3., the La atom is coordinated by nine O and the B atom is planar-triangularly coordinated by three O atoms. Each LaO_9 polyhedron shares edges with six other LaO_9 polyhedra and three BO_3 triangles, whereas each BO_3 triangle shares edges with three LaO_9 polyhedra.

The representation of the aragonite-type LT-$LaBO_3$ structure with LaO_9 groups is given in Figure 1.5. (Nakatsuka et al. 2006).

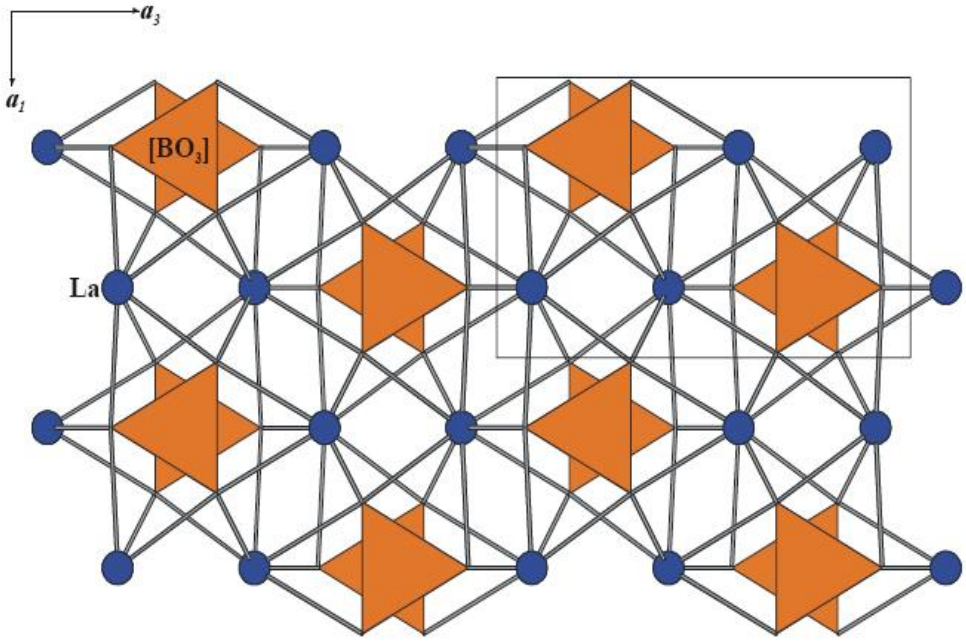

Figure 1.3. The projection of the structure of $LaBO_3$ (Aragonite-Type) paralel to [010] (Gornuyova, 2003)

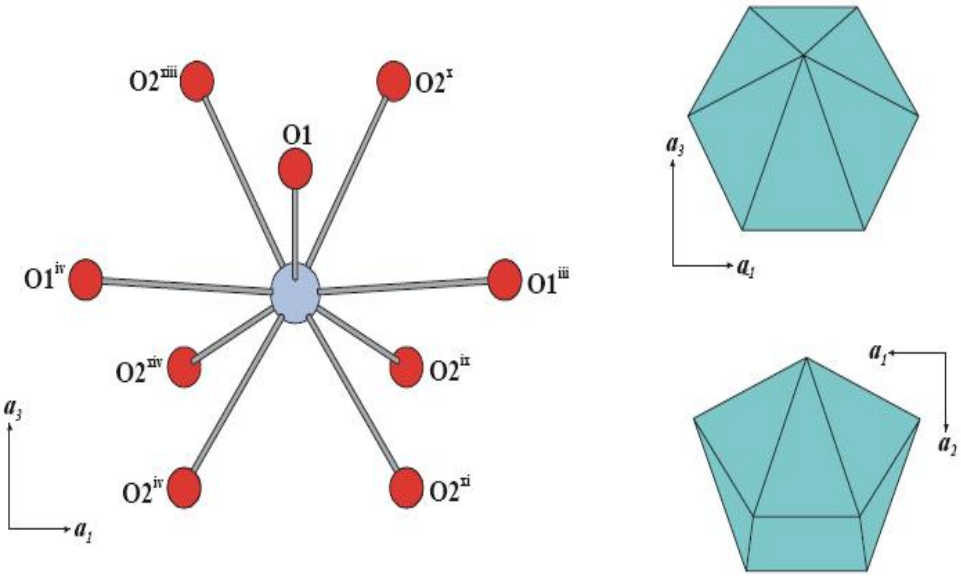

Figure 1.4. The coordination polyhedra of La-Atom in the structure of $LaBO_3$ (Aragonite-type) (Gornuyova, 2003)

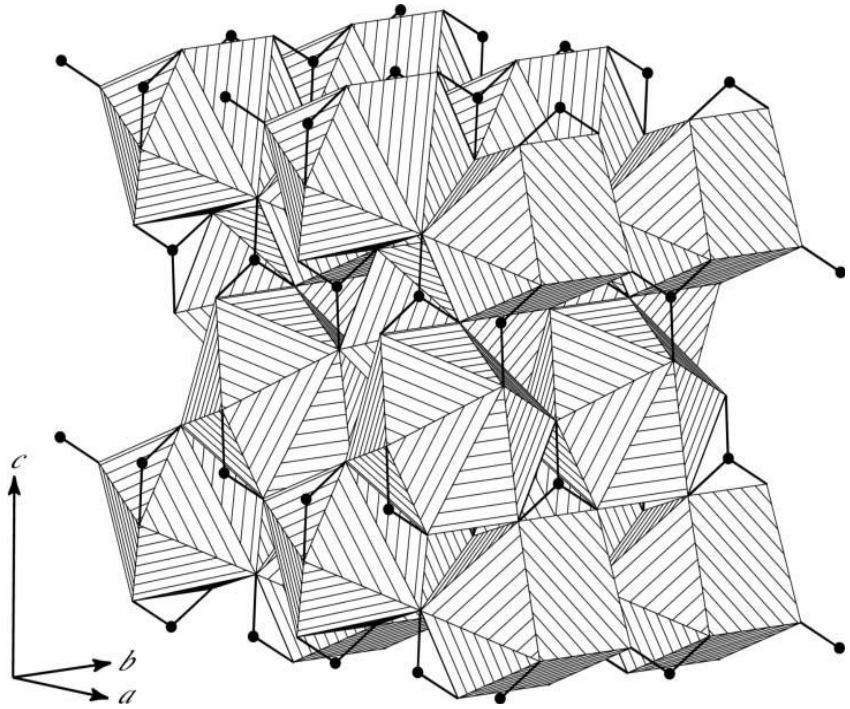

Figure 1.5. Representation of the aragonite-type LT-$LaBO_3$ structure. LaO_9 groups are shown as hatched polyhedra and B atoms as black spheres. B-O bonds are indicated as solid black lines (Nakatsuka et al. 2006).

Meyer and Skokan (1971) have obtained $YbBO_3$ in calcite structure. The structural analysis of single crystal $LuBO_3$ and single crystal structural analysis of $YbBO_3$ were done by Abrahams et al. (1971) and Hupertz (2001), respectively. The space group of them is R-3c symmetry. The octahedral coordination of Lu-atoms and isolated trigonal [BO_3] groups were shown in Figure 1.6.

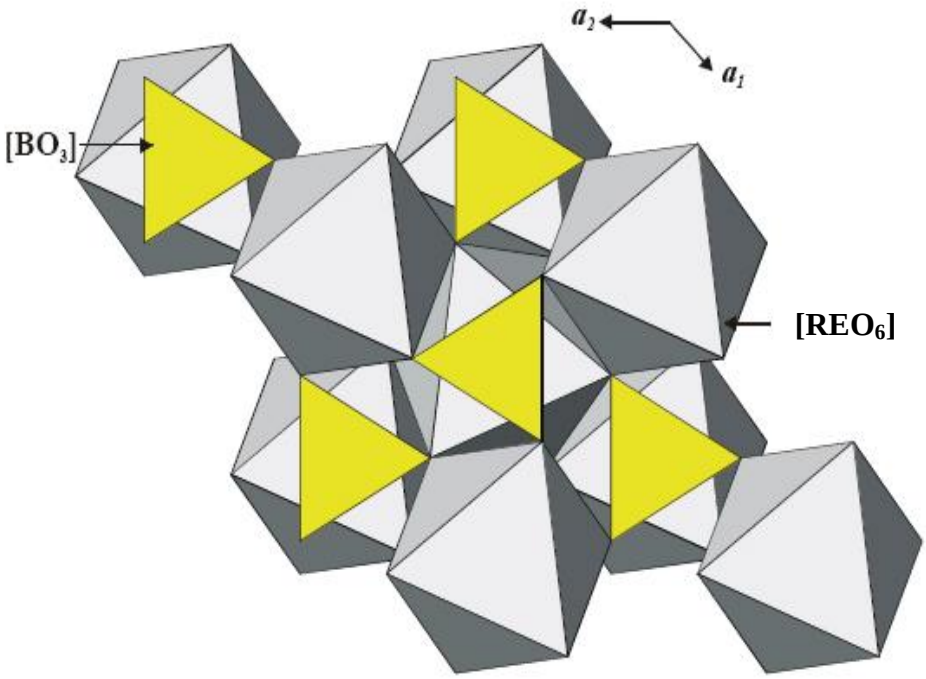

Figure 1.6. The structure of calcite type rare earth orthoborate (Abrahams et al. (1971).

Although most of the anhydrous rare earth borate phases have been known for quite a long time, many controversies about the structures and even the composition remained to be clarified. For example, Corbel et al.(1999) have revised the crystal structure of $EuBO_3$ and assigned it to the space group *P-1*, similarly to the findings of Palkina et al.(1976) for the case of low temperature $SmBO_3$. Triclinic $DyBO_3$ and $ErBO_3$ single crystals with *P-1* space group were obtained by Huppertz et al. (2002) using high-pressure synthesis. Meyer (1972) obtained triclinic rare earth orthoborates $LnBO_3$ (Ln=Pr, Nd, Sm, Eu, Gd, Tb, Dy). Colourless single crystal rods of triclinic *(P-1)* $DyBO_3$ and triclinic *(P-1)* single crystals of $NdBO_3$ were synthesized by Emme and Huppertz (2004) and Noirault et al. (2006) respectively. The structure of triclinic $SmBO_3$ were given in Gornuyova's work (2003) in Figure 1.7. In this figure, it is obvious that structre has [BO_3] group around cationic polyhedra. In Figure 1.8., the [SmO_8] polyhedra in triclinic $SmBO_3$ structure (Gornuyova, 2003).

In the structure of $SmBO_3$, the rare earth atoms occupy the centres of distorted SmO_8 triangulated dodecahedra (Figure 1.8.). Each dodecahedron shares edges with four others to build infnite double chains and also The isolated threefold coordination of boron is regular.

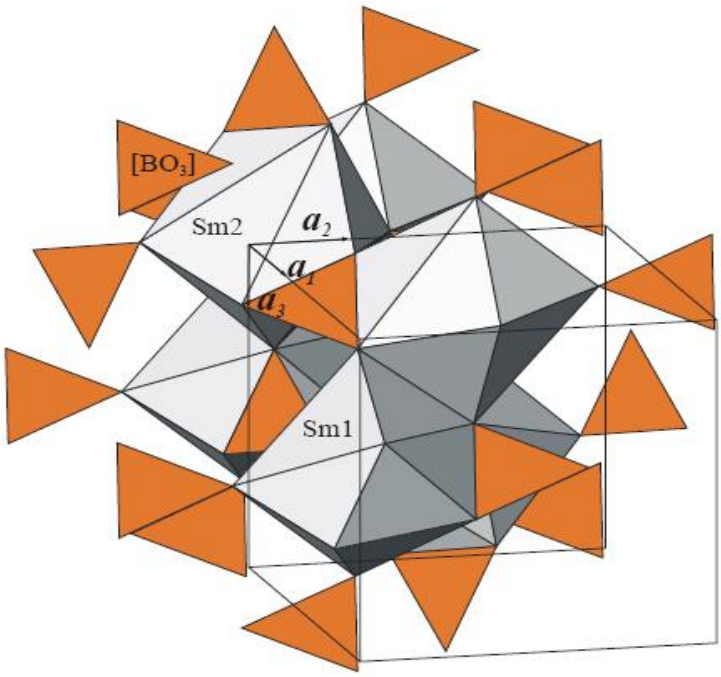

Figure 1.7. The structure of triclinic (P-1) $SmBO_3$ (Gornuyova, 2003).

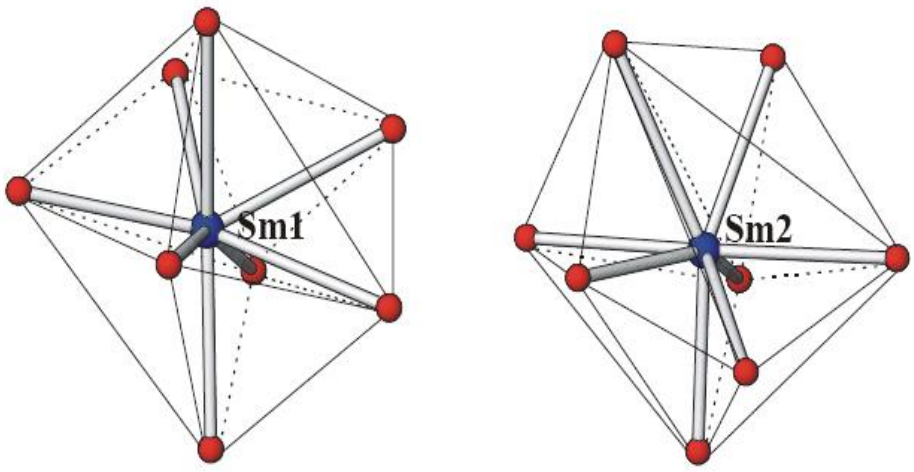

Figure 1.8. The [SmO_8] polyhedra in triclinic $SmBO_3$ structure (Gornuyova, 2003)

For the vaterite-type compounds (Sm to Yb), Newnham et al.(1963) have proposed two possible structure models, a disordered hexagonal ($P6_3/mmc$) structure and an ordered hexagonal ($P6_3/mcm$) structure. Bradley et al. (1966) and Cohen-Adad et al. (2000) described the structure using the P-6c2 space group. A common feature of these models is that the borate group was assumed to be in triangular geometry (BO_3^{3-}). Later IR, NMR, and Raman studies (Laperches and Tarte 1966, Denning and Ross 1972, Kriz and Bray 1969) however, revealed that these compounds contain only the tetrahedral polyborate group of $B_3O_9^{9-}$.

Many researchers have synthesized different vaterite type of $LnBO_3$ compounds using several techniques. Tukia (2005) and coworkers have prepared vaterite type YBO_3 and $GdBO_3$. Felten (1961) prepared rare earth borates (Y, Sm, Eu, Gd, Dy, Ho, Er, Tm, Yb, Lu) of ABO_3 type by the reaction of the constituent oxides in equimolar ratios between 1200 and 1400 ^oC in air and he observed that the borates of ytrrium and smaller rare earth ions (samarium through lutetium) are isostructural with vaterite type $CaCO_3$. In Henkels and Schaak's (2008) work, $LnBO_3$ (Ln=Y, Nd, Sm, Eu, Gd, Ho) and YBO_3:Eu nanocrystallines were synthesized using a borohydride-based solution precursor route and they presented that they found vaterite stucture for $LnBO_3$ orthoborates. Hosokowa et al. (2008) prepared YBO_3 with space grpup $P6_3/m$ by using the glycothermal reaction of the rare earth acetate with trimethoxyborane (Ln/B=1) at 315 ^oC for 2h.

Since yttrium borate compounds have luminescent properties with rare earths, many researcher tried to synthesize this compound by using different techniques. Yttrium orthoborate crystallizes in the vaterite-type structure and has two polymorphic forms, a low and high temperature one. Plewa (2007) and Jüstel have studied the phase transition of YBO_3 and found that the true LT-HT (low temperature to high temperature) transition temperature is 987 ^oC while HT-LT transition is seen around 558 ^oC (Plewa et al. 2007). Single phase YBO_3 (PDF#88-0356, $P6_3/m$) is obtained at the pH 5-6. (Tkachenko et al. 2007).

In Beregi's (Beregi et al. 2002) work, vaterite type $LnBO_3$ (ICDD files for Yb-, Er-, Ho-, Gd- and Y- borates: 19-1427, 13-486, 13-478, 13-483 and 16-277, respectively) were synthesized. YBO_3 pseudo-vaterite structure ($P6_3/m$) in Chadeyron et al. (1997b). Chadeyron et al. (2001) prepared vaterite YBO_3 and H-$LnBO_3$ (Ln=La, Nd, Sm, Eu) orthoborates by sol-gel mineral process. Chadeyron et al.(1997a) reinvestigated the crystal structure of YBO_3 and found that the structure contains the $B_3O_9^{9-}$ group. They described the structure in a hexagonal cell with the space group $P6_3/m$. In their structure model, the boron position and one oxygen position are partially occupied. The structure YBO_3 plane is given is Figure 1.9.

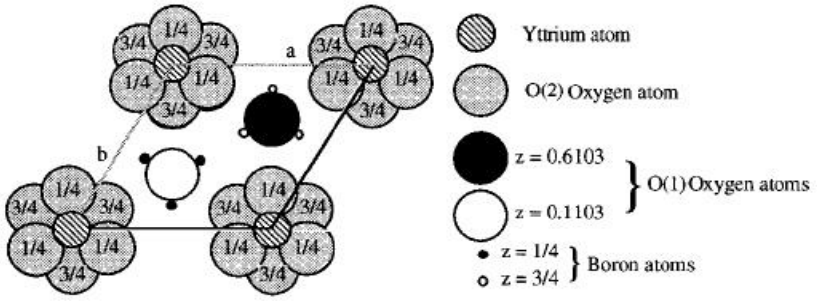

Figure 1.9. Projection of the structure of YBO_3 on the (001) plane (Chadeyron et al. 1997a)

With respect to the large anion size, it is unlikely that the $B_3O_9^{9-}$ group is rotationally distorted in this solid-state structure. Yet, the structure model they proposed provides a reasonable basis for the structure of the vaterite type. The structure and the the sketch of $B_3O_9^{9-}$ ion were given in Figure 1.10.

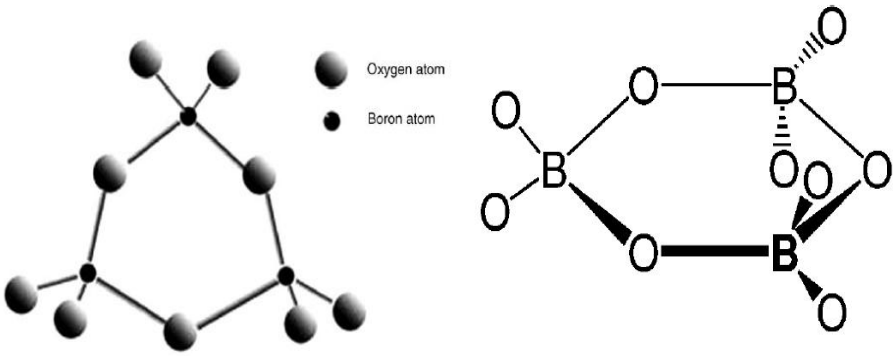

Figure 1.10. a)The Structure of $B_3O_9^{9-}$(Wang et al. 2006), b) Structural sketch map of $B_3O_9^{9-}$ ion (Wei et al. 2002a).

By using powder X-ray and electron diffraction techniques, Ren et al.(1999) have found super-reflections corresponding to a rhombohedral cell, a=6.6357 Å and c= 26.706 Å with space grpup R32, for $GdBO_3$ but the proposed structure model was also questioned for its unphysical bond distances. In this work, Ren et al.(1999) have employed all of the possible space groups (*R3, R-3, R3₂, R3m,* or *R-3m*) for constructing the structure model and only *R3₂* led to a sreasonable solution. The structure defined here was refined by using the Rietveld technique and the boron atoms cannot be identified from the refinement because their scattering power is too small. They were inserted into the structure by considering the structure of the polyborate group $B_3O_9^{9-}$. The B_3O_9 sheet in the *R3₂* structure of LT phase of $GdBO_3$ is given in Figure 1.11.

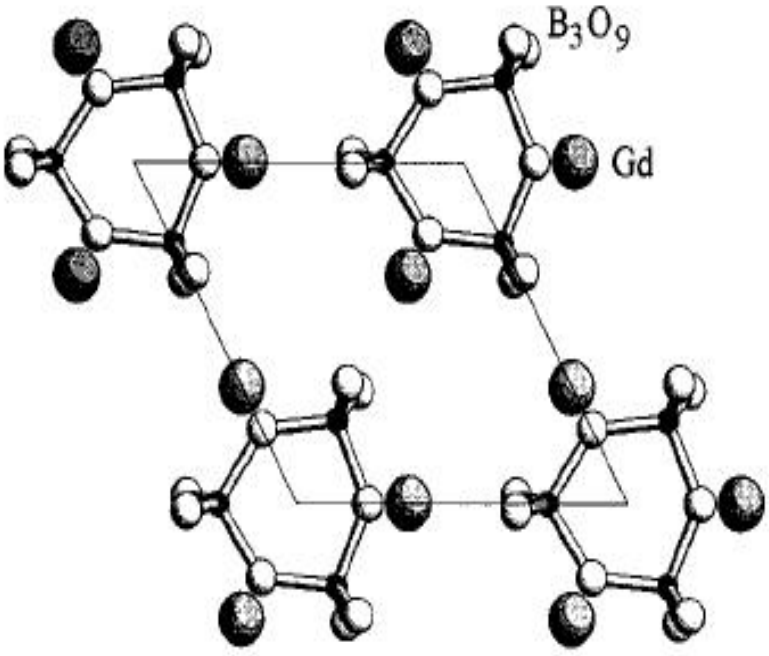

Figure 1.11. The B_3O_9 sheet in the structure of LT phase of $GdBO_3$ (Ren et al. 1999)

The crystal structure of LT phase of $GdBO_3$ with unit cells a=6.6357 Å and c=26.706 Å is shown in Figure 1.12.

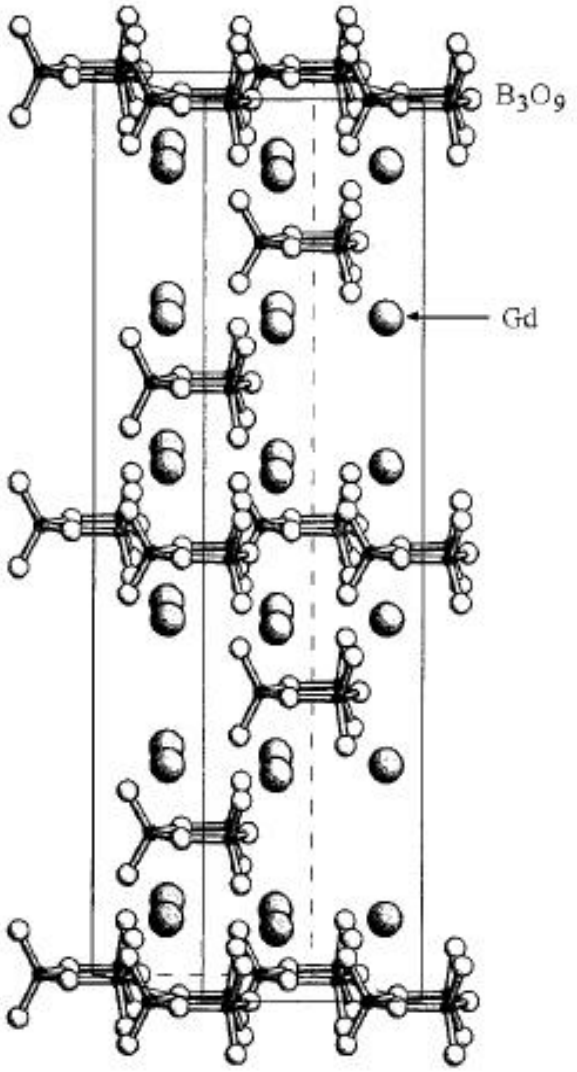

Figure 1.12. The crystal structure of LT phase of $GdBO_3$ (Ren et al. 1999)

Parallel efforts to characterize the vaterite-type rare earth orthoborate have been undertaken through the spectroscopic investigations. Yet, the high resolution luminescence spectra revealed a difficulty in distinguishing between the alternatives of having either two (Hölsa 1987, Chadeyron et al. 1997b) or three (Boyer et at. 2003) cation sites in the structure. In order to clarify the structures of the vaterite-type rare earth orthoborates, one needs to use a special technique that is more sensitive to light atoms.

Lin et al. (2004) reported the use of neutron diffraction as a complementary structure solution tool, since the coherent elastic scattering lengths of rare earths, oxygen, and boron for neutrons have the same order of magnitude. In their work, they have solved the low and high temperature modifications. The low temperature polymorph crystallizes in a C-centered monoclinic cell with *C2/c* space symmetry, the unit cell parameters being a=11.3138(3) Å, b =6.5403(2) Å, c= 9.5499(2) Å, and β=112.902(1)°. The boron atoms in the structure are all tetrahedrally coordinated and form the three-membered ring borate B_3O_9 moiety. The high temperature polymorph also crystallize in *C2/c* space symmetry but the borate groups in the high-temperature structure are all isolated flat BO_3 triangles. In Figure 1.13., the projection of the low temperature structure of monoclinic YBO_3 along b axis, along (001) direction were given.

Figure 1.13a illustrates a projection of the crystal structure of the low-temperature phase of $(Y_{0.92}Er_{0.08})BO_3$ vaterite along the *b*-axis. The structure could be described as alternative stacking of cation sheets and borate layers. The boron atoms are all tetrahedrally coordinated in the BO_4 units, which share vertices, thus forming three membered ring borate B_3O_9 units. Figure 1.13b presents the structure projected along the (001) direction. It can be seen that the yttrium atoms adopt the layers of the almost ideal close-packed arrangement.

In Li's (Li et al. 2008) work, the environmental factors are computed and the corresponding LMCT (ligand-to-metal-charge-transfer-) energies of Eu^{3+} are predicted from space groups *P-6c2* and *C2/c* of the orthoborate YBO_3 based on the dielectric theory of the complex crystal. The result shows that only the space group *C2/c* proposed by Lin et al. (2004) is in good aggreement with the experimental phenomena.

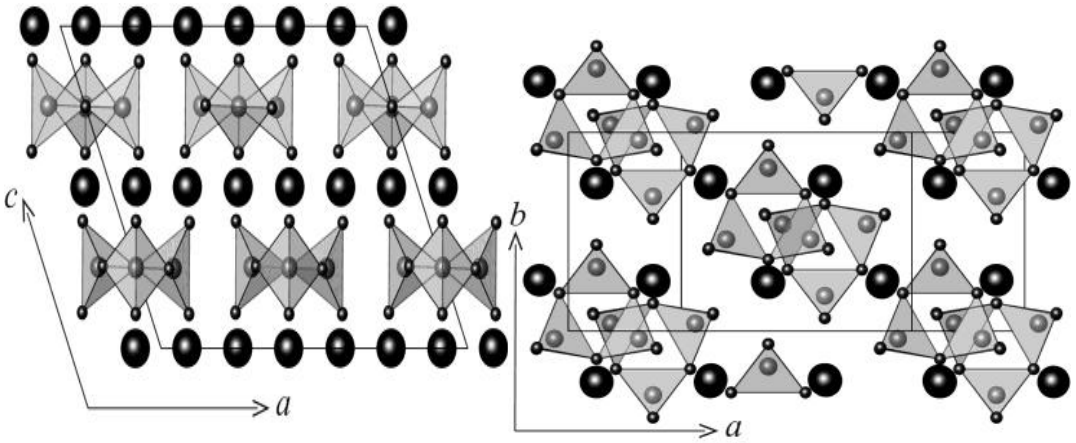

Figure 1.13. (a) Projection of the structure of the low-temperature phase $(Y_{0.92}Er_{0.08})BO_3$ along the *b*-axis. (b) Projection of the structure of the low-temperature phase $(Y_{0.92}Er_{0.08})BO_3$ along the (001) direction. (Lin et al. 2004).

1.4. X-ray Diffraction Structure Determination and the Rietveld Structure Refinement Analysis

1.4.1. The Renaissance of Powder Diffraction

The method of X-ray powder diffraction was devised independently in 1915 by Debye and Scherrer in Germany and in 1916 in the United States, and initially relied on photographic film record the angles and intensities of the diffracted beams. When properly employed, powder diffraction can yield a great deal of structural information about the material under investigation. A given substance always produces a characteristic diffraction pattern. This fact is the basis for the diffraction method of chemical analysis. The powder pattern of a substance is characteristic of that substance and forms a sort of fingerprint by which the substance may be identified (Cullity and Stock, 2001).

Although the diffraction of X-rays from powders (microcrystalline samples) had been discovered by Max von Laue shortly after his historical experiment on a single-crystal of KCI (which he crushed, on purpose, to verify his fresh hypothesis on the nature of such experiment), the Powder Diffraction technique has been seldom

used as a structural tool at the beginning. For more than 50 years powder became a widespread analytical method for the characterisation of soils, ores, rocks, metals, alloys, and, more recently, ceramics, drugs, plastics, dyes and other commodities since it is very clear that powder traces could be used as fingerprints in qualitative analysis of crystalline materials of different origins (Masciocchi, 1997).

At least in principle, every crystalline material shows a unique X-ray diffraction pattern. The potential for qualitative phase identification was certainly recognized from the early days of X-ray diffraction. The most significant milestone of X-ray phase analysis is creating X-ray diffraction databases. Today, the file is produced in annual updates by the International Centre for Diffraction Data (ICDD), which is a nonprofit corporation relying on the volunteer efforts of many of the powder diffractionists. Beside the main ICDD database, there are several other databases for structural studies. The crystallographic and structural information can be obtained from Cambridge Structural Database (CSD) for organic and organometallics, Inorganic Crystal Structure Database (ICSD) for inorganic materials, NRCC Metals Data File for the structure of macromolecules, NIST Crystal Data for inorganic and organic unit cells (Jenkins and Synder, 1996).

1.4.2. Rietveld Theory

The Rietveld (Rietveld 1967, 1969) method refines user-selected parameters to minimize the difference between an experimental pattern (observed data) and a model based on the hypothesized crystal structure and instrumental parameters (calculated pattern). By using Rietveld refinement background profile, atomic parameters, unit cell parameters, unit cell axes, atomic positions, etc. can be refined and three dimensional crystal structure can be finally drawn.

The quality of the Rietveld refinement fit (ie. the quantitative measure of the matching between observations and the calculated pattern), which should give information about the true values of all parameters in calculated model (for which an

estimated standard deviation, in the least-squares sense, is supplied), is normally evaluated by agreement factors, defined as:

$$R_p = \sum i \left| y_{oi} - y_{ci} \right| / i \left| y_{oi} \right| \quad \text{[R-profile]}$$

$$R_{wp} = \sum i\, w_i \left| y_{oi} - y_{ci} \right|^2 / \sum i\, w_i \left| y_{oi} \right|^2 \quad \text{[Weighted R-profile]}$$

$$R_B = \sum k \left| I_{ok} - I_{ck} \right| / \sum k \left| I_{ok} \right| \quad \text{[R-Bragg]}$$

where i runs over all data points, and k runs over all (space-group permitted) reflections. Since Iok (observed integrated intensities) are not readily available, a number of numerical algorithms, partitioning the observed intensities of overlapping peaks into their partial contributions have been developed.

From the above considerations, it is obvious that the Rietveld method requires digitised data and knowledge of an approximate structural model (ie., lattice parameters, space group symmetry and fractional atomic positions). A number of other starting parameters, mostly instrumental, can be guessed by visual inspection (background coefficients, zero angle, etc.) (Masciocchi, 1997).

1.4.2.1. The Rietveld Refinement Steps

For a Rietveld refinement, it is essential that the powder diffraction data be collected appropriately. Factors to consider prior to data collection and calibration are; the most suitable radiation (e.g. conventioanl X-ray, synchrotron X-ray or neutron), the wavelength, appropriate sample preparation and thickness, slit sizes, and necessary counting time (McCusker et al. 1999).

In order to be sure about counting statistics throughout a X-ray powder diffraction pattern, longer time should be spent on the data collection at high angles where intensities are lower. An ideal particle size within a powder sample is around 1-5 μm. Sample rotation will improve the particle homogenity. Any trial to smooth the diffraction profile before doing a Rietveld refinement must be resisted.

Smoothing introduces point-to-point correlations which will give wrongly lowered e.s.d.'s in the refinement. After completing the necessities for sample scanning, Rietveld analysis is composed of the refinement of the following parameters (McCusker et al. 1999):

a) Background Correction: There are two approaches to dealing with the background in a powder diffraction pattern. Background can either be estimated by linear interpolation between selected points between peaks and then substracted, or it can be modelled by an emprical or semiemprical function containing several refinable parameters.

b) Peak Shape Function: The peak shapes observed are a function of both the sample (e.g. domain size, stres/strain, defects) and the instrument (e.g. radiation source, geometry, slit sizes), and they change as function of 2 Theta. Among the analytical peak-shape functions investigated, the pseudo-Voigt aproximation of the Voigt function is probably the most widely used X-ray and constant wavelength neutron data (Thompson et al. 1987). The pseudo-Voigt function can be described as a linear combination of Lorentzian and Gaussian components. This appears to describe the symmetrical part of an X-ray diffraction peak quite well.

c) Profile: If only a partial structural model is available, the calculated intensities may differ significantly from the observed ones, and this can complicate the initial refinement of profile parameters (changes in FWHM and peak asymmetry as a function of 2θ, 2θ correction, unit-cell parameters). In such a case, it is probably best to use a structure-free approach, in which the intensities of the reflections are simply adjusted to fit the observed ones (Le Bail et al. 1988), to obtain initial values for the profile parameters. This Le Bail refinement option, which can also be used to extract a list of integrated intensities from a powder pattern for structure determination, has now been included in most modern Rietveld programs.

d) Completing the Structural Model: In general, refinement of structural parameters should not be started before all (or almost all) atoms in the given structure have been found. Otherwise, refinement is likely to lead to a false minimum, because the algorithm will try to describe all of the electron density with too few atomic positions.

e) Refining the Structure: The Rietveld refinement of structural parameters can begin with a complete structural model and good starting values for the background contribution, the unit-cell parameters and the profile parameters. Because the global minimum of the least-squares residual function is much shallower with powder data than it is with single-crystal data, the refinement needs continuous monitoring. A refinement of a structure of medium complexity can require a hundred cyles, while a structure of more complex compound may easily require several hundred. Refinement is generally done in sets of two to five cycles at a time. In order to monitor the progress of a refinement, the two most useful pieces of information are the profile fit and the nature of the parameters shifts (i.e. shift/e.s.d: are the shifts oscillating, diverging or converging). The profile fit is best seen in a plot of the observed and calculated patterns, but can also be followed numerically with a reliability factor or residual, R, value.

1.4.2.2. Rietveld Programs

There are lots of commercial and free of charge Rietveld programs available. The commercial programs; i.e. Jade, High Score Plus, Topas are softwares of the XRD producer companies. Free of charge programs such as GSAS, Fullprof, EXPO, SIRWARE, QUANTO, BRASS, etc. can be easily downloaded from their web sites. GSAS and Fullprof software packages are most interested by universities and institutions.

1.4.2.2.1. GSAS Software Package (General Structure Analysis System)

GSAS is a set of programs for the processing and analysis of both single crystal and powder diffraction data obtained with X-rays or neutrons and the EXPGUI is the Graphical User Interface fort he GSAS. It is capable of handling all of these types of data simultaneously for a given structural problem. In addition, it can handle powder diffraction data from a mixture of phases refining structural parameters for each phase (Larson and Von Dreele 2000, Toby 2001). By using GSAS in Rietveld refinements, unit cell parameters, background functions, profile parameters, zero shift, atomic positions, and unisotropic thermal parameters can be refined. At the end of refinement, GSAS can provide R_p, R_{wp}, χ^2 shift values and by using final data three-dimensional structure of refined compound can be drawed.

1.5. Purpose of the Thesis

The purpose of this thesis is to synthesize and characterize rare earth containing borates and phosphates, to investigate the crystallographic effect of rare earths on these compounds and to make Rietveld structural analysis for pure rare earth orthoborates. For this purpose, rare earth phosphates, rare earth added pyrophosphates and rare earth orthoborates were synthesized by using solid state reaction and microwave-assisted solid state reaction.

In the phosphate part of the thesis, we divided this group into two separate chapters both including different chemical reactions. In the first part, we synthesized sodium lanthanide oxide phosphates. Since there are only two sodium lanthanide oxide phosphates present in literature, we tried to synthesize other lanthanide oxide containing phosphates and produced Na_2SmOPO_4, Na_2DyOPO_4, Na_2HoOPO_4, Na_2ErOPO_4, and Na_2YbOPO_4 for the first time in the literature.

In the second part of the phosphates, the suitability of $Sr_2P_2O_7$ for its use in TL dosimetry was investigated since our literature survey indicated that the TL and dosimetric properties of rare earth added and pure $Sr_2P_2O_7$ samples have not been studied up to now. For this purpose, $Sr_2P_2O_7$ compound were prepared and rare earths and CuO added into the this compounds. For the characterization of the produced new phases, XRD, IR, and SEM methods were applied to see the changes that may ocur in the crystal structure, and the behavior of the samples due to addition of metal dopants. The dosimetric characteristics of the products were determined by applying TL technique. Thermoluminescence studies showed two glow peaks of Pr, Ho, and Nd along with Cu-added samples, one of them is always at around 90 ^oC and the second TL peak around 180, 275, and 285 ^oC, respectively. Therefore, this study showed that these materials are promising thermoluminescent material for dosimetric applications.

Rare earth borates investigations were divided into two parts. In the first part, the effect of microwave energy on particle size and structure of some $LnBO_3$ (where Ln=La, Nd, Dy, Ho) compounds were investigated. Urea and sucrose were used as a microwave active organic additive.

In the second part of the borates, since there are still uncertainities about the crystal structure of optically important rare earth orthoborates our aim is to investigate the structure of all pure lanthanide borate compounds (Ln= Y, La-Lu). For this purpose, the synthesized powder were subjected to Rietveld structural analysis by using GSAS software.

1.6. Outline of The Thesis

Chapter 1 reveals a detailed literature survey covering general information, uses and reserves of borates, phosphates, definition of TL property and Rietveld refinement.

Chapter 2 deals with the materials used for the synthesis of the borates, and phosphates, the analytical method applied and the experimental procedures implemented throughout the thesis.

In Chapter 3, the experimental results of lanthanide oxide phosphates, pyrophosphates and orthoborates are presented and discussed in detail, based on explanations and comparisons of XRD, FTIR, Raman, SEM, TL and Rietveld analysis studies outputs.

Finally in Chapter 4, the main points that can be drawn from this thesis are emphasized.

CHAPTER 2

EXPERIMENTAL

2.1. Chemicals and Experimental Procedure

2.1.1. Sodium Lanthanide Oxide Phosphates (Na_2LnOPO_4)

The following solid powders were used in the solid state reactions of various rare earth oxides: La_2O_3, Nd_2O_3, Sm_2O_3, Gd_2O_3, Dy_2O_3, Ho_2O_3, Er_2O_3,Yb_2O_3, Na_2CO_3, and $NH_4H_2PO_4$. They are commercial reagents used without further purification and supplied from the Merck, Fluka, Aldrich, and Sigma.

All preparations were made by spontaneous crystallization with stoichiometric proportions of reactants in oxygen atmosphere with the following formula:

$$2Na_2CO_3(s) + Ln_2O_3(s) + 2NH_4H_2PO_4(s) \rightarrow 2Na_2LnOPO_4(s) + 2NH_3(g) + 3H_2O(g) + 2CO_2(g).$$

Desired quantities of salts and oxides were weighed separately and crushed well in agate mortar for homogenization. Then the mixture was transferred into a porcelain crucibles and put into a furnace for heating. The mixtures were heated at 500 ^oC for 11 hours, 700 ^oC for 10 hours, 800 ^oC for 5 hours, 850 ^oC for 5 hours, 900 ^oC for 15 hours, 950 ^oC for 25 hours, 1100 ^oC for 15 hours. The products were taken from the furnaces directly to outside. All the samples were kept in desiccators against moisture. The starting materials weigths are all 1.0000 g for lanthanide oxides. The weigth losses of the products are in good aggrement with the theoretical ones. The products were subjected to X-ray diffraction and IR analysis after each sintering process.

2.1.2. Strontium Pyrophosphates

2.1.2.1. Solid solutions of $Sr_2P_2O_7$ and ZrP_2O_7

The ZrO_2, $SrCO_3$, and $NH_4H_2PO_4$ (from Merck, Aldrich and Allied Chem.) powders were used in the solid state reactions.

The experiments were divided into two sets. All preparations were made in air with the aid of muffle furnaces. Stoichiometric amounts of reactants and heat treatment details of both sets are given in Table 2.1a and 2.1b. Desired quantities of initial reactants were weighed separately and crushed well in agate mortar. Then the mixture was transferred into a porcelain crucible and put into a furnace for heating. The products were subjected to X-ray powder diffraction and IR analysis after each sintering process. All the samples were kept in desiccators against moisture.

Table 2.1. Composition, and heating treatment of $Sr_2P_2O_7$ added ZrP_2O_7 and ZrP_2O_7 added $Sr_2P_2O_7$.

Table 2.1a. Composition, and heat treatment conditions of $Sr_2P_2O_7$ added ZrP_2O_7.

Composition	**900 ^oC**
ZrP_2O_7	14.5h
ZrP_2O_7:10 % $Sr_2P_2O_7$	10.5h
ZrP_2O_7: 5 % $Sr_2P_2O_7$	10.5h
ZrP_2O_7: 1 % $Sr_2P_2O_7$	10.5h
ZrP_2O_7: 0.5 % $Sr_2P_2O_7$	10.5h
ZrP_2O_7: 0.1 % $Sr_2P_2O_7$	10.5h
ZrP_2O_7: 0.05 % $Sr_2P_2O_7$	10.5h
ZrP_2O_7: 0.03 % $Sr_2P_2O_7$	10.5h

Table 2.1. Continued.

Table 2.1b. Composition, and heat treatment conditions of ZrP_2O_7 added $Sr_2P_2O_7$.

Composition	**900 ^oC**
$Sr_2P_2O_7$	14.5h
$Sr_2P_2O_7$: 10% ZrP_2O_7	10.5h
$Sr_2P_2O_7$: 5% ZrP_2O_7	10.5h
$Sr_2P_2O_7$: 1% ZrP_2O_7	10.5h
$Sr_2P_2O_7$: 0.5 % ZrP_2O_7	10.5h
$Sr_2P_2O_7$: 0.25 % ZrP_2O_7	10.5h
$Sr_2P_2O_7$: 0.1 % ZrP_2O_7	10.5h
$Sr_2P_2O_7$: 0.05 % ZrP_2O_7	10.5h

2.1.2.2. Thermoluminescence properties of Copper and Rare Earth Elements added $Sr_2P_2O_7$

The addition was done by mixing previously produced (Section 2.1.2.1.) pure $Sr_2P_2O_7$ with %5 CuO and % 0.5, 1, 2, 3, 4, 5, 10, 15 (by weight) rare earth oxides (Y_2O_3, La_2O_3, CeO_2, Pr_6O_{11}, Nd_2O_3, Sm_2O_3, Eu_2O_3, Gd_2O_3, Tb_2O_3, Dy_2O_3, Ho_2O_3, Er_2O_3, Tm_2O_3, Yb_2O_3, Lu_2O_3).

The mixtures were grounded in an agate mortar. They, then, were transferred in alumina ceramic crucibles and heated at 950 ^oC for 10 hours in muffle furnaces. All preparations were made by spontaneous crystallization in air atmosphere. All the samples were kept in desiccators against moisture.

2.1.3. Rare Earth Orthoborates

In this part of the thesis, rare earth orthoborates were synthesized by using microwave-assisted and solid state synthesis methods.

2.1.3.1. Microwave-Assisted Synthesis of $LnBO_3$ (where Ln=La, Nd, Dy, Ho)

In the present work, we prepared $LnBO_3$ (Ln=La, Nd, Dy, Ho) powder samples by using either urea or sucrose in less energetic microwave-assisted reaction method at 1000 W starting with Ln_2O_3 (where Ln=La, Nd, Dy, Ho) and H_3BO_3 (ratio=1:2) and further two hour heating was applied at 950 ^oC after this process in muffle furnace as shown in Table 2.2.

Microwave processing of materials differs fundamentally from conventional processing in terms of its heat mechanism. In a microwave oven, heat is generated within the sample itself by the interaction of microwaves with the material.

Table 2.2. The composition and heat treatment conditions of orthoborate mixtures prepared by miwrowave-assisted synthesis.

Composition $Re_2O_3+2H_3BO_3$	**%40 Urea or Sucrose By Weight**	**MW treatment (Watt-Minutes)**	**Heat Treatment (^oC-Hours)**
$La_2O_3+ 2H_3BO_3$	%40 Urea	1000W-10 Min.	950 ^oC-2 Hours
$Nd_2O_3+ 2H_3BO_3$	%40 Urea	1000W-10 Min.	950 ^oC-2 Hours
$Dy_2O_3+ 2H_3BO_3$	%40 Urea	1000W-10 Min.	950 ^oC-2 Hours
$Ho_2O_3+ 2H_3BO_3$	%40 Urea	1000W-10 Min.	950 ^oC-2 Hours
$La_2O_3+ 2H_3BO_3$	%40 Sucrose	1000W-10 Min.	950 ^oC-2 Hours
$Nd_2O_3+ 2H_3BO_3$	%40 Sucrose	1000W-10 Min.	950 ^oC-2 Hours
$Dy_2O_3+ 2H_3BO_3$	%40 Sucrose	1000W-10 Min.	950 ^oC-2 Hours
$Ho_2O_3+ 2H_3BO_3$	%40 Sucrose	1000W-10 Min.	950 ^oC-2 Hours

2.1.3.2. Solid State Synthesis of $LnBO_3$ (where Ln= Y, La, Nd, Sm, Eu, Gd, Tb, Dy, Ho, Er, Tm, Yb, Lu)

Starting materials for the preparation of mixtures consisted of reagent grade boric acid, H_3BO_3, powder and thirteen high-purity lanthanide oxides [Ln_2O_3 (where Ln= Y, La, Nd, Sm, Eu, Gd, Dy, Ho, Er, Tm, Yb, Lu) and Tb_4O_7] obtained commercially. The purity of oxides was better than 99.9%.

The mixtures [Ln_2O_3:H_3BO_3=2:1 and Tb_4O_7:H_3BO_3=1/28] were grinded, heated in an Al crucible at 300 ^oC for 5 hours, 500 ^oC for 5 hours, 700 ^oC for 5 hours, 900 ^oC for 10 hours, 1000 ^oC for 5 hours in air atmosphere with intermediate grindings. The compounds were finally quenched to room temperature in air. All the samples were kept in desiccators against moisture.

2.2. Instrumentation

2.2.1. XRD-X-Ray Diffraction

To study the crystal structure of the produced new phases from the solid state reactions, X-ray Diffraction (XRD) investigations were carried out.

Specific d value for each peak was calculated from the corresponding 2θ values by using the Bragg's law given in Equation 2.1.

$$n\lambda = 2d\sin\theta \qquad (2.1.)$$

where,
n: an integer showing order in crystal planes (n=1, 2, 3 .., n)
λ: the wavelength (λ=1.54056 Å for Cu anode)
d: the distance between succesive paralled planes, Å
2θ: the angle between incidence and diffraction of the X-ray beam from the given lattice plane.

The identification was done by comparing those d values with the characteristic d values in the International Centre for Diffraction Data (ICDD) and Inorganic Crystal Structure Database (ICSD) cards of appropriate materials.

In X-ray crystallography, the angstrom (Å) unit has always been the preferred measure of wavelength. Even though the latest recommendation from the International Union of Pure and Applied Chemistry (IUPAC) discourages use of the angstrom and encourages use of the nanometer (nm; 1x 10^{-9} m), the powder diffraction community has fought for retention of the angstrom and this remains the common unit in the use in the field today (Jenkins and Snyder, 1996). For this reason, in this thesis we will use the angstrom unit.

2.2.1.1. Rigaku Diffractometer

The structural analysis of samples was checked by X-ray Powder Diffraction. The XRD data were collected using Rigaku X-ray Diffractometer (Model, Miniflex) with CuK_α (30 kV, 15 mA, λ=1.54051 Å) radiation at room temperature at Chemistry Department of Middle East Technical University. Scanning was performed between 5-145 degree 2 Theta, generally. The measurements were made with 0.01 and 0.05 degree steps and 1 degree/minute rate. The divergence slit was variable and scattering and receiving slit were 4.2 degree and 0.3 mm, respectively. Rigaku Miniflex diffractometer with nickel-filtered CuK_α radiation (15mA, 30kV). This device was used only for preliminary investigation and the X-ray data never used in the Rietveld refinements.

2.2.1.2. Panalytical Diffactometer

For rietveld analysis of lanthanide orthoborate powders, more accurate intensities were then collected on a X'PERT PRO X-ray vertical diffractometer (Bragg-Brentano parafocusing geometry) of PANalytical X-ray systems equipeed with ultrafast solid state detector PIXCEL using CuK_α radiation (45 kV, 40 mA, λ=1.5406 Å) between 10° to 150° with 0.026 sampling rate in continuous mode. The X-ray beam contained $CuK_{\alpha1}$ and CuKα2 wavelengths, respectively with $\lambda K_{\alpha1}$=1.5406 Å and $\lambda K_{\alpha2}$= 1.5444Å and intensity ratio $CuK_{\alpha2}/CuK_{\alpha1}$ of 0.5.

2.2.1.3. Stoe Stadi-P Diffractometer

In order to investigate the differences in powder patterns between dual CuKα radiation and monochromatic CoK_{a1}, some of rare earth borates were scanned by STOE STADI-P CoKα1 (λ=1.78896 Å) with Ge(111) monochromator.

2.2.2. FTIR

The vibrational modes of molecules in the samples were defined by the help of Nicolet 400 and 510 FTIR Infrared Spectrometer in the region 400-2000 cm^{-1}. Spectroscopic grade KBr was used for making IR pellets. KBr was dried at 180 ^{o}C for about 1 day before using. The ratio of KBr to sample was 100 mg:3 mg.

In KBr pellet method, the solid samples is finely pulverized with pure, dry KBr for spectroscopy. The mixture is pressed in a hydraulic press to form a transparent pellet, and the spectrum of the pellet is measured. It is important that the solids be extremely finely divided and well mixed. The pellet is pressed in a special dye that can be evacuated in order to avoid entrapped air, which causes cloudiness in the pellet.

2.2.3. Raman

Jobin Yvon-Horiba was used for Raman scattering spectra. This instrument has He-Ne laser wavelength of 632.83 nm and Peltier cooled CCD detector. Laser power was 10 mWatt, and detector worked at -75 ^{o}C. The slit width was 200 μm, and grating with 600 blazes/cm was used. Data accumulation duration was 60 second, and each accumulation was done for 5 times.

2.2.4. SEM-EDS

The surface characterization of powder specimens were performed by Scanning Electron Microscopy (SEM) technique. Scanning Electron Micrographs were taken by JEOL JSM 6400 (20 kV), equipped with NORAN system 6 X-ray Microanalysis System & Semafore Digitizer at Metallurgical and Materials Engineering Department of Middle East Technical University. The microscope is equipped with secondary and backscattered electron detectors and X-ray microanalysis system, and is capable of providing both topographical and compositional information about the specimen.

Samples were coated with a very thin layer of gold-palladium (Au-Pd) alloy by using HUMMLE VII Sputter Coating Device (ANATECH). The morphology of the samples was investigated by taking microphotographs of SEM images from different parts of the sample surfaces.

2.2.5. Thermoluminescence

In order to investigate the dosimetric properties and to present the thermoluminescence characteristics of the samples were taken by means of TL glow curves. Thermoluminescence glow curves of copper and rare earth added $Sr_2P_2O_7$ compounds were obtained by using a Harshaw QS 3500 Manual type TL reader which has an S-11 response photomultiplier tube at Physics Engineering Department of Gaziantep University. The reader is interfaced to a PC where the TL signals were studied and analyzed. Glow curves were measured using a platinum planchet at a linear heating rate of 1 $^{o}C\ s^{-1}$ from room temperature up to 400 ^{o}C.

A standard clean glass filter was always installed in the reader between sample and photomultiplier tube. This filter allows the light whose wavelength is between ≈250 and ≈1000 nm to pass through it and thereby eliminates unwanted infrared light emitted from the heater.

All samples were irradiated for 5 minutes at room temperature with a $^{90}Sr–^{90}Y$ beta (β) source delivering about 0.9 Gy/min. 15 milligrams of powder were used for each measurement. The time duration between irradiation and TL reading was always kept constant at about 1 min to eliminate the possible fading in the low temperature peak betweenroom temperature and 150 ^{o}C.

All experiments were performed inside a dark room in order to avoid any influence of the environment light on the glow curves.

2.3. Heat Treatment Furnaces

Heat treatment experiment were executed by using Protherm, PLF 125 Model furnace in air atmosphere. To avoid melting, reactions started at room temperature.

2.4. Crystallographic Data Analysis Programs

Although, we always tried to find best conditions for scanning diffractograms in different diffractometers, we have faced difficulties obtaining good peak profiles, background functions, smoothing, peak search, etc. because of the sample characteristics under investigation. In order to correct instrumental broadening and proceed the Rietveld refinement, we used CELREF and GSAS, respectively.

2.4.1. CELREF

CELREF (Altermatt and Brown, 1987), developed at Laboratoire des Matériaux et du Génie Physique Ecole Nationale Supérieure de Physique de Grenoble (INPG) Domaine Universitaire BP 46, 38402 Saint Martin d'Hères France, can refine the unit cell parameters of given compounds whose unit cell parameters and space group previously indexed or solved.

2.4.2. GSAS-General Structure Analysis System

GSAS is a set of programs for the processing and analysis of both single crystal and powder diffraction data obtained with X-rays or neutrons. It is capable of handling all of these types of data simultaneously for a given structural problem. In addition, it can handle powder diffraction data from a mixture of phases refining structural parameters for each phase. EXPGUI is graphical user interface program of GSAS for refinements. (Larson A.C. and Von Dreele, 2000, Toby, 2001).

CHAPTER 3

RESULTS AND DISCUSSION

3.1. Synthesis of Sodium Lanthanide Oxide Phosphates Na_2LnOPO_4 (Ln= La, Nd, Sm, Gd, Dy, Ho, Er, Yb)

The following powders were heated in the solid state reactions of various rare earth oxides: La_2O_3, Nd_2O_3, Sm_2O_3, Gd_2O_3, Dy_2O_3, Ho_2O_3, Er_2O_3,Yb_2O_3, Na_2CO_3, and $NH_4H_2PO_4$ at 500 ^oC for 11 hours, 700 ^oC for 10 hours, 800 ^oC for 5 hours, 850 ^oC for 5 hours, 900 ^oC for 15 hours, 950 ^oC for 25 hours, 1100 ^oC for 15 hours.

Parallel to these experiments, we have tried several experiments to synthesize KTP-like single crystals of Na_2LnOPO_4 by using several chemicals for flux reactions. Unfortunately, our all experiments to obtain single crystal products were failed and it is not possible to find structural data about the related compounds in the literature to perform Rietveld analysis for structural solution.

After the final heating at 1100 ^oC, X-ray diffraction patterns of products were obtained and the final orthorhombic compounds are sectioned into two sets. In the X-ray diffraction pattern of the first set (Figure 3.1), Na_2LaOPO_4, Na_2NdOPO_4, Na_2SmOPO_4 products are differentiated according to their splitting peak as presented by Kizilyalli (Gönen et al. 2000). The second set, Na_2GdOPO_4, Na_2DyOPO_4, Na_2HoOPO_4, Na_2ErOPO_4, and Na_2YbOPO_4, was also indexed in orthorhombic system without having splitting peak.

3.1.1. Results of X-ray Diffraction Investigations

In the synthesis steps of both sets, as the reaction proceeded at 950 ^{o}C for 25 hours, solid state reactions at these stages also did not reveal the expected products and the XRD patterns of the products showed a great similarity with each other but they are not desired ones. The IR spectra of the products obtained at these steps have supported this idea. Therefore, in order to obtain products the temperature was increased. Prolonged heating of the products at 1100 ^{o}C (three 5 hours periods and grinding in between) resulted in single phase product which is orthorhombic Na_2LnOPO_4 (where Ln= La, Nd, and Sm). The XRD patterns of set 1 are presented in Figure 3.1.

It is known from the previous work of (Gönen et al. 2000) that Na_2LaOPO_4 has orthorhombic structure with the refined unit cell parameters of a= 13.657(5), b=11.076(5), and c=6.7295(3) Å. In this study, the diffraction peaks of our Na_2LaOPO_4 can be indexed on the basis of orthorhombic cell with the refined unit cell parameters of a= 13.60(1), b=12.71(1), c=6.96(1) Å using CELREF program (Altermatt and Brown, 1987) and the space group *Pmm2*. Table B.1 shows the X-ray diffraction data of our new Na_2LaOPO_4. The unit cell parameters of previously synthesized sodium lanthanum oxide phosphate and those from new phase show similarities with small differences. The reason of this situation is that former one was containing $Na_3La(PO_4)_2$ together with Na_2LaOPO_4. Another reason for the differences is the production temperature. The former one was obtained at 1000 ^{o}C while our final product Na_2LaOPO_4 was produced at 1100 ^{o}C.

The unit cell parameters of other two products in set 1, Na_2NdOPO_4, and Na_2SmOPO_4, were also indexed in orthorhombic system with the space group *Pmm2*. X-ray diffraction data and hkl values of Na_2LaOPO_4, Na_2NdOPO_4, and Na_2SmOPO_4 are given in Table B.1, B.2, B.3, respectively.

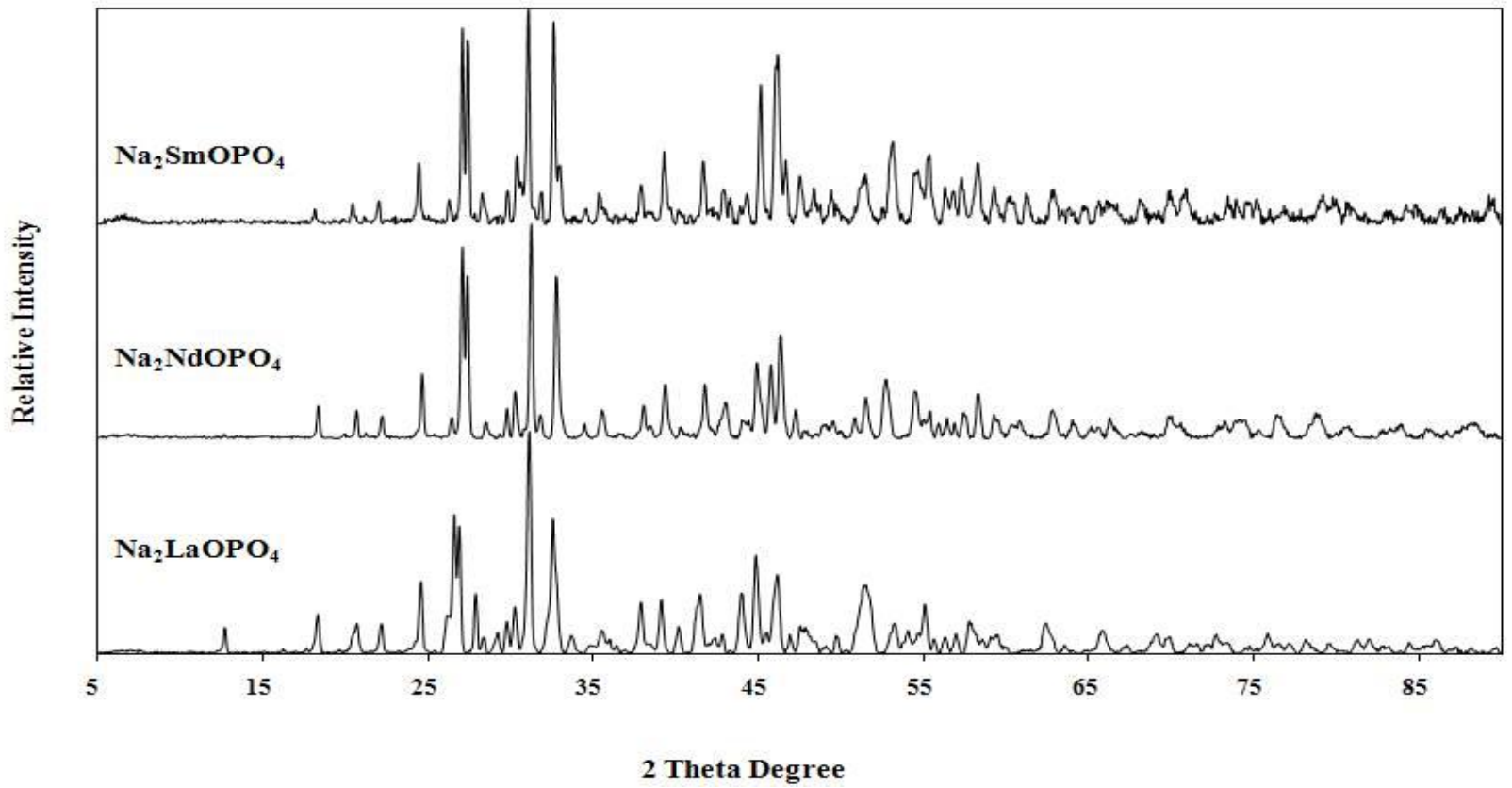

Figure 3.1. X-Ray Diffraction Patterns of Na_2LaOPO_4, Na_2NdOPO_4, Na_2SmOPO_4.

The calculated hkl values and the XRD data of set 1, where samples prepared under the highest temperature 1100 ^{o}C, was in accordance with Gönen's work (Gönen et al. 2000). Table 3.1 summarized the relation between unit cell dimensions of set 1.

Table 3.1. The unit cell parameters of Na_2LaOPO_4, Na_2NdOPO_4, Na_2SmOPO_4.

	Na_2LaOPO_4	**Na_2NdOPO_4**	**Na_2SmOPO_4**
a (Å)	13.60(1)	13.466(5)	13.54(1)
b(Å)	12.71(1)	12.547(6)	12.577(8)
c(Å)	6.96(1)	6.932(5)	7.047(5)

The most intense peaks were observed at d=2.8687, 2.8598, and 2.8732 Å for Na_2LaOPO_4, Na_2NdOPO_4, and Na_2SmOPO_4, respectively. Furthermore, the splitting of peaks were observed at d=3.35 and 3.30 Å, d=3.29 and 3.25 Å, d=3.29 and 3.25 Å, respectively while this splitting observed at 3.27 and 3.23 Å in the XRD data of lanthanum compound (Gönen et al. 2000).

In the second set, Na_2DyOPO_4, Na_2HoOPO_4, Na_2ErOPO_4, and Na_2YbOPO_4 were synthesized for the first time in this study at 1100 ^{o}C and results were given in Seyyidoglu et al. (2008). A new phase of Na_2GdOPO_4 was also obtained by using solid state reaction at the same temperature. The X-ray diffraction patterns of this set were given in Figure 3.2. The indexing of the data showed that Na_2GdOPO_4 and the new products Na_2DyOPO_4, Na_2HoOPO_4, Na_2ErOPO_4, and Na_2YbOPO_4, are also orthorhombic and the space group of this set is also Pmm2. The hkl indices and d observed values are given in Table B.4, B.5, B.6, B.7, and B.8 for Na_2GdOPO_4, Na_2DyOPO_4, Na_2HoOPO_4, Na_2ErOPO_4, and Na_2YbOPO_4, respectively. Table 3.2. represents the unit cell parameters of the second set where there are similarities. Similar hkl values observed in all products and there are some resemblances between these products and the first set, Na_2LnOPO_4 (Ln= La, Nd, and Sm). The splitting of the peak around d=3.45 and 3.25 Å was not observed in these second set products.

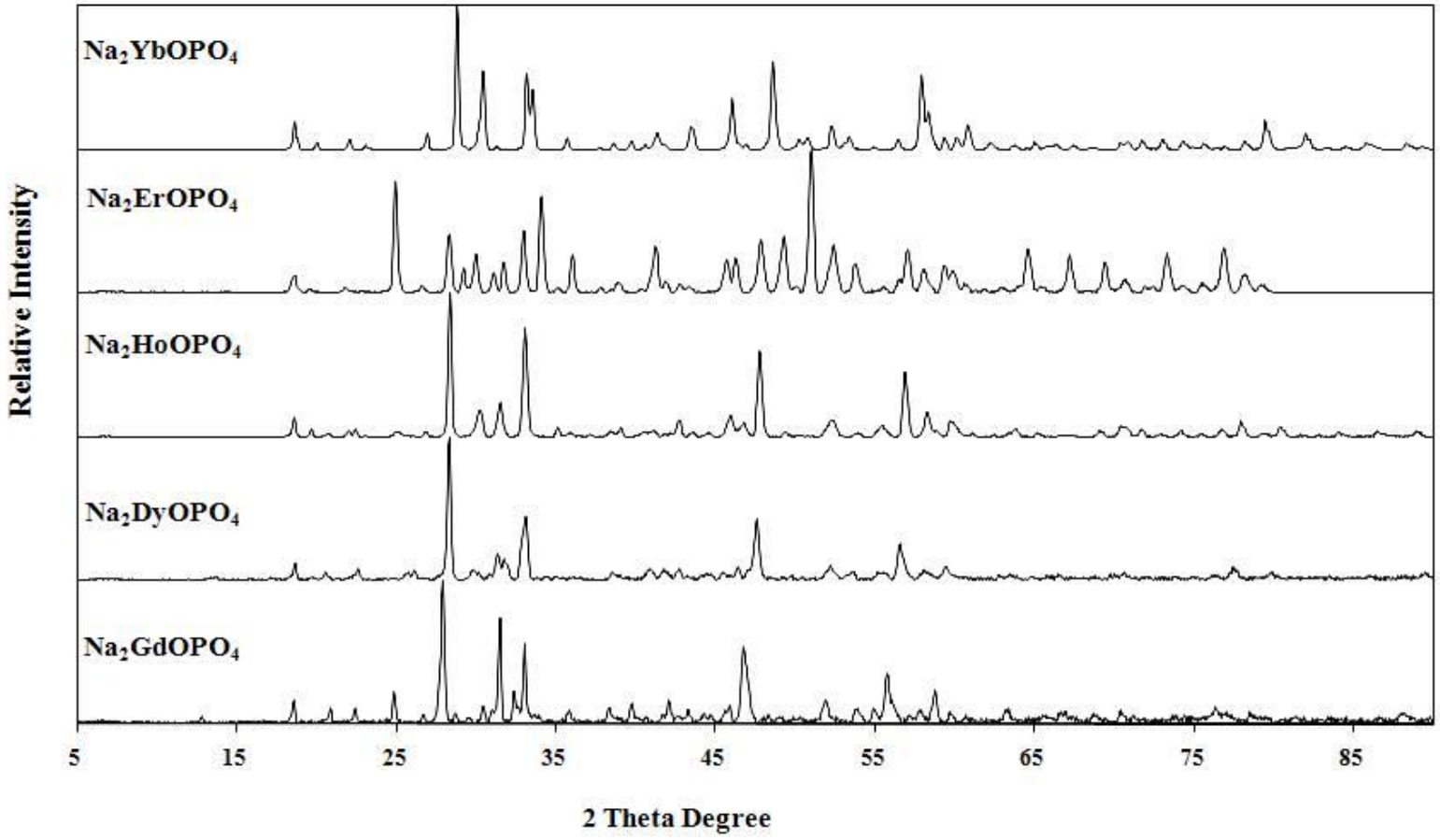

Figure 3.2. X-Ray Diffraction Patterns of Na_2GdOPO_4, Na_2DyOPO_4, Na_2HoOPO_4, Na_2ErOPO_4, Na_2YbOPO_4.

Table 3.2. The unit cell parameters of Na_2GdOPO_4, Na_2DyOPO_4, Na_2HoOPO_4, Na_2ErOPO_4, Na_2YbOPO_4.

	Na_2GdOPO_4	**Na_2DyOPO_4**	**Na_2HoOPO_4**	**Na_2ErOPO_4**	**Na_2YbOPO_4**
a(Å)	13.37(1)	13.66(2)	13.148(4)	13.563(5)	13.501(7)
b(Å)	12.775(9)	12.609(9)	12.577(2)	12.604(4)	17.579(9)
c(Å)	6.910(9)	6.611(6)	6.967(1)	7.003(3)	6.729(4)

3.1.2. Results of FTIR and Raman Investigations

According to Uztetik-Amour et al. (1995), ν_{as} and ν_s bands are assigned as ν_3 (F2), observed between 1136, 1099, 1034, 982, 965, and 945cm^{-1}. Table 3.3 and 3.4. indicate the IR and Raman data and assignments of the first and second sets, respectively. In the IR tables of our results, ν_3 (F2) bands are between 1084-1099, 1030-1053, 976-982, 957-971, and 945-954 cm^{-1} for both sets, respectively. Uztetik-Amour and Kizilyalli (1995) also indicated that bands at 926, and 909 cm^{-1} are due to stretching modes, assigned as ν_1 (A1) and present in our samples in between 921-926 and 913 cm^{-1}. They also stated that the bands around 604, 579, 560, 548, 523, and 470 cm^{-1} are ascribed to the δ (O-P-O) which is assigned as ν_4 (F2). These bands present in between 598-605, 574-579, 559-565, 541- 551, 523-526, 468-472, and 403-409 cm^{-1} for both sets, respectively. Finally, bands at 406, 381, and 367 cm^{-1} are attributed to deformation modes and assigned as ν_3 (E) given by Uztetik-Amour and Kizilyalli (1995). In the IR tables of the both sets, the bands around 403-409 cm^{-1} are obvious. Some of these bands were observed in Raman spectra of the products.

The presence of the tetrahedral PO_4 ion is obvious since the tetrahedral symmetry has four internal modes of vibration, ν_1=938 cm^{-1} (R), ν_2=420 cm^{-1} (R), ν_3=1017 cm^{-1} (IR, R), and ν_4= 567 cm^{-1} (IR, R) (Uztetik-Amour and Kizilyalli 1995). They also mentioned that the antisymmetric stretching modes are found between 1290 and 1050 cm^{-1} and the symmetric modes between 1050 and 900 cm^{-1}. In our results these bands also present.

Husson et al. (1988) and Nakamoto (1971) have reported that the highest frequency observed is due to antisymmetric stretching involving the terminal bond, a bond between a phosphorus atom and a so-called unshared oxygen atom or the shortest bond. For instance in $KTiOPO_4$ compound, ν_{as}P-O was observed at around 1135 cm^{-1}. The streching modes are 926 and 909 cm^{-1} and these bands were observed in both sets in between 921-926 and 913 cm^{-1} (Uztetik-Amour and Kizilyalli 1995).

The bands between 604 and 470 cm^{-1} are fundemental bands for δ(O-P-O) which are 605 and 478 cm^{-1} in this thesis. Finally, our samples have deformation modes which are between 406 and 367 cm^{-1}. The products have bands around 403-409 cm^{-1} and since FTIR instrument can detect peaks to 400 cm^{-1}, the other deformation peaks are not present in this study. These results confirmed that our products have KTP related Na_2GdOPO_4 structure.

Table 3.3. IR band locations for a) Na_2LaOPO_4, Na_2NdOPO_4, Na_2SmOPO_4, and b) Na_2GdOPO_4, Na_2DyOPO_4, Na_2HoOPO_4, Na_2ErOPO_4, Na_2YbOPO_4 (cm^{-1}).

a)

Asssignments	**Na_2LaOPO_4**	**Na_2NdOPO_4**	**Na_2SmOPO_4**
$\nu_3(PO_4)$			1136
	1084	1090	1092
	1053	1044	
	976		978
		957	957
	950	941	945
$\nu_1(PO_4)$	921	924	926
	913	913	
$\nu_4(PO_4)$	599	605	
	574		574
	560	564	564
	547	546	545
		526	523
	472	472	468
$\nu_2(PO_4)$	409	403	408

b)

Asssignments	**Na_2GdOPO_4**	**Na_2DyOPO_4**	**Na_2HoOPO_4**	**Na_2ErOPO_4**	**Na_2YbOPO_4**
$\nu_3(PO_4)$					
	1099	1098	1095		
	1030	1044		1036	
	982	982	982	978	
	963	971		957	
		953	954		
$\nu_1(PO_4)$				926	
$\nu_4(PO_4)$	602	599		598	
	577	579	579	576	576
	561	565	559	559	
	548	541		551	551
	526	520	523	523	523
	471	477	472	472	468
$\nu_2(PO_4)$	405	409	406	408	408

Table 3.4. The Raman data of a) Na_2LaOPO_4, Na_2NdOPO_4, Na_2SmOPO_4, and b) Na_2GdOPO_4, Na_2DyOPO_4, Na_2HoOPO_4, Na_2ErOPO_4, Na_2YbOPO_4 (cm^{-1}).

a)

Assignment	**Na_2LaOPO_4**	**Na_2NdOPO_4**	**Na_2SmOPO_4**
ν_3 (PO_4)			1153
		1023	
	977		
	964	955	958
		944	
ν_1 (PO_4)		932	
ν_4 (PO_4)	625		
	574		585
	574		
	468	464	

b)

Assignment	**Na_2GdOPO_4**	**Na_2DyOPO_4**	**Na_2HoOPO_4**	**Na_2ErOPO_4**	**Na_2YbOPO_4**
ν_3 (PO_4)		1135			
				1108	
		1031		1030	
		977			
	965	958			
		944	932	949	
ν_1 (PO_4)		927			
ν_4 (PO_4)			609	608	
				561	569
				525	
	464			472	

3.1.3. Results of Scanning Electron Microscopy Investigations

The particle size and the morphology of both set of specimens were investigated by using SEM as given in Figure 3.3. These SEM observations showed that some uniformity exists between the specimens of both sets in their shape and particle size. Among these products, particle size can be given as in between 1-10 μm.

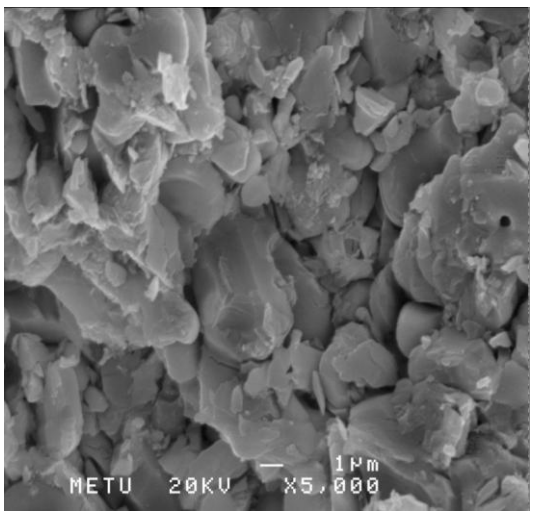

a) Na_2LaOPO_4

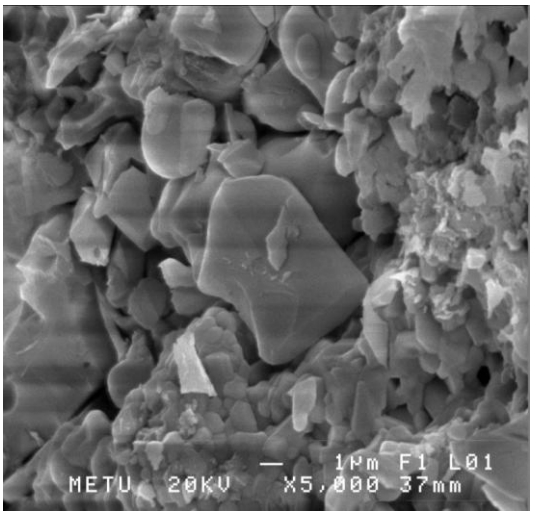

b) Na_2NdOPO_4

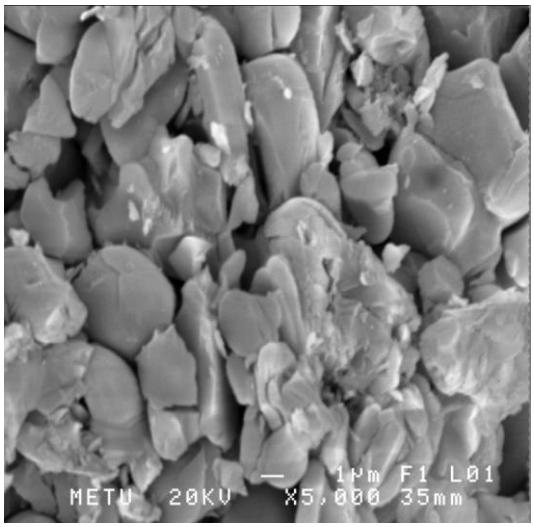

c) Na_2SmOPO_4

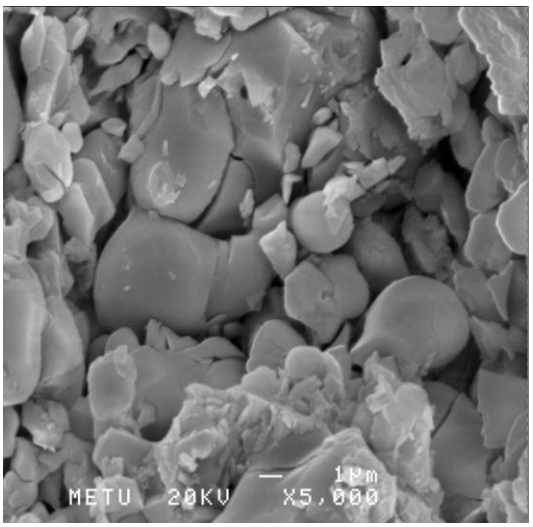

d) Na_2GdOPO_4

Figure 3.3. SEM images of Na_2LaOPO_4, Na_2NdOPO_4, Na_2SmOPO_4, Na_2GdOPO_4, Na_2DyOPO_4, Na_2HoOPO_4, Na_2YbOPO_4.

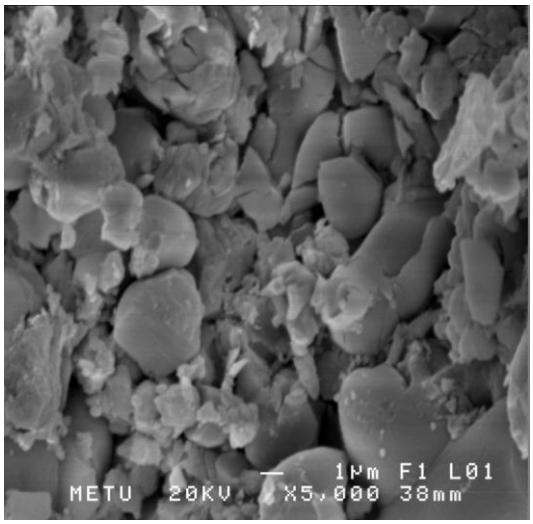

e) Na_2DyOPO_4

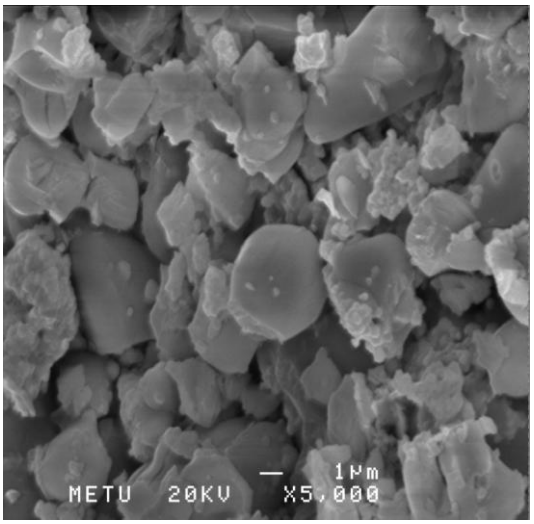

f) Na_2HoOPO_4

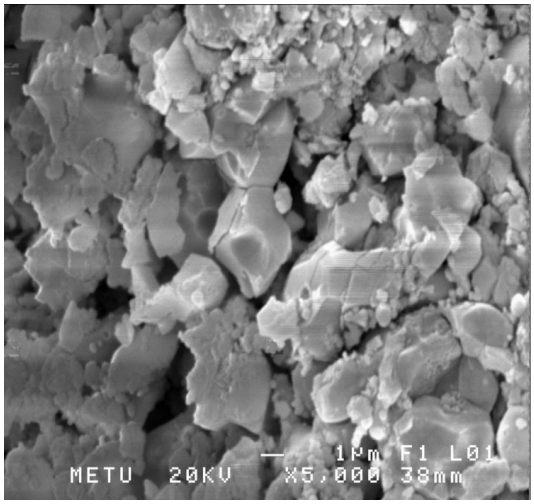

g) Na_2YbOPO_4

Figure 3.3. (continued).

3.2. SYNTHESIS OF $Sr_2P_2O_7$-ZrP_2O_7 SOLID SOLUTION AND SYNTHESIS OF CuO AND RARE EARTH OXIDES ADDED TO $Sr_2P_2O_7$

3.2.1. SYNTHESIS OF $Sr_2P_2O_7$-ZrP_2O_7 SOLID SOLUTION

ZrP_2O_7, zirconium pyrophosphate, was synthesized at 900 ^oC by solid state reaction of ZrO_2 and $NH_4H_2PO_4$ and X-ray diffraction studies indicated that the product was composed of a single phase. The XRD data can be easily indexed into the cubic system with a=8.248(6) Å shown in Table B.9. and the space group is Pa-3. This data is very close to the ICDD Card No: 24-1491 where a=8.245 Å. Khosrovani et al. (1996) solved the structure of cubic ZrP_2O_7 at room temperature and refined by using a combination of modeling and high-resolution neutron powder diffraction data. The cell edge is given as 24.74 Å and the space group is Pa-3. They proposed that the superstructure present at room temperature disappears at about 290 ^oC. Withers et al. (2001) mentioned that the unmodulated parent structure of zirconium pyrophosphate made up of corner-connected ZrO_6 octahedra and PO_4 tetrahedra. They (Withers et al. 2001) also explained that above 294 ^oC, the parent cell parameter is multiplied by 3 to enable direct comparison with the low-temperature superstructure phase. Therefore, our unit cell and space group data are in agreement with these studies (Khosrovani et al. 1996 and Withers et al. 2001).

3.2.1.1. Results of X-ray Diffraction Investigations

XRD patterns of pure and (10, 5, 1, 0.5, 0.1, 0.05, 0.03) % $Sr_2P_2O_7$ added ZrP_2O_7 are given in Figure 3.4. The unit cell parameters of the set 1 has very little change in between 8.248(6)-8.233(8) Å. According to these results it can be concluded that, in this solid solution, orthorhombic addition didn't alter the cubic structure so much. The cell edge length decreased to 8.233(8) from 8.248(6) Å.

The pure $Sr_2P_2O_7$ was synthesized at the same experimental conditions and indexed with respect to ICDD Card No: 24-1011. This X-ray data, which are given in Table B.10., were indexed in the orthorhombic system, and the refined lattice constants were found to be a=8.900(2), b=13.151(2), and c=5.402(2) Å by using CELREF refinement program (Altermatt et al. 1987).

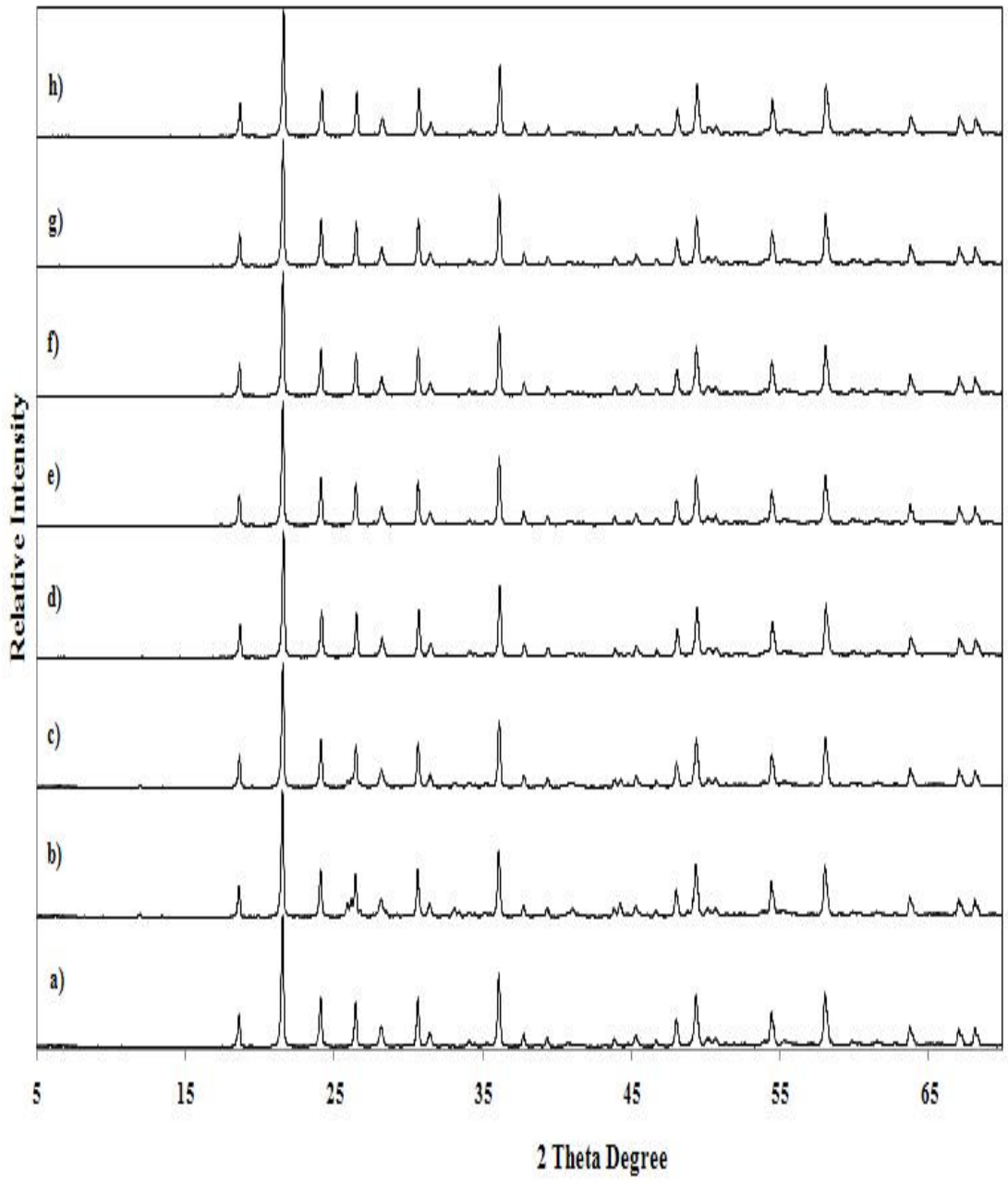

Figure 3.4. X-ray Diffraction Patterns of a) Pure and b)10, c)5, d)1, e)0.5, f)0.1, g)0.05, h)0.03 % $Sr_2P_2O_7$ added ZrP_2O_7.

In Figure 3.5., XRD patterns of pure and (10, 5, 1, 0.5, 0.25, 0.1, 0.05) % ZrP_2O_7 added $Sr_2P_2O_7$ were given. Same trends were observed for three unit cells. They slightly change in between a=8.909(5)-8.877(5), b=13.163(3)-13.12(1), and c=5.403(2)-5.386(4) Å. Since small fluctuations were observed, it can be concluded that cubic ZrP_2O_7 couldn't enter and destroy the orthorhombic $Sr_2P_2O_7$ structure.

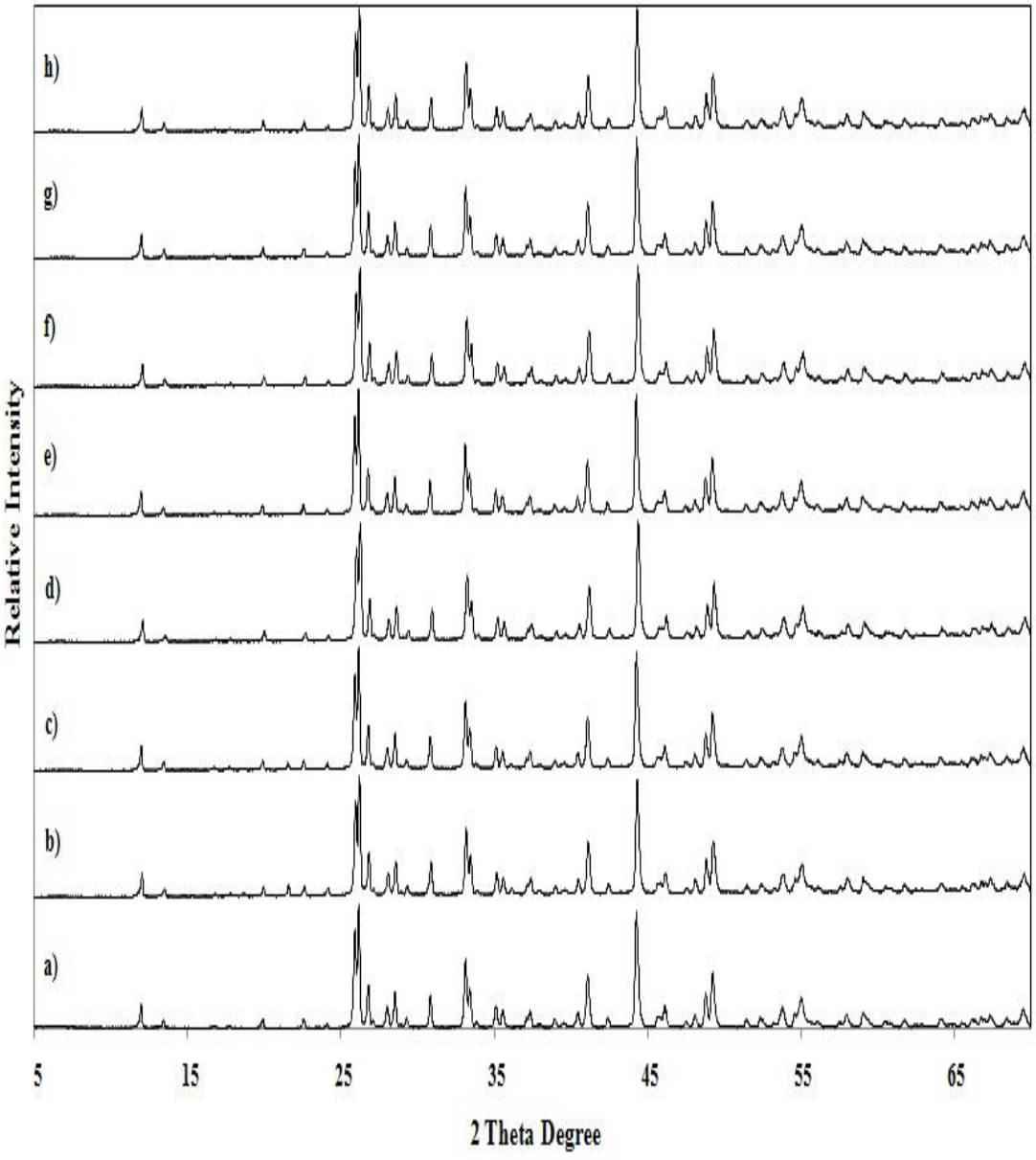

Figure 3.5. X-ray Diffraction Patterns of a)Pure and b)10, c)5, d)1, e)0.5, f)0.25, g)0.1, h)0.05 % ZrP_2O_7 added $Sr_2P_2O_7$.

3.2.1.2. Results of the Infrared and Raman Investigations

In addition to XRD studies, we measured infrared and Raman spectra of the synthesized products in order to confirm the functional groups in all products. The band positions of the Infrared and Raman spectra of the set 1 is given in Table 3.5 and 3.6, respectively and Table 3.7. and Table 3.8. is the band positions of the infrared and Raman spectra for set 2 obtained in this research. Examination of these tables shows that there are some coincidences in the infrared and Raman spectra.

The assignment of the $P_2O_7^{4-}$ modes is carried out in terms of PO_3 and P-O-P vibration [Pillai et al. (1999), Baran et al. (2004)]. The symmetric and antisymmetric stretching frequencies of PO_3 in $P_2O_7^{4-}$ are observed in the region 1157-1002 cm^{-1}. For POP, symmetric modes were observed in the region 779-736 cm^{-1}. Guler et al. (2005) and coworkers observed the bands due to δOPO, δPO_3, δPOP deformations in the region 595-464 cm^{-1}. In our studies, we observed these bands in the between 609-455 cm^{-1}. Khay et al. (2001a, 2001b) mentioned that the deformation bands are between 630 and 373 cm^{-1} and our peaks around these frequencies are consistent with the literature values. They also reported that all bands located below are external vibrational modes. So, the bands below 334 cm^{-1} are external vibrational modes.

Khorosvani et al. (1996) observed unusual P-O-P bond angle in ZrP_2O_7. In their work, the 3x3x3 superstructure present at room temperature disappears at about 290 ^oC, and all P-O-P angles of P_2O_7 are then constrained by symmetry to be 180 ^oC on average. In the same reference, they also mentioned that the angle for P-O-P linkages is normally in the range 130-160^o and the P-O-P bond angle of 180^o is unfavorable, and one expects that a structure containing such a linkage could only be stabilized at high temperature. We expected to have nonlinear POP bond for synthesized strontium pyrophosphate because they are cooled to room temperature after synthesis. Baran et al. (2004) indicated that for a linear bridge the symmetric mode should be only Raman active and the antisymmetric mode only IR active. The

appearance of both vibrations in both spectra is in an agreement with the presence of an angular bridge. We observed this situation in both the IR and Raman spectra.

The infrared and Raman bands observed are in agreement with the reported values for diphosphate compounds of tetravalent, mixed valent cations [Kızılyallı et al. (1993), Khay et al. (2001a, 2001a), Idrissi et al. (2004)] although their crystal systems are different.

Table 3.5. The IR Band Positions (cm^{-1}) for a) Pure and b) 10, c) 5, d) 1, e) 0.5, f) 0.1, g)0.05, h) 0.03 % $Sr_2P_2O_7$ added ZrP_2O_7.

a	**b**	**c**	**d**	**e**	**f**	**g**	**h**
1133	1133	1133	1132	1126	1132	1132	1132
	1115		1115	1112	1115	1115	1113
980	979	980	979	978	979	979	978
745	746	746	746	746	746	746	745
643							
600			592	595			
548	548	548	548	548	548	548	548
		501			508	508	
507	500		502				
493							
483	487						
467		446	446	447	447	447	445
442		434	437	434	438	438	440
	433	409	406	409	409	409	409
415	410						

Table 3.6. The Raman Band Positions (cm^{-1}) for a) Pure and b) 10, c) 5, d) 1, e) 0.5, f) 0.1, g) 0.05, h) 0.03 % $Sr_2P_2O_7$ added ZrP_2O_7.

a	b	c	d	e	f	g	h
1158	1158	1157	1157	1157	1158	1158	1157
1088	1090	1086	1089	1089	1089	1089	1087
735	737	741	736	737	737	742	737
639	638	638	638	640	638	638	637
616	616	614	617	617	617	615	615
557	556	555	556	555	560	556	558
536	537	538	537	537	538	537	535
502	501	503	505	504	503	503	500
476	476	476	476	476	476	477	475
380	381	380	382	383	382	382	379
333	334	333	333	333	333	333	332
246	249	248	248	248	247	247	245
189	189	189	191	190	190	190	188
177	178	177	178	179	179	179	176

Table 3.7. The IR Band Positions (cm^{-1}) for a) Pure and b) 10, c) 5, d) 1, e) 0.5, f) 0.25, g) 0.1, h) 0.05 % ZrP_2O_7 added $Sr_2P_2O_7$.

a	**b**	**c**	**d**	**e**	**f**	**g**	**h**
1187	1188	1187	1188	1188	1189	1188	1190
	1155	1155		1156	1157	1156	1157
1143	1142	1143	1141				
1107	1112	1114	1111	1112		1111	1115
1065	1064	1064	1064	1064	1063	1064	1064
1046	1046	1046	1046	1046	1046	1046	1046
1011	1011	1011	1011	1011	1011	1011	1011
972	970	972	968	969	970	970	970
779							
747	747	747	747	747	747	747	747
683		679					
669	669	669	669	669	669	669	669
649	652	652	651	651	651	651	651
619	619	618	619	618	617	619	619
561	560	561	560	560	560	560	560
543	543	543	542	542	543	542	542
500	501	501	501	500	501	500	500
486	485	486	485	485	484	485	485
469							
456	458	457	456	457	455	458	457
447		441					
432	433		431	431	434	433	433
417	419	419	420	420	420	420	419

Table 3.8. The Raman Band Positions (cm^{-1}) for a) Pure and b) 10, c) 5, d) 1, e) 0.5, f) 0.25, g)0.1, h) 0.05 % ZrP_2O_7 added $Sr_2P_2O_7$.

a	b	c	d	e	f	g	h
1192	1190	1192	1194	1193	1190	1194	1193
1147	1146	1146	1149	1149		1149	1149
1121	1120	1120	1123	1124	1122	1123	1123
1095	1092	1093	1096	1097		1096	1097
1060	1060	1060	1063	1063	1060	1063	1062
1003	1002	1002	1004	1004	1003	1004	1004
963	961	962	965	966	963	966	966
762	761	761	765	765	762	764	765
619	617	618	622	622	619	621	621
607	606	606		609	607	609	609
566	564	565	568	568	565	568	568
551	551	552	555	555	551	555	555
526	526	524	529	528	524	529	528
491	490	490	494	494	491	494	494
442	443	443	446	448	441	446	445
352	351	351	355	355	351	354	355
326	327	324	328	329	325	328	328
222	226	225	224	226	222	228	230
198	202	196	204	201	194	205	200
163	163	163	166	166	163	166	166
124	123	125	126	129		127	126

3.2.1.3. Results of Scanning Electron Microscopy Investigations

The morphology of the products were investigated by taking SEM images. The SEM micrographs of pure ZrP_2O_7 and $Sr_2P_2O_7$ were given in Figure. D.1. In both figures, SEM images demonstrate the small particle size of these phosphates. In $Sr_2P_2O_7$ added ZrP_2O_7 samples, particles, before and after addition of $Sr_2P_2O_7$ to ZrP_2O_7, are around 1μm. Yet, SEM observations of ZrP_2O_7 added $Sr_2P_2O_7$ samples showed that one of the remarkable features of these products is that their sizes are larger than other set. In Figure D.2., EDX analysis of ZrP_2O_7, 10% $Sr_2P_2O_7$ added ZrP_2O_7, $Sr_2P_2O_7$, and 10% ZrP_2O_7 added $Sr_2P_2O_7$ are given. Sr addition was observed in all samples while the same trend was also investigated Zr added samples.

3.2.1.4. Results of Thermoluminescence Studies

The TL characteristics of pure and added strontium pyrophosphate have not been investigated in detail up to now. Natarajan et al. (2004) and his colleagues have recorded the TL glow curve of Eu-doped strontium pyrophosphate and they were reported two glow peaks at 465 and 565 K in the case of samples irradiated by ^{60}Co gamma rays up to 100 and 200 Gy. On the other hand, undoped $Sr_2P_2O_7$ sample did not show any TL (thermoluminescence) peak.

In the present study, all samples were firstly irradiated for 5 mins (≈4.5 Gy) at room temperature in the dark room by beta rays and then their glow curves were recorded. As seen in Figure 3.6., there is no change in the glow curve structure of all samples pure and 10, 5, 1, 0.5, 0.25, 0.1, 0.05 % ZrP_2O_7 added $Sr_2P_2O_7$ samples and their glow curves exhibit one strong glow peak at around 100 ^oC with low intensity glow peaks at about 200 and 350 ^oC. It is seen that the intensity of prominent glow peak at 100 ^oC is continuously increased with decreasing concentration of ZrP_2O_7 and the maximum TL intensity was observed for the sample whose composition is $Sr_2P_2O_7$: 0.05% ZrP_2O_7. Main peak temperature of all samples changes insignificantly by changing the concentration of ZrP_2O_7.

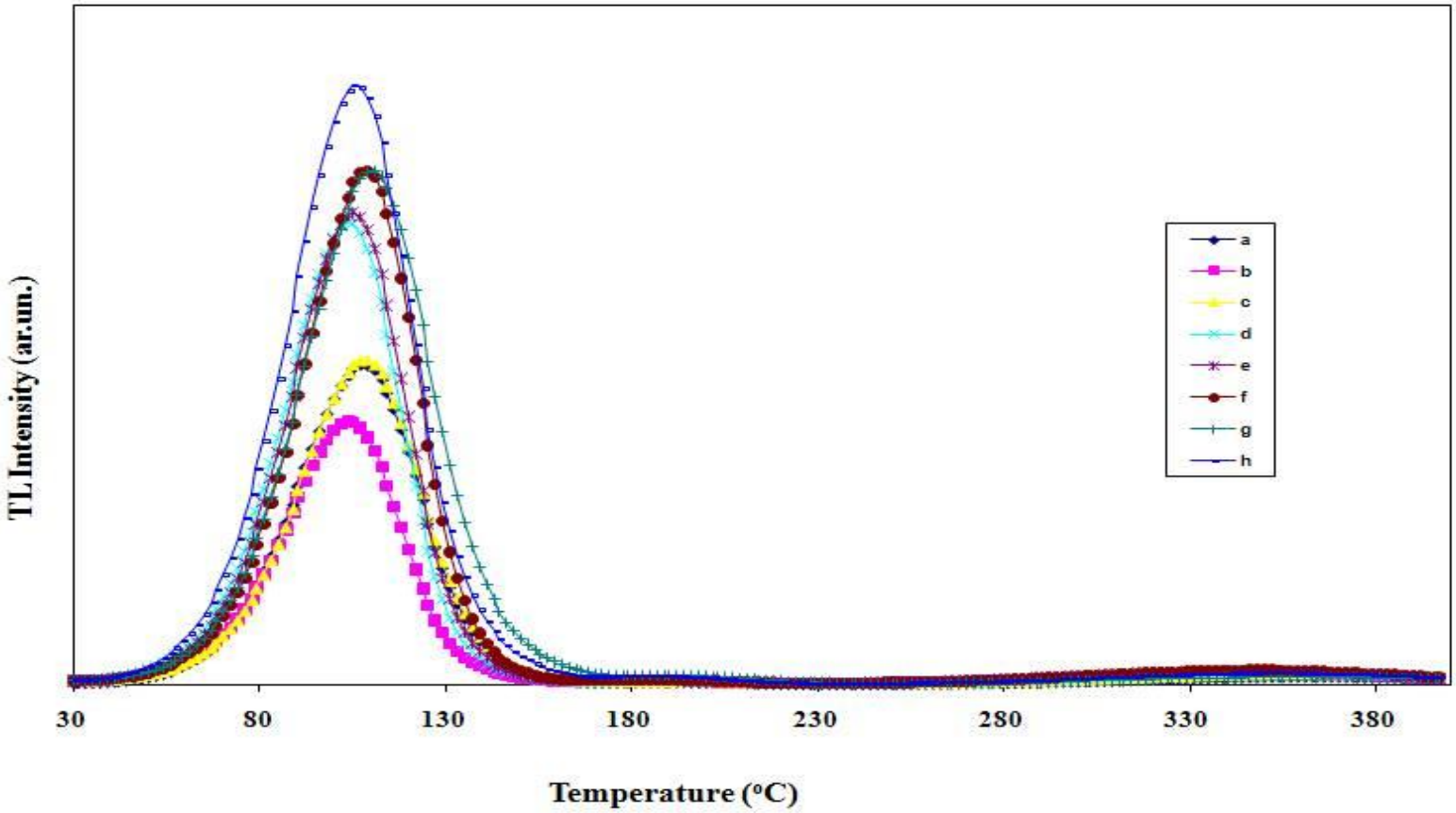

Figure 3.6. Thermoluminescence Glow Curves of a) Pure and b) 10, c) 5, d) 1, e) 0.5, f) 0.25, g) 0.1, h) 0.05) % ZrP_2O_7 added $Sr_2P_2O_7$.

3.2.2. Synthesis of CuO and Rare Earth Added $Sr_2P_2O_7$

The structural analysis of pure strontium pyrophosphate was done in our previous work Seyyidoglu et al. (2007) and it was confirmed that the compound formed was α-$Sr_2P_2O_7$ in orthorhombic structure. In order to obtain good thermoluminsecent phosphors, copper oxide and some rare earth oxides were added into $Sr_2P_2O_7$ host in this study. This work is a continuation of our systematic investigations of pyrophosphates with rare-earth elements. We report the results of these experiments on the synthesis and thermoluminescence properties of the compound, and the determination of their structure.

3.2.2.1. Results of X-ray Diffraction Investigations

Figure 3.7 - 3.12 shows that X-ray diffractions patterns of Pr_6O_{11}, Nd_2O_3 and Ho_2O_3 added with different amounts (0.5, 1, 2, 3, 4, 5, 10, 15%) into $Sr_2P_2O_7$. X-ray diffraction analysis demonstrated that the added rare earth metal oxides did not change patterns which were similar to orthorhombic $Sr_2P_2O_7$ means the structural stabilities of the compounds. As it can be seen from the Figure 3.7. (a), 15% and 10% Pr_6O_{11} addition had small effects on the XRD patterns by lowering the intensities of two most intense peaks while remaining the peaks positions unchanged. As shown in the Figure 3.7. and 3.8., the 5% to 0.5% Pr_6O_{11} added X-ray patterns were very similar to that of orthorhombic $Sr_2P_2O_7$. The X-ray pattern of Nd_2O_3 and Ho_2O_3 added polycrystalline powders showed a great similarity to the X-ray patterns of pure $Sr_2P_2O_7$. Similar XRD patterns were obtained for Nd_2O_3 and Ho_2O_3 addition shown in the Figure 3.9.-3.12.. It can be concluded that X-ray diffraction pattern for the added products in fair agreement with the pattern, indicating the phase purity of the as-synthesized samples of the title compound $Sr_2P_2O_7$.

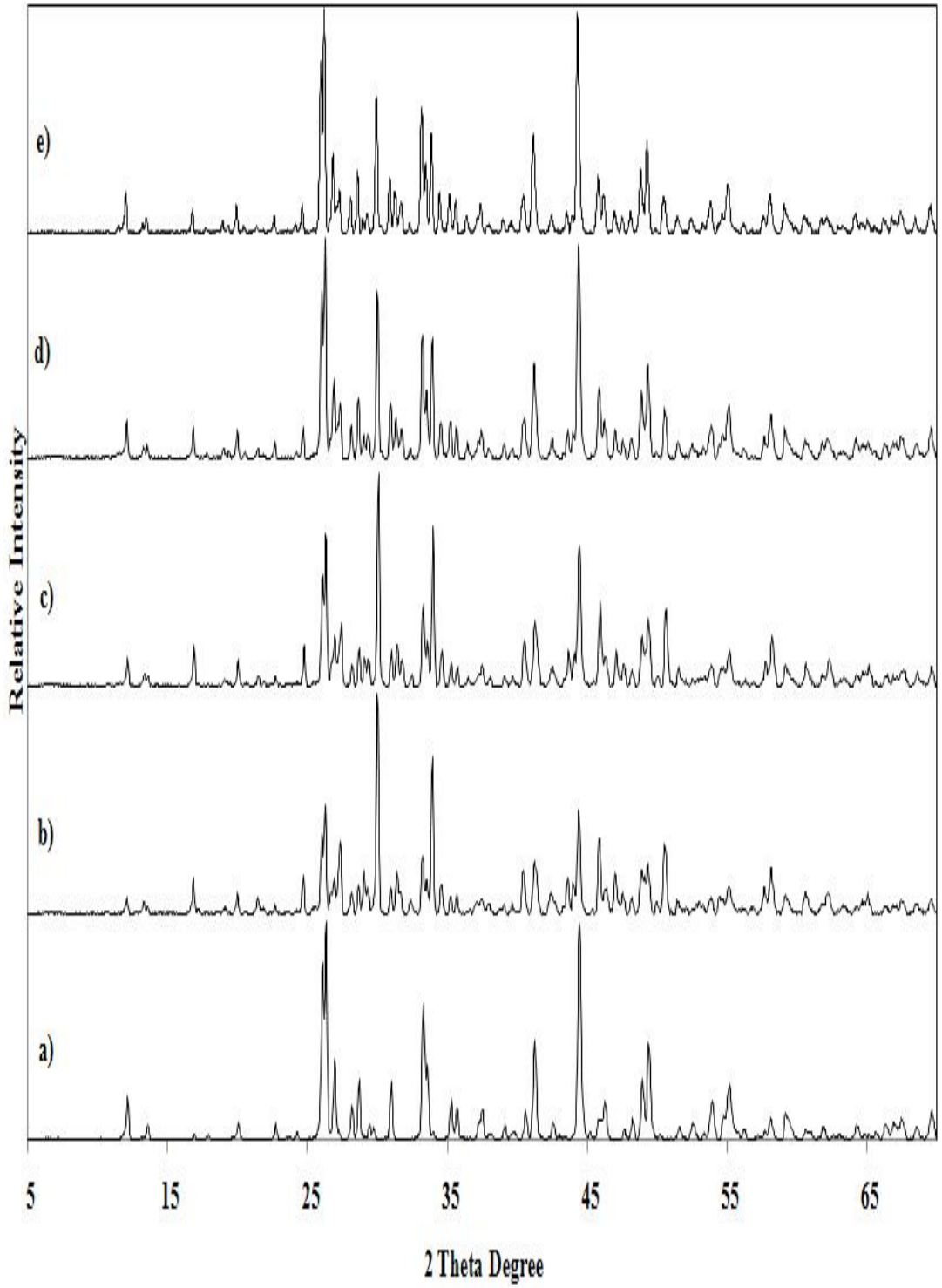

Figure 3.7. X-ray Diffraction Patterns of a) Pure, and 5% CuO and b) 15, c) 10, d) 5, e) 4 % Pr_6O_{11} added $Sr_2P_2O_7$.

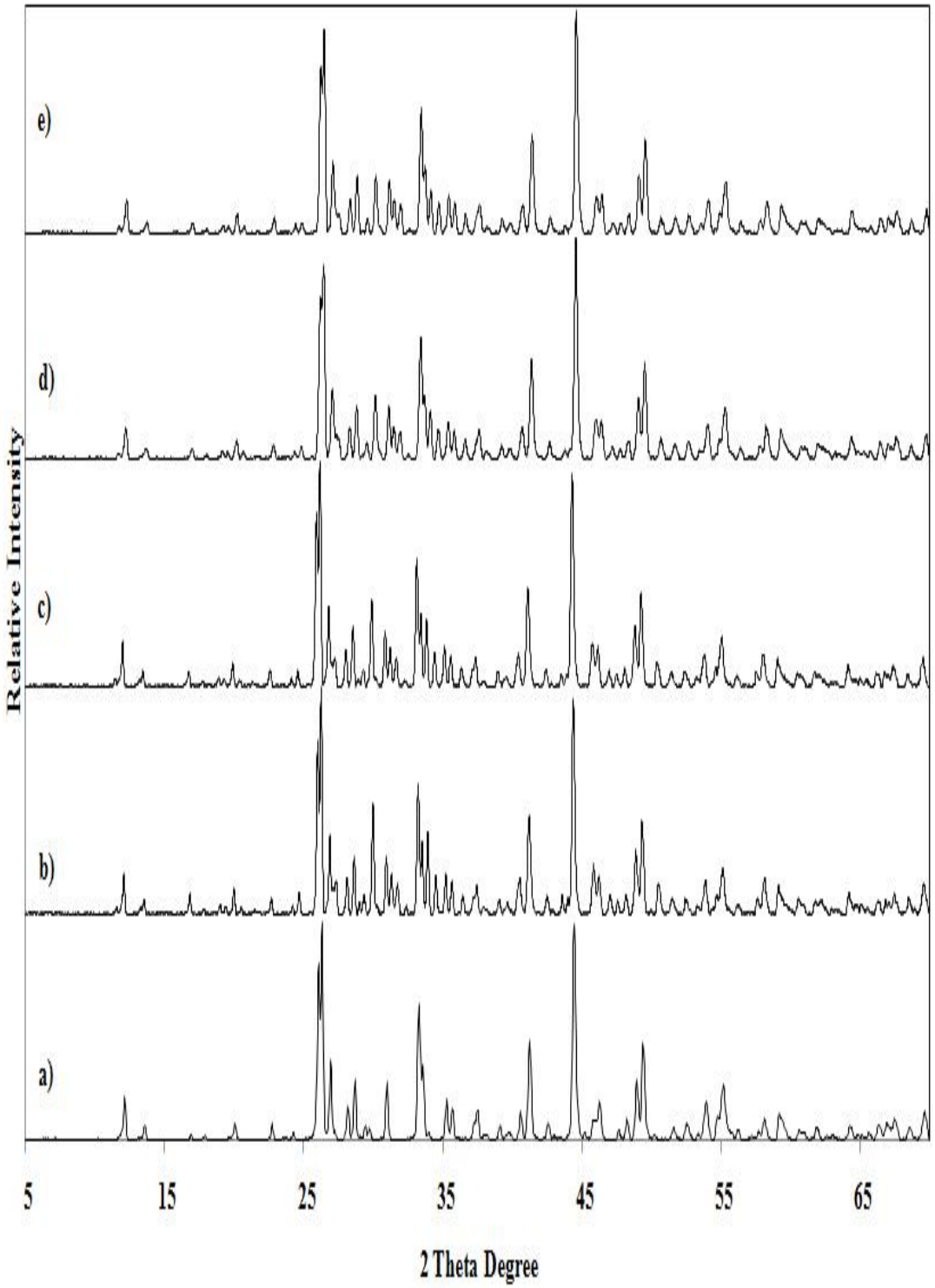

Figure 3.8. X-ray Diffraction Patterns of a) Pure, and 5% CuO and b) 3, c) 2, d) 1, e) 0.5 % Pr_6O_{11} Added $Sr_2P_2O_7$.

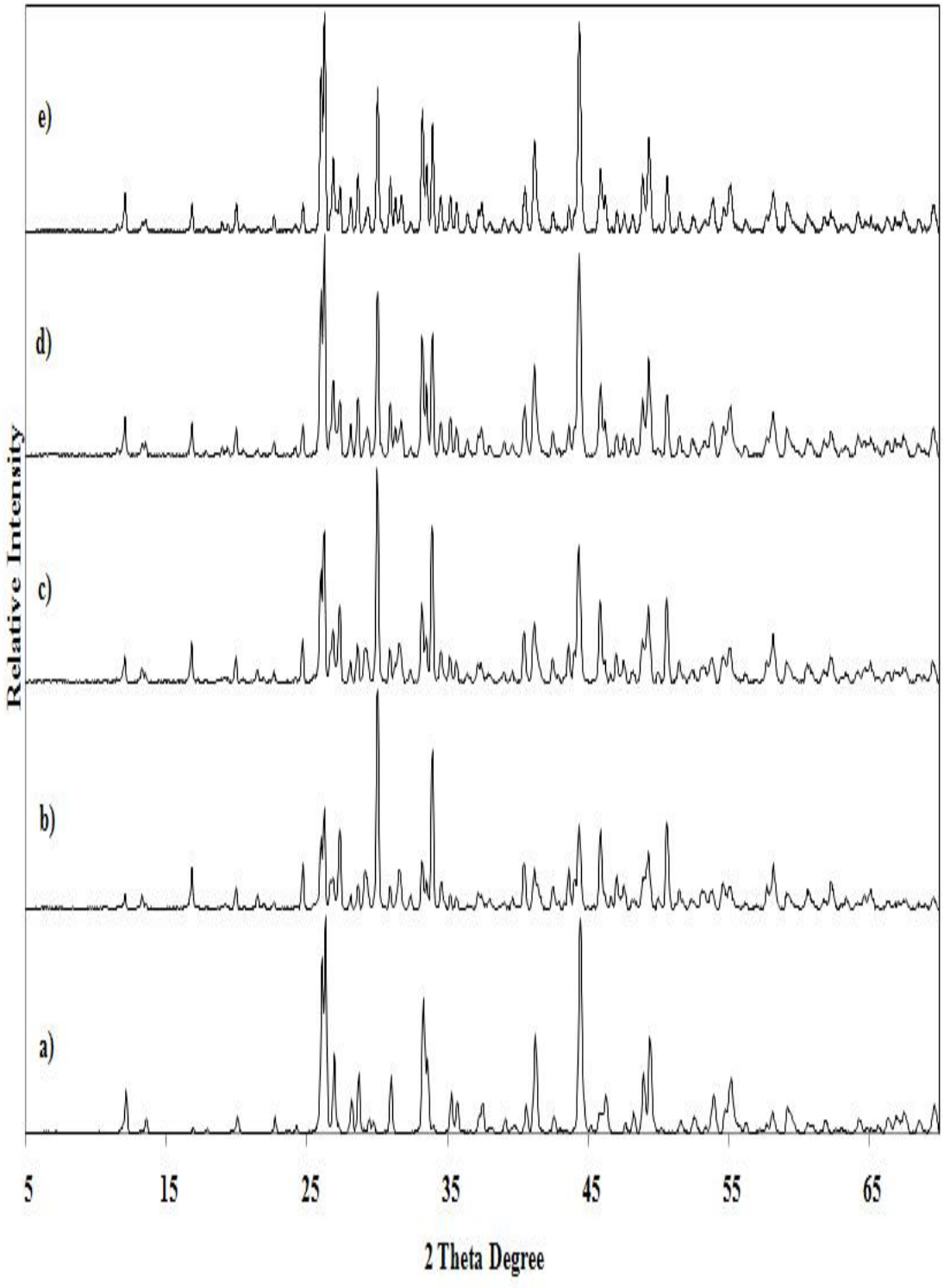

Figure 3.9. X-ray Diffraction Patterns of a) Pure, and 5% CuO and b) 15, c) 10, d) 5, e) 4 % Nd_2O_3 Added $Sr_2P_2O_7$.

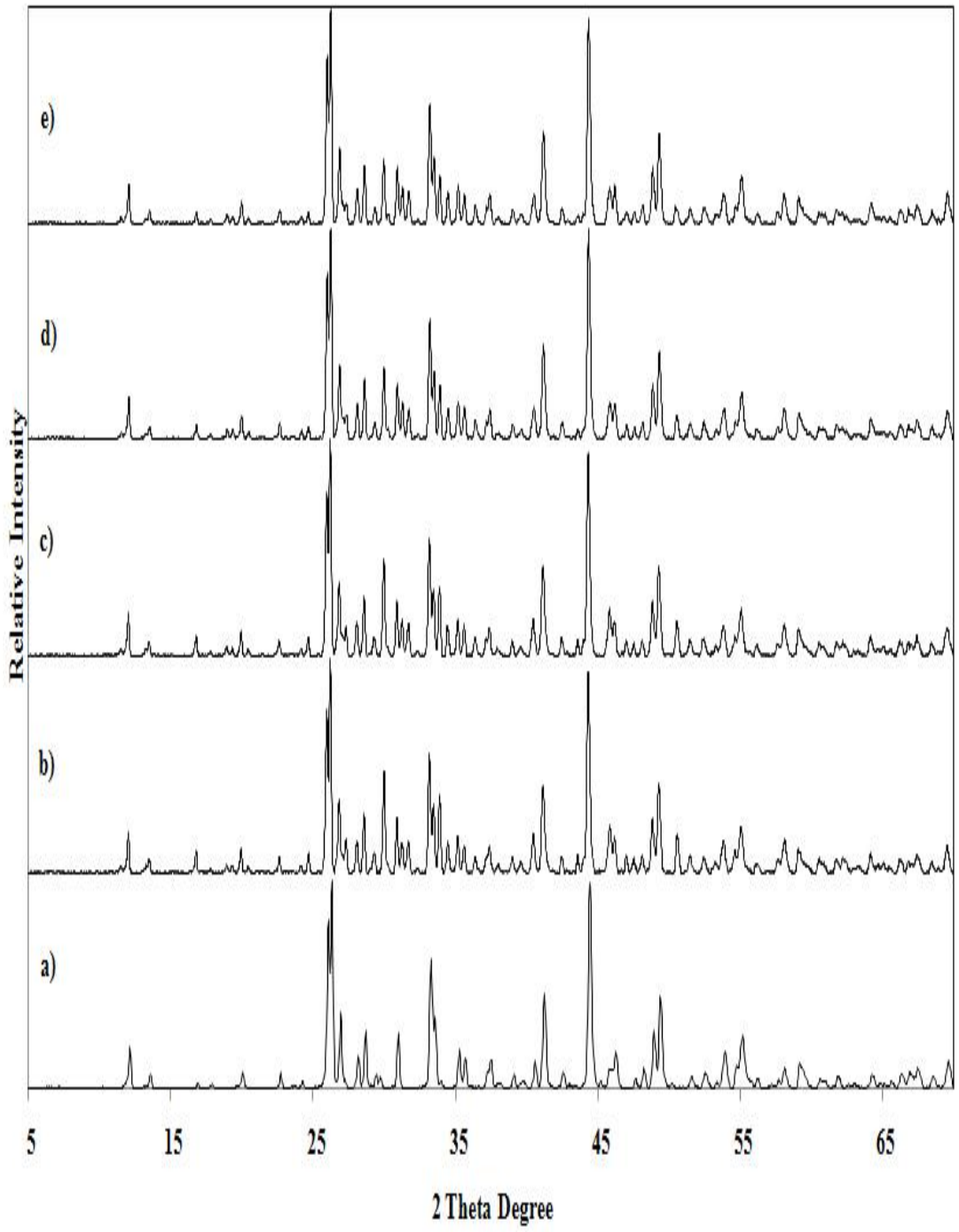

,Figure 3.10. X-ray Diffraction Patterns of a) Pure, and 5% CuO and b) 3, c) 2, d) 1, e) 0.5 % Nd_2O_3 Added $Sr_2P_2O_7$.

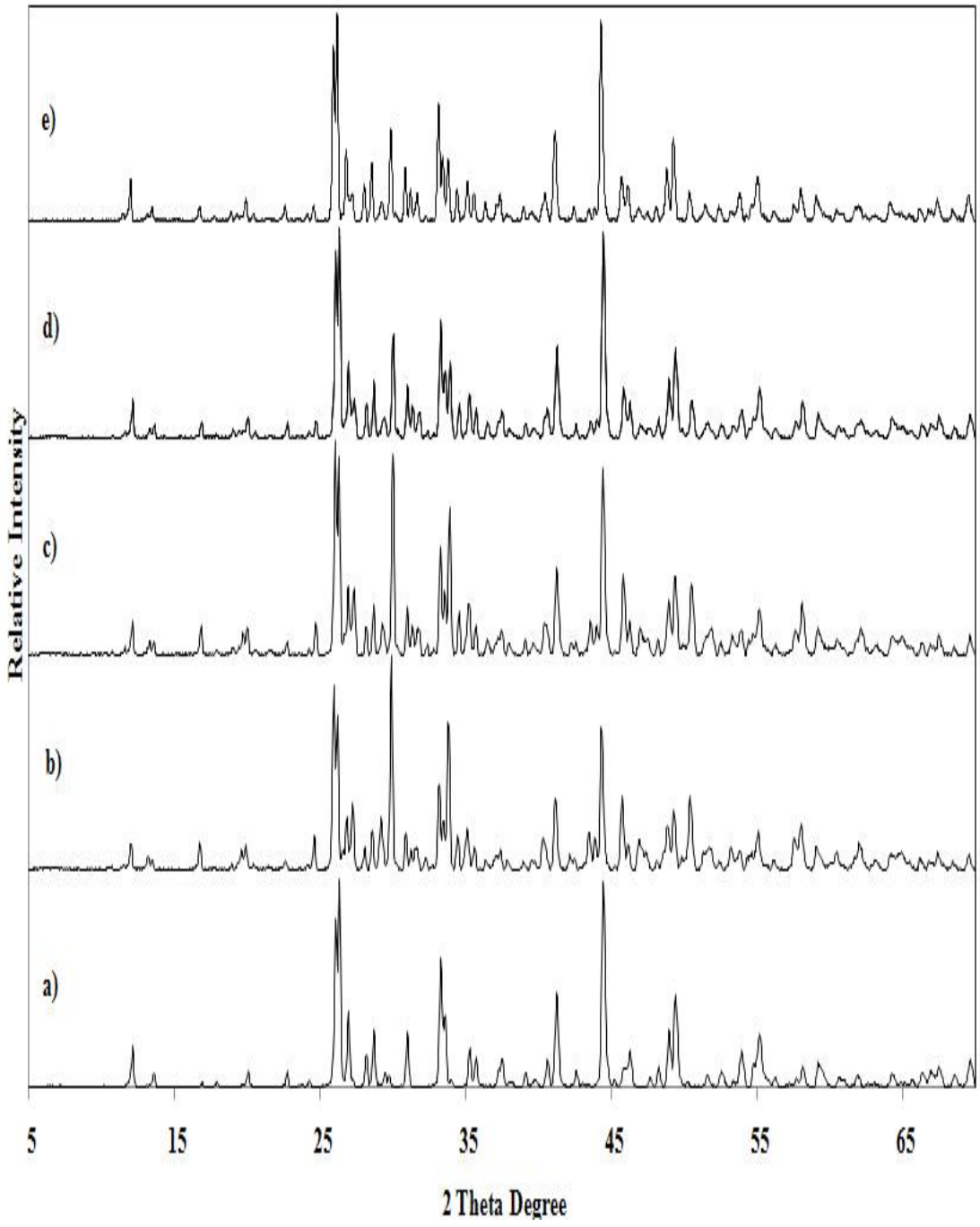

Figure 3.11. X-ray Diffraction Patterns of a) Pure, and 5% CuO and b) 15, c) 10, d) 5, e) 4 % Ho_2O_3 Added $Sr_2P_2O_7$.

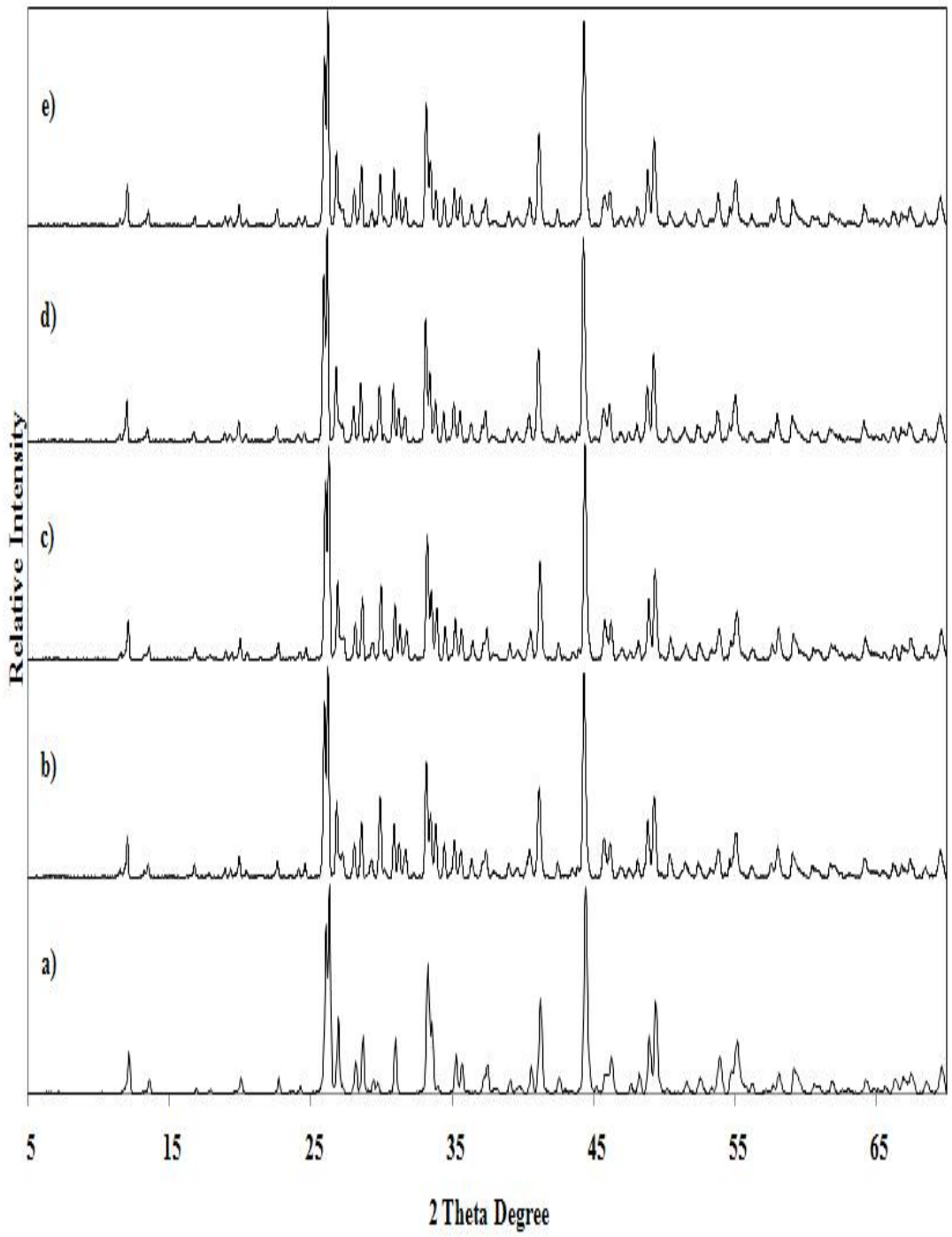

Figure 3.12. X-ray Diffraction Patterns of a) Pure and 5% CuO b) 3, c) 2, d) 1, e) 0.5 % Ho_2O_3 Added $Sr_2P_2O_7$.

3.2.2.2. Results of Thermoluminescence Studies

The TL characteristics of pure and rare earth oxides (Y_2O_3, La_2O_3, CeO_2, Pr_6O_{11}, Nd_2O_3, Sm_2O_3, Eu_2O_3, Gd_2O_3, Tb_2O_3, Dy_2O_3, Ho_2O_3, Er_2O_3, Tm_2O_3, Yb_2O_3, Lu_2O_3) and CuO added strontium pyrophosphate have not been investigated until now (Seyyidoglu et al. 2007). It is well known that copper and rare earths are highly efficient elements to increase the TL intensity in many crystals. The attractive feature of lanthanides is their highly efficient narrow band f-f photoluminescence coming from trivalent lanthanide ions almost regardless of their environment: the luminescence was obtained in inorganic glass, sol-gel materials, polymers and in liquid crystals (Palewska et al. (2007). The luminescence of lanthanide complexes originates from transitions between f-levels of central ions that are effectively shielded from the influence of external forces by filled 5s and 5p-shells (Palewska et al. (2007). Therefore, CuO and some rare earth oxides added into host $Sr_2P_2O_7$ in order to obtain high TL intensity in this study. Figure 3.13 (a-f). shows some of the selected TL glow curves for samples prepared after different amounts of rare earth oxides addition. Based on the results presented in Figure 3.13 (a-f), it can be summarized that all $Sr_2P_2O_7$ products after addition have a TL peak around 90 ^oC as pure samples and another peaks above 150 ^oC in all samples at different temperatures and TL intensities (i.e, a glow peak at around 180 ^oC for Pr_6O_{11}, 275 ^oC for Nd_2O_3, 285 ^oC for Ho_2O_3, 225 ^oC for Er_2O_3, and two glow peaks at around 185 and 305 ^oC for Tm_2O_3 and Dy_2O_3 added samples). These results show us that rare earths along CuO addition into $Sr_2P_2O_7$ increased the intensity of TL glow peaks above 150 ^oC of $Sr_2P_2O_7$. In particular, Pr_6O_{11}, Nd_2O_3, Ho_2O_3 and Er_2O_3 added samples gave us the best TL results among them. Therefore, this study showed that these materials can be a promising thermoluminescent material for dosimetric applications since they have TL peaks over 100 ^oC and the intensity of the peaks is relatively higher.

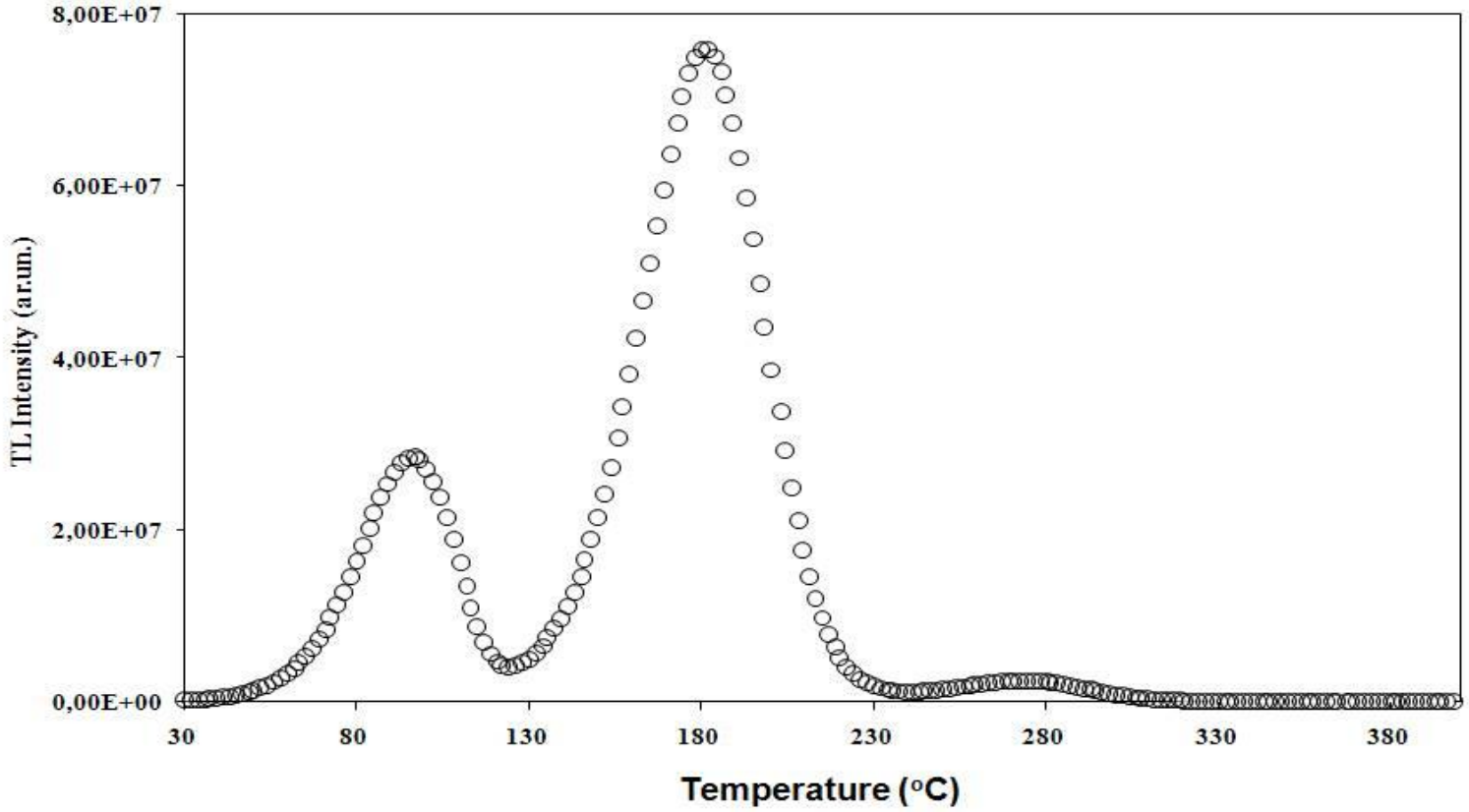

a)

Figure 3.13. The thermoluminescence Glow Curves of 5% CuO and a) 5% Pr_6O_{11}, b) 2 % Nd_2O_3, c) 5% Ho_2O_3, d) 15% Er_2O_3, e) 5% Tm_2O_3, f-) 5% Dy_2O_3 Added $Sr_2P_2O_7$.

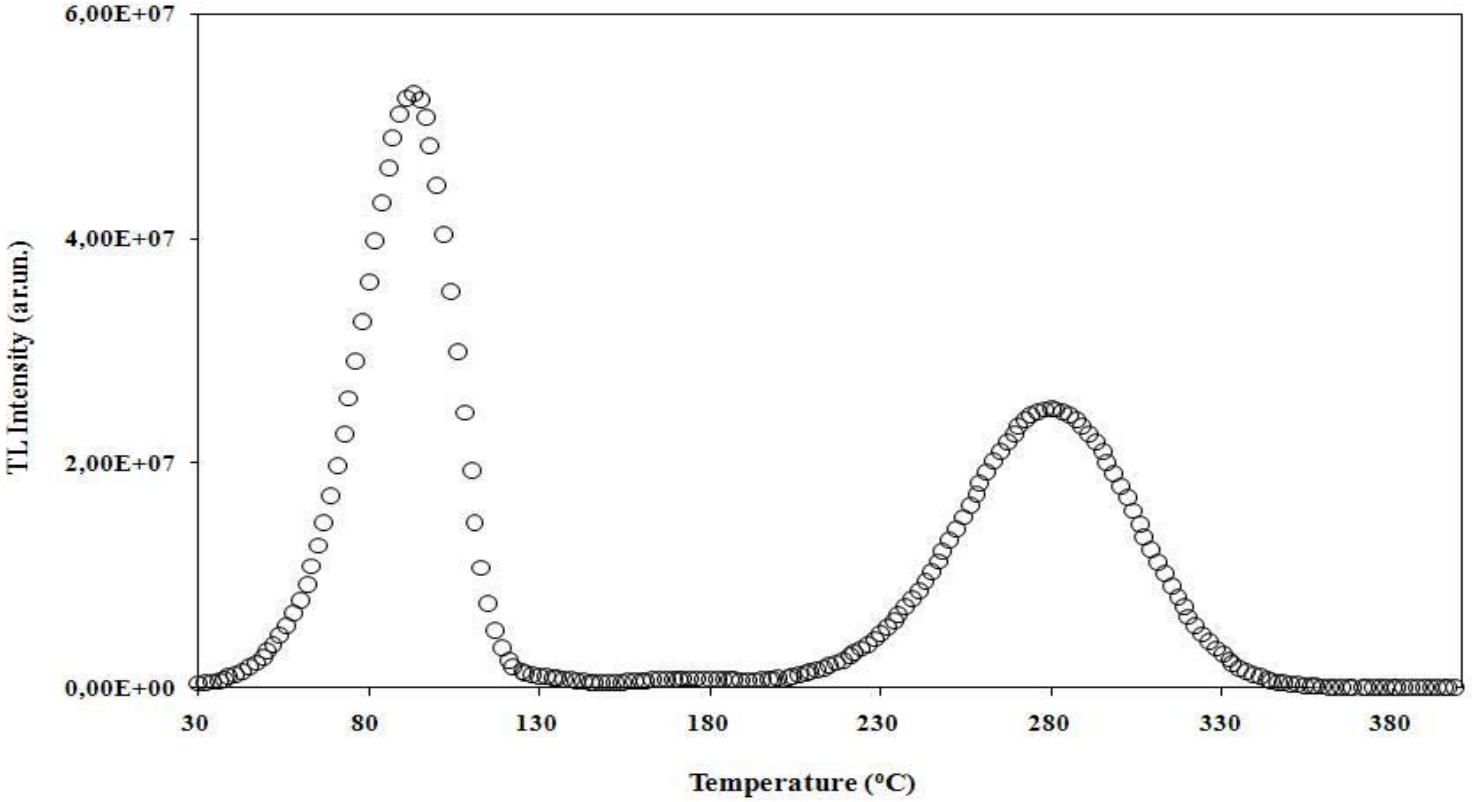

b)

Figure 3.13. Continued.

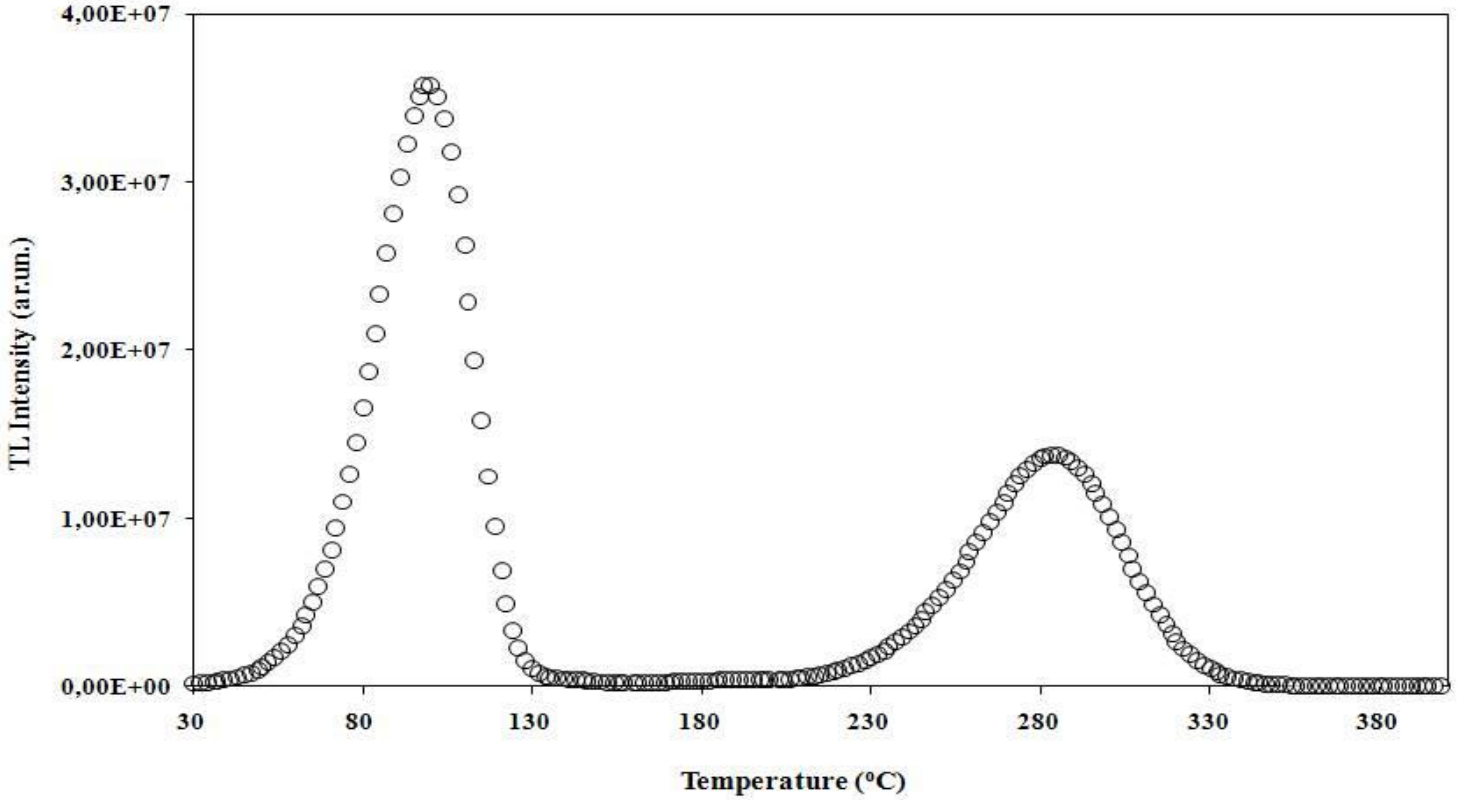

c)

Figure 3.13. Continued.

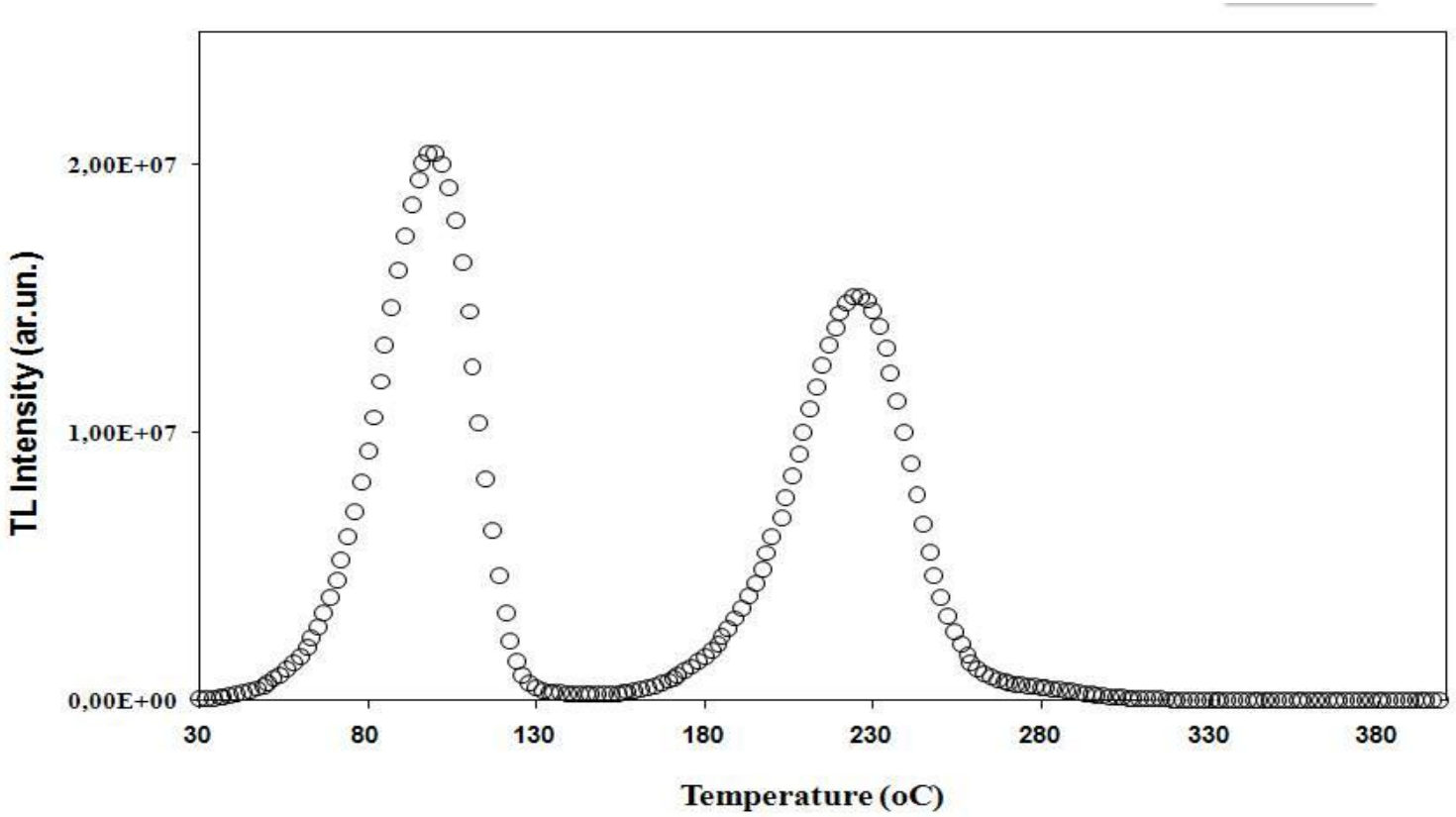

d)

Figure 3.13. Continued.

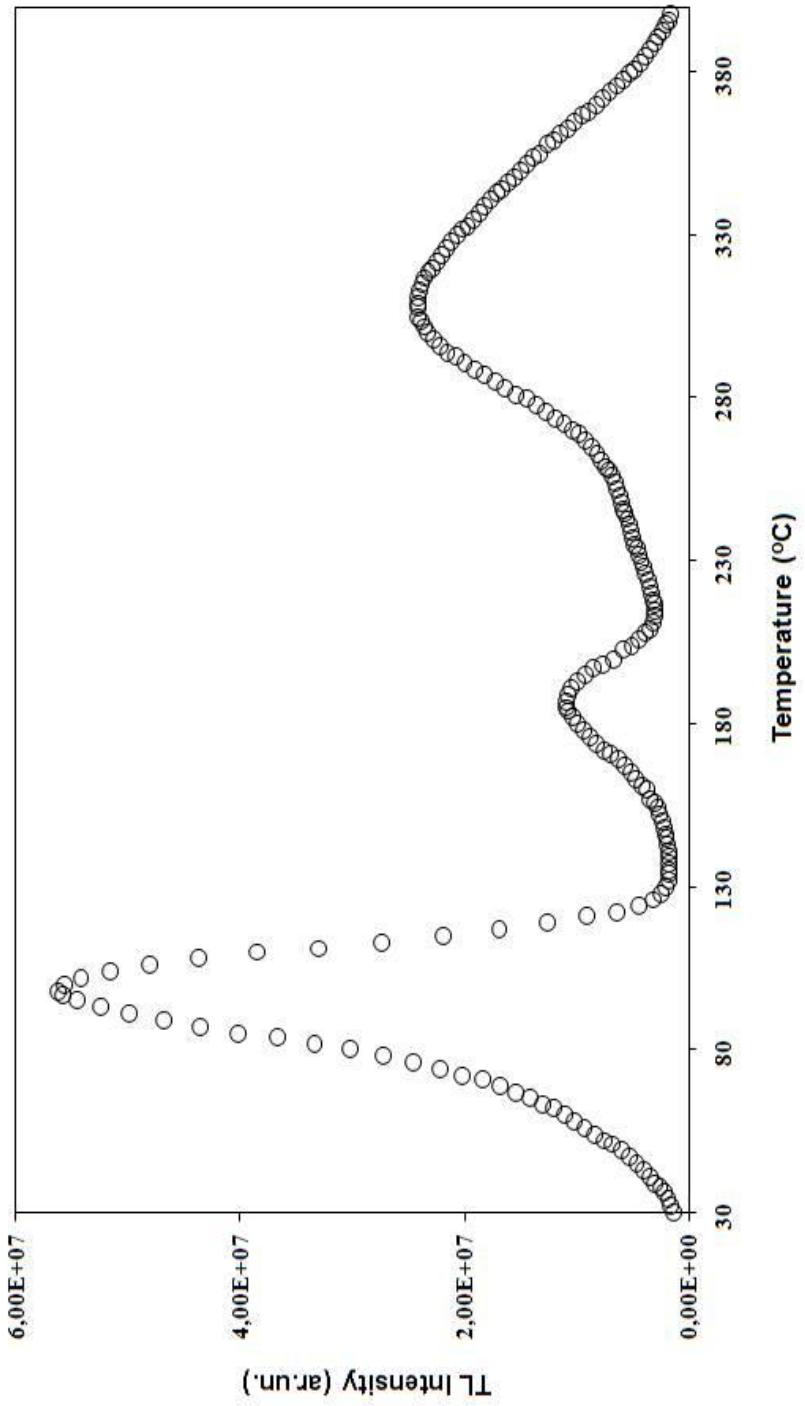

e)

Figure 3.13. Continued.

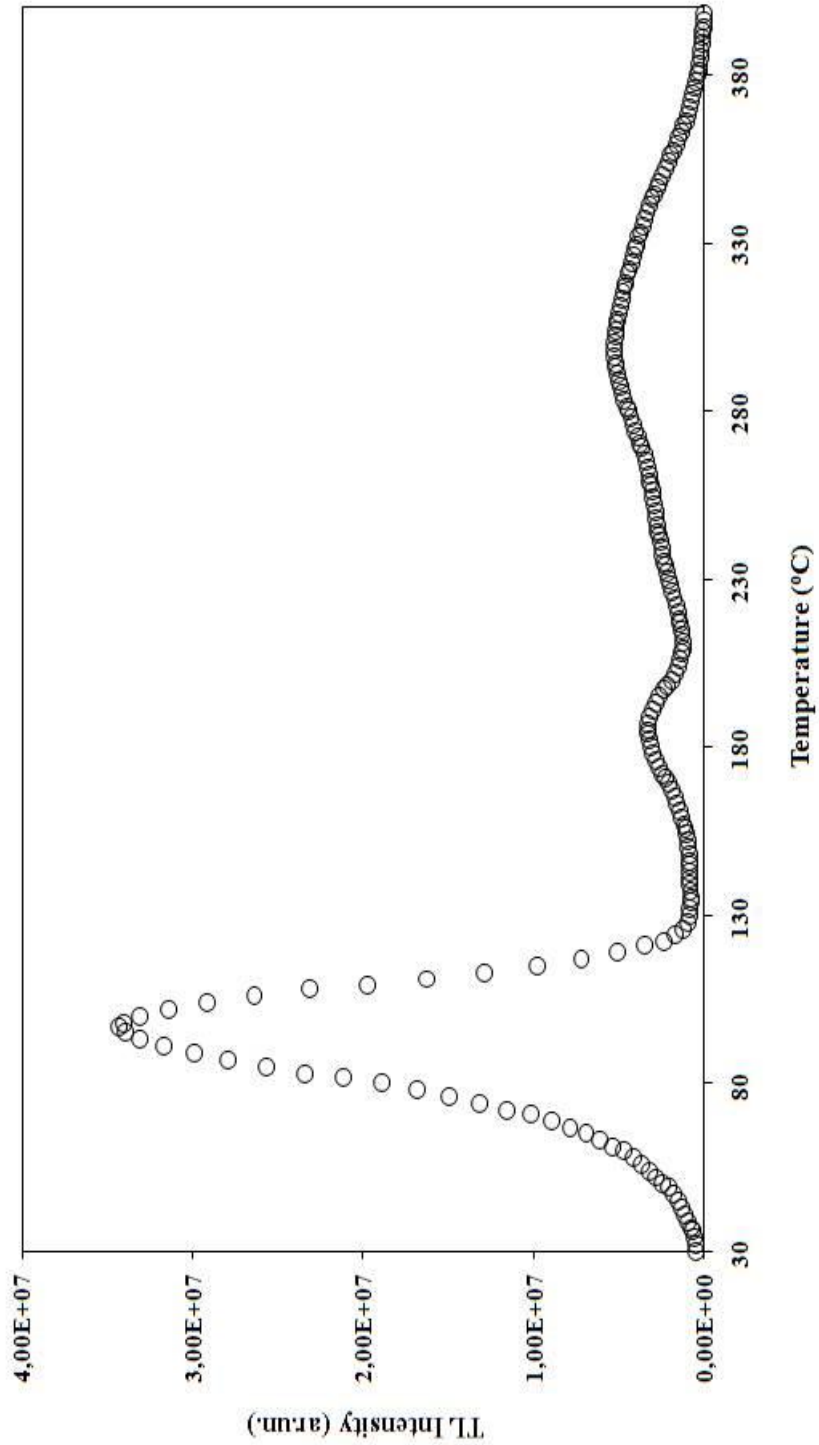

f)

Figure 3.13. Continued.

3.3. SYNTHESIS OF $LnBO_3$ (where Ln=La, Nd, Dy, Ho) BY USING MICROWAVE-ASSISTED SOLID STATE REACTION

3.3.1. Microwave-Assisted Synthesis

The microwave-assisted synthesis is a rapidly developing area of research (Gomez at al. 2004, Wang et al. 2004, Dhage et al. 2002, Mirji et al. 2004). Microwave synthesis is generally quite faster, simpler, and very energy efficient. The exact nature of the interaction of microwaves with the reactants during the synthesis of ceramic materials is somehow unclear and speculative. However, energy transfer from microwaves to material is believed to occur either through resonance or by relaxation, both of which results in rapid heating.

In this part of the thesis, $LnBO_3$ (Ln=La, Nd, Dy, Ho) powder samples were prepared by using either urea or sucrose in less energetic microwave-assisted reaction method at 1000 W for 10 minutes starting with Ln_2O_3 (where Ln=La, Nd, Dy, Ho) and H_3BO_3 (ratio=1:2). Further two hours heating was applied at 950 ^oC after this process in muffle furnace to complete the reaction. The percentage of microwave active organic substances; urea and sucrose, were not chosen arbitrary. From zero percent to 100% (by weight) is tried for microwave experiments. Among these, below 40% samples did not activate the reaction and organic substances stayed unreacted which has no further effect in XRD patterns. The above 40%, organic microwave active reagant added samples did active in a very short time (in the first minutes) and this activation is so fast and uncontrollable. The mixtures of Ln_2O_3 (where Ln=La, Nd, Dy, Ho) and H_3BO_3 (ratio=1:2) without any microwave active organic substance addition did not activated by microwave and XRD investigations of these powders showed Ln_2O_3 and H_3BO_3 stayed unreacted and give only rare earth oxide peaks.

3.3.1.1. Results of X-ray Diffraction Investigations

In our case, the well mixed urea and sucrose were reacted during the microwave heating part of the experiments. This bubling action of the additive microwave active organic additives happens generally in the last minute of ten minute microwave heating. The very viscous black samples were left to cool. Then, their XRD patterns were taken and given. As seen in Figure 3.14.b- Figure 3.23.b, after microwave heating part of the synthesis, patterns show pure Ln_2O_3 (where Ln=La, Nd, Dy, Ho) phase patterns.

However, because of the existence of residual unburned organic impurities as well as the uncompleted crystallization at lower temperatures, as prepared samples were subjected to solid state reaction to complete the reaction. The XRD patterns (Figure 3.14.c-3.21.c) taken after the two hours solid state reaction in muffle furnaces shows us that microwave-assisted synthesized $LnBO_3$(where Ln=La, Nd, Dy, Ho) samples has same diffraction pattern with samples prepared by direct solid state reaction (Figure 3.14.a-3.21.a).

This is confirmed by the d-spacing values of the samples as shown in Table B.11.-B.14. In these tables, X-Ray Diffraction Data of $LnBO_3$ after a) Solid State Reaction, b) Microwave Heating With Urea and 2 hours Conventional Heating, c) Microwave Heating With Sucrose and 2 hours Conventional Heating were given. We have seen that while $LaBO_3$ and $NdBO_3$ samples prepared by both methods has same orthorhombic crystal structure with *Pnma* (aragonite-type) space group as seen by d-spacing values in Table B.11-B.14., the $DyBO_3$ and $HoBO_3$ orthoborates has hexagonal crystal structure with space group of *P-6c2* (vaterite-type). XRD data of $LnBO_3$ (where Ln=La, Nd, Dy, Ho) samples were subjected to CELREF (Altermat et al. 1987) program and unit cell parameters (given in Å) of were refined and summarized in Table 3.9.

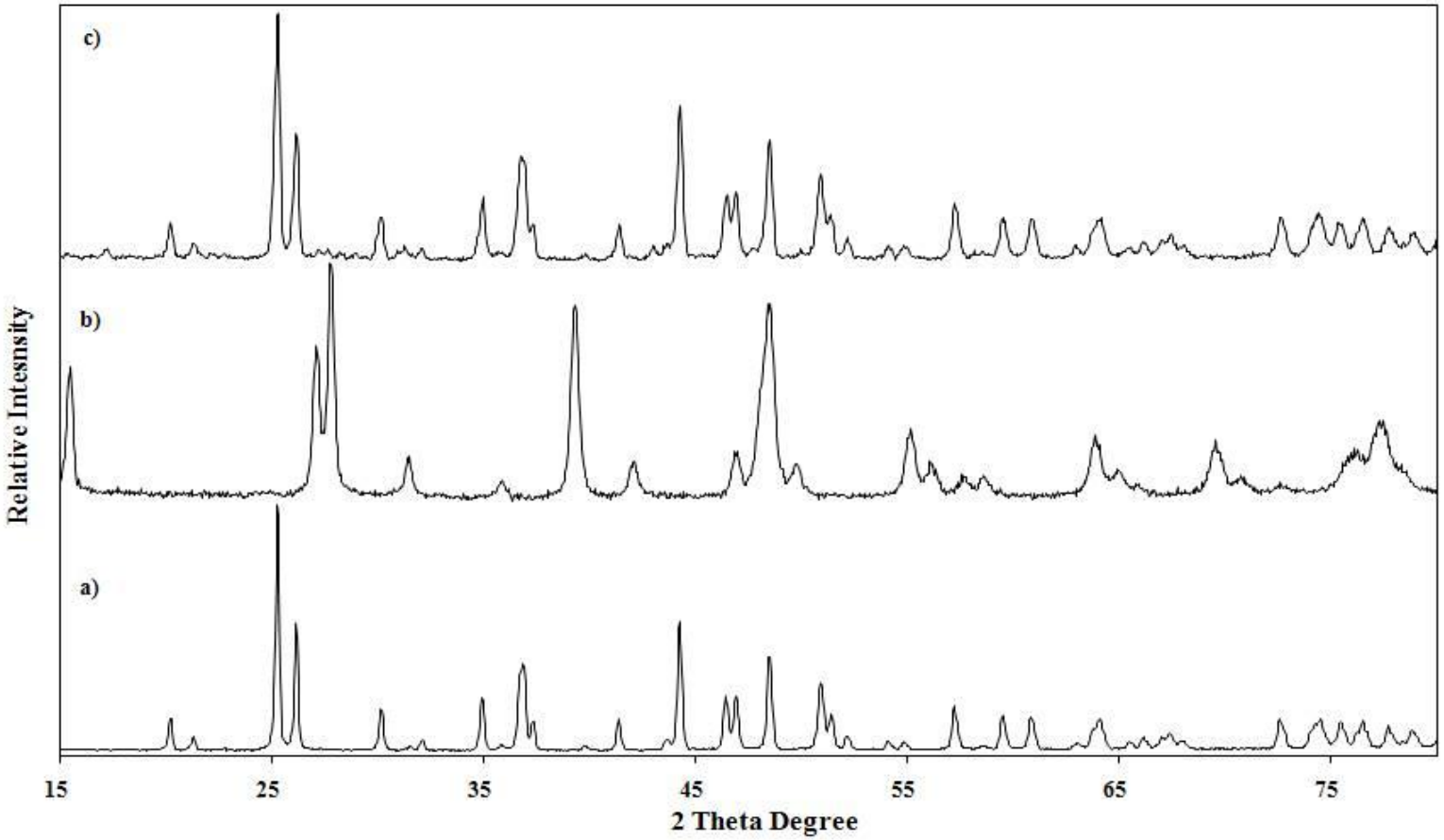

Figure 3.14. X-Ray Diffraction Patterns of $LaBO_3$ after a) Solid State Reaction, b) Microwave Heating With Urea, and c) Microwave and 2 hours Conventional Heating.

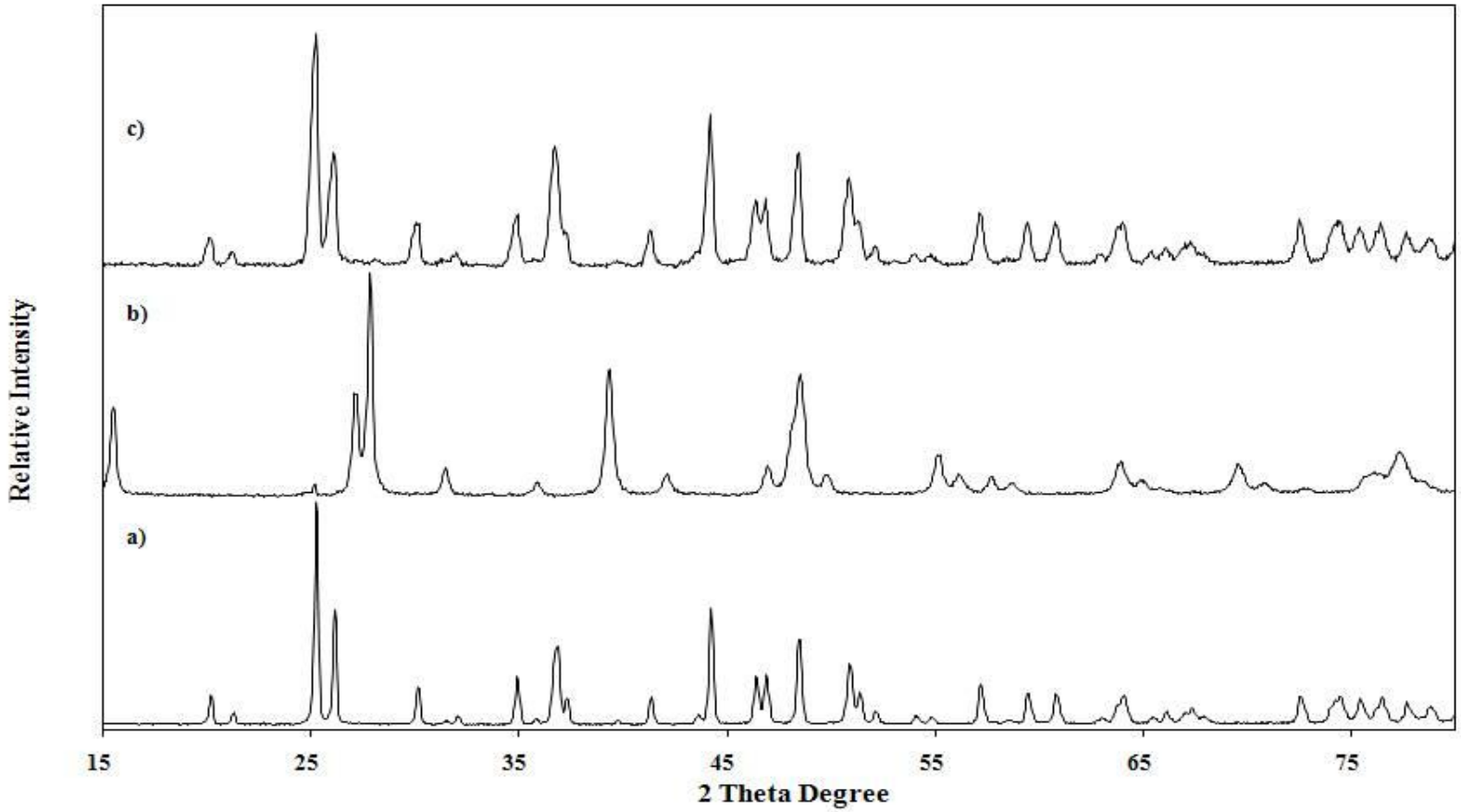

Figure 3.15. X-Ray Diffraction Patterns of $LaBO_3$ after a) Solid State Reaction, b) Microwave Heating With Sucrose, and c) Microwave and 2 hours Conventional Heating.

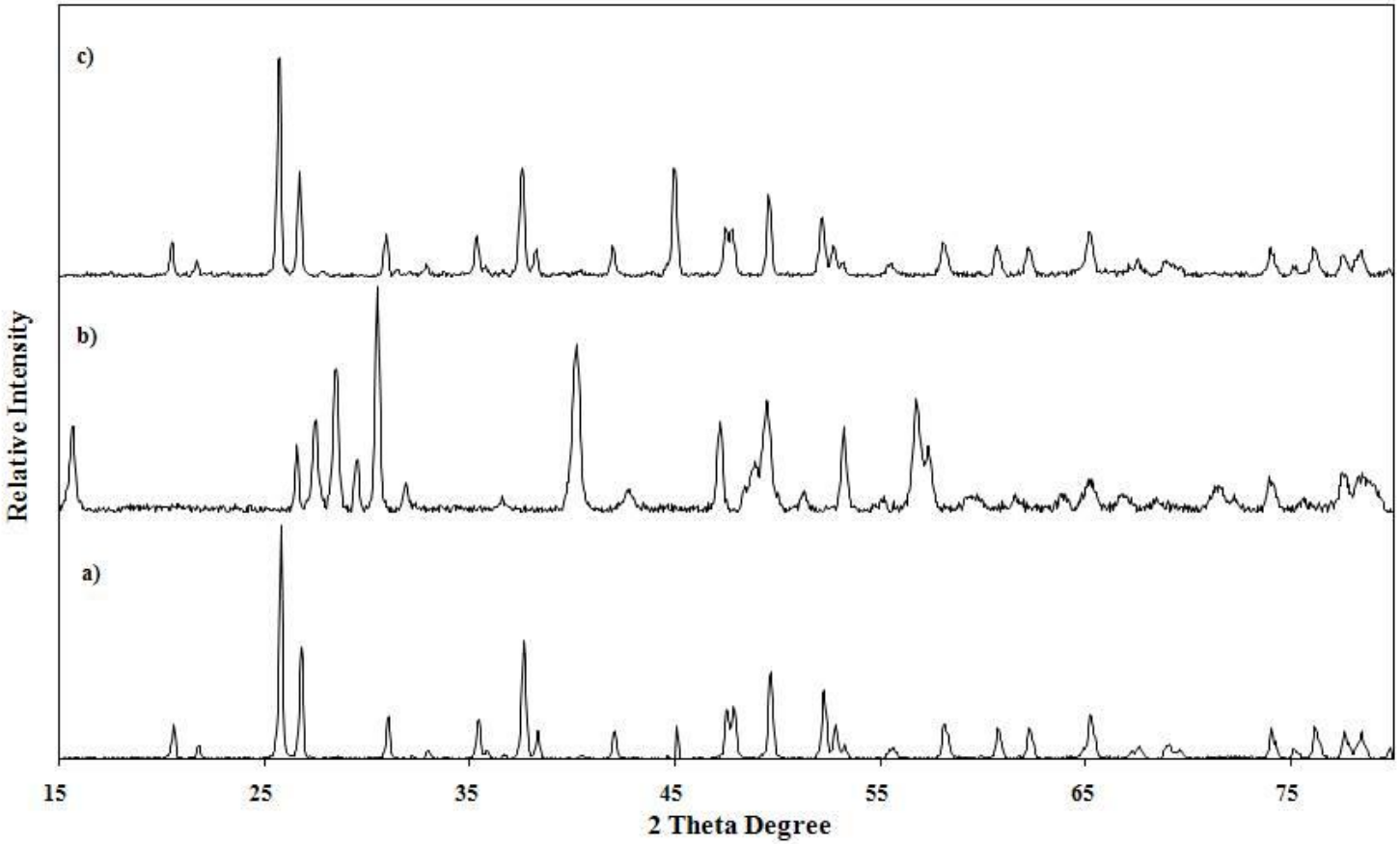

Figure 3.16. X-Ray Diffraction Patterns of $NdBO_3$ after a) Solid State Reaction, b) Microwave Heating With Urea, and c) Microwave and 2 hours Conventional Heating.

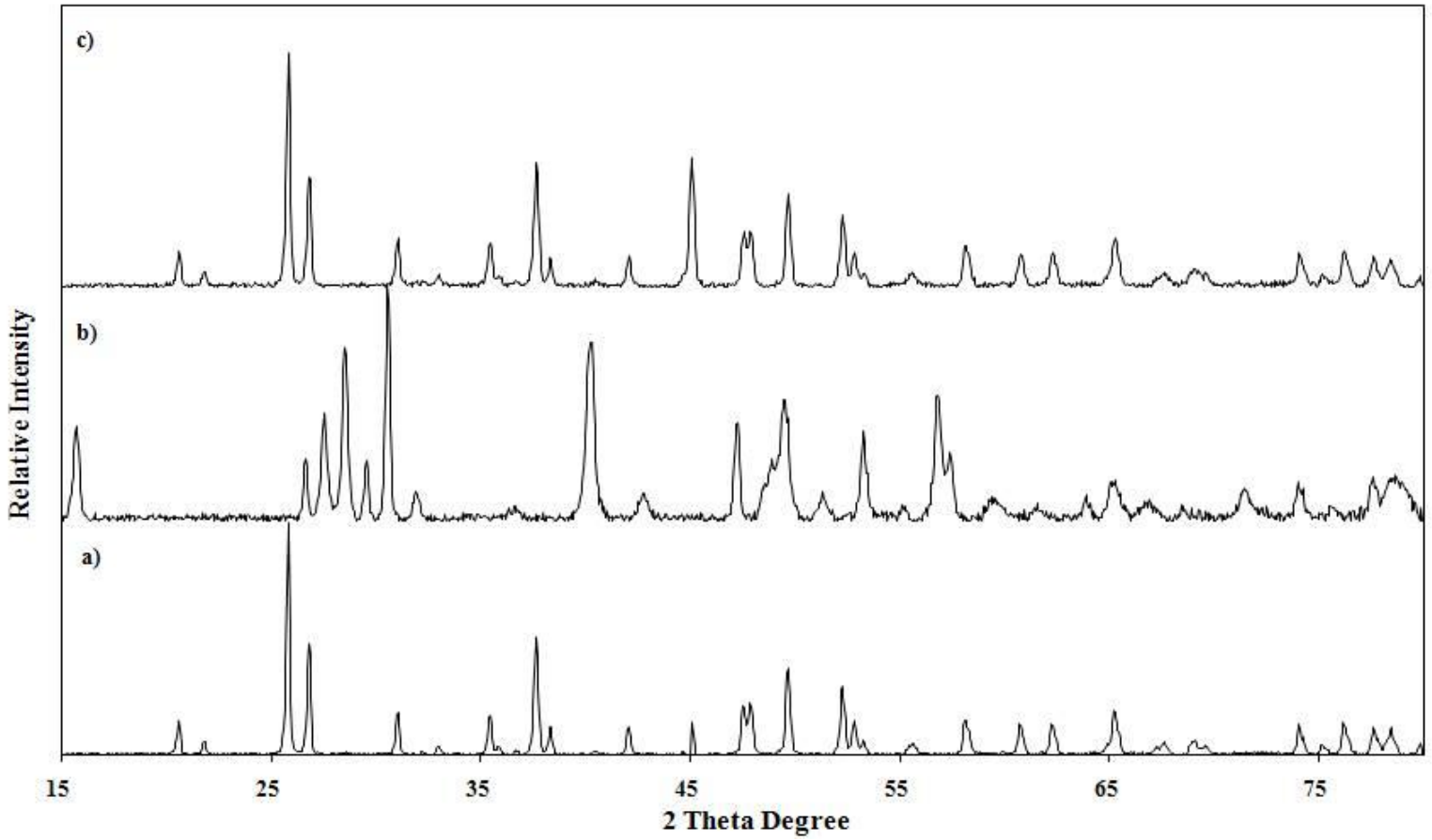

Figure 3.17. X-Ray Diffraction Patterns of $NdBO_3$ after a) Solid State Reaction, b) Microwave Heating With Sucrose, and c) Microwave and 2 hours Conventional Heating.

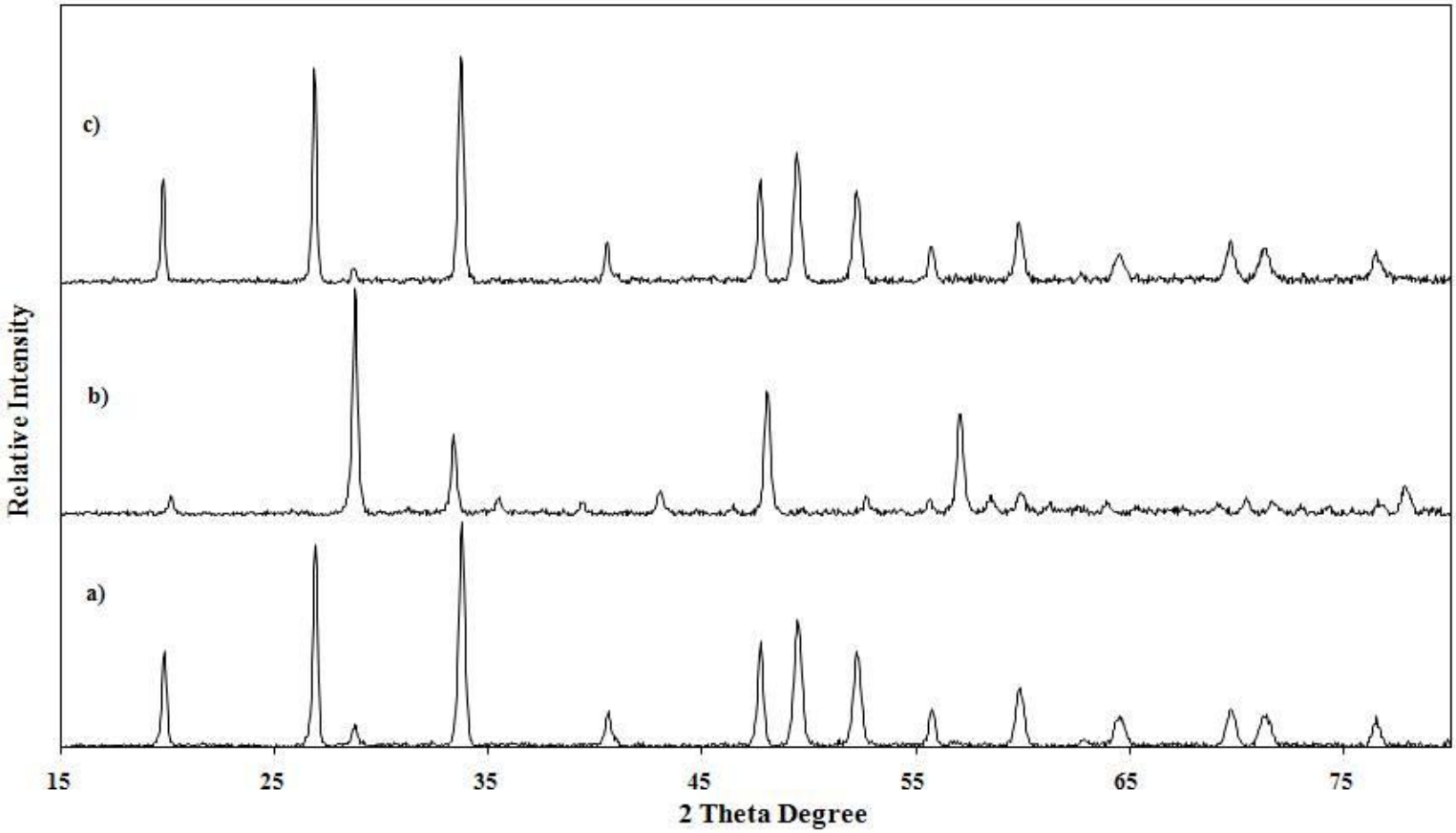

Figure 3.18. X-Ray Diffraction Patterns of $DyBO_3$ after a) Solid State Reaction, b) Microwave Heating With Urea, and c) Microwave and 2 hours Conventional Heating.

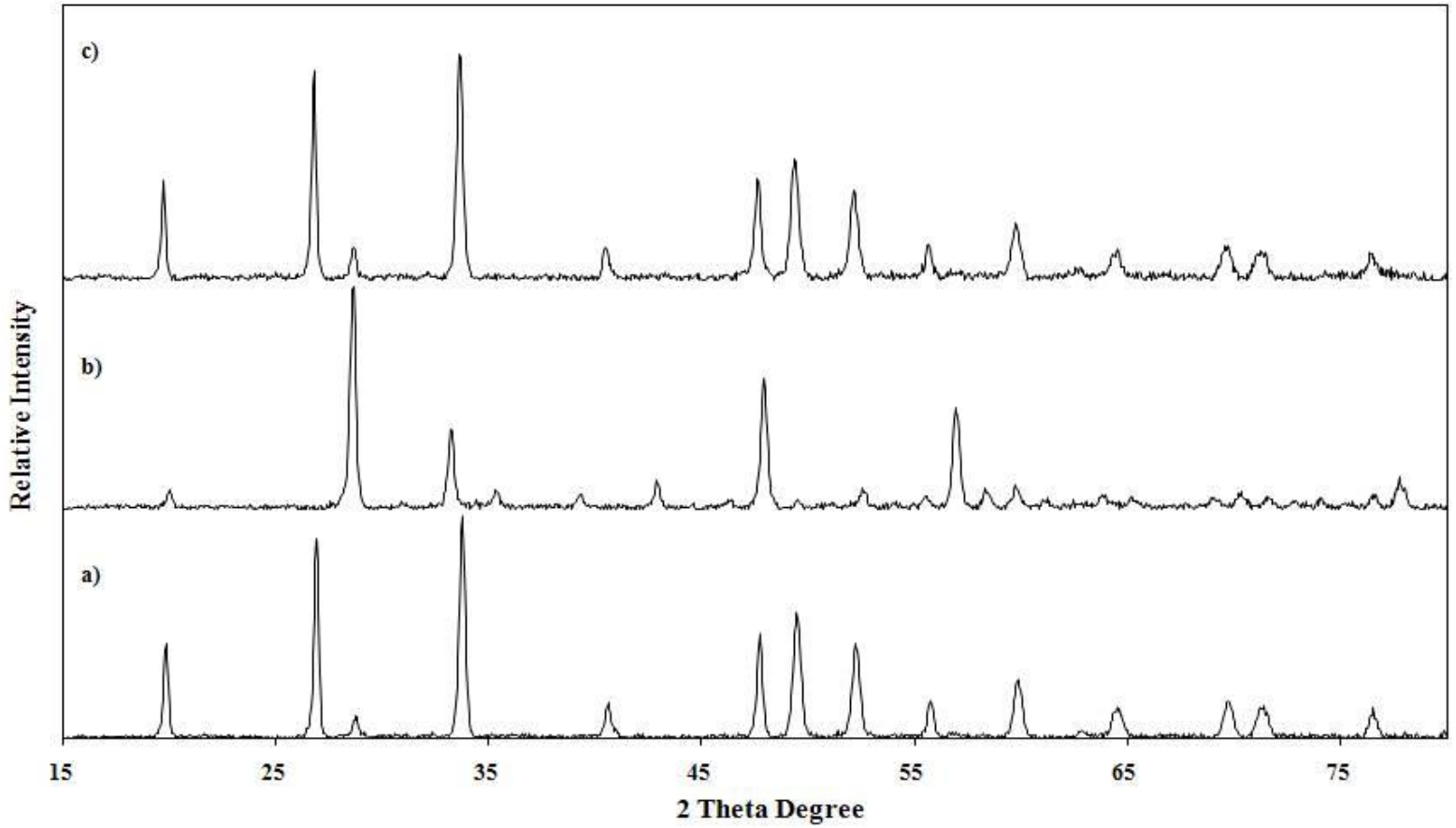

Figure 3.19. X-Ray Diffraction Patterns of $DyBO_3$ after a) Solid State Reaction, b) Microwave Heating With Sucrose, and c) Microwave and 2 hours Conventional Heating.

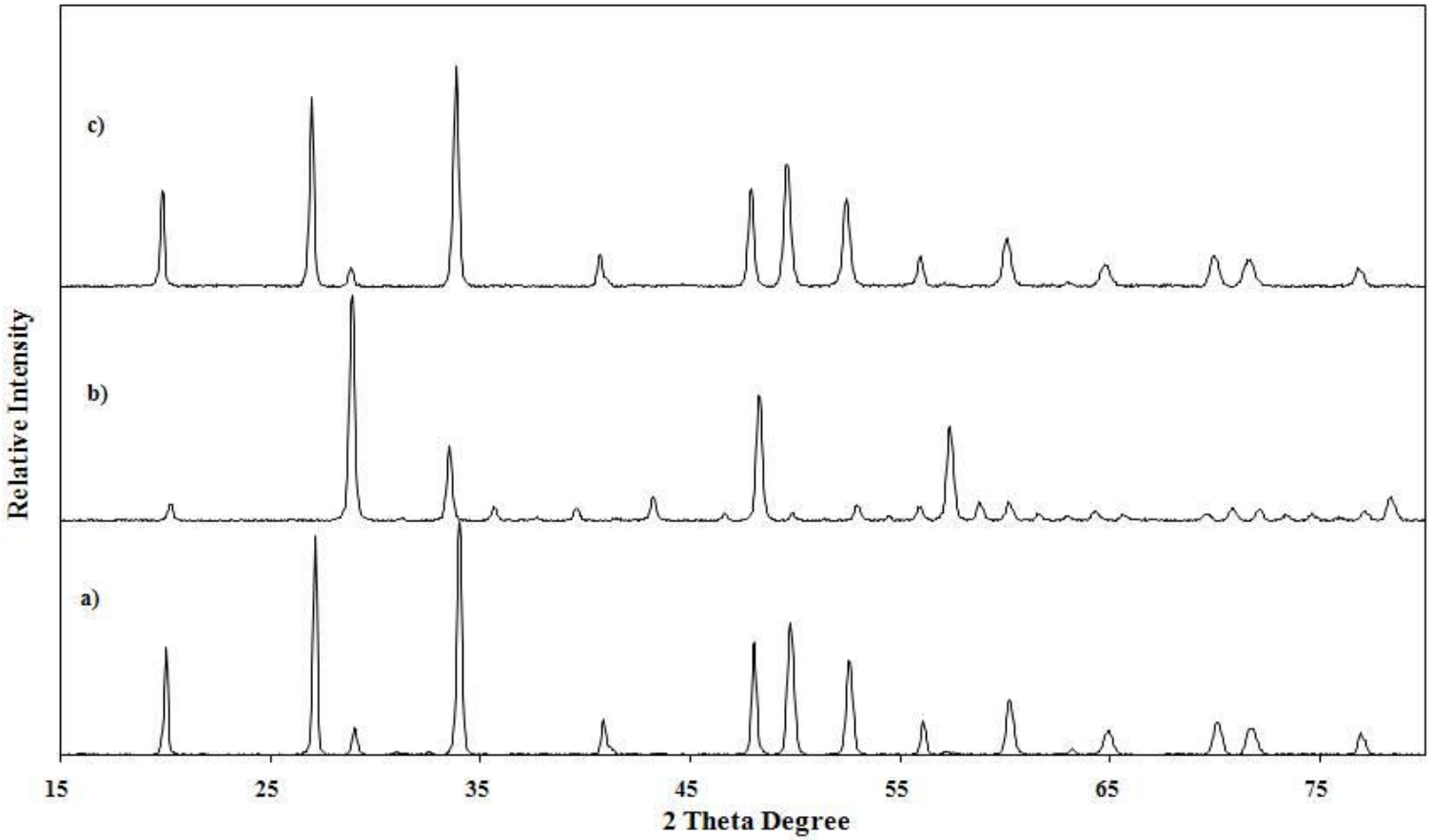

Figure 3.20. X-Ray Diffraction Patterns of $HoBO_3$ after a) Solid State Reaction, b) Microwave Heating With Urea, and c) Microwave and 2 hours Conventional Heating.

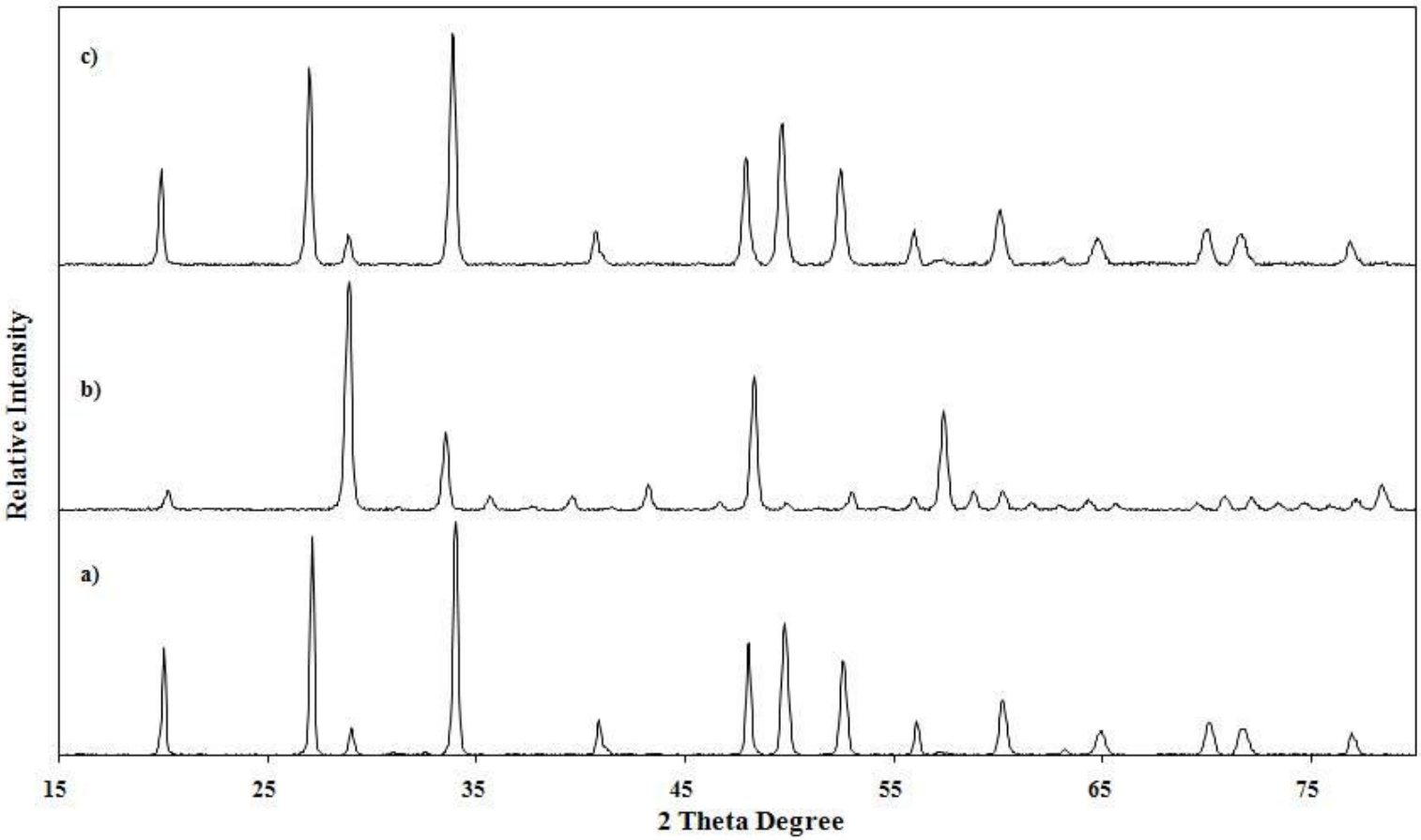

Figure 3.21. X-Ray Diffraction Patterns of $HoBO_3$ after a) Solid State Reaction, b) Microwave Heating With Sucrose, and c) Microwave and 2 hours Conventional Heating.

Table 3.9. Space groups and refined unit cell values of $LnBO_3$ (where Ln=La, Nd, Dy, Ho) prepared by microwave-assisted synthesis method.

	$LaBO_3$	**$NdBO_3$**	**$DyBO_3$**	**$HoBO_3$**
Space Group	Pnma	Pnma	P-6c2	P-6c2
Solid State	a= 5.910(6)Å	a= 5.749(3)Å	a= 3.810(6)Å	a= 3.786(3)Å
	b= 8.35(2)Å	b= 8.145(6)Å		
	c= 5.135(6)Å	c= 5.059(3)Å	c= 8.879(2)Å	c= 8.8300(9)Å
MW-Urea + Solid State	a= 5.927(5)Å	a= 5.762(4)Å	a= 3.809(5)Å	a= 3.794(7)Å
	b= 8.33(1)Å	b= 8.17(1)Å		
	c= 5.113(6)Å	c= 5.066(4)Å	c= 8.888(2)Å	c= 8.858(2)Å
MW-Sucrose + Solid State	a= 5.929(3)Å	a= 5.75(4)Å	a= 3.815(5)Å	a= 3.793(5)Å
	b= 8.334(6)Å	b= 8.109(7)Å		
	c= 5.122(4)Å	c= 5.059(4)Å	c= 8.911(2)Å	c= 8.851(2)Å

3.3.1.2. Results of Scanning Electron Microscopy Investigations

The results of XRD pattern of $LnBO_3$ samples (Figure 3.14.c.-3.21.c), indicates that FWHM of the samples after microwave activated solid state heating are larger than samples prepared by direct solid state reaction. These results showed the decrease in particle sizes of products. For this reason, products sent to Scanning Electron Microscope analysis to see the changes in morphology and particle sizes of microwave-assisted synthesized $LnBO_3$ samples.

In Figure D.3.-D.6., SEM images of $LnBO_3$ (where Ln=La, Nd, Dy, Ho) obtained by using a) Microwave-Assisted synthesis with urea, b) microwave-assisted synthesis with sucrose and c) solid-state reaction were given. In these figures, it is obviously seen that particles has submicron (<1μm) size and equally distributed for samples prepared by urea and sucrose. The particle sizes of direct solid solid state products are larger than 1μm and particles have not equal size and the distribution is random.

By using organic additives such as urea and sucrose, in the first part of the reaction, particles are equally distributed and probable mechanism is expected that during bubling part of the organic substance activation in microwave-assisted part, these activators surrounded the other particles giving homogeneous distribution and while heating them at high temperatures these substances resist to agglomeration of residual powders. Most of the samples in Figure D.3.-D.6., has around 500 nm particle size in diameter.

3.4. RIETVELD REFINEMENT ANALYSIS OF $LnBO_3$ (where Ln= Y, La, Nd, Sm, Eu-Lu) STRUCTURES

Herein, in this final chapter of the thesis, we report the solid state reactions of Ln_2O_3 (where Ln= Y, La, Nd, Sm-Lu) and H_3BO_3 (ratio=1:2) performed at 900 ^oC for 10 hours and 1000 ^oC for 5 hours. The structure of the produced phases was identified by X-ray Diffraction studies. Then, their crystallographic studies were performed by using Rietveld refinement structural analysis. The Rietveld method is a full-pattern fit method. The measured profile and calculated profile are compared. By the variation of many parameters (background, profile, structural, zero shift, atomic positions, instrumental parameters, scale factor, unisotropic thermal parameters, etc.) the difference between the two profiles is minimized. After refining of these parameters, three dimensional structural analysis of the molecules can be drawn by, Diamond 2.1a.(Branderburg, 1996-1999) software packages were used.

3.4.1. Results of X-ray Diffraction Investigations

The X-ray diffraction patterns of the produced samples were collected by using Rigaku Miniflex Diffractometer and Panalytical X'Pert PRO Diffractometer.

3.4.1.1. Results of X-ray Diffraction Investigations of $LnBO_3$ scanned by using Rigaku Diffractometer

The X-ray Diffraction patterns of the $EuBO_3$ products scanned by Rigaku diffractometer were given in Figure 3.22. Based on the $EuBO_3$ XRD results, we deduced that the rise of the background level is due to absorption of the CuKα radiation and subsequent X-ray fluorescence. By using a K_β filter subsequent X-ray fluorescence and the K_β radiation can be avoided. The slight rise of the background was observed for the YBO_3, $LaBO_3$, $YbBO_3$, $LuBO_3$ and the strong rise of the bakground level for $NdBO_3$, $SmBO_3$, $GdBO_3$, $TbBO_3$, $DyBO_3$, $HoBO_3$, $ErBO_3$, $TmBO_3$ were observed.

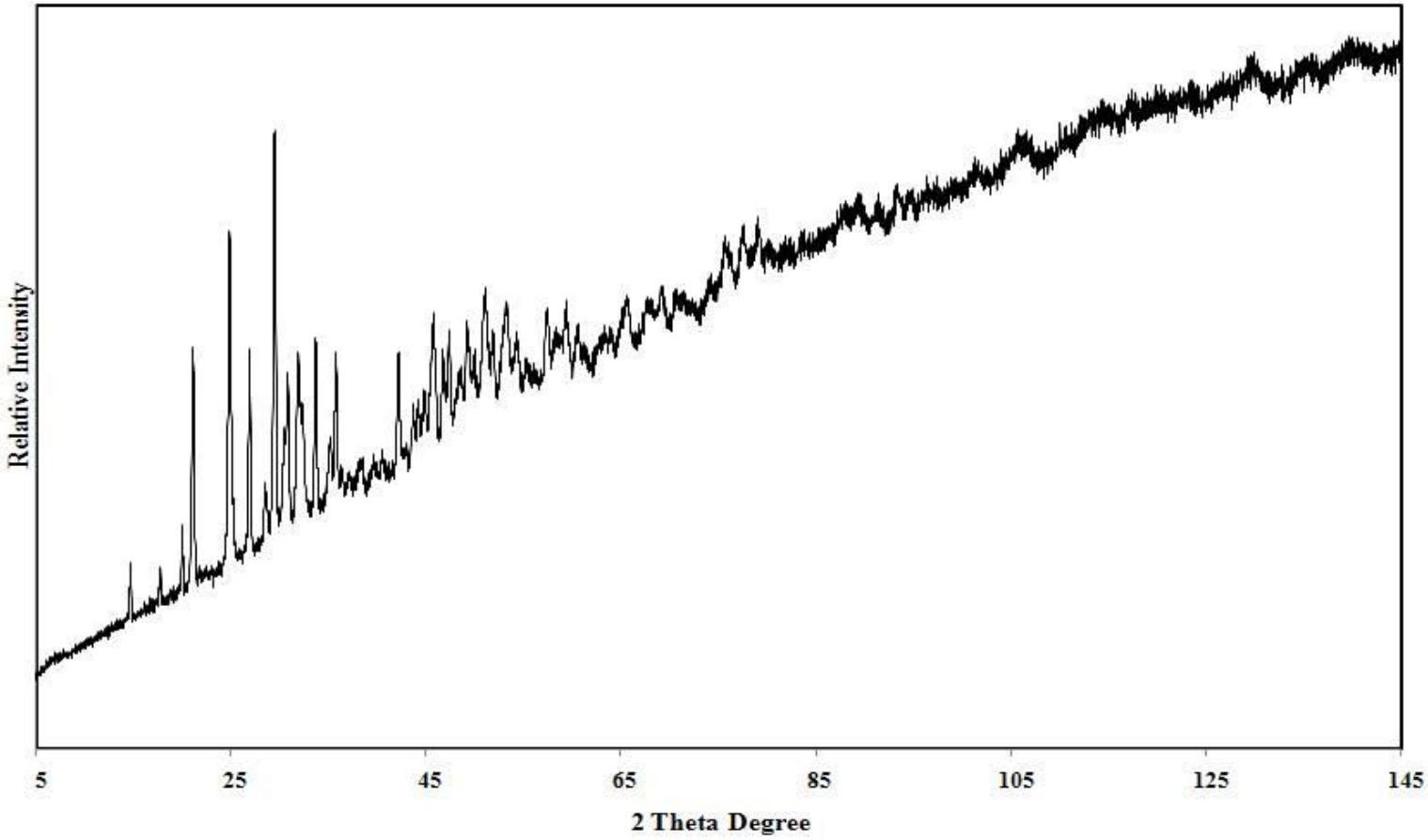

Figure 3.22. X-Ray Diffraction Pattern of $EuBO_3$ Scanned by Using Rigaku Miniflex Diffractometer Between 5-145^{o} 2 Theta.

3.4.1.2. Results of X-ray Diffraction Investigations of $LnBO_3$ scanned by using Panalytical Diffractometer

Same samples were subjected to Cu radiation with K_β filter using Panalytical Diffractometer. For $EuBO_3$, the background level is seem normal in Figure 3.23. The slight increase of the background in the low angles resulted from the fixed divergence slit. Yet, it is normalized for the higher angles and we obtained nearly smooth background for whole sample. The same smooth background were observed for YBO_3, $LaBO_3$, $NdBO_3$, $SmBO_3$, $GdBO_3$, $TbBO_3$, $DyBO_3$, $HoBO_3$, $ErBO_3$, $TmBO_3$ $YbBO_3$, $LuBO_3$. Since our aim is to solve the crystal structure of rare earth orthoborates, high quality data were needed. All of these X-ray patterns has high quality data for Rietveld refinement with good FWHM values and with relatively much higher intensities with good peak shape.

X-ray Diffraction (XRD) patterns were analyzed by the X'Pert High Score Plus software version 2.2c (High Score Plus, 2007) with reference to the patterns of the International Centre for Diffraction Data database (Powder Diffraction File. PDF-2, 2002) as well as the Inorganic Crystal Structure Database (ICSD, 2005). According to these qualitative analysis by using search and match mode of the program, the following results firstly depicted from the library match (Table 3.10). The X-ray diffraction data of all lanthanide orthoborates were given in Table B.15.-B.27.

The $LaBO_3$ and $NdBO_3$ has correct space group as mentioned in ICSD cards. $SmBO_3$ has also triclinic crystal structure with *P-1* space group. For vaterite type of orthoborates (YBO_3, $GdBO_3$, $TbBO_3$, $DyBO_3$, $HoBO_3$, $ErBO_3$, $TmBO_3$ $YbBO_3$, $LuBO_3$) some of these cards are not fit well because of the structural differences in lanthanide orthoborates where all possible point groups has same d-spacings with different intensity values.

Yet, since atoms and atomic positions directly affects the intensity values of the given molecule, all possible space groups *($R3_2$, $P6_3/mmc$, $P6_3/m$, $C2/c$)* were tried for vaterite type of orthoborates and the results of these trials is given in the Rietveld refinement results part. Among these crystal structures only *$P6_3/mmc$* contains BO_3 groups in the structure while other (*$R3_2$, $P6_3/m$, $C2/c$*) has BO_4 groups in $B_3O_9^{9-}$ ring (Ren et al. 1999, Lin et al. 2004, Chadeyron et al. 1997b). This is proved by using IR spectroscopy in Chapter 3.4.2.

Table 3.10. Space groups, reference cards, unit cell parameters of lanthanide orthoborates.

$LnBO_3$	**Space Groups (ICSD / ICDD Cards), Unit Cell Parameters**
YBO_3	*$P6_3/mmc$* (01-074-1929), a=3.778, c=8.814 Å
$LaBO_3$	*Pnma* (00-012-0762), a=5.872, b=257, c=5.107 Å
$NdBO_3$	*Pnma* (01-041-2407), a=5.7351, b=5.0564, c=8.0916 Å
$SmBO_3$	*P-1* (01-040-0745), a=6.493, b=6.499, c=6.242 Å, α=107.79, β=107.42, γ=93.33 ^{o}
$EuBO_3$	*$P6_3/mmc$* (01-074-1931) + *P-1* (01-088-0201) a=3.842, c=8.937 Å + a=6.468, b=6.477, c=6.22 Å, α=107.78, β=108.00, γ=92.07 ^{o}
$GdBO_3$	*$P6_3/mmc$* (01-074-1932), a=3.839, c=8.906 Å
$TbBO_3$	*$P6_3/mmc$* (01-074-1933), a=3.793, c=8.847 Å
$DyBO_3$	*$P6_3/mmc$* (01-074-1933) , a=3.793, c=8.847 Å
$HoBO_3$	*$P6_3/mmc$* (01-074-1934), a=3.784, c=8.836 Å
$ErBO_3$	*$P6_3/mmc$* (01-074-1935), a=3.767, c=8.807 Å
$TmBO_3$	*$P6_3/mmc$* (01-074-1936), a=3.753, c=8.789 Å
$YbBO_3$	*$P6_3/mmc$* (01-074-1937), a=3.735, c=8.747 Å
$LuBO_3$	*$P6_3/mmc$* (01-074-1938) + *R-3c* (01-016-0525) a=3.727, c=8.722 Å + a=4.913, c=16.212 Å

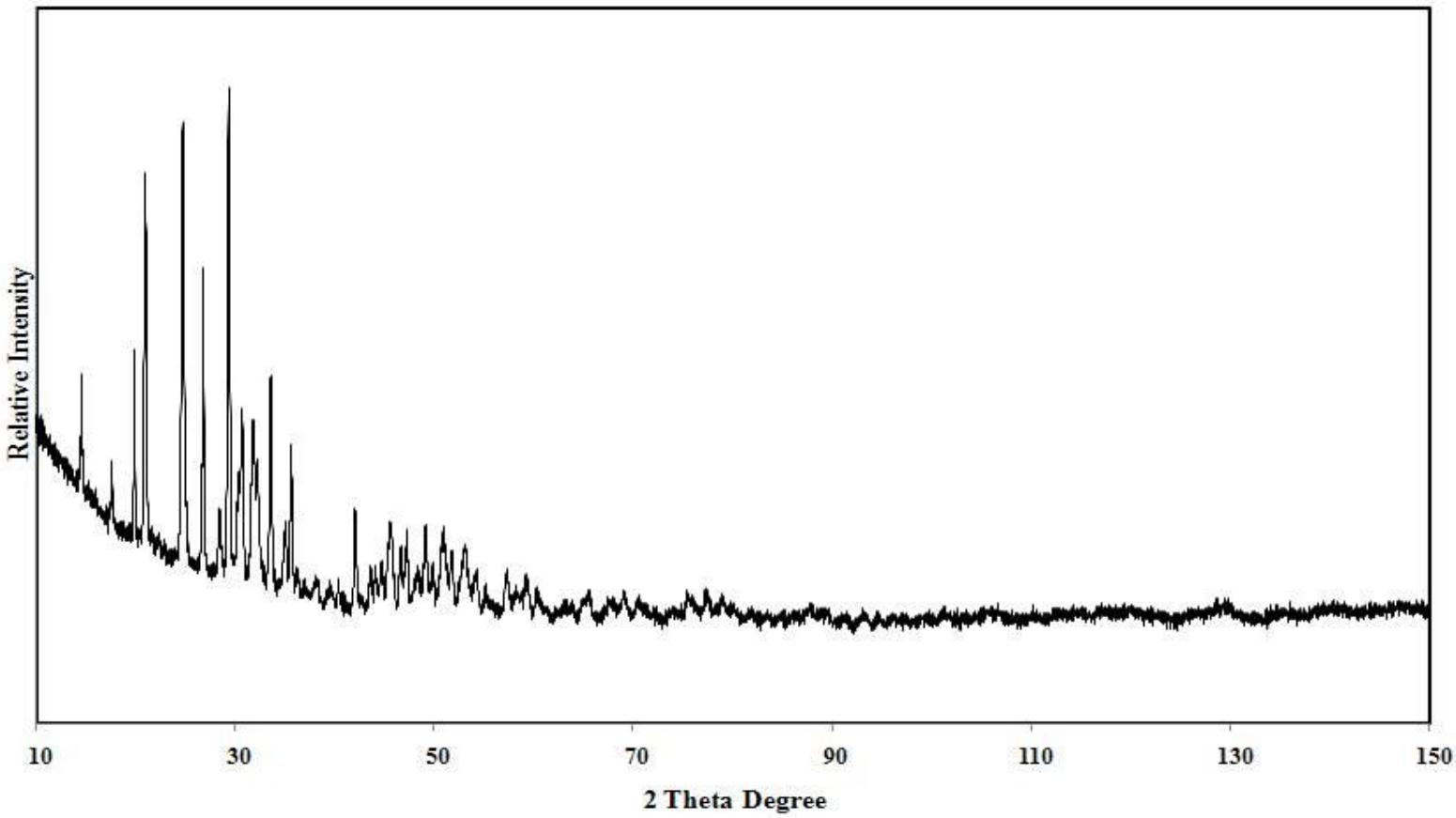

Figure 3.23. X-Ray Diffraction Pattern of $EuBO_3$ Scanned by Using Panalytical Diffractometer with PIXCEL Detector Between 10-150^o 2 Theta.

3.4.2. Results of FTIR Investigations

IR spectroscopy was carried out with the objective of specifying and comparing the coordination of boron in $LnBO_3$ borates synthesized in this study. Aragonite type of orthoborates ($LaBO_3$ and $NdBO_3$) have vibration modes which can be described as follows: υ3 (asymmetric stretching) in the region 1100 and 1400 cm^{-1}, υ1 (symmetric stretching) near 940 cm^{-1}, υ2 (out of plane bending) in the region 700-800 cm^{-1}, and υ4 (in-plane bending) below 670 cm^{-1} (Lemanceau et al. 1999). The close similarities in the IR spectra of $LaBO_3$ and $NdBO_3$ are evident as in Figure 3.24. and C.1, respectively. The υ3 (asymmetric stretching) bands observed at 1277, 1246 and 1281, 1258 cm^{-1}, υ1 (symmetric stretching) bands 947 and 966 cm^{-1}, υ2 (out of plane bending) bands 819, 796, 718, and 788, 706 cm^{-1}, and υ4 (in-plane bending) bands 609, 601, 539, 493 and 617, 594, 547 cm^{-1} for $LaBO_3$ and $NdBO_3$, respectively. It will be noted that the behavior of υ3 bands in the two structures serves as a distinguishing feature. For these compounds it is clear that boron atoms are in threefold coordination. The observed frequencies between 1350 and 1150 cm^{-1} range correspond to the strectching frequencies of a coordinated BO_3 group (Lemanceau et al. 1999).

According to XRD results there is only one triclinic phase for $SmBO_3$ and two phases (triclinic and vaterite) for $EuBO_3$. There FTIR spectra of these compounds were presented in Figure 3.25. and Figure C.2. The structure of these compounds consist of triclinic phases where the structure consist of BO_3^{3-} anions and Nd^{3+} and Eu^{3+} cations. The BO_3^{3-} anions are in the form of equilateral triangles with boron in the center. And the bands over 1150 cm^{-1} explained the presence of BO_3 in these structures (Lemanceau et al. 1999). For borates and calcite and aragonite structures, the boron atoms are threefold coordinated (Chadeyron et al. (1997b). The only calcite containing phase is $LuBO_3$ which has also vaterite phase in the structure. As shown in its IR spectrum (Figure C.3h.) the bands between 1350 and 1150 cm^{-1} corresponds to BO_3 groups in the structure.

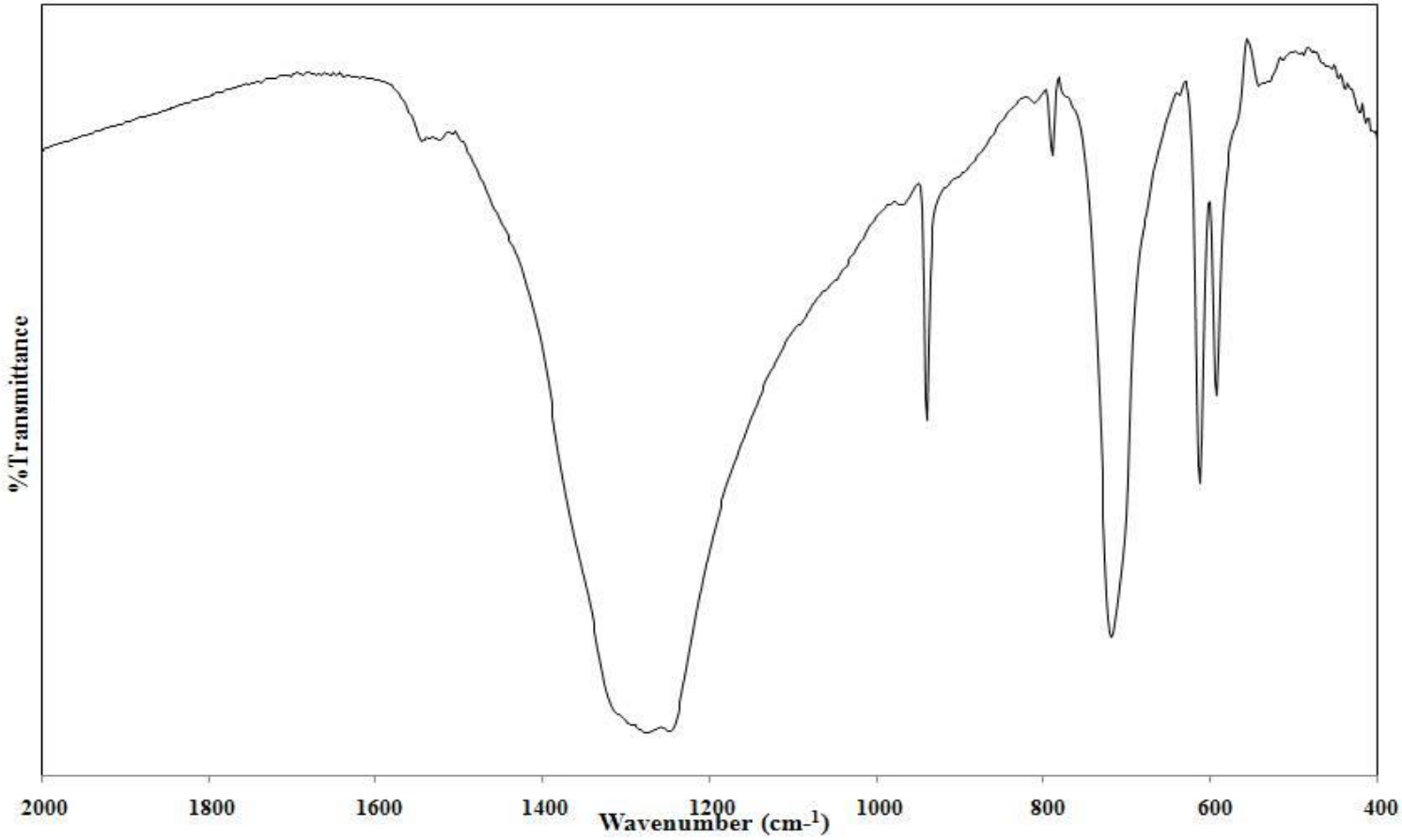

Figure 3.24. FT-IR spectrum of $LaBO_3$

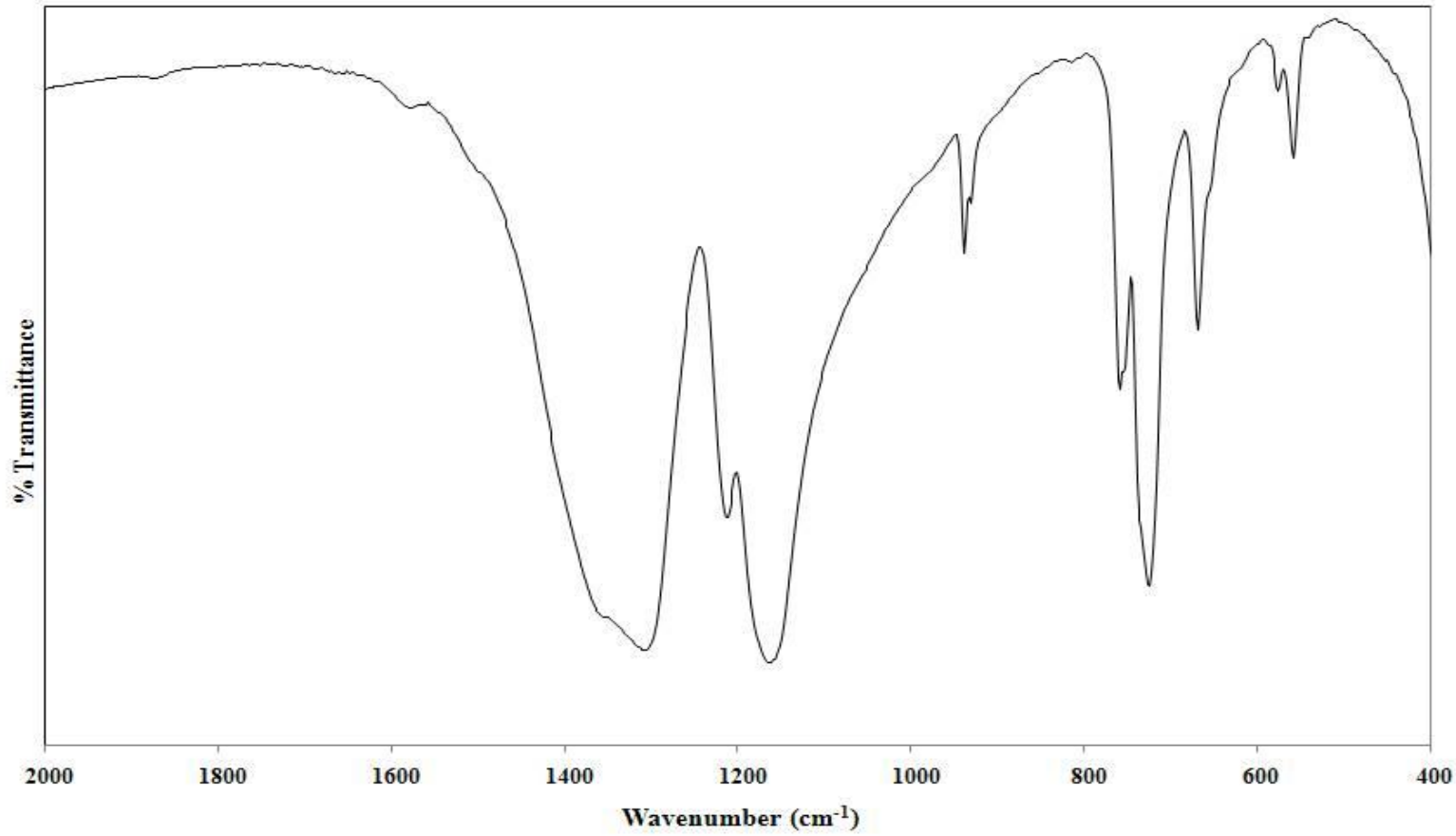

Figure 3.25. FT-IR spectrum of $SmBO_3$

The rest of the orthoborates $LnBO_3$ (Ln=Y, Gd, Tb-Yb) have single phase according to XRD phase analysis. They have vaterite type of structure. According to IR, NMR, and Raman studies (Laperches and Tarte 1966, Denning and Ross 1972, Kriz and Bray 1969), these compounds contain only the tetrahedral polyborate group of $B_3O_9^{9-}$ in their structure and this structure contains BO_4 groups not BO_3 anions.

Therefore, the bands between 1150-1350 cm^{-1} are not seen in the FTIR spectra of YBO_3 and $LnBO_3$(Ln=Gd, Tb, Dy, Ho, Er, Tm, Yb) in the Figure 3.26. and C.3.(a-g), respectively. The IR absorption peaks between 900 and 1050 cm^{-1} are those typical for the tetrahedral borate group BO_4 (Ren et al. 1999) and our results are consistent with these and $LnBO_3$ (Ln=Y, Gd, Tb-Yb) products is composed of $B_3O_9^{9-}$ in their structure.

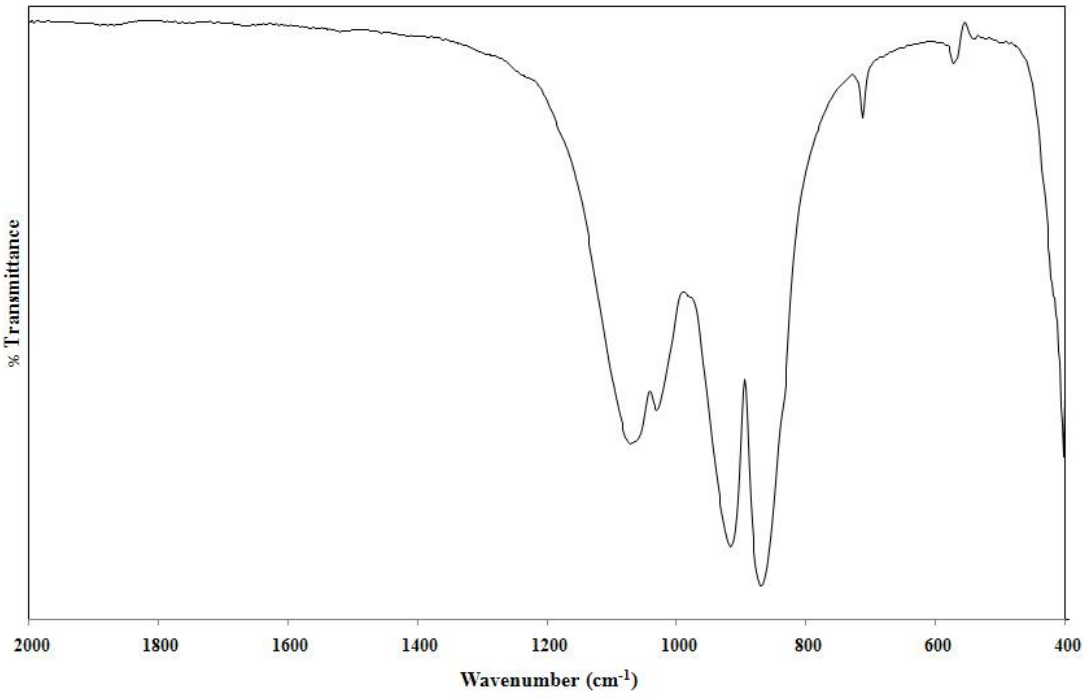

Figure 3.26. FT-IR spectrum of YBO_3

3.4.3. Results of Rietveld Refinement Structural Analysis

The proper space group and the corresponding atomic positions either from ICSD database, CIF (Crystallographic Information Files) Files, or from references in the literature were tried to find the best crystallographic starting point for the rare earth orthoborates. Structure refinements were carried out using the XRD data and we used the Rietveld refinement program contained in the GSAS suite (Larson et al. 2000) for all refinements.

The Bragg peak profile was modeled using a pseudo-Voigt function. The instrumental background was emprically fitted using a cosine series polynomial of the second kind with 7 variable coeffients. The 2 theta–zero shift was accurately refined in all the patterns of the data set. One scale factor and the unit-cell parameters were allowed to vary for all histograms.

As anticipated, a tentative structure refinement using the structure model given in Lin et al. (2004) was also attempted for the structure of YBO_3, $DyBO_3$ and $HoBO_3$ and their crystal structure is found in monoclinic system with C2/c space group. The structure refinements with the *P63/m, P63/mmc, C2/c* and $R3_2$ models have been performed comparatively in a rigorous way using the same data set for $LnBO_3$ (where Ln= Y, Dy, Ho). The scale factor, the unit cell parameters and the structure parameters were independently refined whereas the background and peak profile parameters were kept identical in the two refinements to rule out any possible correlation. The most probable space group for the produced YBO_3, $DyBO_3$ and $HoBO_3$ compounds is found as *C2/c*. For YBO_3, Co sourced STOE STADI-P Diffractometer was used to see any preferred orientation by using transmission geometry and no preferred orientation was observed as seen in Figure A.2. The similar d-spacing values were also observed with other diffractometer (Table B.15.)

As mentioned before, $LaBO_3$ and $NdBO_3$ compounds produced in this study have aragonite structure with Pnma space group, while $SmBO_3$ has triclinic structure

with *P-1* space group. The produced $GdBO_3$ structure was solved according to Ren et al. (1999) with $R3_2$ space group.

In the light of refinement results carried out to determine the most probable space group for the other rare earth borates $LnBO_3$ (Ln= Eu, Tb, Er, Tm, Yb, Lu) having vaterite structure but proper solution could not be found. The structural problem of all vaterite type of compound is due to their high and low temperature forms and the transition between these structures. Generally, the high temperature phase is $P6_3/mmc$. They are not quenchable compounds. They formed mixed of several space groups during cooling.

The reason for different space groups and why $ErBO_3$, $TmBO_3$, $YbBO_3$, $LuBO_3$ are problematic are lanthanides ionic radius. Since the ionic radius of Y (0.893 Å), Ho (0.894 Å), and Dy (0.908 Å) are close to each other, YBO_3, $HoBO_3$, $DyBO_3$ form the same space group *C2/c*. From Y to Dy and then to Ho, unit cell parameters are also increasing. For La (1.016 Å) and Nd (0.995 Å) which have the largest ionic radius among lanthanides, $LaBO_3$ and $NdBO_3$ have same orthorhombic *Pnma* space group. For Gd (0.938 Å), ionic radius is larger than Y, Ho, and Dy and this could be the reason of why $GdBO_3$ has different $R3_2$ space group. Eu (0.950 Å) and Sm (0.964 Å) have relatively larger ionic radius than Gd and Y, Ho, and Dy and smaller than La and Nd. This also could be reason why $EuBO_3$ and $SmBO_3$ have triclinic *P-1* space group in their structure. The rest Er (0.881 Å), Tm (0.87 Å), Yb (0.858 Å), Lu (0.85 Å) have smallest ionic radius among lantanides which could be reason why $ErBO_3$, $TmBO_3$, $YbBO_3$, $LuBO_3$ are not stable in one of these space groups mentioned above. Since the ionic radius of Er, Tm, Yb, Lu are so small, they probably enter many sites in different space groups making them having many space groups. They are not stable in definite space group (Weast 1977).

3.4.3.1. Structures of YBO_3, $DyBO_3$ and $HoBO_3$ with C2/c Space Group

Chadeyron et al. (1997) revised the structure of YBO_3 orthoborate. They achieve to synthesize YBO_3 single crystals by using $LiBO_2$ flux and they found that YBO_3 crystallize in *$P6_3/m$*. The same space group found and were given for $YbBO_3$ synthesized by glycothermal method (Hosokawa et al. 2008). We use these data for the refinements at the beginning. Although refinements seems converges at the beginning the intensity order of this space group totally different than the produced phase. This creates differences in difference plot curves. So, we dicided to apply *C2/c* space group which was done for YBO_3 in neutron and did not tried for X-ray Diffraction before. The refinement converges with good residual values.

The results of the Rietveld refinement of YBO_3 are summarized in Table 3.11., and the corresponding profiles are shown in Figure 3.27. The difference curve given in Figure 3.27. and the matching of calculated lines with observed lines shows this model fitted well including intensity matches which means that proposed crystallographic structure is correct. The difference curve is resulted from intensity differences. The calculated lines are calculated by GSAS program (Larson et al. 2000). The refinement converged smoothly and the calculated goodness-of-fit parameters ($\chi^2=(R_{wp}/R_{exp})^2$) remained low ($\chi^2$= 3.289) showing good fit and chemically reasonable structure. The overall value of goodness-of-fit (χ^2) is obviously better than 12.7 given in Lin et al. (2004) showing good fit for this model. The summary of $(Y_{0.92}Er_{0.08})BO_3$ Rietveld refinement results and corresponding atomic structures were tabulated in Table 3.12.

The refined unit cell parameters for YBO_3 at room temperature are a=11.3276(3), b=6.5444(2) Å, c=9.5589(1) Å, β=112.955(1) ^{o},V=652.512 (9)Å^3. The refinement leads to the residual values of R_p=0.0301, R_{wp}=0.0421 which are good agreement with the reported data.

The final atomic coordinates and the equivalent isotropic displacement parameters for YBO_3 given in Table 3.13. These data are in consistency with the data given in Table 3.12. The selected bond length and angles of monoclinic *C2/c* were demonstrated in Table 3.14. In the YBO_3 structure, the B-O distances were found between 1.13915(3) Å and 1.995(5) Å, respectively. The Y-O bond distances are in between 2.22027(5) Å and 2.53378(4) Å. The three O-B-O angle were found as 108.003(1) ^{o}, 119.369(1) ^{o} and 112.102(3) ^{o}. The atomic positions, bond lengths and angles between atoms in YBO_3 are in good agreement with the reported data (Lin et al. 2004).

These refinement results were used to draw crystal structure of YBO_3 by using Diamond (2000-2006) software and the structure is given in Figure 3.28. The same structure with Lin et al. (2004) was obtained and $B_3O_9^{9-}$ anions are seen in this monoclinic cell.

The same space group *C2/c* is tried for $DyBO_3$ and $HoBO_3$ and refinement converges with good residual values which were given in Table E.1. and E.2, respectively. It is found 1.96 and 3.968 for χ^2 values for $DyBO_3$ and $HoBO_3$ showing a good fit and chemically reasonable structure. The difference curves for these orthoborates were given in Figure A.3. and A.4., respectively. The same behaviour of good match with the calculated models are seen in these figures. The final atomic coordinated and the equivalent isotropic displacement parameters for $DyBO_3$ given in Table E.7. and E.8., respectively. The selected bond length and distances of these monoclinic compounds *C2/c* were demonstrated in Table E.14. E.15. respectively. And the corresponding crystal structures were drawn in Figure F.1 and F.2., respectively. In these figures, monoclinic cell with $B_3O_9^{9-}$ anions are shown. These crystal structures are same with YBO_3 crsytal structure.

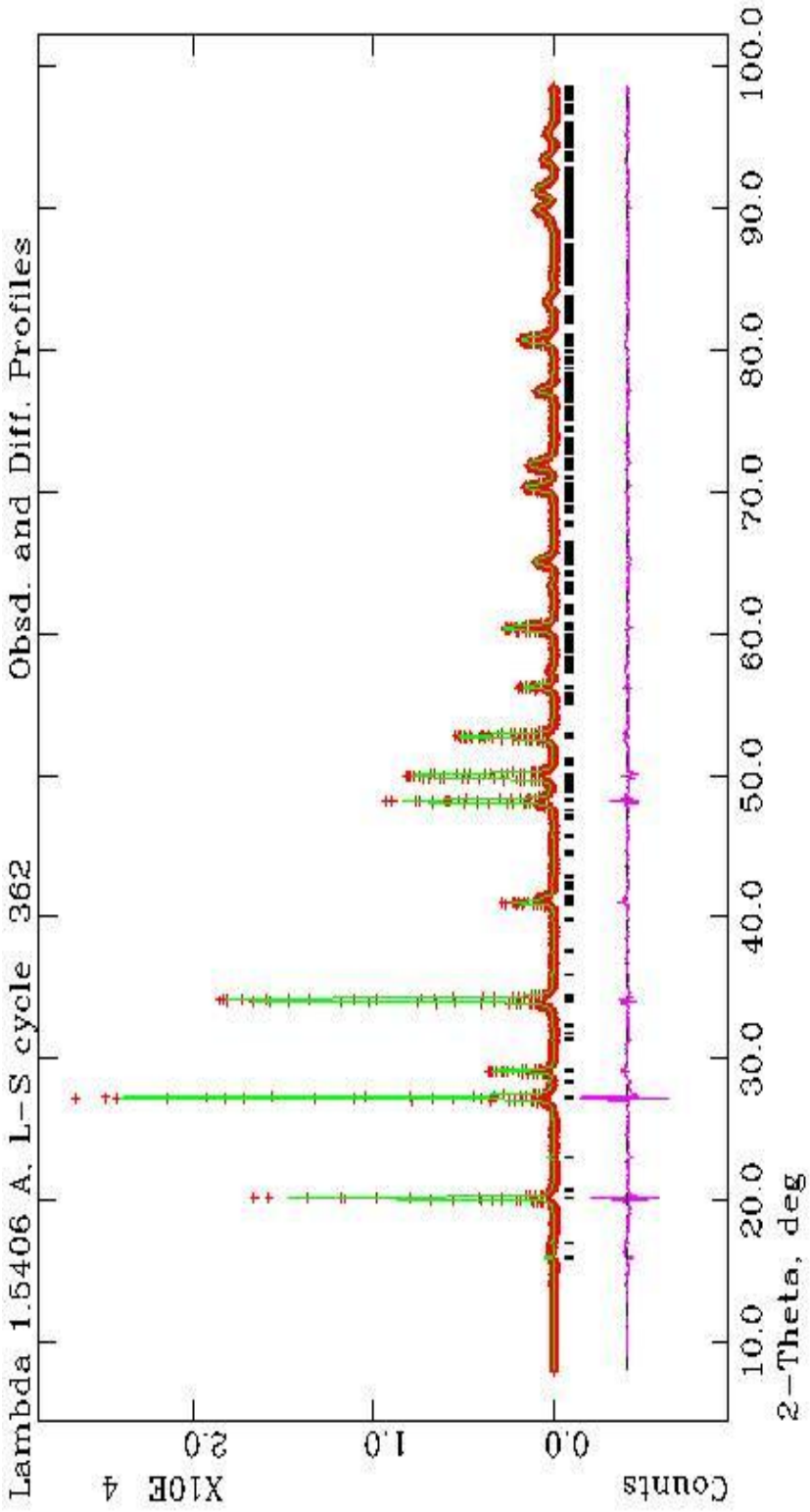

Figure. 3.27. Observed, calculated and difference X-ray diffraction profile for YBO_3 with approximate intensity scale depending upon the angular area. Crosses indicate the observed data and the solid line shows the calculated profile. All possible Bragg reflections are indicated with vertical markers below the profile.

Table 3.11. Crystal data and structure refinement results for YBO_3

Emprical Formula	YBO_3
Molar mass	147.7 g/mol
Crystal System	Monoclinic
Space Group	*C2/c*
Powder diffractometer	Panalytical X'Pert Pro
Radiation	CuKα(λ=1.54051Å)
Unit-cell dimensions	a=11.3276(3) Å
	b=6.5444(2) Å
	c=9.5589(1) Å
	β=112.955(1) ^{o}
Volume	652.512 (9)Å^3
Step (^{o})	0.013
2 Theta Range	10-150 ^{o}
R_{wp}	0.0421
R_p	0.0301
χ^2	3.289

Table 3.12. Crystallographic data of the Low-Temperature Phase of $(Y_{0.92}Er_{0.08})BO_3$ (Lin et al. 2004).

Emprical Formula	$(Y_{0.92}Er_{0.08})BO_3$		
Molar mass	147.7 g/mol		
Crystal System	Monoclinic		
Space Group	*C2/c*		
Synchrotron Radiation	Swiss Light Source		
Radiation	λ=0.9531Å		
Unit-cell dimensions	a=11.3140(3) Å		
	b=6.5404(2) Å		
	c=9.5503(2) Å		
	β=112.902(1) ^{o}		
R_{wp}	4.72%		
R_p	3.61%		
χ^2	12.7		
Atom	x	y	z
Y1/Er1	0.25	0.25	0
Y2/Er2	0.843(5)	0.2561(6)	0.5007(8)
B1	0.1220(5)	0.0382(9)	0.2476(5)
B2	0	0.678(1)	0.25
O1	0.1258(6)	0.083(1)	0.1057(5)
O2	0.2209(5)	0.090(1)	0.3894(4)
O3	0.0478(5)	0.565(1)	0.3938(5)
O4	0.3932(6)	0.309(1)	0.2543(7)
O5	0	0.1399(17)	0.25

Table 3.13. Fractional atomic coordinates and isotropic displacement parameters $U_{iso}(Å^2)$ for YBO_3

Atom	x	y	z	$U_{iso}(Å^2)$
Y1	0.25	0.25	0.0	0.02157
Y2	0.0827(6)	0.2522(4)	0.500(1)	0.02508
B1	0.154(3)	0.013(2)	0.242(3)	0.025
B2	0.0	0.699(3)	0.25	0.025
O1	0.128(1)	0.098(3)	0.1074(7)	0.0068
O2	0.228(1)	0.083(4)	0.3894(8)	0.02656
O3	0.049(1)	0.557(3)	0.3895(7)	0.02245
O4	0.362(2)	0.342(1)	0.252(2)	0.06537
O5	0.0	0.150(2)	0.25	0.02997

Table 3.14. Selected bond distances and angles for YBO_3.

Distances			
B1-O1	1.33816(2)	Y1-O1	2.25268(4)
B1-O2	1.41094(2)	Y1-Y2	3.79339(8)
B1-O4	1.13935(3)	Y2-Y2	3.74671(8)
B1-O5	1.995(5)	Y1-B1	2.85347(4)
B2-O3	1.42794(2)	Y2-B1	2.74627(4)
Y2-O1	2.40792(6)	O4-O2	2.06944(4)
Y2-B2	2.93645(4)	O4-O1	2.13223(4)
Angles			
O1-B1-O2	131.091(1)	O1-Y1-O4	99.752(1)
O1-Y1-O1	179.980(0)	O2-Y1-O3	68.880(1)
B1-Y2-O1	28.868(0)	B1-Y2-O4	24.050(0)
O1-Y2-O1	78.150(1)	O2-Y2-O3	175.466(0)
O1-Y2-O4	98.609(1)	O2-Y2-O4	79.421(1)
O1-Y2-O3	110.284(1)	O3-Y2-O4	69.929(1)
O1-Y2-O5	95.34(24)	O4-Y2-O5	146.54(23)
Y2-B1-O1	64.490(2)	Y1-O3-Y2	99.775(2)
Y2-B1-O4	55.163(1)	Y2-O3-Y2	105.582(1)
Y1-O1-B1	132.401(1)	Y1-O4-Y2	145.407(1)
Y2-O1-Y2	101.850(1)	Y1-O4-B1	106.127(1)
Y2-O1-B1	113.883(1)	Y2-O4-B1	100.786(1)
Y2-O1-B1	86.642(1)	Y2-O5-Y2	146.1(5)

Distances are given in Å and angles in degrees (^{o}).

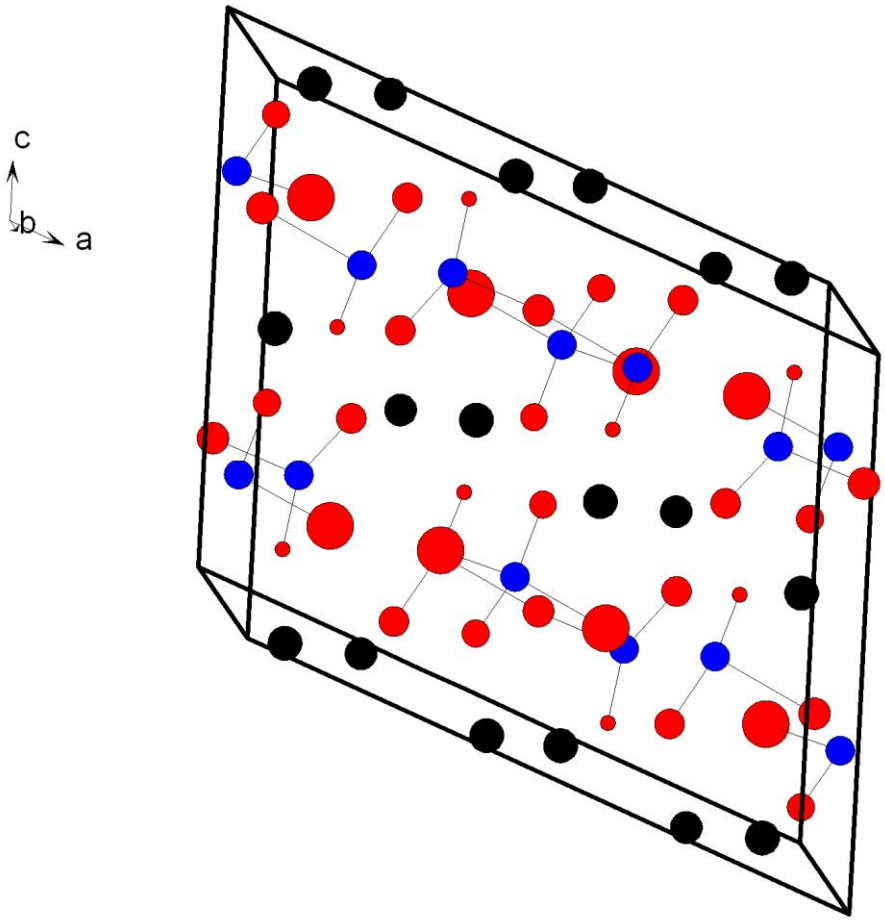

Figure 3.28. Crystal structure of YBO_3 (Blacks: Y atoms, Blues: B atoms, Reds: O atoms).

3.4.3.2. Structures of $LaBO_3$, and $NdBO_3$ with Pnma Space Group

According to structural model of $NdBO_3$ (ICSD Card No: 01-041-2407) we refined the structure parameters of $LaBO_3$ and $NdBO_3$ from the X-ray diffraction data by Rietveld method using the computer program GSAS. Figure A.5. and the Figure A.6. shows the Rietveld refinement results for $LaBO_3$ and $NdBO_3$, respectively.

The results of the Rietveld refinements of $LaBO_3$ and $NdBO_3$ are summarized in Table E.3. and Table E.4., respectively. The refinements converged smoothly as seen in Figure A.5. and A.6. The $LaBO_3$ crystallize in orthorhombic system with the following refined unit cell parameters at room temperature a=5.8761(1) Å, b=5.10535(9) Å, c=8.252(1) Å. The refinement leads to the residual values of R_p=0.0844, R_{wp}=0.1076 and χ^2= 5.101. Since Müller-Bunz et al. (2003) synthesized single crystal product, we can not compare the residual values which is always lower than X-ray diffraction results but these values are quite reasonable. χ^2 value 5.101 seems quite higher but this is resulted from using $NdBO_3$ data for $LaBO_3$ indexing which is quite larger in atomic size. The residual values of $NdBO_3$ are R_p=0.0691, R_{wp}=0.0544 and χ^2=1.958 with better fit to the Muller-Bunz structural model (Table E.4.).

The final atomic coordinates and the equivalent isotropic displacement parameters for orthorhombic $LaBO_3$ and $NdBO_3$ given in Table E.9. and Table E.10., respectively. These final positions are quite similar with the values given in ICSD Card No: 01-041-2407. The selected bond length and angles of orthorhombic lanthanide and neodymium orthoborates were demonstrated in Table E.16. and Table E.17. While the B-O distances were found between 1.35(1) Å and 1.40(3) Å for $LaBO_3$ structure, the very similar bonds lenths found as 1.352(5) Å and 1.40685(2) Å for $NdBO_3$. The Nd-O bond distances are in between 2.22027(5) Å and 2.53378(4) Å. The two O-B-O angle were found as 117.0(1) ^{o} and 122.6(2) ^{o} for $LaBO_3$ structure.

The crystal structure of $LaBO_3$ and $NdBO_3$ were obtained from these refinement results and crystal structures were given in Figure 3.29. and Figure F.3., respectively, by using Diamond (2000-2006). Trigonal BO_3 anions are easily seen in this orthorhombic structure.

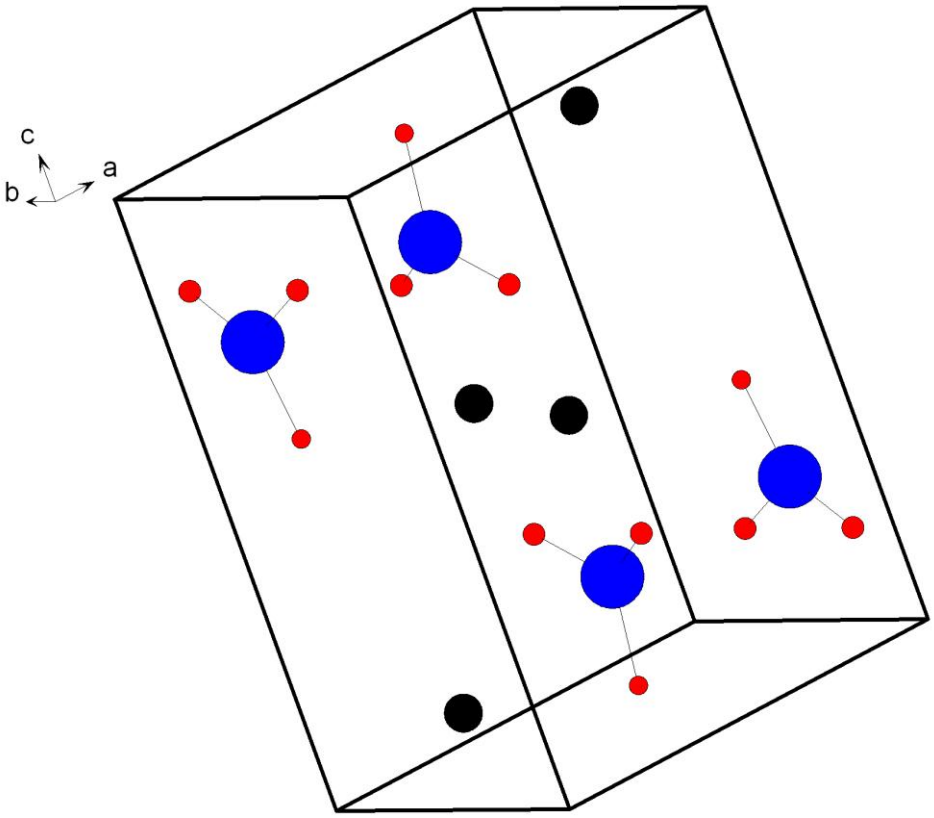

Figure 3.29. The crystal structure of $LaBO_3$. (Blacks: La atoms, Blues: B atoms, Reds: O atoms)

3.4.3.3. Structure of $SmBO_3$ P-1 with Space Group

By using the structural model given in $SmBO_3$ (ICSD Card No: 01-040-0745) we refined the structure parameters of our products from the X-ray diffraction data by Rietveld method using the computer program GSAS. The Rietveld refinement profile for triclinic $SmBO_3$ is given Figure A.7.

The results of the Rietveld refinements of $SmBO_3$ are summarized in Table E.5. The refinements converged smoothly as seen in Figure A.7. The $SmBO_3$ crystallize in triclinic system with the following refined unit cell parameters at room temperature a=6.4904(3) Å, b=6.4962(3) Å, c=6.2431(3) Å, α=107.764(3) ^{o}, β=107.703(3) ^{o}, γ=93.385(2) ^{o}. The space group of $SmBO_3$ is *P-1*. The refinement leads to the residual values of R_p=0.0532, R_{wp}=0.0682 and χ^2=3.227. The residual values of triclinic samarium orthoborate fit better with the structural model given in ICSD Card No: 01-040-0745.

The final atomic coordinates and the equivalent isotropic displacement parameters for orthorhombic $SmBO_3$ given in Table E.11. These final positions are quite similar with the values given in ICSD Card No: 01-040-0745. The selected bond length and angles of $SmBO_3$ orthoborate were demonstrated in Table E.18. The six B-O bond distances were found between 1.13935(3) Å and 1.995(5) Å for triclinic system while the Sm-O bond distances are in between 2.21042(6) Å and 3.00654(14) Å. The two O-B-O angles were found in between 91.045(3) ^{o} and 130.750(2) ^{o}.

Figure 3.30. shows the crystal structure of triclinic $SmBO_3$ along direction. The trigonal BO_3 groups can be seen from the figure. The samarium is in nine coordination in the triclinic cell.

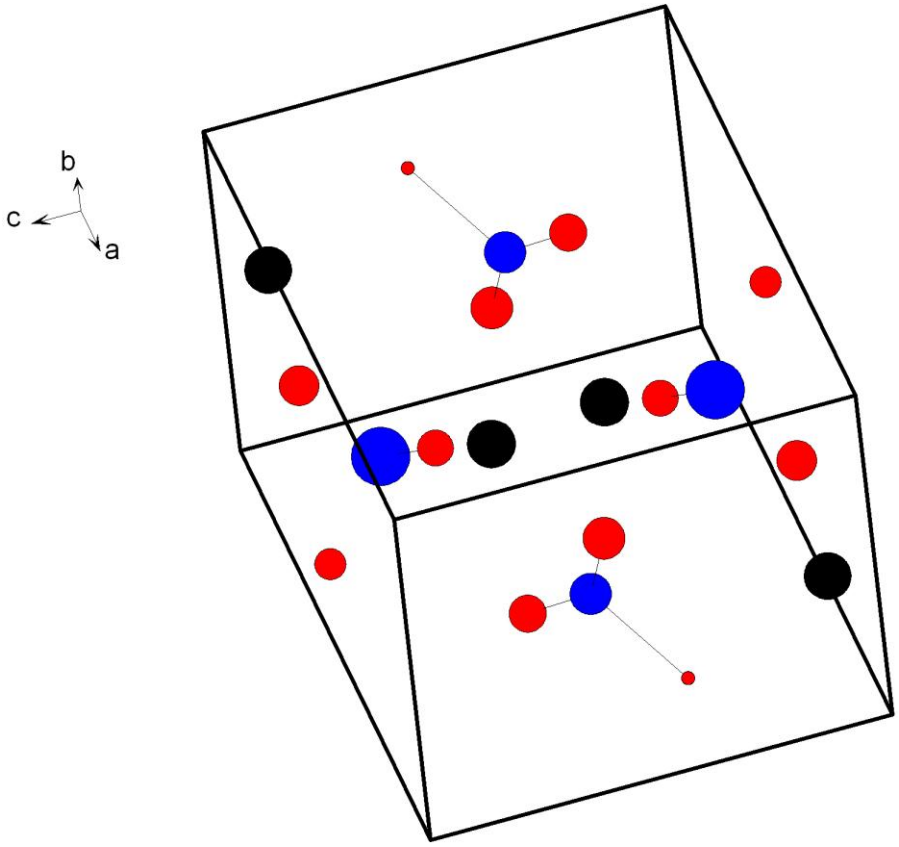

Figure 3.30. Crystal structure of $SmBO_3$ (Blacks: Sm atoms, Blues: B atoms, Reds: O atoms)

3.4.3.4. Structure of $GdBO_3$ with $R3_2$ Space Group

Since the space group work of vaterite structure is problematic, we used the all possible space groups mentined before to find out the best possible space group All attempts were failed and the refinements generally diverges for other space groups for $GdBO_3$. Only possible space group is $R3_2$ as mentioned in Ren et al. (1999).

Ren et al. (1999) reported the structure of $GdBO_3$ orthoborate structure. In this work, the phase purity of $GdBO_3$ powder samples was examined by X-ray diffraction. They derived the rhombohedral lattice constants from electron diffraction and refined from X-ray diffraction pattern, are a=6.6357(2) Å and c=26.706(1) Å. Ren et al. (1999) could not identify the boron atoms from the refinement, because their scattering power is too small. They were inserted into the structure by considering the structure of the polyborate group $B_3O_9^{9-}$. The unit cell values and the atomic positions given in Table E.12. were used as a structural model for our $GdBO_3$ product. The refinement converged and the calculated goodness-of-fit parameters remained low (χ^2= 2.590) showing good fit and chemically reasonable structure. The refined unit cell parameters for $GdBO_3$ at room temperature are a=6.63899(8), c=26.7219(5) Å for our case.

Table E.6 summarized the results of the Rietveld refinement and the corresponding profiles are shown in Figure A.8. The differecence plot are very similar to profile given in Ren et al. (1999) and the same difference curve was obtained in this work. Their refinement leads to the residual value of R_p=0.12 and R_{wp}=0.16, while same residuals were found as R_p=0.032 and R_{wp}=0.0454. When we compare the better residual values with the literature ones, one can easily see that this hexagonal model was fitted well.

The final atomic coordinates and the equivalent isotropic displacement parameters for $GdBO_3$ given in Table E.13.

The selected bond lengths and angles of rhombohedral $R3_2$ cell were demonstrated in Table E.19. In the $GdBO_3$ structure, the B-O distances were found as 1.28037(2) Å, 1.68689(1) and 1.75480(1) Å, respectively. The Gd-O bond distances are in between 2.21827(2) Å and 2.54225(3) Å. The O-B-O angle were found between 103.580(1) ^{o} and 143.991(1) ^{o}. Diamond (2000-2006) software program was used to draw crystal structure of $GdBO_3$ and the structure is given in Figure 3.31. The long c-cell and the $B_3O_9^{9-}$ anions can be derived from the structure. This structure was solved from the diffraction and it is very similar to the structure (Figure 1.12.) represented by Ren et al. (1999) in section 1.3.2.

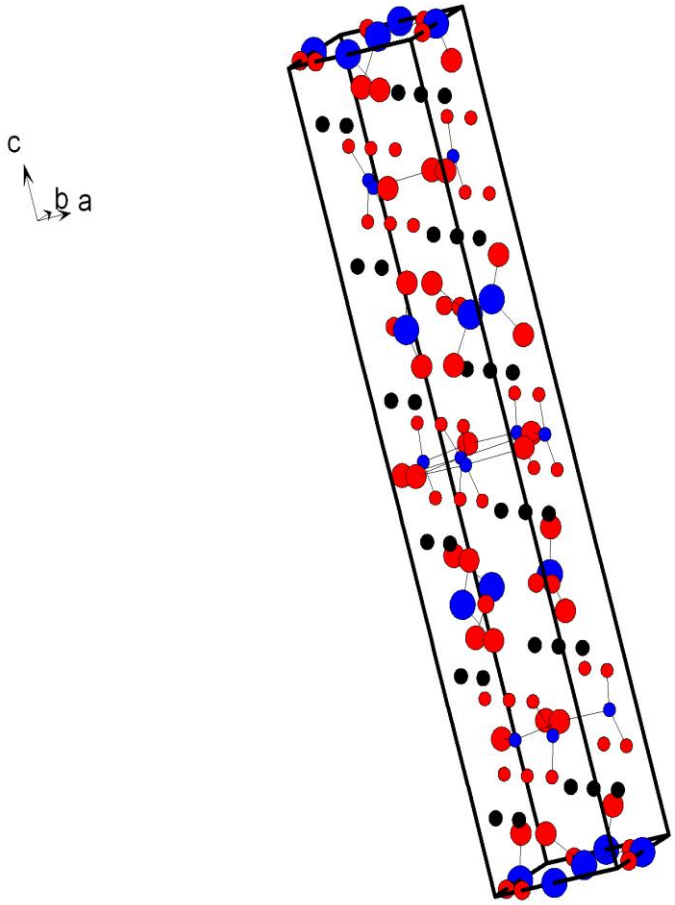

Figure 3.31. Shows the crystal structure of $GdBO_3$ (Blacks: Gd atoms, Blues: B atoms, Reds: O atoms)

CHAPTER 4

CONCLUSIONS AND RECOMMENDATIONS

Borate and phosphate compounds are currently very attractive to the scientific community owing to their wide range of applications. In this thesis, it was aimed to synthesize and characterize sodium lanthanide oxide phosphates, rare earth added strontium pyrophosphates and rare earth orthoborates. It was shown for the first time in this study that new orthorhombic lanthanide oxide phosphates were synthesized; thermoluminescence and structural studies of rare earth added $Sr_2P_2O_7$ were applied; $LnBO_3$ (Ln= La, Nd, Dy, Ho) were synthesized by using microwave-assisted solid state synthesis with submicron particle sizes; and structural determination of all rare earth borates (Ln=Y, La-Lu) were investigated via Rietveld refinement. In the light of experimental test results obtained at the end of this investigation, the following conclusions can be driven:

1. In the first set of sodium lanthanide oxide phosphate compounds, Na_2LaOPO_4, Na_2NdOPO_4, and Na_2SmOPO_4 have unit cell parameters of a= 13.60(1), b=12.71(1), c=6.96(1); a= 13.466(5), b=12.547(6), c=6.932(5); a= 13.54(1), b=12.577(8), c=7.047(5) Å, respectively and the space group is *Pmm2*. The splitting of the peaks in the X-ray diffraction patterns was observed in all compounds in the first set at d=3.35 and 3.30 Å, d=3.29 and 3.25 Å, d=3.29 and 3.25 Å, respectively. By the help of the same procedure, new orthorhombic Na_2DyOPO_4, Na_2HoOPO_4, Na_2ErOPO_4, and Na_2YbOPO_4 were synthesized the first time in the literature at 1100 ^oC. The indexing of the data showed that Na_2GdOPO_4 and the new products are also orthorhombic with the unit cell paramaters a=13.37(1), b=12.775(9), c=6.910(9); a= 13.66(2), b=12.609(9), c=6.611(6); a=13.148(4), b=12.577(2), c=6.967(1);

a=13.563(5), b=12.604(4), c=7.003(3); a=13.501(7), b=17.579(9), c=6.729(4) Å for Na_2DyOPO_4, Na_2HoOPO_4, Na_2ErOPO_4, and Na_2YbOPO_4, respectively and the space group of this set is also *Pmm2*. However, splitting of X-ray diffraction peaks between d=3.35 and 3.30 Å were not observed throughout the second set. If the single crystals of these compounds would be obtained, structural results will be more reliable.

2. The orthorhombic $Sr_2P_2O_7$ were obtained by solid state reaction with a=8.900(2), b=13.151(2), and c=5.402(2) Å unit cell parameters. The unit cell parameters of the other samples were fluctuated in between a=8.909(5)-8.877(5), b=13.163(3)-13.12(1), and c=5.403(2)-5.386(4) Å. The cubic ZrP_2O_7 (a=24.74(1) Å) addition is the reason for these changes. The glow curves of the $Sr_2P_2O_7$ added with ZrP_2O_7 exhibit one strong glow peak at around 100 ^oC. The intensity of prominent glow peak at 100 ^oC is continuously increased with decreasing concentration of ZrP_2O_7 among the set 2. The TL sensitivity of these samples when compared with the well known dosimetric material LiF:Mg,Ti (TLD-100) are much more than TLD-100.

3. XRD studies of 5% CuO and rare earth oxides (Y_2O_3, La_2O_3, CeO_2, Pr_6O_{11}, Nd_2O_3, Sm_2O_3, Eu_2O_3, Gd_2O_3, Tb_2O_3, Dy_2O_3, Ho_2O_3, Er_2O_3, Tm_2O_3, Yb_2O_3, Lu_2O_3) 0.5-15% (by weight) added $Sr_2P_2O_7$ showed that addition did not affect our host structure but only small shifts observes in XRD patterns of added samples. The TL glow curve of pure $Sr_2P_2O_7$ consists of only one glow peak at around 100 ^oC [Seyyidoğlu et al (2007)]. On the other hand, Pr, Ho, and Nd along with Cu-added samples showed two glow peaks, one of them is always at around 90 ^oC and the second TL peak around 180, 275, and 285 ^oC, respectively. So, it can be thought that the first peak at ≈90 ^oC in all samples should be related with host samples but the second peak above 150 ^oC with the added elements.

As a conclusion, this work investigated the TL properties of $Sr_2P_2O_7$ which is added with rare-earth oxides series and CuO together. Many of the results gave TL glow curves but not so intense and no glow peaks around 200 ^oC. Yet, Pr, Nd, Ho, and Er along Cu-added samples resulted with very intense, sharp peaks in TL glow curves around 200 ^oC. In order to investigate effect of different metal oxides addition on the TL properties of $Sr_2P_2O_7$, various metal oxides will be added together with rare earth metal oxides.

4. XRD studies revealed that while $LaBO_3$ and $NdBO_3$ samples prepared by both solid state and microwave-assisted synthesis with urea and sucrose has the same orthorhombic crystal structure with *Pnma* (aragonite-type) space group, the $DyBO_3$ and $HoBO_3$ orthoborates has hexagonal crystal structure with space group of *P-6c2* (vaterite-type). It is obviously seen that particles has submicron (<1μm) size, most of them has around 500 nm particle size in diameter and homogenously distributed for samples prepared by urea and sucrose. The particle sizes of direct solid state products are larger than 1μm and particles have not equal size and the distribution is random. This microwave irradiation method, with using cheap microwave active organic additives such as sucrose and urea and requiring no expensive equipments, will ensure good purity in the products, reduce the particle size of products and greatly reduce the production cost, and will thus offer a simple and rapid synthetic route for other functional inorganic materials. The effects of various microwave active organic molecules on the structure and the size of rare earth orthoborate particles can be investigated in future.

5. YBO_3 crystallize in monoclinic system at room temperature with the unit cell parameters of a=11.3276(3), b=6.5444(2) Å, c=9.5589(1) Å, β=112.955(1) ^{o}, V=652.512(9) $Å^3$ with the *C2/c* space group. The overall value of goodness-of-fit (χ^2) 3.289 is obviously better than 12.7 given in Lin et al. (2004) showing good fit for this model.

The same space group *C2/c* is tried for $DyBO_3$ and $HoBO_3$ and it is found 1.96 and 3.968 for χ^2 values for $DyBO_3$ and $HoBO_3$ showing a good fit and chemically reasonable structure.

6. The $LaBO_3$ crystallize in orthorhombic system (Pnma) with the following refined unit cell parameters at room temperature a=5.8761(1) Å, b=5.10535(9) Å, c=8.252(1) Å. The refinement leads to the residual values of R_p=0.0844, R_{wp}=0.1076 and χ^2 = 5.101 while the residual values of $NdBO_3$ are R_p=0.0691, R_{wp}=0.0544 and χ^2=1.958 with better fit to the Muller-Bunz (2003) structural model.

7. The $SmBO_3$ crystallize in triclinic system with the following refined unit cell parameters at room temperature a=6.4904(3) Å, b=6.4962(3) Å, c=6.2431(3) Å, α=107.764(3) ^{o}, β=107.703(3) ^{o}, γ=93.385(2) ^{o}. The space group of $SmBO_3$ is *P-1*. The refinement leads to the residual values of R_p=0.0532, R_{wp}=0.0682 and χ^2=3.227. The residual values of triclinic samarium orthoborate fit better with the structural model given in ICSD Card No: 01-040-0745.

8. The refined unit cell parameters for $GdBO_3$ at room temperature were found as a=6.63899(8), c=26.7219(5) Å. Ren et al. (1999) find the residuals as R_p=0.12 and R_{wp}=0.16, while same residuals were found as R_p=0.032 and R_{wp}=0.0454 for our product showing better fit for this $R3_2$ rhombohedral model. All of rare earth orthoborate structures will be confirmed by synthesizing single crystals of these compounds and making single crystal structural analysis.

REFERENCES

Abdullaev G.K., Dzhafarov G.G., Mamedov Kh.C., Azerbaidzhanskii Khim. Zh., 3, 1976, 117-120.

Abrahams S.C., Bernstein J.L., Keve E.T., J. Appl. Cryst., 4, 1971, 284-290.

Altermatt U.D., Brown I.D., Acta Cryst., A34, 1987, 125-130.

Amezawa K., Tomii Y., Yamamoto N., Solid State Ionics, 176, 2005, 143-148.

Amezawa K., Tahahashi, N., Kitamura N., Tomii Y., Yamumoto N., Solid State Ionics, 175, 2004, 575-579.

Antic-Fidancev E., Aride J., Chaminade J., Lemaitre-Blaise M., Porcher P., J. Solid State Chem., 97, 1992, 74-81.

Assaaoudi H., Butler I.S., Kozninski J.A., Solid State Sciences, 8, 2006, 1353-1360.

Assaaoudi H., Butler I.S., Kozinski J., Belanger-Gariepy F., J. Chemical Crystallography, 35, 10, 2005, 809-820.

Baran E.J., Mercader R.C., Massafero A., Kremer E., Spectrochimica Acta Part A, 60, 2004, 1001-1005.

Becker, P., Z. Kristallogr. 216, 2001, 523–533.

Belokoneva E.L., Crystallography Reviews, 11, 3, 2005, 151-198.

Beregi E., Watterich A., Madarasz J., Toth M., Polgar K., J. Cryst. Growth, 237-239, 2002, 874-878.

Bhaumik I., Moorthy S.G., Bhatt R., Sundar R., Karnal A.K., Wadhawan V.K., J. Crystal Growth, 243, 2002, 522-525.

Bradley W.F., Graf D.L., Roth R.S., Acta Cryst., 20, 1966, 283-287.

Brandenburg. K.. Diamond (Version 2.1a), Crystal Impact GbR. Bonn. Germany 1996-1999.

Bohlhoff R., Bambauer H.U., Hoffman W., Z.Kristallogr., 133, 1971, 386.

Boutfessi A., Boukhari A., Holt E.M., Acta Cryst. C42, 1996a, 1594-1597.

Boutfessi A., Boukhari A., Holt E.M., Acta Cryst. C42, 1996b, 1597-1599.

Boyer D., Bertrand-Chadeyron G., Mahiou R., Lou L., Brioude A., Mugnier J., 16 Opt. Mater., 2001, 21.

Boyer D., Bertrand-Chadeyron G., Mahiou R., Caperaa C., Cousseins J.C., J. Mater. Chem., 9, 1999, 211.

Boyer D., Bertrand G., Mahiou R., J. Luminescence, 104, 2003, 229-237.

Carvajal J.J., Nikolov V., Sole R., Gavalda J., Massons J., Aguilo M., Diaz F., Chem. Mater. 14, 2002, 3136-3142.

Carvajal J.J., Sole R., Gavalda J., Massons J., Aguilo M., Diaz F., Crystal Growth & Design 1 (6), 2001, 479-484.

Chadeyron G., El-Ghozzi M., Boyer D., Mahiou R., Cousseins C., J. Alloys Comp., 317-318, 2001, 183-185.

Chadeyron G., El-Ghozzi M., Mahiou R., Arbus A., Cousseins C.,J. Solid State Chem., 128, 1997a, 261-266.

Chadeyron G., Mahiou R., El-Ghozzi M., Arbus A., Cousseins J.C., J. Luminescence, 72-74, 1997b, 564-566.

Chani V.I., Shimamura K., Endo S., Fukuda T., J. Cryst. Growth 169, 1996, 604-605.

Chani V.I., Shimamura K., Endo S., Fukuda T., J. Cryst. Growth 173, 1997, 117-122.

Chani V.I., Fukuda T., J. Cryst. Growth 206, 1999, 245-248.

Chen, R., Mckeever, S.W.S. *Theory Of Thermoluminescence And Related Phenomena.* Singapoure: World Scientific, 1997.

Chernaya V.V., Mitaev A.S., Chizhov P.S., Dikarev E.V., Shapanchenko R.V., Antipov E.V., Korolenko M.V., Fabritchnyi P.B., Chem. Mater., 17, 2005, 284-290.

Chinn S.R., Hong H.Y.P., Optical Communication, 18, 1976, 87.

Cohen-Adad M.T., Aloui-Lebbou O., Goutadier C., Panczer G., Dujardin C., Pedrimi C., Florian P., Massiot D., Gerard F., Kappenstein C., J. Solid State Chem., 154, 2000, 204-213.

Corbel G., Leblanc M., Antic-Fidancev E., Lemaitre-Blaise M., Krupa J.C., J. Alloys Comp., 287, 1999, 71-78.

Cui X., Zhuang, W., Yu, Z., Xia T., Huang, X., Li H., J. Alloys Comp., 451, 2008, 280-285.

Cullity B.D., Stock S.R., Elements of X-ray Diffraction, 3rd Edition, Prentice- Hall Inc., New Jersey, 2001.

Cuong, T.T., Dung, P.T. , Hain,Q., Ha V.T.T Hung N.M., Khoi N.T., Ku N.X., Quang V.X., Thanh N.T. ,Thanh N.Q. "Preparation And Dosimetric Characterization Of Some Thermallystimulated Luminescence Materials In The Radiotherapy." *Proceedings Of The Ninth Asia Pacific Physics Conference.* Hanoi, Vietnam, 2004.

Dhage S.R., Khollam Y.B., Potdar H.S., Deshpande S.B., Bakare P.P., Sainkar S.R., Date S.K., Materials Letters, 57, 2002, 457-462.

Denning J.H., Ross S.D., Spectochim. Acta, 28A, 1972, 1775-1785.

Doat A., Pelle F., Lebugle A., J. Solid State Chem., 178, 2005, 2354-2362.

Emme H., Huppertz H., Acta Cryst., C60, 2004, i117-i119.

Felten E.J., Journal of Inorganic Nuclear Chemistry, 19, 1961, 61-64.

Ferid M., Horchani-Naifer K., Mat. Res. Bull., 39, 2004a, 2209-2217.

Ferid M., Horchani K., Amami J., Mat. Res. Bull., 39, 2004b, 1949-1955.

Filatov, S. K. & Bubnova, R. S., Phys. Chem. Glasses, 41, 2000, 216–224.

Fukuda K., Moriyama A., Hashimoto S., J. Solid State Chem., 177, 2004, 3514-3521.

Gomez I., Hernandez M., Aguilar J., Hinojosa M.,Ceramics International, 30, 2004, 893-900.

Goryunova A., PhD. Thesis, 2003, Üniversitat zu Köln, 'Beitrag zur Kristallchemie und Kristallsynthese binaer Seltenerdborate vom Typ SEB_3O_6 und $SEBO_3$'.

Goubin F., Montardi Y., Deniard P., Rocquefelte X., Brec R., Jobic S., J.Solid State Chem., 117, 2004, 89-100.

Gover R.K.B., Withers N.D., Allen S., Withers R.L., Evans J.S.O., J. Solid State Chem., 166, 2002, 42-48.

Gönen Z.S., Kizilyalli M., Pamuk H.Ö., J. Alloys and Compounds 303-304, 2000, 416-420.

Griesel L., Bartley J.K., Wells R.P.K., Hutchings G.J., J. Molecular Catalysis A: Chemical 220, 2004, 113-119.

Guler H., Kurtulus F., J. Material Science, 40, 2005, 6565-6569.

Hamady A., Zid M.F., Jouini T., J. Solid State Chem., 113, 1994, 120-124.

Henkels A.E., Schaak R.E., J. Solid State Chem., 181, 2008, 3264-3268.

High Score Plus Software, Version 2.2c., Panalytical, Nederland, 2007.

Hirai H., Masui T., Imanaka N., Adachi G.Y., J. Alloys Comp., 374, 2004, 84-88.

Hosokawa S., Tanaka Y., Iwamoto S., Inoue M, J. Mater. Sci. , 43, 2008, 2276-2285.

Hölsa J., Inorg. Chim. Acta, 139, 1987, 257-259.

Huili L., Jing Z., Lei M., Quiu Z., Journal of Rare Earths, 25, Suppl., 2007, 34-36.

Huppertz H., Z. Naturforsch., 2001, 56 b, 697–703.

Husson E., Genet F., Lachar A., Piffard Y., J. Solid State Chem., 75, 1988, 305.

Hu X.B., Liu H., Wang J.Y., Zhang H.J., Jiang H.D., Jiang S.S., Li Q., Tian Y.L., Huang Y.Y., Huang W.X., He W., Optical Materials 23, 2003, 369-372.

Inorganic Crystal Structure Database (ICSD), Fachinformationszentrum Karlsruhe. Germany, 2005

ICSD Card No: 01-040-0745.

ICSD Card No: 01-041-2407.

ICSD Card No: 01-074-1929.

ICSD Card No: 01-074-1931.

ICSD Card No: 01-074-1932.

ICSD Card No: 01-074-1933.

ICSD Card No: 01-074-1934.

ICSD Card No: 01-074-1935.

ICSD Card No: 01-074-1936.

ICSD Card No: 01-074-1937.

ICSD Card No: 01-074-1938.

ICSD Card No: 01-072-1053.

ICSD Card No: 01-089-7988.

Idrissi M.S., Rghioui L., Nejjar R., Benarafa L**.,** Lorriaux A., Wallart F., Spectrochimica Acta Part A 60, 2004, 2043-2052.

Inoue S., Ohtaki N., J. Chromatography, 645, 1, 1993, 57-65.

Jazouli A.E., Krımı S., Manoun B., Chaminade J.P., Gravereau P., Waal D.D., Ann. Chim. Sci. Mat. 23, 1998, 7-10.

Jenkins R., Snyder R.L., Introduction to X-ray Powder Diffractometry, A Wiley-Interscience Publication, New York, 1996.

Jiang X.C., Sun L.D., Feng W., Yan C.H., Crystal Growth and Design, 4, 3, 2004a, 517-520.

Jiang X-C., Sun L-D., Yan C-H., 108, J. Phys. Chem. B, 2004b, 3387.

Jiang X.C., Yan C.H., Sun L.D., Wei Z.G., Liao C.S., J. Solid State Chem., 175, 2003, 245-251.

Ketatni M., Abraham F., Mentre O., Solid State Sciences 1, 1999, 449-460.

Ketatni E.M., Huve M., Abraham F., Mentre O., J. Solid State Chem. 172, 2003, 327-338.

Khay N., Ennaciri AA., Harcharras M., Vibrational Spectroscopy 27, 2001a, 119-126.

Khay N., Ennaciri AA., J. Alloys Comp., 323-324, 2001b, 800-805.

Khosrovani N., Korthuis V., Sleight A.W., Inor. Chem., 35, 1996, 485-489.

Klassen N.V., Shmurak S.Z., Shmyt'ko I.M., Strukova G.K., Derenzo S.E., Weber M.J., Nuclear Instruments and Methods in Physics Research A, 537, 2005, 144-148.

Kling A., Rico M., Zaldo C., Aguilo M., Diaz F., Nuclear Instrumnets and Methods in Physics Research B, 218, 2004, 271-276.

Kloss M., Finke B., Schwarz L., Haberlandl D., J. Luminescence 72-74, 1997, 684-686.

Kim C.H., Yim H.S., Solid State Communications 110, 1999, 137-142.

Kim D.S., Lee R.Y., J. Materials Science, 35, 2000, 4777-4782.

Kim K.N., Jung H.K., Park H.D., Kim D. J Mater. Res., 17, 2002, 907.

Kim T., Kang S., 40, Mater. Res. Bull., 2005 , 1945.

Kistler, R.B., and Helvacı, C., Industrial Minerals and Rocks, 6th Edition, D.D. Carr, Senior Editor, Published by Society for Mining and Metallurgy and Exploration Inc., Littleton, Colorado, 171-186, 1994.

Kizilyalli M., Darras M., J. Solid State Chem., 107, 1993, 373-380.

Kizilyalli M., J. the Less-Common Metals, 127, 1987, 147-154.

Koseva J., Nikolov V., Peshev P., J. Alloys Comp., 353, 2003, L1-L4.

Kriz H.M., Bray P.J., J. Chem. Phys., 51, 1969, 3624-3625.

Laparches J., Tarte P., Spectochim. Acta, 22, 1996, 1201-1210.

Larson A.C. and Von Dreele R.B., "General Structure Analysis System (GSAS)", Los Alamos National Laboratory Report LAUR **2000**, 86-748.

Laureiro Y., Veiga M.L., Fernandez F., Saez-Puche R., Jerez A., Pico C., Journal of the Less-Common Metals, 167, 1991, 387-393.

Laureiro Y., Veiga M.L., Fernandez F., Saez-Puche R., Jerez A., Pico C., Journal of the Less-Common Metals, 157, 1990, 3335-341.

Le Bail A., Duroy H., Fourquet J.L., Mater. Res. Bull. 23, 1988, 447-452.

Ledain S., Leclaire A., Borel M.M., Raveau B., Acta Cryst. C42, 1996, 1593-1594.

Lemanceau S., Chadeyron G.B., Mahiou R., El-Ghozzi M., Cousseins J.C., Conflant P., Vannier R.N., J. Solid State Chem., 148, 1999, 229-235.

Leonyuk N.I., Leonyuk L.I., Crystal Chemistry of Anhydrous Borates, MSU, Moscow., 1983, in Russian.

Leonyuk N.I., J. Cryst. Growth, 174, 1997, 301-307.

Levin E.M., Roth R.S., Martin J.B., The American Minerologist, 46, September-October, 1961, 1030-1055.

Li L., Zhou S., Zhang S., Solid State Sciences, 10, 2008, 1173-1178.

Li Z., Zeng J., Chen C., Li Y., 286, J. Cryst. Growth, 2006, 487.

Li M.R., Liu W., Chen H.H., Yang X.X., Wei Z.B., Cao D.H., Gu M., Zhao J.T., European, J. Inorganic Chemistry, 23, 2005, 4693-4696.

Lin. J., Sheptyakov D., Wang Y., Allenspach P., Chem. Mater., 16, 2004, 2418-2424.

Lin J., Huang Y., Zhang J., Ding X., Qi S., Tang C., Materials Letters, 61, 2007, 1596-1600.

Lisnyak V.V., Stus N.V., Slobodyanik N.S., Belyavina N.M., Markiv V.Y., J. Alloys Comp., 309, 2000, 83-87.

Liu W., Shen H.Y., Zhang G.F., Zhang D.Y., Zhang G., Lin W.X., Zeng R.R., Huang C.H., Optics Communications 185, 2000, 191-196.

Lucas S., Champion E., Bregiroux D., Bernache-Assollant D., Audubert F., , J. Solid State Chem., 177, 2004a, 1302-1311.

Lucas S., Champion E., Bernache-Assollant D., Leroy G., J. Solid State Chem. 177, 2004b, 1312-1320.

Mahesh K., Weng, P.S., Furetta, C. *Thermoluminescence In Solids And Its Applications.* Ashford, Kent,England: Nuclear Technology Publishing, 1989.

Manoun B., El Jazouli A., Gravereau P., Chaminade J.P., Mat. Res. Bull., 40, 2005, 229-238.

Marcu I.C., Millet J.M.M., Herrmann J.M., Catalysis Letters, 78, 1-4, 2002, 273-279.

Masciocchi N., The Rigaku Journal, 14, 2, 1997, 9-16.

McCusker L.B., Von Dreele R.B., Cox D.E., Louer D., Scardi P., J. Appl. Crys. 32, 1999, 36-50.

Meyer H.J., Skokan A., Naturwissenschaften, 58, 1971, 566.

Meyer H.J., Naturwissenschaften, 56, 9, 1969, 458-459.

Meyer H.J., Naturwissenschaften, 59, 5, 1972, 215.

Mirji S.A., Khollam Y.B., Deshpande S.B., Potdar H.S., Bathe R.N., Sainkar S.R., Date S.K., Materials Letters, 58, 2004, 837-841.

Miyamoto A., Mori Y., Okada Y., Sasaki T., Nakai S., J. Cryst. Growth, 156, 1995, 303-306.

Mizrahi A., Wignacourt J.P., Steinfink H., J. Solid State Chem., 133, 1997, 516-521.

Moorthy S.G., Kumar F.J., Subramanian C., Bocelli G., Ramasamy P., Materials Letters, 36, 1998, 266-270.

Moreno-Real L, Losilla E.R., Aranda M.A.G., Martinez-Lara M., Bruque S., Gabas M., J. Solid State Chemistry, 137, 1998, 289-294.

Müller-Bunz H., Nikelski T., Schleid T., Zeitschrift Naturforschung, 58b, 2003, 375-380

Nakamoto K., 'Infrared Spectra of Inorganic Compounds', Wiley Interscience, New York, 1971.

Nakatsuka A., Ohtaka O., Arima H., Nakayama N., Mizota T., Acta Cryst. E62, 2006, i103-i105.

Natarajan V., Bhide M.K., Dhobale A.R., Godbole S.V., Seshagari T.K., Page A.G., Lu C.H., Mat. Res. Bull. 39, 2004, 2065-2075.

Newnham R.E., Redman M.J., Santoro R.P., J. the American Ceramic Society, 46, 6, 1963, 253-256.

Noirault S., Joubert O., Caldes M.T., Piffard Y., Acta Cryst., E62, 2006, i228-i230.

Onada H., Nariai H., Maki H., Mtooka I., Materials Chemistry and Physics 73, 2002, 19-23.

Palkina K. K., Kuznetsov V. G., Butman L. A., Dzhurinskii B. F., 2Russ. J. Coord. Chem., 2, 1976, 286-289.

Palewska K., Miniewicz A., Bartkiewicz S., Legendziewicz J., Strek W., J. Luminescence, 124, 2007, 265-272.

Pelova V.A., Grigorov L.S., J. Luminescence 72-74, 1997, 241-243.

Pillai V.P.M., Thomas B.R., Nayar V.U., **Lii** K.H., Spectrochimica Acta Part A, 55, 1999, 1809-1817.

Plewa J., Jüstel T., Journal of Thermal Analysis and Calorimetry, 88, 2, 2007, 531-535.

Powder Diffraction File, Joint Committee on Powder Diffraction Standards, Swathmore, PA.

Powder Diffraction File No: 00-012-0762 ICDD, USA.

Powder Diffraction File No: 00-013-0478 ICDD, USA.

Powder Diffraction File No: 00-013-0483 ICDD, USA.

Powder Diffraction File No: 00-013-0486 ICDD, USA.

Powder Diffraction File No: 00-016-0277 ICDD, USA.

Powder Diffraction File No: 00-019-1427 ICDD, USA.

Powder Diffraction File No: 00-024-1011 ICDD, USA.

Powder Diffraction File No: 00-024-1491 ICDD, USA.

Powder Diffraction File No: 00-088-0356 ICDD, USA.

Pradhan, A.S,. "Thermoluminescence Dosimetry And Its Applications." *Radiation Protection Dosimetry*, 1981, 153-167.

Ren M., Lin J.H., Dong Y., Yang L.Q., Su M.Z., Chem. Mater. 11, 1999, 1576-1580.

Rietveld H.M., Acta Crystallogr. 22, 1967, 151-152.

Rietveld H.M., J. Appl. Crystallogr., 2, 1969, 65-71.

Roskill, The Economics of Boron, 10th Edition, 2002.

Roth M., Angert N., Tseitlin M., Schwarzman G., Zharov A., Optical Materials 26 (4), 2004, 465-470.

Roth M., Angert N., Tseitlin M., Alexandrovski A., Optical Materials 16, 2001, 131-136.

Schipper W.J., Piet J.J., De Jager H.J., Blasse G., Mat. Res. Bull., 29, 1994, 23-30.

Schwarz L., Finke B., Kloss M., Rhohmann A., Sasum U., Haberlandl D., J. Luminescence 72-74, 1997, 257-259.

Schwarz L., Kloss M., Rhohmann A., Sasum U., Haberlandl D., J. Alloys Comp. 275-277, 1998, 93-95.

Seyyidoglu S., Ozenbas M., Yazici N., Yilmaz A., J. Materials Science 42, 2007, 6453-6463.

Seyyidoglu S., Ozenbas M., Yilmaz A., Turkish J. Chemistry, 32, 2008, 1-20.

Smaalen S.V., Dinnebier R., Hanson J., Gollwitzer J., Bullesfeld F., Prokofiev A., Assmus W., J. Solid State Chemistry 178, 2005, 2225-2230.

Sole R., Ruiz X., Cabre R., Gavalda J., Aguilo M., Diaz F., Nikolov V., Solans X., J. Crystal Growth 167, 1996, 681-685.

Srilakshmi C., Ramesh K., Nagaraju P., Lingaiah N., Prasad P.S.S., Catalysis Letters 106, 3-4, 2006, 115-122.

Srivastava A.M., US Patent Application 0030067008, 2003.

Stock N., Ferey G., Cheetham A.K., Solid State Sciences, 2, 2000, 307-312.

Stus N.V., Dub S.N., Stratiychuk D.A., Linsyak V.V., J. Alloys Comp., 366, 2004, L13-L15.

Tie S.L., Li Y.Y., Yang Y.S., J.Phys.Chem Solids 58, 6, 1997, 957-961.

Tkachenko E.A., Mahiou R., Chadeyron G., Boyer D., Fedorov P.P., Kuznetsov S.V., Russian Journal of Inorganic Chemistry, 52, 6, 2007, 829-834.

Thompson, P., Cox, D.E., Hastings, J.B. J.Appl. Cryst. 20, 1987, 79-83.

Toby G.H., EXPGUI, a graphical user interface for GSAS, J. Appl.Crystallogr. 2001, 34, 210-213.

Touboul, M., Penin, N. & Nowogrocki, G., Solid State Sciences, 5, 2003, 1327–1342.

Trunov V.K., Oboznenko Y.V., Sirotikin S.P., Tskhelashvili N.B., Inorganic Materials, 27, 9, 1990, 1993-1994.

Trunov V.K., Oboznenko Y.V., Sirotikin S.P., Tskhelashvili N.B., Inorganic Materials, 27, 11, 1991, 2370-2374.

Tukia M., Hölsa J., Lastusaari M., Niittykoski J., Optical Materials, 27, 2005, 1516-1522.

Uztetik- Amour A., Kizilyalli M., J. Solid State Chem. 120, 1995, 275-278.

Varga T., Wilinson A.P., Haluska M.S., Payzant E.A., J. Solid State Chem., 178, 2005, 3541-3546.

Veenis A.W., Bril A., Philips J. Res., 33, 1978, 124.

Wang. F., Fan X., Pi D., Wang M., J. Solid State Chem., 177, 2004a, 3346-3350.

Wang X., Yuan X., Li W., Qi J., Wang S., Shen D., J. Cryst. Growth 237-239 (1), 2002, 672-675.

Wang Y.H., Wu C.F., Zang J.C., Mat. Res. Bull., 41, 2006, 1571-1577.

Weast R.C., CRC Handbook of Chemistry and Physics, 58th edition, CRC Press Inc., Florida, 1977, pp.213-214.

Wei Z., Sun L., Liao C., Yin J., Jiang X., Yan C., J. Phys. Chem. B, 106, 2002a, 10610-10617.

Wei Z-G., Sun L-D., Liao C-S., Jiang X-C., Yan C-H., 12, J. Mater. Chem., 2002b, 3665.

Withers R.L., Tabira Y., Evans J.S.O., King I.J., Sleight A.W., J. Solid State Chem., 157, 2001, 186-192.

Yang J., Zhang C., Wang L., Hou Z., Huang S., Lian H., Lin J., J. Solid State Chem., 181, 2008, 2672-2680.

Yuan G., Xue D., Acta Cryst., B63, 2007, 353-362.

Zaldo C., Rico M., Diaz F., Carvajal J.J., Optical Materials 13, 1999, 175-180.

Zaldo C., Martin M.J., Diaz F., Materials Letters 45, 2000, 107-110.

Zaldo C., Rico M., Martin M.J., Massons J., Aguilo M., Diaz, F. J. Luminescence, 79, 1998, 127-132.

Zhang J., Wang J., Ge B., Liu Y., Hu X., Boughton R.I., J. Cryst. Growth, 267, 2004, 517-521.

Zhang D.Y., Shen H.Y., Liu W., Chen W.Z., Zhang G.F., Zhang G., Zeng R.R., Huang C.H., Lin W.X., Liang J.K., J. Cryst. Growth 218 (2000), 98-102.

Zhang J., Lin J., J. Cryst. Growth, 271, 2004, 207-215.

Zhang Z., Zhang Y., Li X., Xu J., Huang Y., J. Alloys Comp., 455, 2008, 280-284.

Zhu H., Zhang L., Zuo T., Gu X., Wang Z., Zhu L., Yao K., Applied Surface Sciences, 254, 2008, 6362-6365.

APPENDIX A

XRD PATTERNS OF THE PRODUCED PHASES

Individual XRD patterns of the produced phases from the solid state reactions are presented in the following figures.

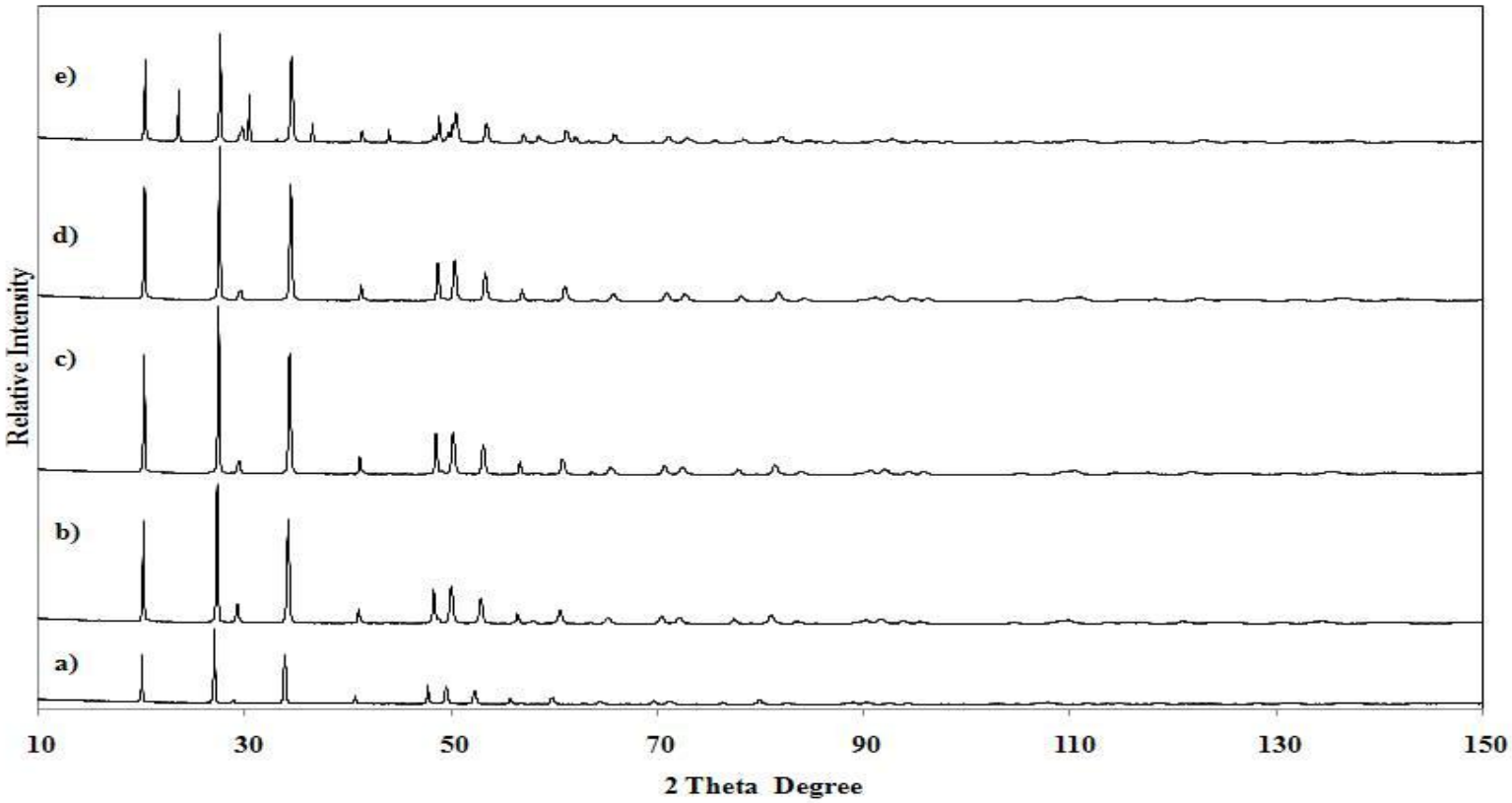

Figure A.1. X-Ray Diffraction Pattern of a) $TbBO_3$, b) $ErBO_3$, c) $TmBO_3$, d) $YbBO_3$, e) $LuBO_3$ Scanned by Using Panalytical Diffractometer.

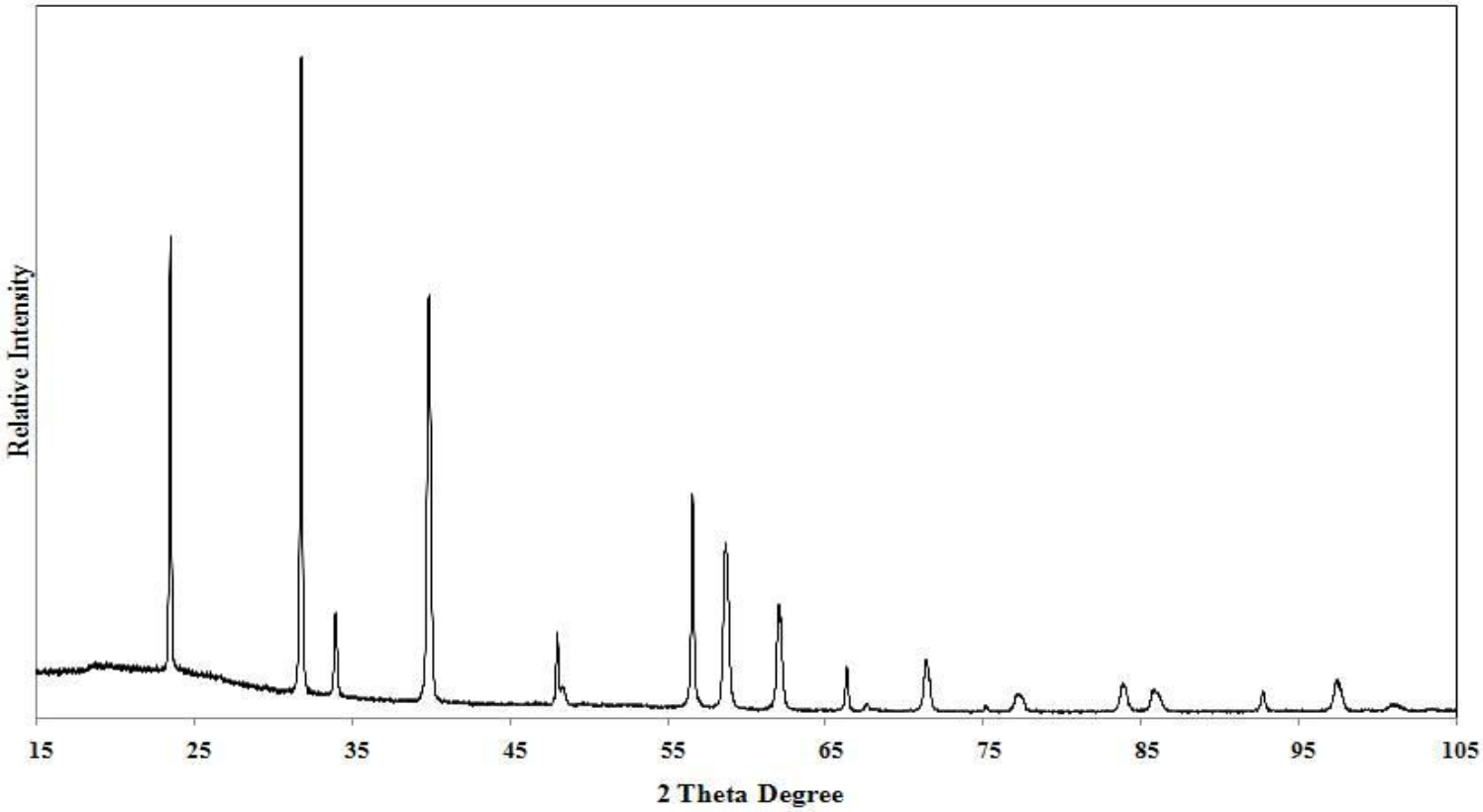

Figure A.2. X-Ray Diffraction Pattern of YBO_3 Scanned by Using STOE STADI-P Diffractometer.

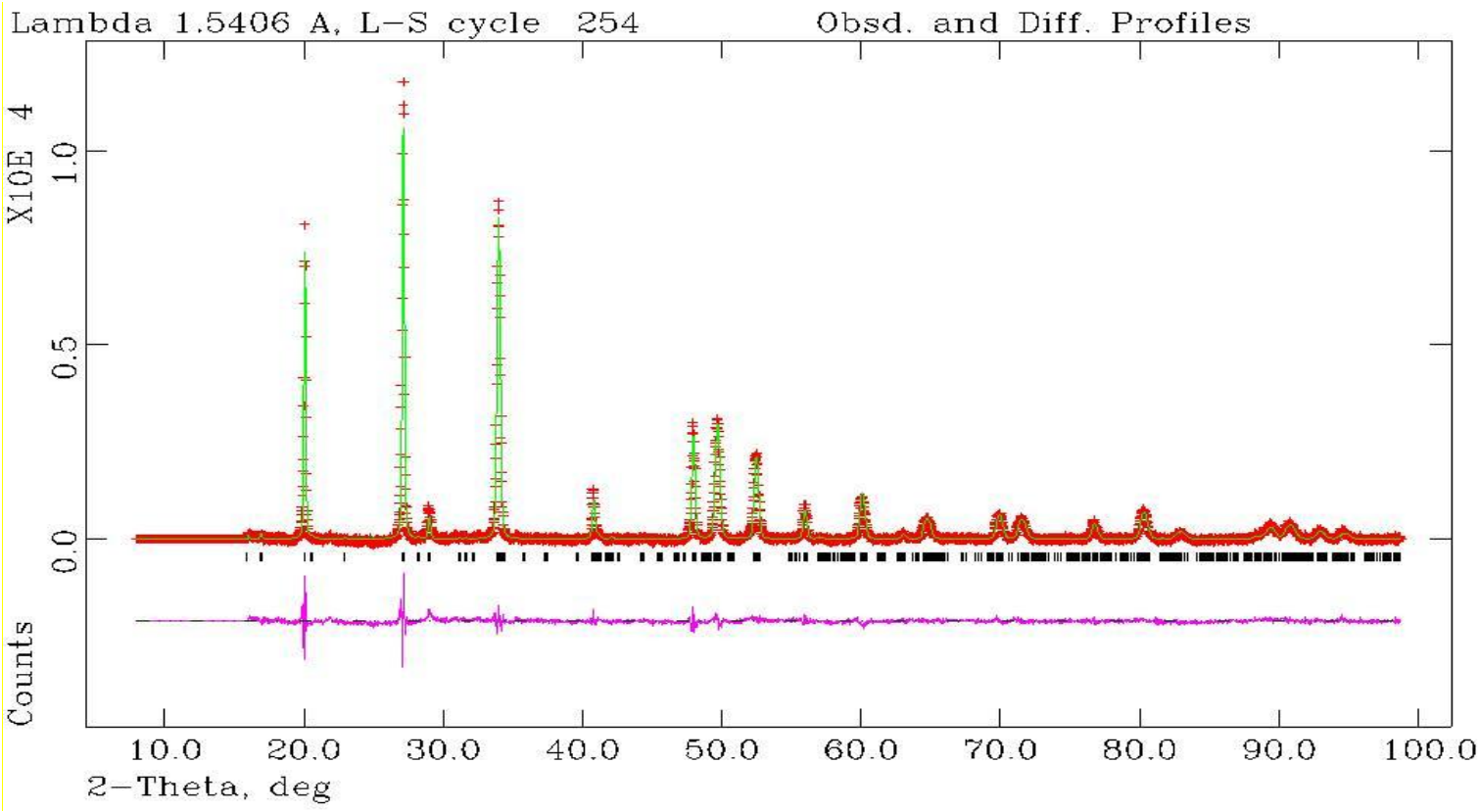

Figure A.3. Observed. calculated and difference X-ray diffraction profile for $DyBO_3$ with approximate intensity scale depending upon the angular area. Crosses indicate the observed data and the solid line shows the calculated profile. All possible Bragg reflections are indicated with vertical markers below the profile.

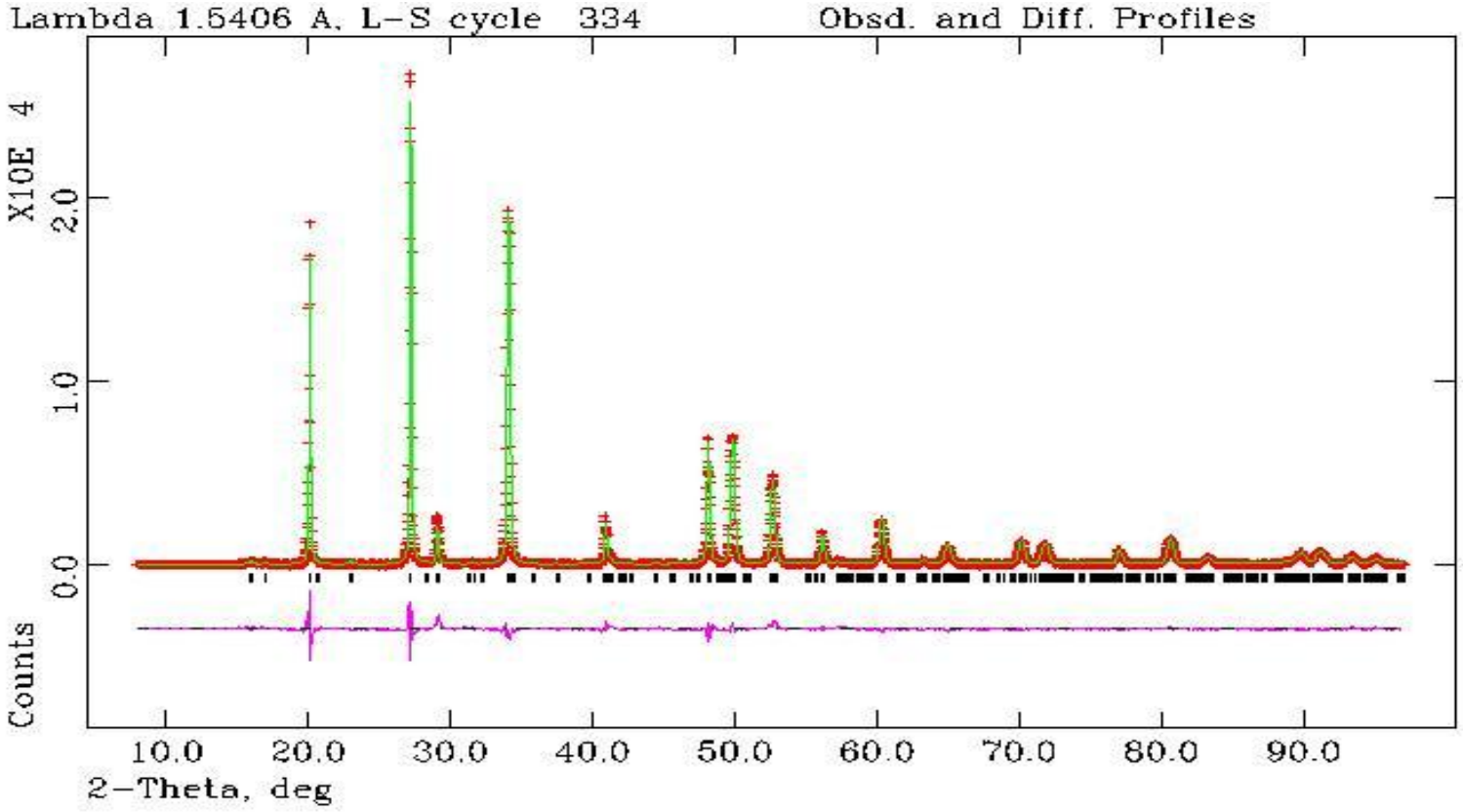

Figure A.4. Observed. calculated and difference X-ray diffraction profile for $HoBO_3$ with approximate intensity scale depending upon the angular area. Crosses indicate the observed data and the solid line shows the calculated profile. All possible Bragg reflections are indicated with vertical markers below the profile.

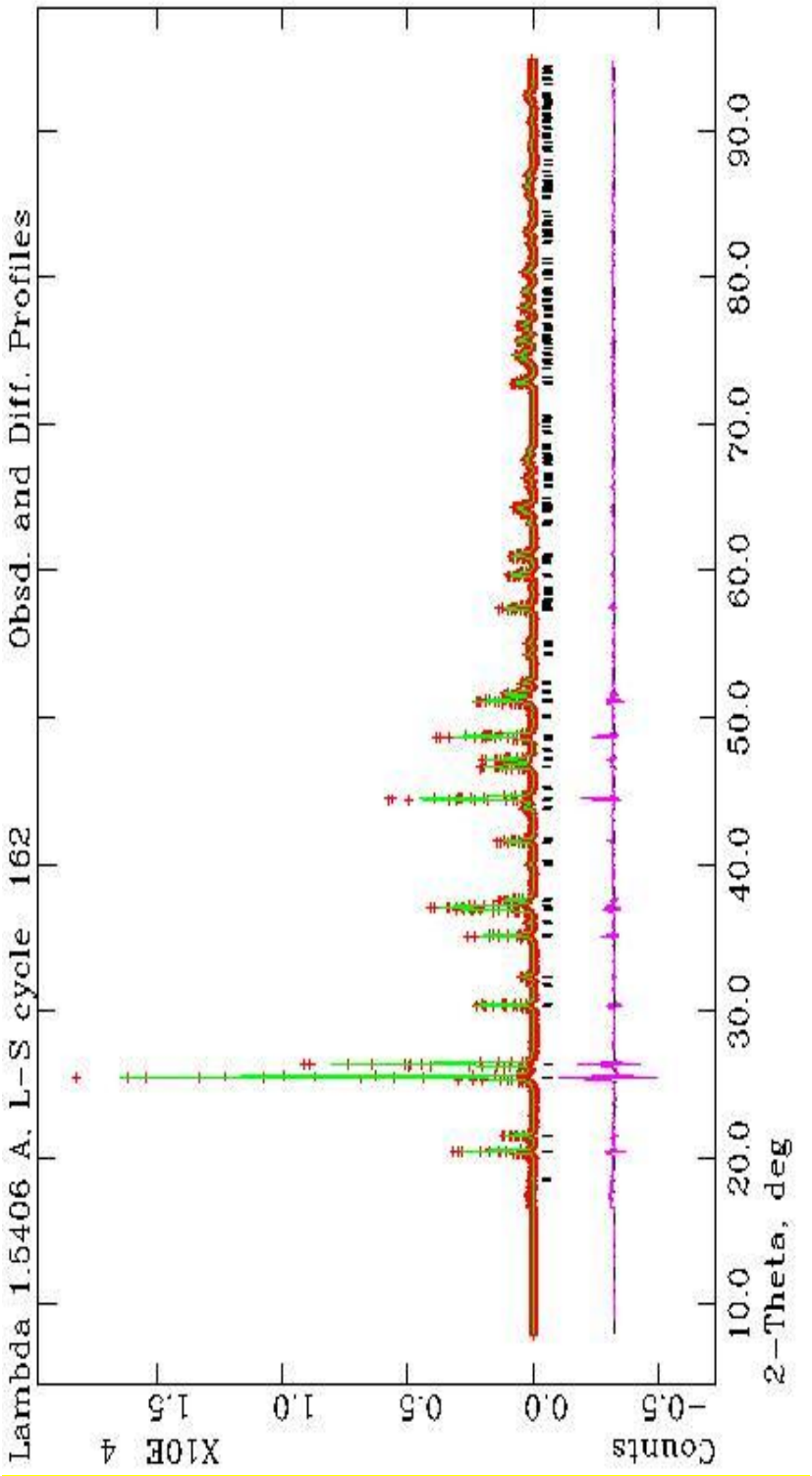

Figure. A.5. Observed, calculated and difference X-ray diffraction profile for $LaBO_3$ with approximate intensity scale depending upon the angular area. Crosses indicate the observed data and the solid line shows the calculated profile. All possible Bragg reflections are indicated with vertical markers below the profile.

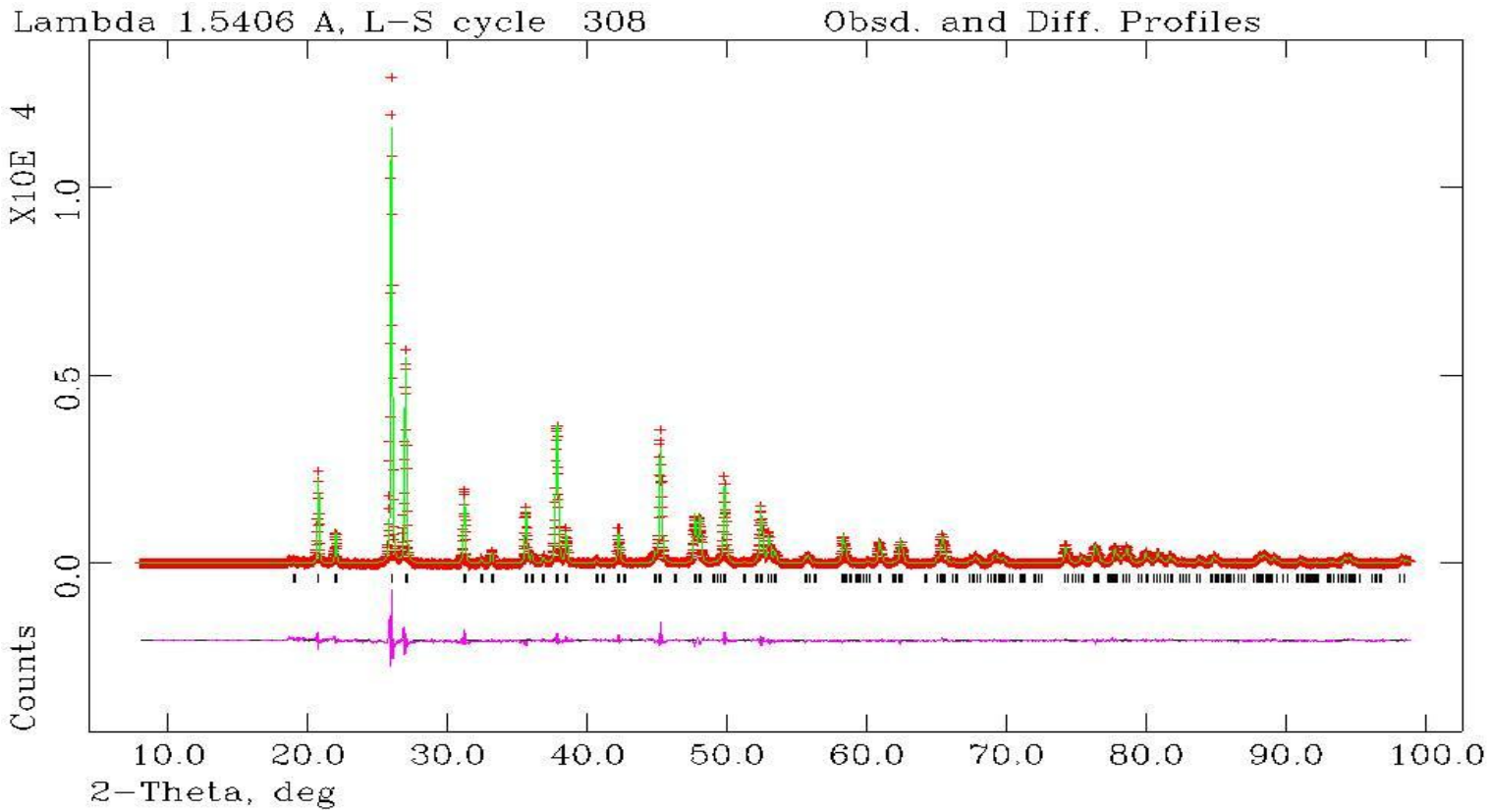

Figure A.6. Observed. calculated and difference X-ray diffraction profile for $NdBO_3$ with approximate intensity scale depending upon the angular area. Crosses indicate the observed data and the solid line shows the calculated profile. All possible Bragg reflections are indicated with vertical markers below the profile.

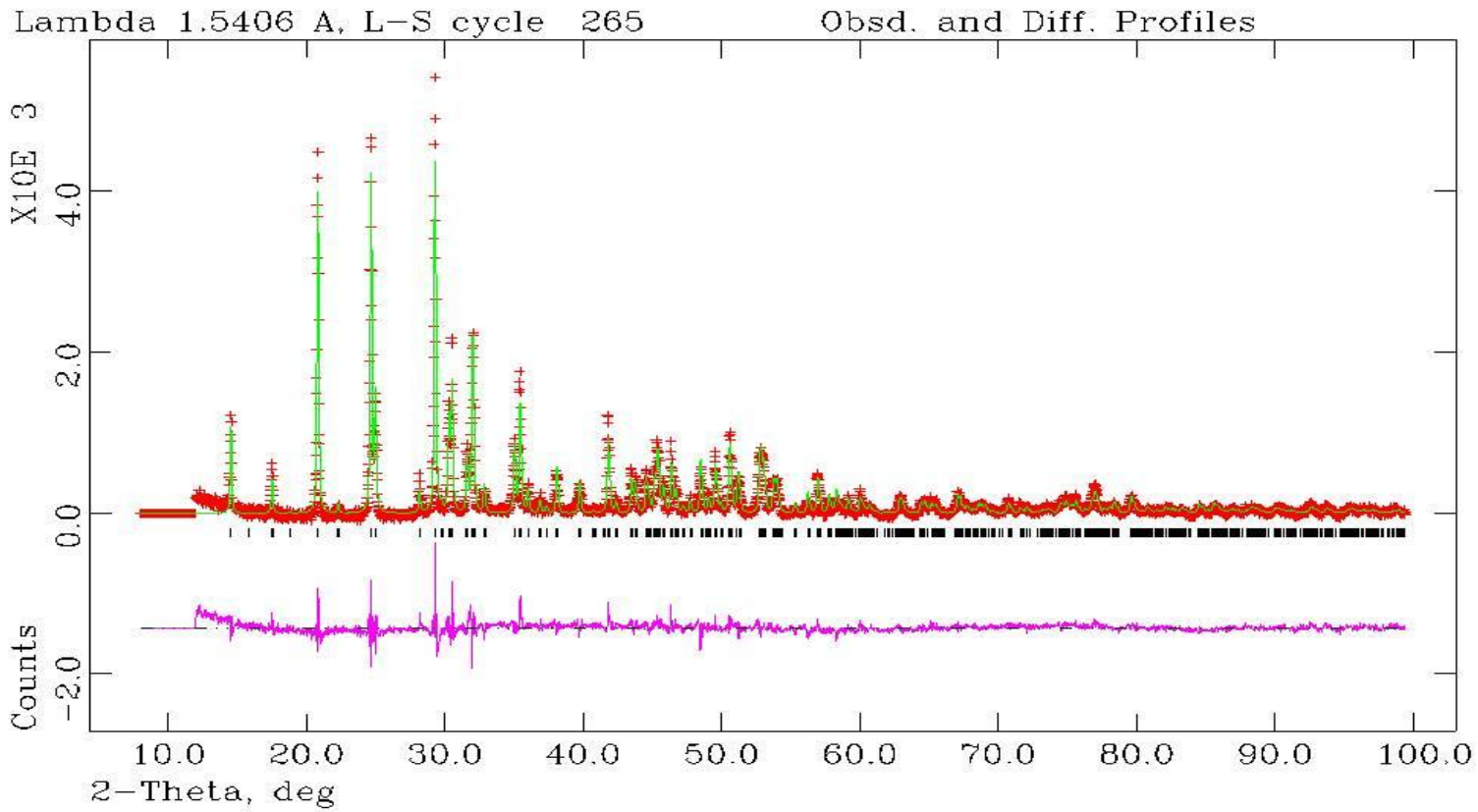

Figure A.7. Observed, calculated and difference X-ray diffraction profile for $SmBO_3$ with approximate intensity scale depending upon the angular area. Crosses indicate the observed data and the solid line shows the calculated profile. All possible Bragg reflections are indicated with vertical markers below the profile.

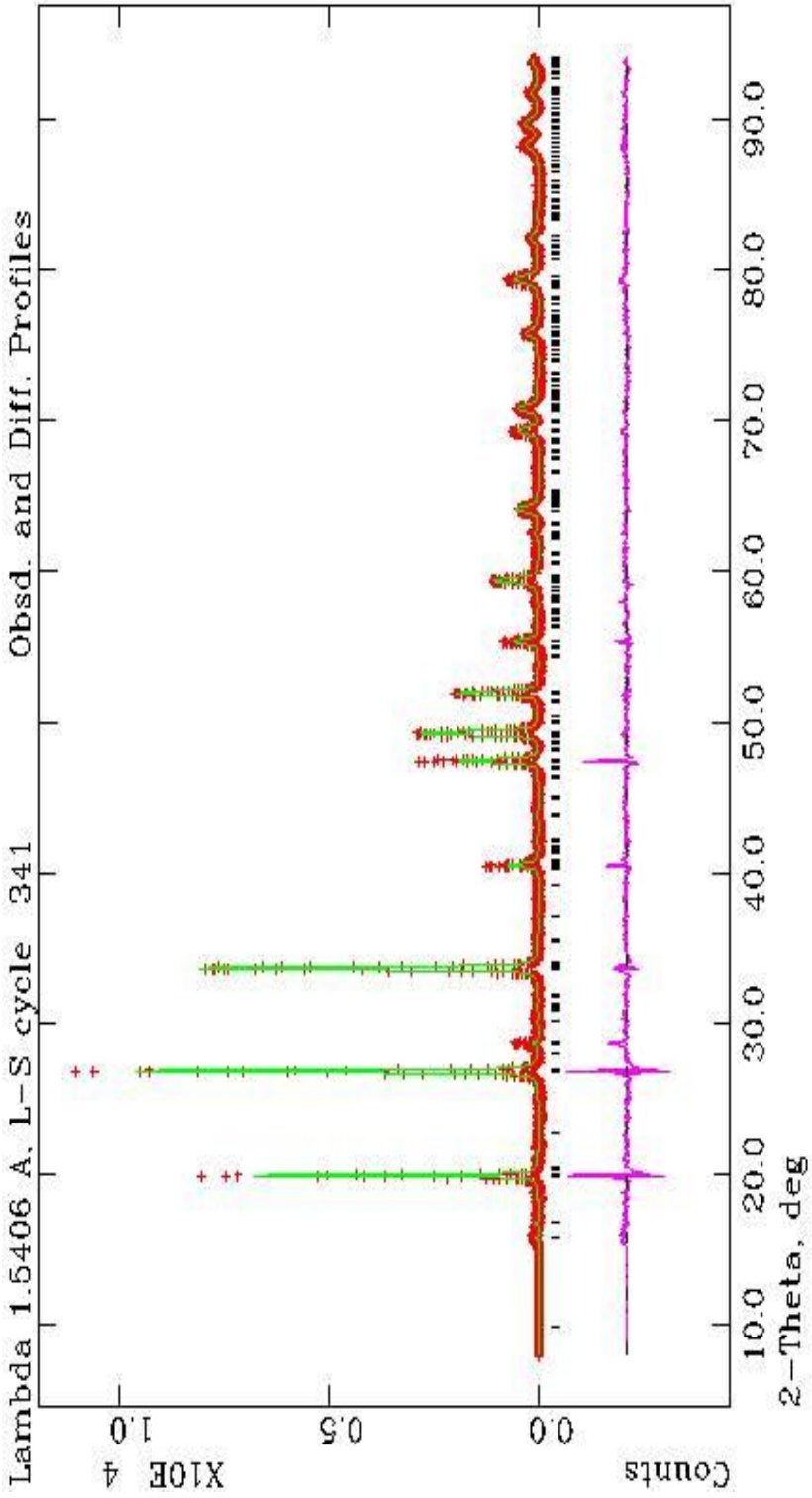

Figure A.8. Observed, calculated and difference X-ray diffraction profile for $GdBO_3$ with approximate intensity scale depending upon the angular area. Crosses indicate the observed data and the solid line shows the calculated profile. All possible Bragg reflections are indicated with vertical markers below the profile.

APPENDIX B

XRD DATA OF THE PRODUCED PHASES

The following tables represent the XRD data of the produced phases.

Table B.1. X-ray Diffraction Data of Na_2LaOPO_4 (a=13.60(1), b=12.71(1), c=6.96(1) Å) (Intensities over 5 were given).

d_{obs} (Å)	d_{cal} (Å)	$(I/I_o)_{obs}$	h k l		d_{obs} (Å)	d_{cal} (Å)	$(I/I_o)_{obs}$	h k l
6.9642	6.9642	12	0 0 1		1.8993	1.8983	12	6 0 2
4.8307	4.8629	18	2 0 1		1.8772	1.8775	6	6 1 2
4.2873	4.2660	14	3 1 0		1.8329	1.8349	9	4 2 3
4.0009	4.0439	14	1 3 0		1.8294	1.8189	8	6 2 2
3.6671	3.6378	6	3 1 1		1.7730	1.7761	32	5 4 2
3.6157	3.6191	33	0 3 1		1.7263	1.7269	10	1 0 4
3.4048	3.3966	18	4 0 0		1.7187	1.7140	14	0 5 3
3.3482	3.3583	63	0 4 0		1.6952	1.6953	11	7 0 2
3.3115	3.2814	58	4 1 0		1.6780	1.6792	10	0 2 4
3.1951	3.1941	27	2 3 1		1.6667	1.6665	23	1 2 4
3.1400	3.1769	8	0 4 0		1.6515	1.6500	7	8 0 1
3.0506	3.0529	10	4 0 1		1.6327	1.6301	8	2 2 4
2.9956	2.9955	15	4 2 0		1.6156	1.6120	10	3 1 4
2.9520	2.9684	22	4 1 1		1.5951	1.5970	15	8 2 1
2.8687	2.8778	100	2 4 0		1.5727	1.5740	6	7 3 2
2.7485	2.7517	61	4 2 1		1.5534	1.5543	9	1 6 3
2.6573	2.6572	9	5 1 0		1.4890	1.4890	13	7 0 3
2.5266	2.5314	11	5 0 1		1.4209	1.4211	9	4 6 3
2.4926	2.4982	7	1 5 0		1.3573	1.3567	9	2 1 5
2.3719	2.3804	24	2 5 0		1.3488	1.3488	7	6 2 4
2.3363	2.3469	5	0 4 2		1.3454	1.3455	8	5 8 1
2.2960	2.2882	25	1 0 3		1.3176	1.3180	5	4 7 3
2.2440	2.2520	13	1 1 3		1.2957	1.2960	6	7 0 4
2.1741	2.1730	27	5 3 1		1.2926	1.2937	5	10 3 0
2.1300	2.1330	8	6 2 0		1.2539	1.2537	10	2 4 5
2.1110	2.1120	9	3 5 1		1.2435	1.2449	5	1 10 1
2.0562	2.0529	28	0 5 2		1.2226	1.2230	7	4 8 3
2.0192	2.0220	45	2 6 0		1.1830	1.1812	7	6 1 5
1.9918	1.9970	10	6 3 0		1.1747	1.1757	7	9 4 3
1.9653	1.9651	36	2 5 2		1.1472	1.1470	6	2 6 5
1.9106	1.9117	13	5 3 2		1.1289	1.1285	7	10 6 1

Table B.2. X-ray Diffraction Data of Na_2NdOPO_4 (a=13.466(5), b=12.547(6), c=6.932(5) Å) (Intensities over 10 were given).

d_{obs} (Å)	d_{cal} (Å)	$(I/I_o)_{obs}$	h k l		d_{obs} (Å)	d_{cal} (Å)	$(I/I_o)_{obs}$	h k l
4.8177	4.8310	16	2 0 1		1.6300	1.6276	10	4 4 3
4.2873	4.2256	14	3 1 0		1.6182	1.6173	8	3 0 4
3.9920	3.9854	11	1 3 0		1.6040	1.6040	13	3 1 4
3.6085	3.6085	31	3 1 1		1.6001	1.6010	11	0 3 4
3.3669	3.3669	10	4 0 0		1.5826	1.5827	21	8 2 1
3.2876	3.2513	90	4 1 0		1.5582	1.5576	12	2 3 4
3.2522	3.2432	76	1 1 2		1.5523	1.5541	9	1 8 0
3.1292	3.1292	8	0 4 0		1.5221	1.5230	9	8 3 1
2.9956	2.9933	15	2 1 2		1.4784	1.4788	14	7 0 3
2.9473	2.9428	22	4 1 1		1.4535	1.4528	9	9 1 1
2.8598	2.8522	100	0 4 1		1.4306	1.4319	6	6 4 3
2.8116	2.7966	12	3 3 1		1.4095	1.4085	10	9 3 0
2.7321	2.7263	76	4 2 1		1.4086	1.4070	9	4 6 3
2.5231	2.5132	14	3 2 2		1.3463	1.3467	11	10 0 0
2.3629	2.3546	16	0 5 1		1.3429	1.3426	11	5 6 3
2.2878	2.2893	26	1 4 2		1.3338	1.3334	8	0 6 4
2.2387	2.2226	6	2 5 1		1.2919	1.2917	9	2 3 5
2.1616	2.1684	26	0 2 3		1.2769	1.2757	9	4 1 5
2.1447	2.1409	6	1 2 3		1.2747	1.2747	9	6 6 3
2.0993	2.0971	17	5 1 2		1.2733	1.2732	9	7 5 3
2.0562	2.0552	9	3 0 3		1.2428	1.2405	11	3 9 2
2.0386	2.0414	9	5 4 0		1.2161	1.2159	10	9 6 0
2.0170	2.0211	36	6 2 1		1.2148	1.2139	12	7 8 0
1.9815	1.9767	35	6 3 0		1.2122	1.2117	12	2 10 1
1.9572	1.9583	49	5 4 1		1.1539	1.1545	6	11 0 2
1.9220	1.9239	14	7 0 0		1.1528	1.1518	7	3 9 3
1.7941	1.7922	10	2 4 3		1.1098	1.1101	7	1 3 6
1.7730	1.7733	20	4 6 0		1.1088	1.1079	7	12 0 1
1.7354	1.7372	18	5 1 3		1.1078	1.1076	8	2 11 1
1.6837	1.6834	23	8 0 0		1.1073	1.1073	7	7 2 5
1.6667	1.6673	10	7 1 2		1.1048	1.1047	8	12 2 0
1.6570	1.6581	13	1 2 4		1.1034	1.1036	7	12 1 1

Table B.3. X-ray Diffraction Data of Na_2SmOPO_4 (a=13.54(1), b=12.577(8), c=7.047(5) Å) (Intensities over 10 were given).

d_{obs} (Å)	d_{cal} (Å)	$(I/I_o)_{obs}$	h k l		d_{obs} (Å)	d_{cal} (Å)	$(I/I_o)_{obs}$	h k l
4.3391	4.2482	10	3 1 0		1.6065	1.6038	22	7 4 1
4.0277	3.9998	11	1 3 0		1.5826	1.5854	29	4 7 0
3.6375	3.6375	29	3 1 1		1.5582	1.5595	18	1 8 0
3.3857	3.3857	12	4 0 0		1.5347	1.5348	14	6 6 0
3.2876	3.2888	91	1 1 2		1.5131	1.5145	15	8 1 2
3.2522	3.2514	86	3 2 1		1.4773	1.4764	17	3 6 3
3.1508	3.1400	15	0 4 0		1.4219	1.4208	12	7 6 0
2.9956	2.9951	16	1 2 2		1.4133	1.4101	12	2 5 4
2.9378	2.9651	32	4 1 1		1.4095	1.4084	11	0 0 5
2.8732	2.8678	100	0 4 1		1.4067	1.4070	10	6 6 2
2.8030	2.8056	16	1 4 1		1.4048	1.4045	10	6 7 0
2.7444	2.7445	94	4 2 1		1.4011	1.4008	10	1 0 5
2.7120	2.7109	28	3 1 2		1.3766	1.3767	12	5 7 2
2.3719	2.3659	19	0 5 1		1.3721	1.3723	10	8 4 2
2.2906	2.3023	34	4 4 0		1.3463	1.3465	16	10 1 0
2.1666	2.1641	30	5 3 1		1.3446	1.3445	16	3 0 5
2.1087	2.1084	16	4 3 2		1.3429	1.3418	14	2 9 1
2.0924	2.0933	11	0 6 0		1.3338	1.3337	12	5 8 1
2.0878	2.0912	13	2 2 3		1.3313	1.3325	14	9 4 1
2.0429	2.0449	15	0 5 2		1.3280	1.3284	17	1 3 5
2.0064	2.0065	65	0 6 1		1.2889	1.2889	14	6 8 0
1.9713	1.9691	68	5 4 1		1.2814	1.2814	12	2 8 3
1.9632	1.9598	78	2 3 3		1.2733	1.2733	10	4 2 5
1.9454	1.9393	30	4 5 1		1.2631	1.2625	12	2 4 5
1.9125	1.9121	23	7 1 0		1.2617	1.2615	10	5 7 3
1.8808	1.8800	17	0 4 3		1.2129	1.2129	10	8 7 1
1.8754	1.8788	11	6 1 2		1.2116	1.2115	12	4 9 2
1.8663	1.8656	10	7 0 1		1.2090	1.2087	14	2 5 5
1.8433	1.8440	17	4 2 3		1.2014	1.2014	13	4 4 5
1.8398	1.8418	12	5 5 0		1.1989	1.1995	12	0 9 3
1.8329	1.8328	10	6 4 0		1.1915	1.1921	11	10 5 0
1.7778	1.7787	22	1 7 0		1.1897	1.1895	11	6 1 5
1.7746	1.7739	24	5 0 3		1.1434	1.1439	10	9 0 4
1.7217	1.7245	39	1 7 1		1.1423	1.1428	10	11 2 2
1.6851	1.6841	24	2 7 1		1.0970	1.0972	14	12 2 1
1.6612	1.6625	32	2 5 3		1.0960	1.0958	10	1 4 6
1.6584	1.6563	33	5 6 0		1.0951	1.0957	12	9 7 2
1.6327	1.6331	18	6 5 1		1.0941	1.0941	13	8 8 2
1.6195	1.6225	16	3 7 1					

Table B.4. X-ray Diffraction Data of Na_2GdOPO_4 (a=13.37(1), b=12.775(9), c=6.910(9) Å) (Intensities over 10 were given).

d_{obs} (Å)	d_{cal} (Å)	$(I/I_o)_{obs}$	h k l		d_{obs} (Å)	d_{cal} (Å)	$(I/I_o)_{obs}$	h k l
4.7791	4.8043	17	2 0 1		1.9434	1.9472	54	2 6 1
4.2568	4.2601	11	0 3 0		1.7602	1.7612	16	2 7 0
3.9656	4.0590	11	1 3 0		1.6995	1.6981	11	1 1 4
3.5799	3.5925	22	2 3 0		1.6723	1.6726	11	2 0 4
3.1951	3.1951	100	0 4 0		1.6488	1.6548	34	1 2 4
2.9331	2.9286	12	4 1 1		1.6393	1.6392	17	7 4 0
2.8777	2.8827	10	2 4 0		1.5951	1.5950	10	7 4 1
2.8377	2.8341	74	1 4 1		1.5913	1.5937	10	4 6 2
2.7650	2.7667	23	2 2 2		1.5703	1.5691	24	2 7 2
2.7403	2.7304	12	3 0 2		1.4710	1.4701	10	7 0 3
2.7080	2.7220	56	4 2 1		1.4690	1.4694	10	3 8 1
2.3480	2.3458	11	0 4 2		1.4669	1.4643	11	8 2 2
2.2657	2.2646	14	5 3 0		1.3362	1.3368	10	10 0 0
2.1469	2.1467	16	2 1 3		1.2462	1.2462	12	2 4 5
1.9774	1.9743	13	6 3 0					

Table B.5. X-ray Diffraction Data of Na_2DyOPO_4 (a=13.66(2), b=12.609(9), c=6.611(6) Å) (Intensities over 5 were given).

d_{obs} (Å)	d_{cal} (Å)	$(I/I_o)_{obs}$	h k l		d_{obs} (Å)	d_{cal} (Å)	$(I/I_o)_{obs}$	h k l
4.7663	4.7663	12	2 0 1		1.6543	1.6539	6	1 5 3
4.3182	4.3401	6	1 2 1		1.6247	1.6254	27	7 2 2
3.9310	4.0151	9	1 3 0		1.5938	1.5936	5	5 3 3
3.4112	3.4112	7	4 0 0		1.5888	1.5888	7	6 0 3
3.1508	3.1508	100	0 4 0		1.5850	1.5839	7	0 7 2
3.0005	2.9999	8	4 2 0		1.5534	1.5520	10	3 1 4
2.8553	2.8605	19	2 4 0		1.4658	1.4656	5	3 3 4
2.8159	2.8002	15	3 3 1		1.4048	1.4008	5	3 4 4
2.7037	2.7001	45	2 2 2		1.3471	1.3479	5	9 2 2
2.2228	2.2206	5	0 0 3		1.3437	1.3436	5	6 0 4
2.2046	2.2047	8	3 5 0		1.3321	1.3323	6	0 0 5
2.1616	2.1644	8	5 3 1		1.2846	1.2849	5	0 8 3
2.1493	2.1522	6	6 0 1		1.2476	1.2485	5	2 3 5
2.1157	2.1115	9	2 0 3		1.2346	1.2345	5	11 1 0
2.0386	2.0367	5	6 2 1		1.2319	1.2333	10	1 10 1
2.0234	2.0272	5	4 5 0		1.2306	1.2306	9	10 4 1
1.9960	1.9954	6	3 0 3		1.2279	1.2281	7	9 2 3
1 9553	1 9493	9	7 0 0		1.2021	1.2024	5	4 8 3
1.9317	1.9280	8	2 5 2		1.2008	1.2000	6	10 5 0
1.9087	1.9070	43	3 6 0		1.9996	1.9999	6	9 3 3
1.7508	1.7537	11	5 4 2		1.0965	1.0961	5	0 10 3
1.7083	1.7090	7	7 3 1		1.0941	1.0934	6	0 2 6
1.7054	1.7056	7	8 0 0		1.0926	1.0926	5	1 10 3
1.6653	1.6654	6	0 0 4					

Table B.6. X-ray Diffraction Data of Na_2HoOPO_4 (a=13.148(4), b=12.577(2), c=6.967(1) Å) (Intensities over 5 were given).

d_{obs} (Å)	d_{cal} (Å)	$(I/I_o)_{obs}$	h k l
4.7791	4.7790	14	2 0 1
4.5139	4.5464	6	2 2 0
4.0277	4.1410	5	3 1 0
3.9569	3.9957	6	1 3 0
3.1454	3.1454	100	0 4 0
2.9473	2.9651	18	1 2 2
2.8377	2.8377	24	2 4 0
2.7080	2.6882	77	4 2 1
2.5544	2.5559	8	3 4 0
2.3046	2.2969	7	1 4 2
2.1134	2.0983	12	5 0 2
1.9733	1.9844	15	6 2 1
1.9414	1.9431	11	6 3 0
1.9031	1.9027	60	4 4 2
1.7493	1.7455	12	5 4 2
1.6556	1.6534	9	7 0 2
1.6169	1.6163	46	3 0 4
1.5813	1.5804	18	6 1 3
1.5475	1.5444	12	1 6 3
1.4576	1.4573	7	8 4 0
1.3590	1.3582	5	0 2 5
1.3362	1.3385	8	0 6 4
1.3160	1.3156	6	10 0 0
1.2769	1.2769	5	7 7 1
1.2414	1.2397	6	4 6 4
1.2394	1.2387	5	9 4 2
1.2380	1.2381	4	0 10 1
1.2253	1.2252	12	4 3 5
1.1940	1.1948	8	8 0 4

Table B.7. X-ray Diffraction Data of Na_2ErOPO_4 (a=13.563(5), b=12.604(4), c=7.003(3) Å) (Intensities over 5 were given).

d_{obs} (Å)	d_{cal} (Å)	$(I/I_o)_{obs}$	h k l		d_{obs} (Å)	d_{cal} (Å)	$(I/I_o)_{obs}$	h k l
4.7537	4.6837	12	0 2 1		1.7446	1.7437	34	0 7 1
3.5658	3.5726	78	2 3 0		1.7025	1.7041	21	5 2 3
3.1508	3.1508	41	0 4 0		1.6130	1 6156	31	0 3 4
3.0557	3.0548	17	4 0 1		1.5888	1.5901	17	1 7 2
2.9809	2.9852	27	1 2 2		1.5558	1.5557	20	4 0 4
2.8732	2.8732	14	0 4 1		1.5267	1.5272	7	1 8 1
2.8159	2.8187	21	3 3 1		1.4425	1.4440	31	6 4 3
2.7160	2.7160	44	5 0 0		1.3939	1.3917	27	9 3 1
2.6270	2.6280	68	1 3 2		1.3529	1.3523	21	9 2 2
2.4926	2.4942	27	5 2 0		1.3313	1.3330	10	5 4 4
2.3132	2.3120	8	3 3 2		1.2904	1.2890	28	3 6 4
2.1892	2.1884	33	0 2 3		1.2588	1.2585	8	8 4 3
1.9836	1.9902	23	1 6 1		1.2567	1.2550	7	0 7 4
1.9612	1.9586	25	2 5 2		1.2394	1.2392	32	2 10 0
1.8993	1.9006	37	6 0 2		1.2213	1.2209	14	5 2 5
1.8468	1.8476	40	5 5 0		1.2084	1.2094	7	3 7 4
1.7892	1.7864	100	5 5 1		1.2065	1.2062	6	6 7 3

Table B.8. X-ray Diffraction Data of Na_2YbOPO_4 (a=13.501(7), b=17.579(9), c=6.729(4) Å) (Intensities over 5 were given).

d_{obs} (Å)	d_{cal} (Å)	$(I/I_o)_{obs}$	h k l		d_{obs} (Å)	d_{cal} (Å)	$(I/I_o)_{obs}$	h k l
4.7663	4.7663	20	2 0 1		1.6300	1.6300	7	8 1 1
4.4357	4.4256	6	2 3 0		1.5913	1.5913	52	3 10 1
4.0187	4.0058	7	3 2 0		1.5801	1.5818	27	3 9 2
3.3055	3.3055	11	0 1 2		1.5558	1.5554	9	2 11 0
3.0973	3.1169	100	0 5 1		1.5392	1.5408	9	5 9 1
2.9331	2.9305	55	0 6 0		1.5221	1.5221	17	3 3 4
2.7001	2.7001	54	5 0 0		1.4912	1.4917	5	7 7 1
2.6688	2.6688	42	5 1 0		1.4336	1.4323	6	5 9 2
2.5129	2.5119	8	0 7 0		1.3362	1.3361	5	0 8 4
2.3276	2.3832	5	1 7 1		1.3297	1.3296	6	1 8 4
2.2684	2.2876	6	2 5 2		1.3152	1.3156	7	10 3 0
2.1816	2.1810	12	1 6 2		1.2949	1.2953	8	3 13 0
2.0809	2.0854	16	3 7 1		1.2755	1.2758	6	7 10 1
1.9693	1.9728	36	4 5 2		1.2567	1.2572	5	0 5 5
1.9336	1.9335	4	1 9 0		1.2220	1.2218	6	1 12 3
1.8718	1.8732	62	1 5 3		1.2052	1.2050	22	10 4 2
1.8158	1.8142	7	7 2 1		1.1741	1.1736	12	3 10 4
1.7974	1.7921	9	3 9 0		1.1315	1.1317	6	2 8 5
1.7477	1.7437	17	3 5 3		1.1063	1.1064	5	8 12 0
1.7158	1.7174	9	5 1 3					

Table B.9. X-ray Diffraction Data of Cubic ZrP_2O_7.

d_{PDF}[24-1491]	d_{obs}	hkl	$(I/I_o)_{obs}$
4.760	4.7612	111	25
4.13	4.1219	200	100
3.69	3.6866	210	38
3.37	3.3644	211	34
2.915	2.9144	220	37
2.487	2.4853	221	57
2.382	2.381	222	10
2.288	2.2866	230	7
2.205	2.2072	321	3
2.062	2.0629	400	6
2.002	2.0001	410	9
1.9449	1.9438	141	5
1.8930	1.8919	331	21
1.8447	1.8444	240	38
1.7990	1.8000	241	6
1.7583	1.7762	332	2
1.6833	1.6837	242	27
1.5872	1.5875	151	40
1.5326	1.5384	250	3
1.5051	1.5058	251	4
1.4580	1.4580	440	15
1.3944	1.3943	351	13

Table B.10. X-ray Diffraction Data of Orthorhombic $Sr_2P_2O_7$.

d_{PDF} [24-1011]	d_{obs}	hkl	$(I/I_o)_{obs}$		d_{PDF} [24-1011]	d_{obs}	hkl	$(I/I_o)_{obs}$
7.4000	7.3750	1 1 0	21		2.2300	2.2270	4 0 0	12
6.6000	6.5727	0 2 0	7		2.1950	2.1933	0 6 0	43
5.3000	5.2790	1 2 0	2		2.1320	2.1295	1 6 0	9
5.0100	4.9898	0 1 1	3		2.0440	2.0434	2 3 2	95
4.4620	4.4511	2 0 0	8		1.9870	1.9856	4 3 0	8
3.9400	3.9327	1 3 0	8		1.9820	1.9807	1 6 1	9
3.6940	3.6911	2 2 0	4		1.9660	1.9665	4 2 1	16
3.4390	3.4345	2 0 1	80		1.9130	1.9129	3 2 2	4
3.4060	3.4010	0 3 1	100		1.8910	1.8908	2 4 2	10
3.3270	3.3237	2 1 1	34		1.8660	1.8649	4 3 1	28
3.2910	3.2864	0 4 0	5		1.8500	1.8489	2 6 1	42
3.1820	3.1806	1 3 1	17		1.7760	1.7759	0 7 1	6
3.1280	3.1249	2 3 0	28		1.7470	1.7458	4 4 1	8
3.0480	3.0445	2 2 1	7		1.7420	1.7434	1 7 1	7
2.9000	2.8959	3 1 0	27		1.7220	1.7211	5 2 0	3
2.7000	2.7009	0 0 2	57		1.7030	1.7031	0 6 2	14
2.6800	2.6789	1 4 1	30		1.6690	1.6695	2 0 3	10
2.6480	2.6474	2 4 0	4		1.6650	1.6667	0 3 3	23
2.5540	2.5537	3 1 1	18		1.6510	1.6524	2 7 1	2
2.5250	2.5231	1 5 0	14		1.6370	1.6380	1 3 3	4
2.4220	2.4206	3 2 1	8		1.6009	1.6011	4 3 2	5
2.4060	2.4055	1 2 2	14		1.5903	1.5900	3 7 0	10
2.3770	2.3773	2 4 1	3		1.5643	1.5635	4 6 0	11
2.3100	2.3086	2 0 2	8		1.5554	1.5582	1 4 3	8

Table B.11. X-Ray Diffraction Data of $LaBO_3$ after a) Solid State Reaction, b) Microwave Heating With Urea and 2 hours Conventional Heating, c) Microwave Heating With Sucrose and 2 hours Conventional Heating.

a)		**b)**		**c)**	
$\mathbf{d_{obs}}$ **(Å)**	$\mathbf{(I/I_o)_{obs}}$	$\mathbf{d_{obs}}$ **(Å)**	$\mathbf{(I/I_o)_{obs}}$	$\mathbf{d_{obs}}$ **(Å)**	$\mathbf{(I/I_o)_{obs}}$
4.3815	13	4.3923	15	4.3923	13
3.5241	100	3.5172	100	3.5241	100
3.4048	52	3.3984	49	3.4048	45
2.9568	17	2.9664	19	2.9664	20
2.5686	22	2.5650	26	2.5722	22
2.4338	33	2.4434	39	2.4434	48
2.4056	10	2.4056	12	2.4087	11
2.1816	14	2.1791	15	2.1841	17
2.0451	53	2.0429	63	2.0473	66
1.9553	21	1.9553	22	1.9553	25
1.9356	21	1.9356	26	1.9375	25
1.8772	38	1.8754	49	1.8772	50
1.7924	26	1.7924	31	1.7941	34
1.7762	13	1.7778	15	1.7762	15
1.6091	18	1.6091	23	1.6104	23
1.5534	14	1.5523	17	1.5534	19
1.5221	14	1.5221	16	1.5233	19
1.4535	11	1.4546	13	1.4586	14
1.3019	12	1.3011	15	1.4026	20
1.2725	10	1.2718	12	1.2733	15
1.2589	10	1.2610	11	1.2596	12
1.2442	11	1.2439	13	1.2455	15

Table B.12. X-Ray Diffraction Data of $NdBO_3$ after a) Solid State Reaction, b) Microwave Heating With Urea and 2 hours Conventional Heating, c) Microwave Heating With Sucrose and 2 hours Conventional Heating.

a)		**b)**		**c)**	
$\mathbf{d_{obs}}$ **(Å)**	$\mathbf{(I/I_o)_{obs}}$	$\mathbf{d_{obs}}$ **(Å)**	$\mathbf{(I/I_o)_{obs}}$	$\mathbf{d_{obs}}$ **(Å)**	$\mathbf{(I/I_o)_{obs}}$
4.3079	15	4.3287	16	4.3079	16
3.4502	100	3.4568	100	3.4436	100
3.3237	48	3.3359	48	3.3237	47
2.8778	19	2.8868	20	2.8778	21
2.5300	17	2.5369	19	2.5300	19
2.3871	51	2.3932	49	2.3871	53
2.3480	12	2.3510	12	2.3480	12
2.1469	12	2.1518	14	2.1445	14
2.0107	15	1.0149	49	2.0107	55
1.9125	20	1.9144	21	1.9106	23
1.8993	21	1.8975	13	1.8993	23
1.8346	37	1.8381	38	1.8346	41
1.7493	29	1.7540	25	1.7493	30
1.7323	13	1.7354	13	1.7308	13
1.5863	14	1.5875	15	1.5863	18
1.5244	13	1.5256	14	1.5233	14
1.4901	13	1.4923	13	1.4891	14
1.4297	18	1.4297	19	1.4297	18
1.2792	13	1.2799	14	1.2792	14
1.2490	14	1.2490	13	1.2490	13
1.2293	11	1.2306	10	1.2293	12
1.2181	11	1.2181	12	1.2187	11

Table B.13. X-Ray Diffraction Data of $DyBO_3$ after a) Solid State Reaction, b) Microwave Heating With Urea and 2 hours Conventional Heating, c) Microwave Heating With Sucrose and 2 hours Conventional Heating.

a)		**b)**		**c)**	
$\mathbf{d_{obs}}$ **(Å)**	$\mathbf{(I/I_o)_{obs}}$	$\mathbf{d_{obs}}$ **(Å)**	$\mathbf{(I/I_o)_{obs}}$	$\mathbf{d_{obs}}$ **(Å)**	$\mathbf{(I/I_o)_{obs}}$
4.4689	43	4.4801	47	4.4913	46
3.3116	91	3.3176	96	3.3237	95
3.1025	11	3.1131	7	3.1185	14
2.6535	100	2.6573	100	2.6650	100
2.2201	16	2.2228	18	2.2281	15
1.9050	47	1.9050	46	1.9087	44
1.8416	55	1.8433	57	1.8451	51
1.7508	40	1.7508	41	1.7524	38
1.6488	16	1.6502	16	1.6502	16
1.5440	25	1.5452	26	1.5464	24
1.4435	13	1.4435	13	1.4435	12
1.3479	16	1.3479	18	1.3505	14
1.3232	12	1.3224	13	1.3223	12
1.2435	10	1.2449	11	1.2449	11

Table B.14. X-Ray Diffraction Data of $HoBO_3$ after a) Solid State Reaction, b) Microwave Heating With Urea and 2 hours Conventional Heating, c) Microwave Heating With Sucrose and 2 hours Conventional Heating.

a)		**b)**		**c)**	
$\mathbf{d_{obs}}$ **(Å)**	$\mathbf{(I/I_o)_{obs}}$	$\mathbf{d_{obs}}$ **(Å)**	$\mathbf{(I/I_o)_{obs}}$	$\mathbf{d_{obs}}$ **(Å)**	$\mathbf{(I/I_o)_{obs}}$
4.4248	47	4.4689	45	4.4578	43
3.2816	95	3.2995	86	3.2995	88
3.0763	12	3.0920	9	3.020	14
2.6345	100	2.6458	100	2.6458	100
2.2072	15	2.2149	15	2.2149	15
1.8937	48	1.8975	45	1.8975	46
1.8312	56	1.8363	55	1.8346	60
1.7400	40	1.7446	38	1.7431	40
1.6393	15	1.6420	14	1.6420	15
1.5359	23	1.5382	21	1.5382	23
1.4346	10	1.4385	10	1.4385	11
1.3421	13	1.3437	14	1.3421	14
1.3136	11	1.3168	11	1.3160	12

Table B.15. The X-ray Diffraction Data of YBO_3 scanned by Panalytical and Stoe (Intensities over 5 were given).

Panalytical d_{obs} (Å)	**$(I/I_o)_{obs}$**	**STOE-d_{obs} (Å)**	**$(I/I_o)_{obs}$**
4.40132	63	4.39298	63
3.26972	100	3.26598	100
3.06055	13	3.06627	6
2.63029	55	2.62641	60
2.20074	11	2.19922	13
1.88834	35	1.88750	31
1.82594	30	1.8274	48
1.73395	21	1.73709	3
1.63552	7	1.63463	9
1.53080	10	1.53440	12
1.33882	6	1.33978	14
1.31271	5	1.31521	6
1.23647	2	1.23563	4
1.18873	7	1.19174	10
1.09046	4		

Table B.16. X-ray Diffraction Data of $LaBO_3$ (Intensities over 5 were given).

d_{obs} (Å)	$(I/I_o)_{obs}$
4.34381	17
4.12792	7
3.49100	100
3.48944	46
3.37610	49
3.37470	23
2.93543	12
2.55256	14
2.55212	9
2.43255	17
2.42196	22
2.42162	13
2.39267	7
2.17125	8
2.03658	31
2.03625	16
1.94699	11
1.94689	6
1.92671	11
1.92648	6
1.78413	6
1.76853	6
1.60369	8
1.54832	5
1.51764	5

Table B.17. X-ray Diffraction Data of $NdBO_3$ (Intensities over 5 were given).

d_{obs} (Å)	$(I/I_o)_{obs}$
4.27776	19
4.04259	7
3.42616	100
3.42470	50
3.30112	44
2.86360	15
2.52022	12
2.38018	23
2.37477	27
2.33679	7
2.13859	7
2.00378	26
2.00360	16
1.90538	9
1.89239	9
1.82895	18
1.82876	9
1.74392	12
1.74351	6
1.72685	6
1.58116	5
1.42619	6
1.42619	6

Table B.18. X-ray Diffraction Data of $SmBO_3$ (Intensities over 5 were given).

d_{obs} (Å)	$(I/I_o)_{obs}$		d_{obs} (Å)	$(I/I_o)_{obs}$
6.08808	21		2.07941	10
5.06425	12		2.06601	8
4.26497	82		2.03123	10
3.98915	2		2.00633	9
3.60736	87		1.99857	15
3.55798	28		1.97920	6
3.16715	9		1.95722	15
3.04843	100		1.94447	6
2.94892	26		1.87423	9
2.92948	39		1.83899	13
2.83133	15		1.80351	17
2.79036	39		1.78464	8
2.56147	16		1.73416	12
2.53130	32		1.72476	14
2.53068	20		1.70358	8
2.49264	6		1.69590	8
2.35996	8		1.61595	9
2.26439	6		1.54000	6
2.15953	22		1.23789	6

Table B.19. X-ray Diffraction Data of $EuBO_3$ (Intensities over 5 were given).

d_{obs} (Å)	$(I/I_o)_{obs}$	d_{obs} (Å)	$(I/I_o)_{obs}$
6.08845	24	2.52189	28
5.04278	12	2.15149	19
4.46773	39	2.07490	7
4.24212	77	2.05484	7
3.60359	88	2.02729	8
3.59713	91	1.98829	16
3.33161	63	1.94667	11
3.14970	11	1.92487	14
3.04290	100	1.88290	5
3.03853	92	1.85504	15
2.95196	19	1.83054	7
2.91481	35	1.79367	14
2.82020	32	1.76685	10
2.77478	22	1.72592	11
2.67746	32	1.68947	6
2.55910	13	1.60815	8

Table B.20. X-ray Diffraction Data of $GdBO_3$ (Intensities over 5 were given).

d_{obs} (Å)	$(I/I_o)_{obs}$
4.45351	73
3.31737	100
3.31645	57
3.11075	5
2.66506	60
2.22647	11
1.91620	26
1.91579	15
1.84982	25
1.84596	24
1.75833	18
1.65921	8
1.55634	9
1.35435	5
1.20861	5

Table B.21. X-ray Diffraction Data of $TbBO_3$ (Intensities over 5 were given).

d_{obs} (Å)	$(I/I_o)_{obs}$
4.42782	64
3.29247	100
3.29120	51
2.64971	51
2.64439	66
2.64381	51
2.21657	10
2.21626	6
1.90338	26
1.90310	15
1.84386	15
1.83966	23
1.83551	19
1.75219	14
1.74766	17
1.64885	8
1.54794	7
1.54312	8
1.19900	5

Table B.22. X-ray Diffraction Data of $DyBO_3$ (Intensities over 5 were given).

d_{obs} (Å)	$(I/I_o)_{obs}$
4.42420	72
3.28372	100
3.28220	55
3.07979	7
2.64264	56
2.63633	72
2.21136	11
1.89662	25
1.83882	18
1.83519	26
1.74119	18
1.64218	8
1.54205	8
1.53736	9
1.34391	6
1.19363	6

Table B.23. X-ray Diffraction Data of $HoBO_3$ (Intensities over 5 were given).

d_{obs} (Å)	$(I/I_o)_{obs}$
4.41156	7
3.27237	100
3.27114	58
3.06393	10
2.63195	62
2.20488	10
2.20442	6
1.88991	25
1.88943	16
1.82582	25
1.73957	14
1.73513	18
1.63677	6
1.53597	8
1.53198	9
1.19220	5
1.18942	5

Table B.24. X-ray Diffraction Data of $ErBO_3$ (Intensities over 5 were given).

d_{obs} (Å)	$(I/I_o)_{obs}$
4.39766	73
3.25910	100
3.25805	56
3.04398	13
2.61955	72
2.19846	10
2.19780	6
1.88245	24
1.88199	15
1.82334	25
1.73214	16
1.63008	7
1.52973	8
1.52605	9
1.33702	5
1.18761	5
1.18473	5

Table B.25. X-ray Diffraction Data of $TmBO_3$ (Intensities over 5 were given).

d_{obs} (Å)	$(I/I_o)_{obs}$
4.38338	71
3.24459	100
3.24352	54
3.04258	6
3.02537	7
2.60901	71
2.19172	11
2.19141	6
1.87421	25
1.87380	14
1.82068	15
1.81333	23
1.72556	15
1.72142	17
1.62304	7
1.52397	8
1.52055	9
1.33310	5
1.18285	5
1.17966	5

Table B.26. X-ray Diffraction Data of $YbBO_3$ (Intensities over 5 were given).

d_{obs} (Å)	$(I/I_o)_{obs}$
4.37447	73
3.23671	100
3.01463	6
2.60271	76
2.18658	10
2.18634	7
1.86745	24
1.86764	14
1.81046	27
1.72041	14
1.61721	7
1.51480	9
1.41824	5
1.32899	5
1.17864	5

Table B.27. X-ray Diffraction Data of $LuBO_3$ (Intensities over 5 were given).

d_{obs} (Å)	$(I/I_o)_{obs}$	d_{obs} (Å)	$(I/I_o)_{obs}$
4.36241	75	1.86306	14
3.76990	47	1.82921	9
3.22668	100	1.81782	16
3.22546	52	1.80734	27
3.02727	5	1.80454	25
3.00273	14	1.71558	15
2.93399	43	1.71143	17
2.93313	21	1.61354	8
2.59623	76	1.61391	5
2.45677	17	1.57782	7
2.45645	10	1.51493	10
2.18098	10	1.51109	10
2.18041	7	1.49510	6
2.05808	12	1.41862	8
2.05781	7	1.41865	7
1.88395	6	1.32570	6
1.86354	24	1.41862	7

APPENDIX C

INFRARED AND RAMAN SPECTRA OF THE PRODUCED PHASES

The separate FTIR and Raman spectrum and tables for produced compounds at different conditions are demonstrated in this section.

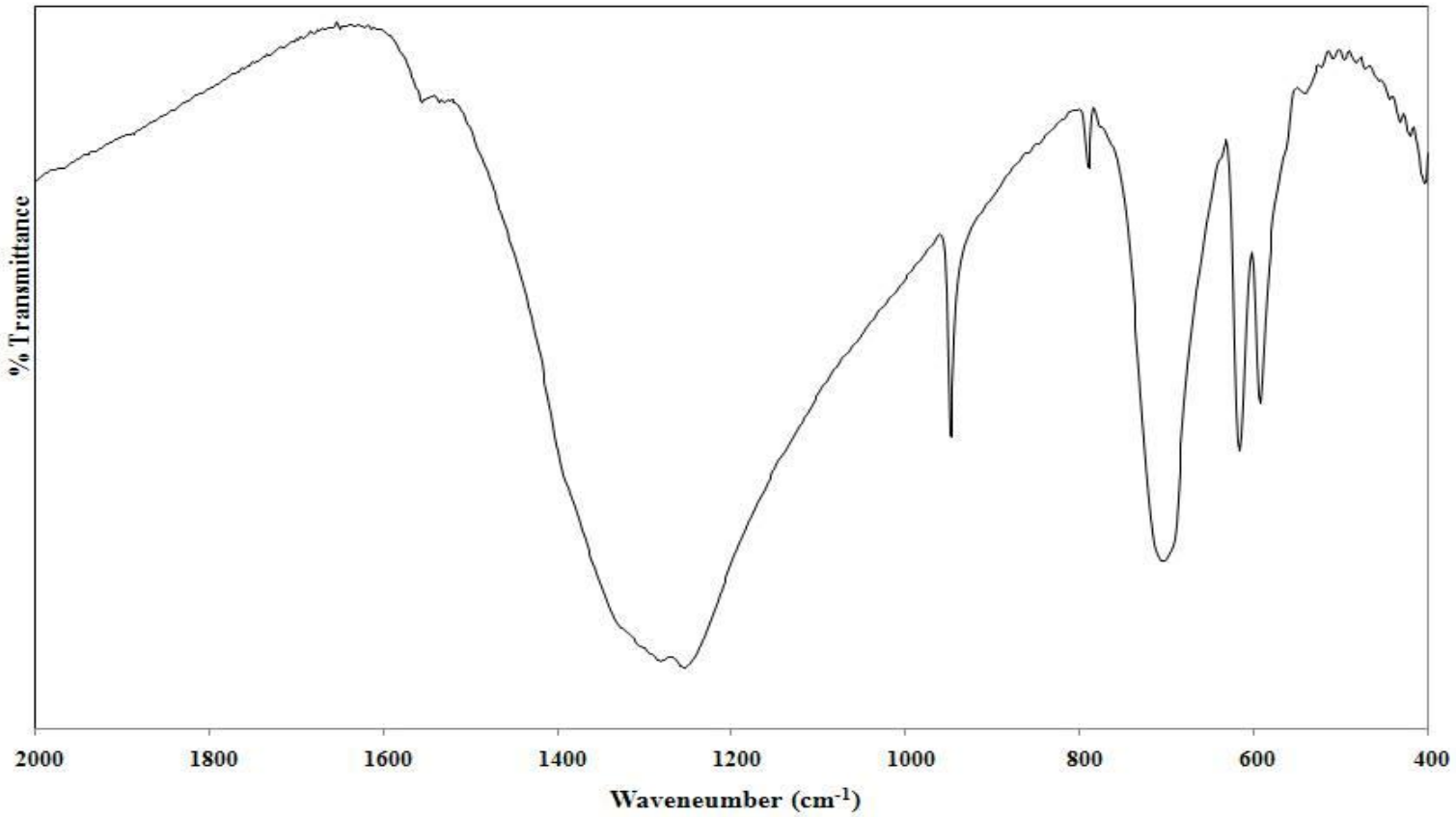

Figure C.1. FT-IR spectrum of $NdBO_3$.

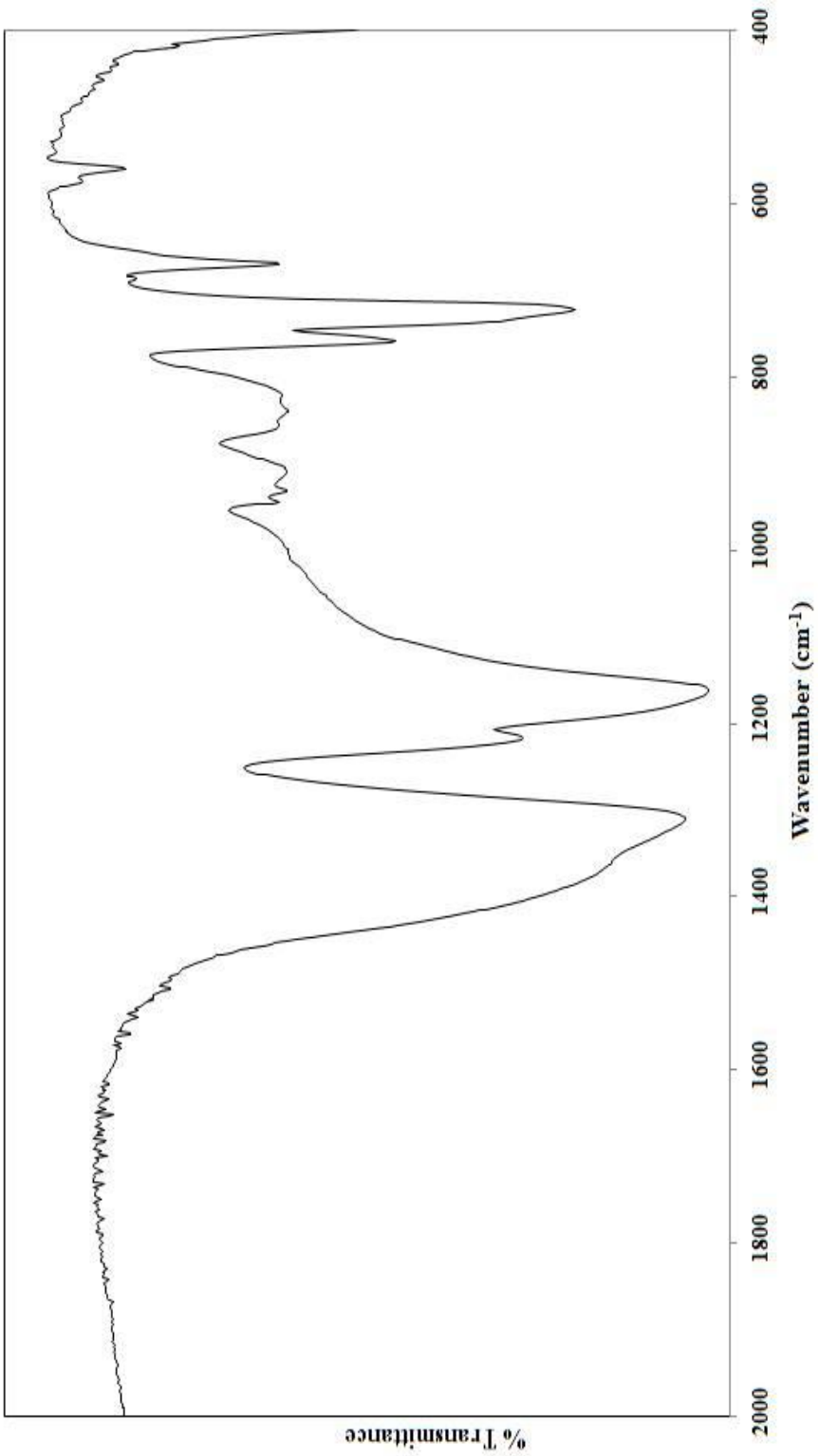

Figure C.2. FT-IR spectrum of $EuBO_3$.

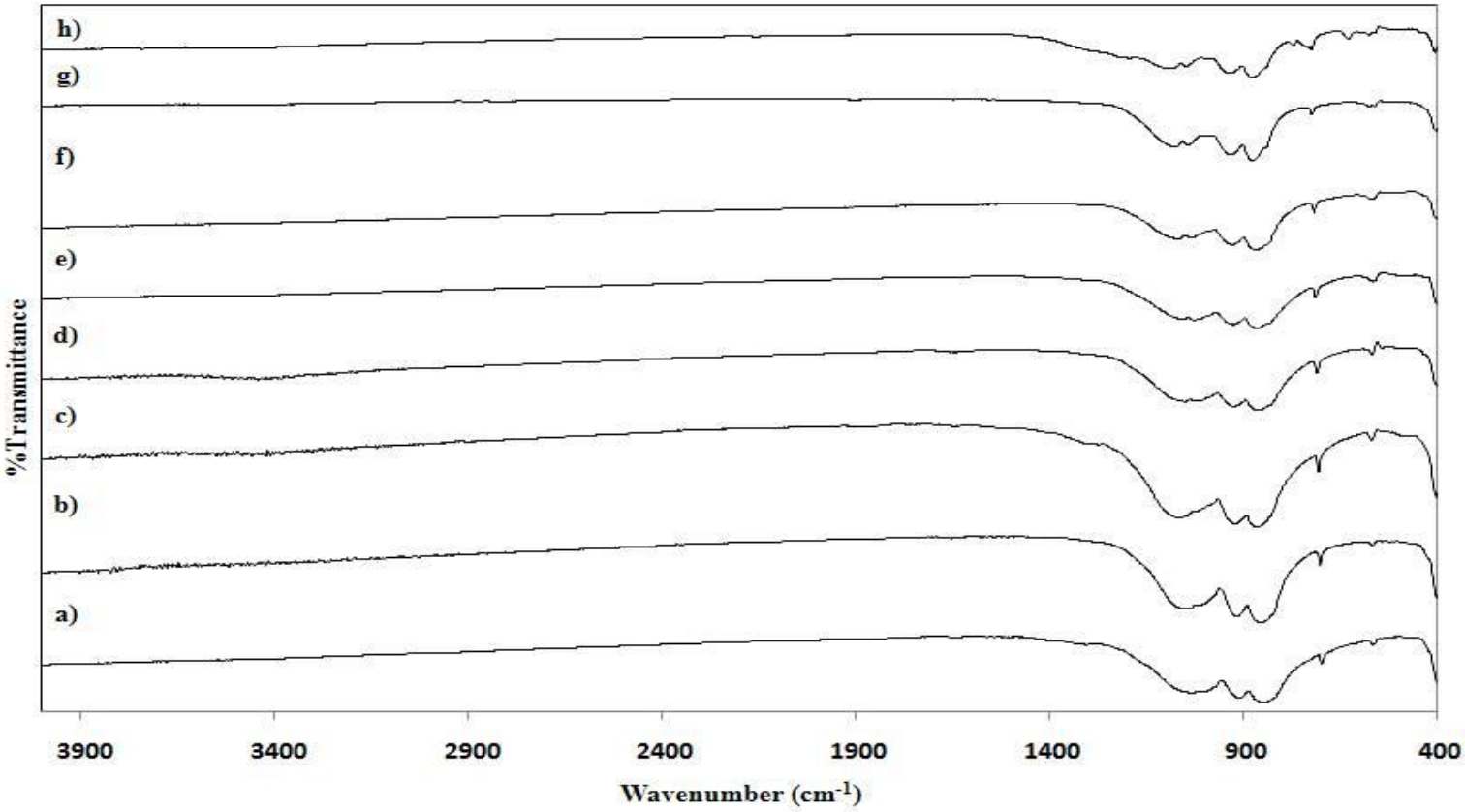

Figure C.3. FT-IR spectra of a) $GdBO_3$, b) $TbBO_3$, c) $DyBO_3$, d) $HoBO_3$, e) $ErBO_3$, f) $TmBO_3$, g) $YbBO_3$, h) $LuBO_3$.

APPENDIX D

SEM MONOGRAPHS and EDX ANALYSIS OF PRODUCED PHASES

The surface morphology of $Sr_2P_2O_7$ and ZrP_2O_7 compounds synthesized by solid state reaction are demonstrated in SEM pictures given in the following figures. The composition of ZrP_2O_7, 10% $Sr_2P_2O_7$ added ZrP_2O_7, $Sr_2P_2O_7$, and 10% ZrP_2O_7 added $Sr_2P_2O_7$ compounds given in EDX spectrum.

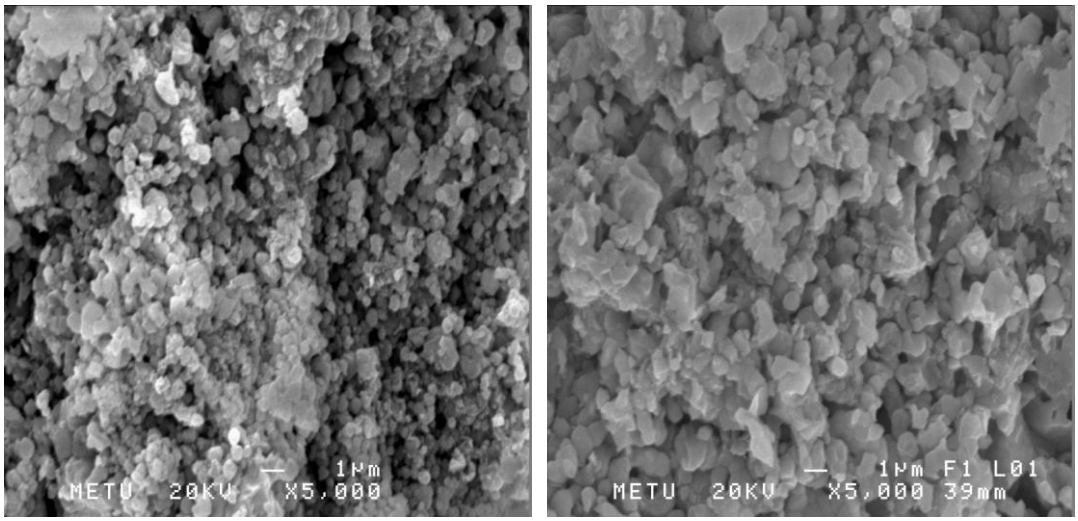

a. ZrP_2O_7 b. $Sr_2P_2O_7$

Figure D.1. SEM Micrographs of Pure ZrP_2O_7 and $Sr_2P_2O_7$.

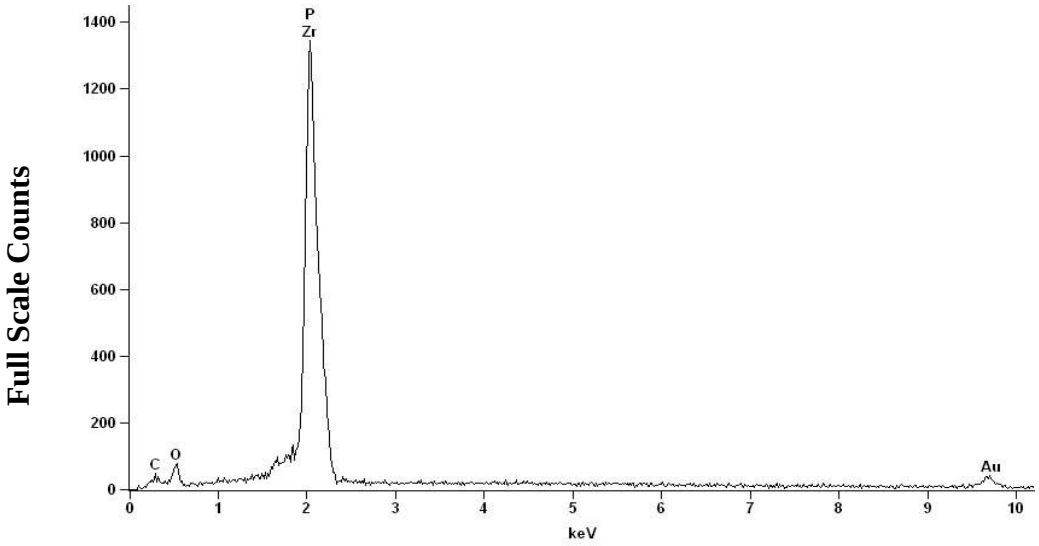

a. ZrP_2O_7

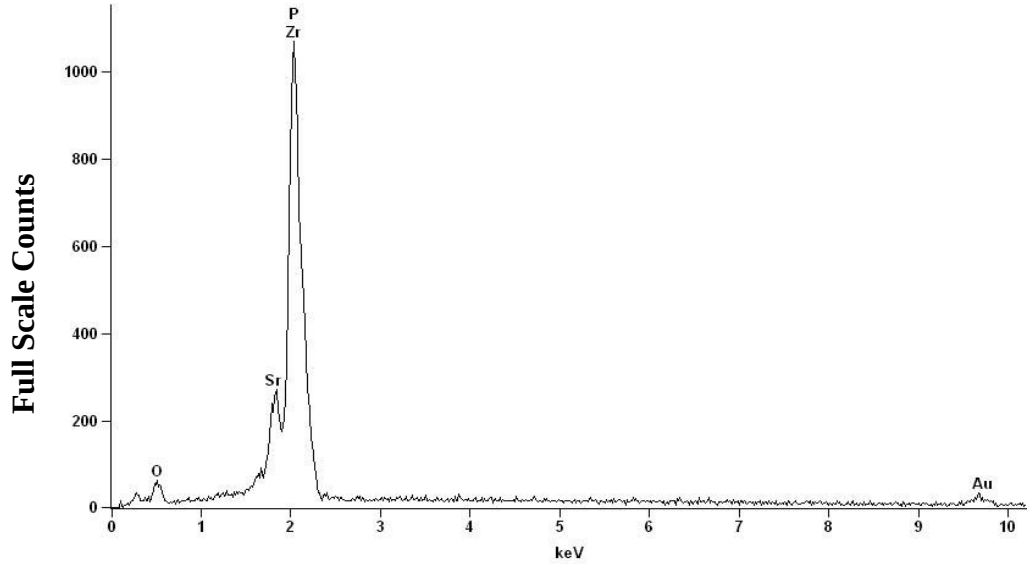

b. 10% $Sr_2P_2O_7$ doped ZrP_2O_7.

Figure D.2. EDX Analysis of ZrP_2O_7, 10% $Sr_2P_2O_7$ added ZrP_2O_7, $Sr_2P_2O_7$, and 10% ZrP_2O_7 added $Sr_2P_2O_7$.

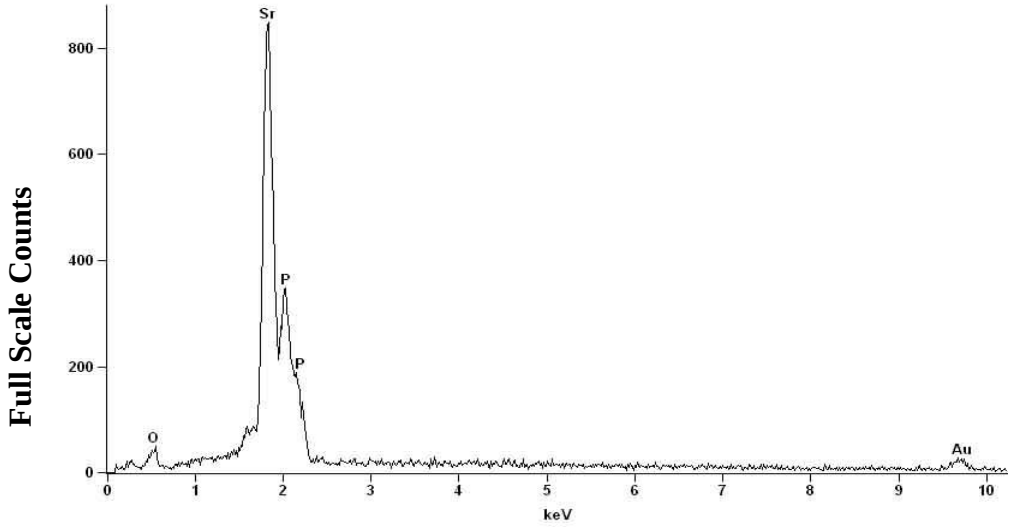

c. $Sr_2P_2O_7$

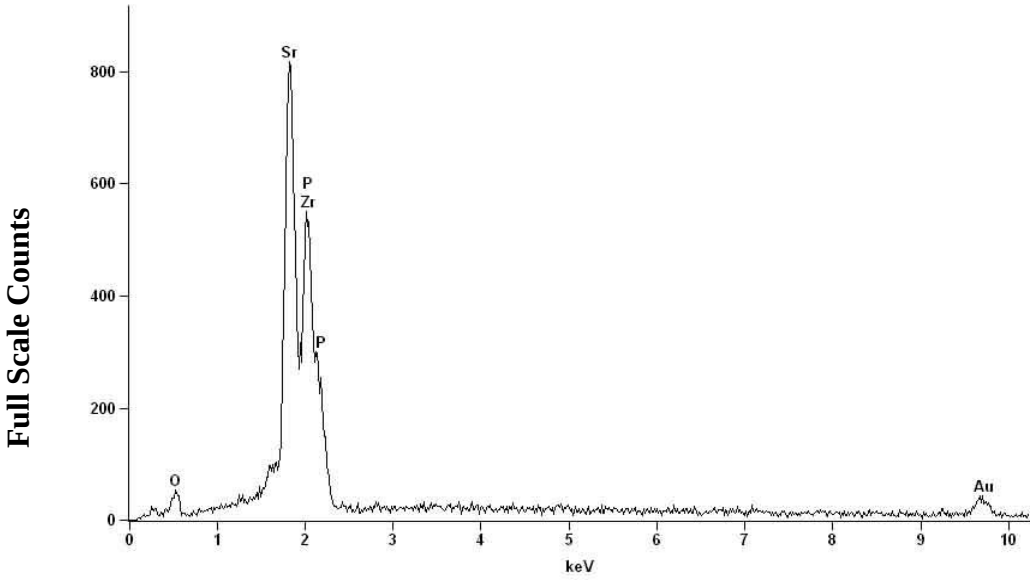

d. 10% ZrP_2O_7 added $Sr_2P_2O_7$.

Figure D.2. Continued.

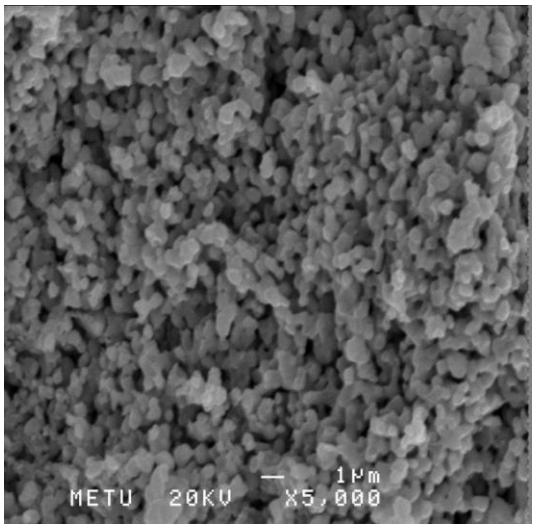

a)

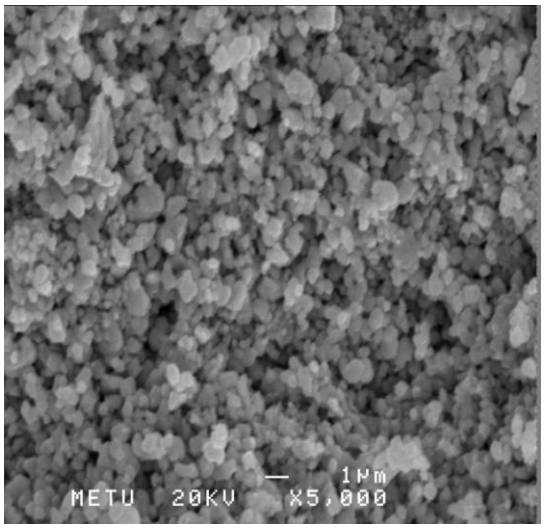

b)

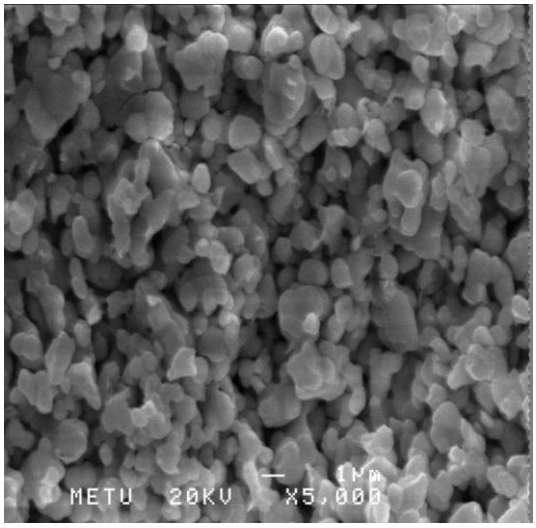

c)

Figure D.3. SEM Images of $LaBO_3$ Obtained by using a)Microwave-Assisted Synthesis with Urea, b)Microwave-Assisted Synthesis with Sucrose and c)Solid-State Reaction.

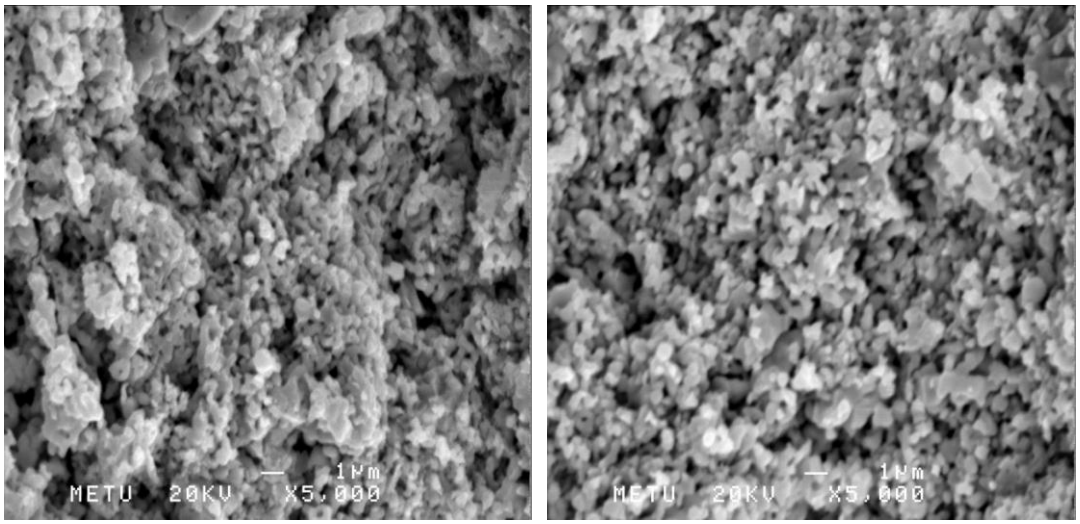

a) **b)**

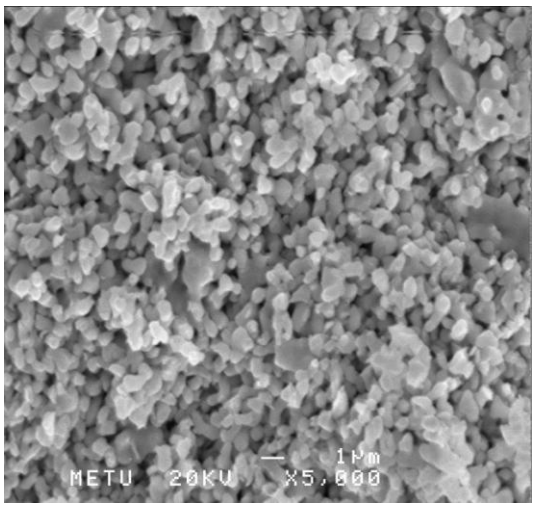

c)

Figure D.4. SEM Images of $NdBO_3$ Obtained by using a)Microwave-Assisted Synthesis with Urea, b)Microwave-Assisted Synthesis with Sucrose and c)Solid-State Reaction.

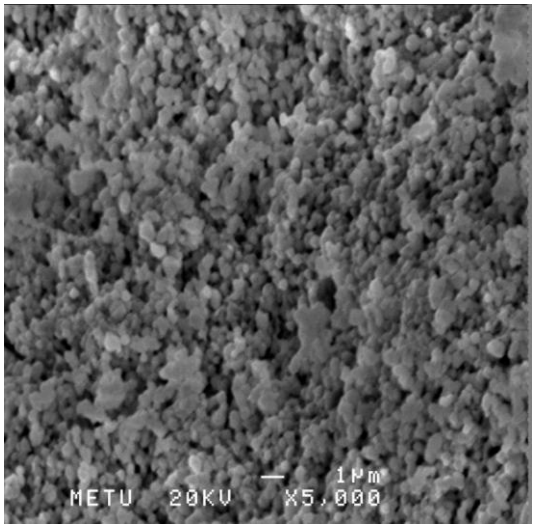

a)

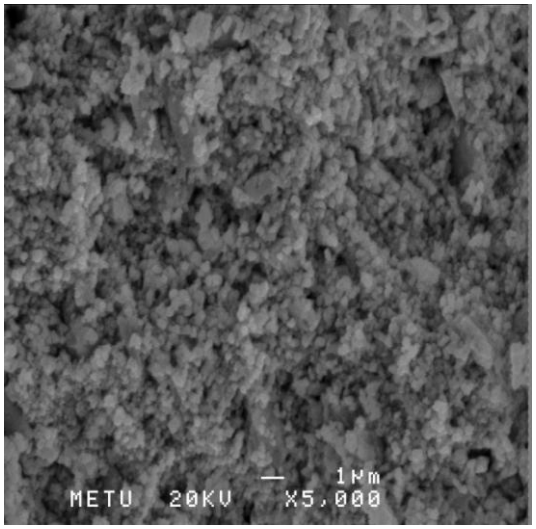

b)

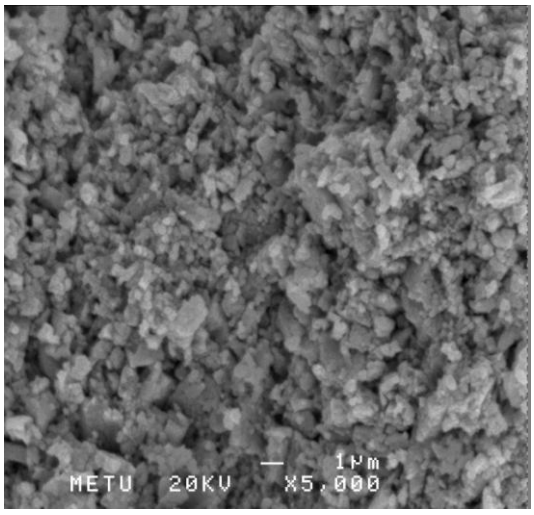

c)

Figure D.5. SEM Images of $DyBO_3$ Obtained by using a)Microwave-Assisted Synthesis with Urea, b)Microwave-Assisted Synthesis with Sucrose and c)Solid-State Reaction.

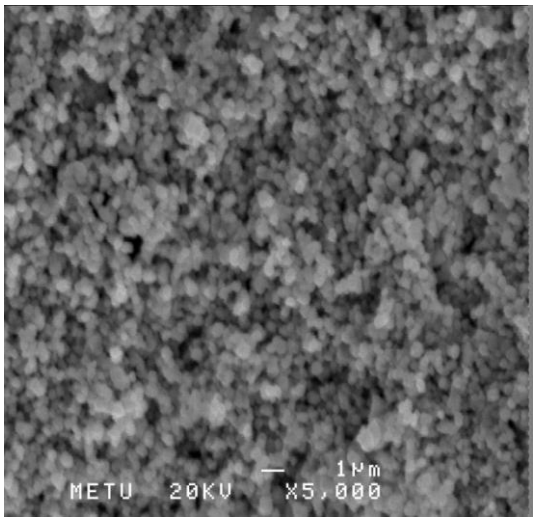

a)

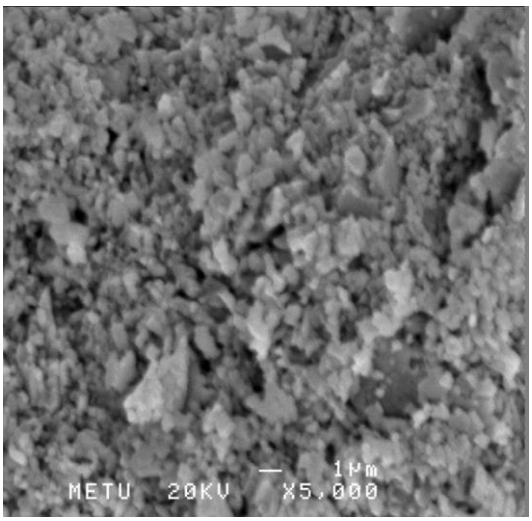

b)

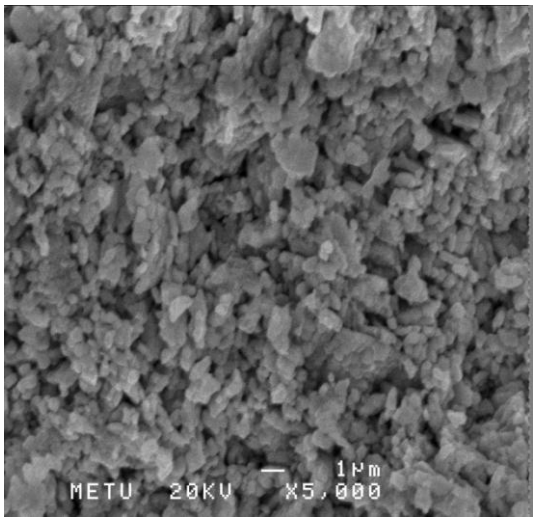

c)

Figure D.6. SEM Images of $HoBO_3$ Obtained by using a)Microwave-Assisted Synthesis with Urea, b)Microwave-Assisted Synthesis with Sucrose and c)Solid-State Reaction.

APPENDIX E

CRYSTAL DATA, STRUCTURE REFINEMENT RESULTS, ATOMIC POSITIONS, SELECTED BOND LENGTHS AND DISTANCES OF $NdBO_3$, $DyBO_3$, $HoBO_3$

The crystal system, space group, residual rietvel values, and unit cell parameters of $NdBO_3$, $DyBO_3$, $HoBO_3$ compounds were given in crystal data and structure refinement results. Atomic positions, the bond lengths and distances of these compounds were given.

Table E.1. Crystal data and structure refinement results for $DyBO_3$.

Emprical Formula	$DyBO_3$
Molar mass	221.3 g/mol
Crystal System	Monoclinic
Space Group	*C2/c*
Powder diffractometer	Panalytical X'Pert Pro
Radiation	CuKα1(λ=1.54051Å)
Unit-cell dimensions	a=11.3708(6) Å
	b=6.5718(3) Å
	c=9.6012(2) Å
	β=112.922(2) ^{o}
Volume	660.80(1) $Å^3$
Step (^{o})	0.013
2 Theta Range	10-150 ^{o}
R_{wp}	0.036
R_p	0.027
χ^2	1.96

Table E.2. Crystal data and structure refinement results for $HoBO_3$.

Emprical Formula	$HoBO_3$
Molar mass	223.7 g/mol
Crystal System	Monoclinic
Space Group	*C2/c*
Powder diffractometer	Panalytical X'Pert Pro
Radiation	CuKα1(λ=1.54051Å)
Unit-cell dimensions	a=11.3317(4) Å
	b=6.5475(3) Å
	c=9.5749(2) Å
	β=112.944(1) ^{o}
Volume	654.20(1) $Å^3$
Step (^{o})	0.013
2 Theta Range	10-150 ^{o}
R_{wp}	0.0581
R_p	0.0421
χ^2	3.968

Table E.3. Crystal data and structure refinement results for $LaBO_3$.

Emprical Formula	$LaBO_3$
Molar mass	197.7 g/mol
Crystal System	Orthorhombic
Space Group	*Pnma*
Powder diffractometer	Panalytical X'Pert Pro
Radiation	CuKα(λ=1.54051Å)
Unit-cell dimensions	a=5.8761(1) Å
	b=5.10535(9) Å
	c=8.252(1) Å
Volume	247.570 (8) $Å^3$
Step (^{o})	0.013
2 Theta Range	10-150 ^{o}
R_{wp}	0.1076
R_p	0.0844
χ^2	5.101

Table E.4. Crystal data and structure refinement results for $NdBO_3$.

Emprical Formula	$NdBO_3$
Molar mass	203.1 g/mol
Crystal System	Orthorhombic
Space Group	*Pnma*
Powder diffractometer	Panalytical X'Pert Pro
Radiation	CuKα1(λ=1.54051Å)
Unit-cell dimensions	a=5.73221(7) Å
	b=5.04199(6) Å
	c=8.0833(1) Å
Volume	233.621(3) $Å^3$
Step (^{o})	0.013
2 Theta Range	10-150 ^{o}
R_{wp}	0.0691
R_p	0.0544
χ^2	1.958

Table E.5. Crystal data and structure refinement results for $SmBO_3$.

Emprical Formula	$SmBO_3$
Molar mass	209.2 g/mol
Crystal System	Triclinic
Space Group	*P-1*
Powder diffractometer	Panalytical X'Pert Pro
Radiation	CuKα(λ=1.54051Å)
Unit-cell dimensions	a=6.4904(3) Å
	b=6.4962(3) Å
	c=6.2431(3) Å
	α=107.764(3) ^{o}
	β=107.703(3) ^{o}
	γ=93.385(2) ^{o}
Volume	235.437 (7) $Å^3$
Step (^{o})	0.013
2 Theta Range	10-150 ^{o}
R_{wp}	0.0682
R_p	0.0532
χ^2	3.227

Table E.6. Crystal data and structure refinement results for $GdBO_3$.

Emprical Formula	$GdBO_3$
Molar mass	216.1 g/mol
Crystal System	Rhombohedral
Space Group	$R3_2$
Powder diffractometer	Panalytical X'Pert Pro
Radiation	CuKα(λ=1.54051Å)
Unit-cell dimensions	a=6.63899(8) Å
	c=26.7219(5) Å
Volume	1020.00 (2) $Å^3$
Step (^{o})	0.013
2 Theta Range	10-150 ^{o}
R_{wp}	0.0454
R_p	0.0320
χ^2	2.590

Table E.7. Fractional atomic coordinates and isotropic displacement parameters $U_{iso}(Å^2)$ for $DyBO_3$.

Atom	x	y	z	$U_{iso}(Å^2)$
Dy1	0.25	0.25	0.0	0.02157
Dy2	0.0833(9)	0.2461(1)	0.499(2)	0.02497
B3	0.144(6)	0.016(6)	0.233(8)	0.01403
B4	0.0	0.65(1)	0.25	0.04684
O5	0.115(3)	0.064(7)	0.108(1)	0.01223
O6	0.220(3)	0.057(6)	0.389(2)	0.03598
O7	0.051(3)	0.563(7)	0.394(7)	0.02413
O8	0.388(3)	0.320(7)	0.252(4)	0.05726
O9	0.0	0.148(3)	0.25	0.02153

Table E.8. Fractional atomic coordinates and isotropic displacement parameters $U_{iso}(Å^2)$ for $HoBO_3$.

Atom	x	y	z	$U_{iso}(Å^2)$
Ho1	0.25	0.25	0.0	0.02470
Ho2	0.0842(4)	0.2526(5)	0.500(1)	0.02439
B3	0.188(3)	0.011(3)	0.252(6)	0.025
B4	0.0	0.624(6)	0.25	0.025
O5	0.128(1)	0.098(3)	0.1074(7)	0.0068
O6	0.228(1)	0.083(4)	0.3894(8)	0.02656
O7	0.049(1)	0.557(3)	0.3895(7)	0.02245
O8	0.362(2)	0.342(1)	0.252(2)	0.06537
O9	0.0	0.150(2)	0.25	0.02997

Table E.9. Fractional atomic coordinates and isotropic displacement parameters $U_{iso}(Å^2)$ for $LaBO_3$.

Atom	x	y	z	$U_{iso}(Å^2)$
La1	0.2568(4)	0.25	0.5844(1)	0.02378
O2	0.404(1)	0.25	0.078(1)	0.00558
O3	0.413(1)	0.481(1)	0.3230(8)	0.00787
B4	0.435(4)	0.25	0.246(4)	0.06470

Table E.10. Fractional atomic coordinates and isotropic displacement parameters $U_{iso}(Å^2)$ for $NdBO_3$.

Atom	x	y	z	$U_{iso}(Å^2)$
Nd1	0.257(3)	0.25	0.5847(1)	0.02381
B1	0.425(3)	0.25	0.246(2)	0.03092
O1	0.402(1)	0.25	0.073(1)	0.02058
O2	0.4080(8)	0.013(1)	0.3228(7)	0.01048

Table E.11. Fractional atomic coordinates and isotropic displacement parameters $U_{iso}(Å^2)$ for $SmBO_3$.

Atom	x	y	z	$U_{iso}(Å^2)$
Sm1	-0.1533(5)	0.2688(5)	0.0544(6)	0.03671
Sm2	0.2797(5)	0.18890(5)	0.5568(6)	0.03879
B1	-0.279(7)	0.241(8)	0.518(9)	0.02845
B2	-0.319(9)	-0.223(9)	-0.09(1)	0.05670
O1	0.472(4)	0.213(3)	-0.017(5)	0.01623
O2	0.234(4)	0.130(4)	0.176(4)	0.02141
O3	0.698(4)	0.203(4)	-0.350(4)	0.02309
O4	0.104(3)	-0.140(4)	-0.388(4)	0.00294
O5	0.220(4)	0.523(4)	0.505(5)	0.02930
06	-0.158(4)	0.638(4)	0.091(5)	0.02641

Table E.12. Selected Atomic Parameters for LT Phase of $GdBO_3$ (Ren et al. 1999).

Atom	x	y	z
Gd1	0.3358	-0.0014(2)	0.0820(2)
O1	-0.009(2)	0.667(4)	0.120(6)
O2	0.021(4)	0.673(4)	0.049(7)
O3	0.0	0.214(6)	0.0
O4	0.0	0.202(8)	0.5
B1	0.760	0.0	0.0
B2	0.760	0.0	0.5

Table E.13. Fractional atomic coordinates and isotropic displacement parameters $U_{iso}(Å^2)$ for $GdBO_3$.

Atom	x	y	z	$U_{iso}(Å^2)$
Gd1	0.335(1)	-0.001(1)	0.0810(1)	0.02485
O2	-0.002(9)	0.67(1)	0.1211(4)	0.02
O3	0.02(1)	0.654(9)	0.0494(5)	0.05795
O4	0.0	0.223(3)	0.0	0.03524
O5	0.0	0.196(3)	0.5	0.05847
B6	0.487(7)	0.0	0.0	0.08784
B7	0.60(1)	0.0	0.5	0.02

Table E.14. Selected bond distances and angles for $DyBO_3$.

Distances			
B3-O5	1.15744(3)	B3-O9	1.915(10)
B3-O6	1.42925(4)	B4-O8	1.69343(6)
B3-O8	1.36030(6)	B4-O7	1.40156(3)
Dy1-Dy2	3.79481(20)	Dy2- Dy2	3.75076(15)
Dy1-B3	2.94336(7)	Dy2-B3	3.07345(10)
Dy1-O8	2.35835(6)	Dy2-O8	2.33150(5)
B4-Dy1	2.99141(12)	O5-O8	2.09881(7)
O6-O8	2.11352(7)	B4-Dy2	2.99233(6)
Angles			
O5-B3-O6	147.539(1)	O5-Dy1-O7	101.435(3)
O6-B3-O8	98.486(1)	O5-Dy1-O8	93.289(3)
O7-B4-O7	130.373(3)	O6-Dy1-O7	108.431(2)
O8-B4-O8	97.907(4)	O6-Dy1-O8	54.545(1)
O5-Dy1-O5	180.000(0)	O7-Dy1-O7	179.972(0)
B3-Dy2-O5	86.064(2)	B3-Dy2-O7	88.711(2)
O5-Dy2-O9	58.40(22)	O6-Dy2-O9	123.18(24)
O7-Dy2-O7	72.760(2)	O8-Dy2-O9	148.6(4)
Dy2-O6-B3	129.985(1)	Dy2-B3-O	55.256(2)
Dy2-O7-B4	138.846(0)	Dy2-O7-Dy2	107.240(2)
Dy1-O8-Dy2	141.874(2)	B3-O8-B4	148.973(1)

Distances are given in Å and angles in degrees (^{o}).

Table E.15. Selected bond distances and angles for $HoBO_3$.

Distances			
B3-O5	1.35955(3)	B4-O7	1.27808(2)
B3-O6	1.28912(2)	B4-O8	2.04474(6)
B3-O8	1.29884(4)	Ho2-Ho2	3.75658(15)
Ho2-B3	2.82010(5)	Ho1-Ho2	3.75982(11)
Ho1-B3	2.78570(5)	Ho1-O5	2.44310(6)
Ho1-B4	3.02404(9)	Ho2-O6	2.34909(7)
Ho1-O6	2.33783(7)	Ho2-Ho2	3.76113(11)
O6-O8	2.07002(5)	O8-O5	2.02055(5)
Angles			
O5-B3-O8	98.914(2)	O7-B4-O7	144.459(1)
O5-Ho1-O5	180.000(0)	O5-Ho2-O6	76.021(2)
O6-B3-O8	106.234(1)	Ho2-O9-Ho2	148.8(9)
Ho1-O5-Ho2	104.722(3)	Ho2-O6-B3	117.119(1)
Ho2-O5-B3	137.887(1)	Ho2-O7-Ho2	103.586(2)

Distances are given in Å and angles in degrees (^{o}).

Table E.16. Selected bond distances and angles for $LaBO_3$.

Distances			
B4-O2	1.40(3)	La1-O2	2.47040(3)
B4-O3	1.35(1)	La1-B4	2.980(29)
La1-La1	4.07755(4)	La1-O3	2.59829(3)
Angles			
O2-B4-O3	117.0(1)	O2-La1-O3	81.209(1)
O3-B4-O3	122.6(2)	O2-La1-O3	95.106(1)
O2-La1-O2	139.386(1)	O2-La1-O3	144.992(1)
La1-O2-La1	139.386(1)	O3-La1-O3	77.067(1)
La1-O2-B4	91.48(34)	O3-La1-O3	66.662(1)
La1-O2-La1	107.554(0)	La1-O2-B4	115.4(10)

Distances are given in Å and angles in degrees (^{o}).

Table E.17. Selected bond distances and angles for $NdBO_3$.

Distances			
B1-O1	1.40685(2)	Nd1-O1	2.68386(3)
B1-O2	1.352(5)	Nd1-B1	2.90325(3)
Nd1-Nd1	3.91847(3)	Nd1-O2	2.522(6)
Angles			
O1-B1-O2	116.8(2)	O2-Nd1-O2	103.85(13)
O2-B1-O2	124.5(5)	O1-Nd1-O2	141.88(12)
O1-Nd1-O1	139.874(1)	O2-Nd1-O2	65.53(23)
O2-Nd1-O2	174.62(21)	O2-Nd1-O2	120.56(5)
O2-Nd1-O2	74.78(21)	O2-Nd1-O2	77.13(13)

Distances are given in Å and angles in degrees (^{o}).

Table E.18. Selected bond distances and angles for $SmBO_3$.

Distances			
B1-O1	1.33816(2)	Sm1-O2	2.69261(1)
B1-O2	1.41094(2)	Sm1-O2	2.48169(12)
B1-O4	1.13935(3)	Sm1-O3	2.30936(8)
B1-O5	1.995(5)	Sm1-Sm1	3.85488(13)
B2-O3	1.42794(2)	Sm1-O5	3.00654(14)
B2-O4	1.93248(4)	Sm2-B1	2.68607(12)
Sm1-Sm2	3.71193(13)	Sm2-Sm2	3.96366(14)
Sm1-B2	3.05196(12)	Sm2-O1	2.52116(8)
Angles			
O1-Sm1-O2	81.616(3)	O3-Sm2-O4	94.127(3)
O1-Sm1-O3	76.852(3)	O3-Sm2-O5	144.730(2)
O1-Sm1-O4	88.261(2)	O3-Sm2-O6	131.336(2)
Sm2-B1-O3	69.413(3)	O3-B1-O5	130.730(2)
Sm2-B1-O4	66.307(2)	O3-B1-O4	123.224(2)
B1-Sm2-O1	81.536(3)	O1-B2-O2	142.113(2)
B1-Sm2-O4	92.840(3)	Sm2-O1-B2	106.487(3)
B1-Sm2-O5	163.404(1)	Sm1-O2-Sm2	111.087(3)
O1-Sm2-O4	122.565(2)	Sm2-O3-Sm2	101.865(3)
O2-Sm2-O4	111.307(3)	Sm1-O4-B1	106.631(2)
O2-Sm2-O4	78.352(3)	Sm2-O4-Sm2	110.389(3)
O3-Sm2-O6	116.126(3)	Sm1-O6-Sm2	136.376(2)

Distances are given in Å and angles in degrees (^{o}).

Table E.19. Selected bond distances and angles for $GdBO_3$.

Distances			
B7-O2	1.28037(2)	Gd1-Gd1	3.80957(5)
B6-O3	1.68689(2)	B6-O4	1.75480(1)
O2-O3	1.92691(4)	O3-O2	1.92691(4)
Gd1-O3	2.21827(2)	Gd1-O3	2.54225(3)
Gd1-O2	2.46459(3)	Gd1-B6	2.38703(4)
Gd1-O3	2.35600(3)	Gd1-B7	2.91671(4)
Angles			
O1-B1-O2	131.091(1)	O2-Gd1-B6	90.852(1)
O2-Gd1-O3	125.018(0)	O3-Gd1-O3	109.189(0)
O2-Gd1-O3	128.536(0)	O3-Gd1-B6	42.778(0)
O2-Gd1-O3	45.359(1)	O4-Gd1-O5	159.864(0)
O2-Gd1-O3	128.756(0)	O4-Gd1-B6	44.002(1)
O2-Gd1-O4	105.128(1)	O5-Gd1-B6	140.292(1)
Gd1-O2-Gd1	101.320(1)	Gd1-O3-B6	73.956(1)
Gd1-O2-B7	124.438(0)	Gd1-O4-Gd1	141.807(1)
Gd1-O2-Gd1	102.341(1)	Gd1-O4-B6	70.903(0)
Gd1-O2-B7	123.138(0)	Gd1-B6-Gd1	130.189(1)
Gd1-O3-Gd1	103.970(0)	Gd1-B6-O4	65.095(0)
Gd1-O3-B6	131.097(0)	O2-B7-O2	143.991(1)
O3-B6-O4	128.210(1)	O3-B6-O3	103.580(1)

Distances are given in Å and angles in degrees (^{o}).

APPENDIX F

CRYSTAL STRUCTURES OF $NdBO_3$, $DyBO_3$, $HoBO_3$

Three dimensional crsytal structures of $NdBO_3$, $DyBO_3$, $HoBO_3$ are demonstrated in this section.

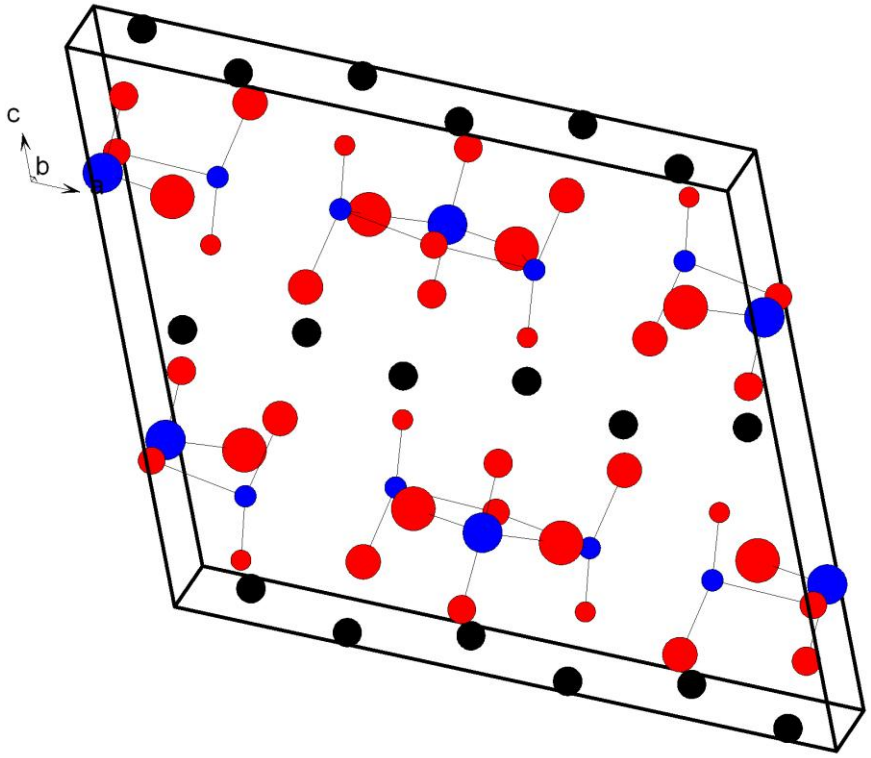

Figure F.1. Crystal structure of $DyBO_3$ (Blacks: Dy atoms, Blues: B atoms, Reds: O atoms).

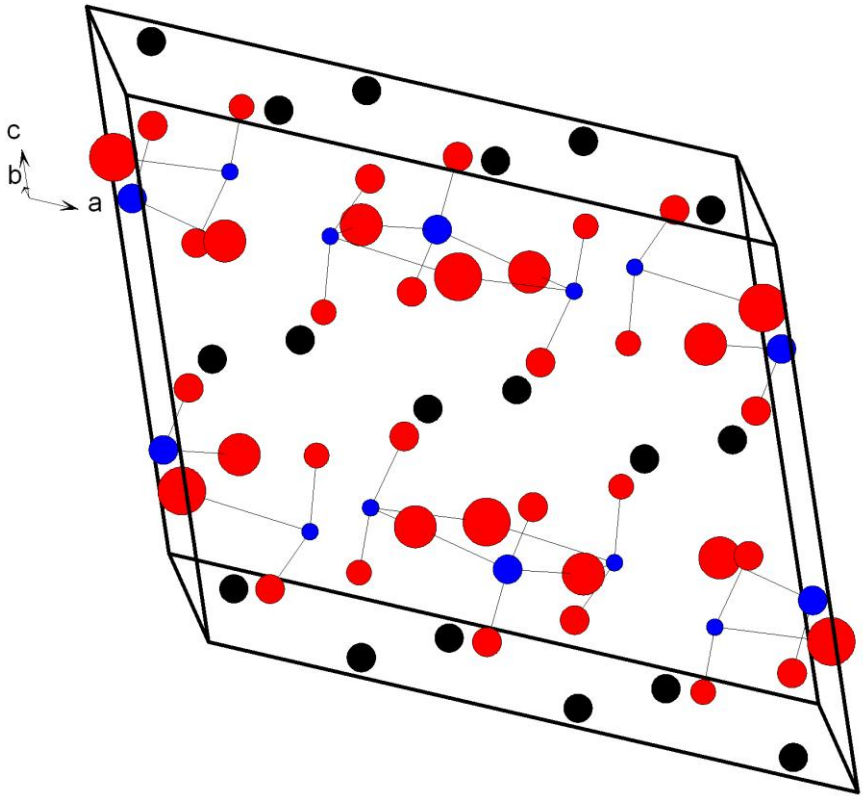

Figure F.2. Crystal structure of $HoBO_3$ (Blacks: Ho atoms, Blues: B atoms, Reds: O atoms).

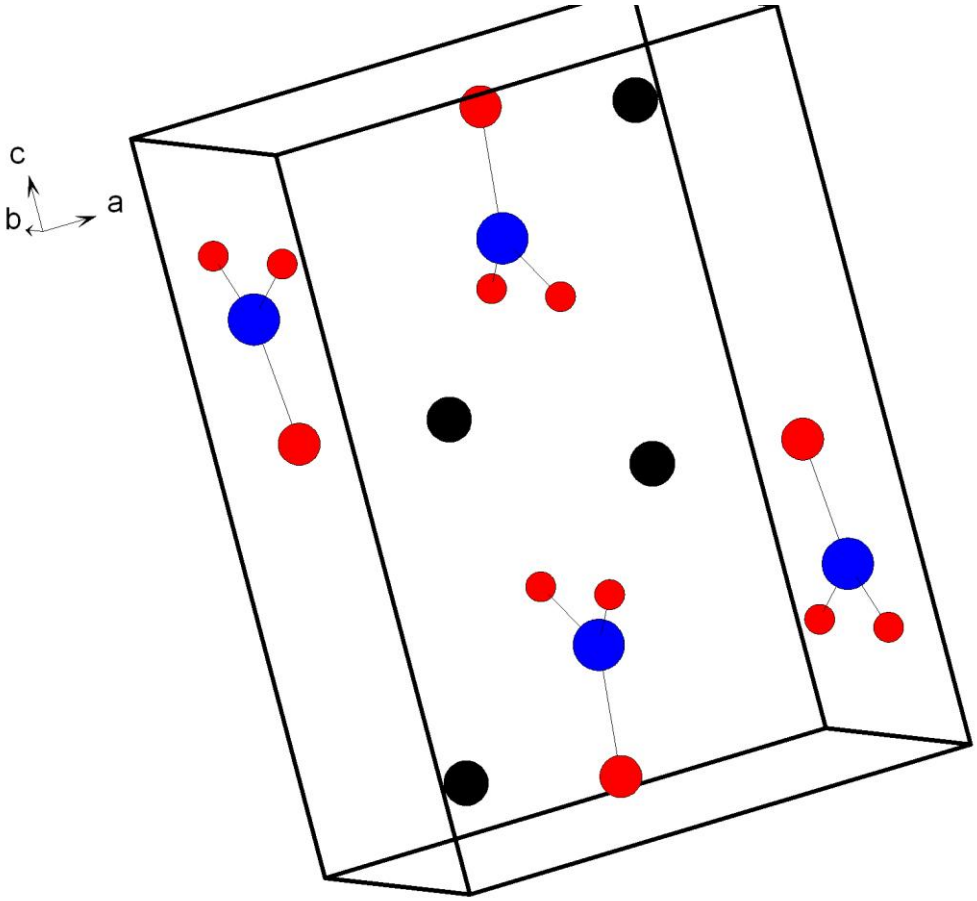

Figure F.3. Crystal structure of $NdBO_3$ (Blacks: Nd atoms, Blues: B atoms, Reds: O atoms).

CURRICULUM VITAE

Surname, Name: Seyyidoğlu, Semih
Nationality: Turkish (TC)
Date and Place of Birth: 19 July 1977, Istanbul
Marital Status: Married
Phone: +90 312 210 32 10
Fax: +90 312 210 32 00
e-mail: semihseyyidoglu@yahoo.com

EDUCATION

Degree	Institution	Year of Graduation
Ph.D.	METU, Chemistry Department	2009
MSc.	METU, Chemistry Department	2003
BS	METU, Chemistry Department	2001

WORK EXPERIENCE

Year	Place	Enrollment
2009-	Seyyidoglu Ultrasonic Solutions	Owner
2007-2008	Panalytical, TETRA	XRD Specialist
2001-2007	Chemistry Department	Research Assistant

AWARDS

2007 June Full Scholarship for ICDD- XRD Clinics 1&2 Education

MEMBERSHIPS

2002-2007 Member of ***Executive*** Board Turkey Chemistry Association, Ankara, Turkey

2007-present Member of Chemists Society, Izmir, Turkey

2009-present Member of American Chemical Society, Washington DC, USA

FOREIGN LANGUAGES

Advanced English, Good Russian

PUBLICATIONS

Refereed Journals

1. Katzenmeyer A.M., Bayam Y., Logeeswaran V.J., Pitcher M.W., Nur Y., Seyyidoglu S., Toppare L.K., Talin A.A., Han H., Davis C.E., Islam M.S., Journal of Nanomaterials, Vol 2009 .

2. Seyyidoglu S., Ozenbas M., Yazıcı N., Yilmaz A., *"Investigation of Solid Solution of ZrP_2O_7- $Sr_2P_2O_7$"*, J. Material Science, 2007, 42, 6453-6463.

3. Seyyidoglu S., Ozenbas M., Yilmaz A., *"Investigation of Novel Sodium Rare-Earth Oxyphosphates"*, Turk J. Chem., 32, 2008, 1-20.

4. Pekgozlu I., Seyyidoglu S., Tascioglu S., *"A Novel Blue-Emitting Phosphor: $BaAl_2B_2O_7:Pb^{2+}$"*, J. Luminescence, 128, 2008, 1541-1543.

5. Nur Y., Pitcher M.W., Seyyidoglu S., Toppare L., *"A Facile Synthesis of Poly(hydridocarbyne): A Precursor to Diamond and Diamond-like Ceramics"*, J. Macromolecular Science, Part A Pure and Applied Chemistry, 2008, 45, 358-363.

6. Pitcher W., Neshat A., Seyyidoglu S., *"Formation of Metastable Vaterite Crystals in a Polymer Matrix by Gaseous Diffusion"*, J. Chil.Chem. Soc., 53, 2, 2008, 1393-1394.

In preparation:

1. Seyyidoglu S., Kayhan M., Aysen Y., "Tailoring the morphology and particle size of BPO_4 by solvothermal and microwave assisted synthesis methods" .

2. Yazıcı A.N., Seyyidoğlu S., Toktamış H., Yılmaz A., "Thermoluminescent Properties of $Sr_2P_2O_7$ Doped with Copper and Rare Earth Elements*"* .

3. Seyyidoglu S., Hoffmann K., Albert B., Yilmaz A., *"*Structural Investigations of $LnBO_3$ (Ln= Y, La, Nd, Sm, Eu, Gd, Dy, Ho, Er,Yb, Lu) by Rietveld Method*"*.

4. Seyyidoglu S., Ozenbas M., Yilmaz A., *"*Microwave-Assisted Synthesis of $LnBO_3$ (Ln=La, Nd, Dy, Ho)*"*.

International Conference Presentations:

1. *"*Structural Investigations of $LnBO_3$ (Ln= Y, La, Nd, Sm, Eu, Gd, Dy, Ho, Er,Yb, Lu) by Rietveld Method", Seyyidoglu S, Hoffmann K., Albert B., Yılmaz A., ECM-25 European Crystallography Meeting-25, Instanbul, Turkey, August, 2009.

2. "Formation of Conducting Micro-Nanostructures of Carbon from Poly(Hydridocarbyne) Synthesized Via Electro-polymerization", Aaron M. Katzenmeyer[1], Yavuz Bayam[1,2], Logeeswaran VJ[1], Michael W. Pitcher[3], Yusuf Nur[3], Semih Seyyidoğlu[3], Levent K. Toppare[3], A. Alec Talin[4] and M. Saif Islam[1,] IEEE Nanotechnology Conference, Texas, USA, August, 2008.

3. "Electrically produced polycarbynes: Polymeric precursors to diamond and diamond-like carbon", Michael W. Pitcher, Yusuf Nur, Semih Seyyidoğlu, Asli Taşkın, Halime Cengiz, Levent Toppare, Poster Presentation at American Chemical Society 234th National Meeting & Exposition, Boston, USA, August, 2007.

4. "Controlling the crystallization of calcium carbonate: Metastable vaterite formation using a polymer matrix", Michael W. Pitcher, Abdollah Neshat, Semih Seyyidoğlu, Poster Presentation at American Chemical Society 234th National Meeting & Exposition, Boston, USA, August, 2007.

5. "Synthesis and Characterization of Speciality Boron Products Produced by Microwave Energy", Seyyidoglu S., Aysen Yilmaz, Macit Ozenbas, Oral Presentation at the *3rd International Boron Symposium*, Ankara, Turkey, November , 2006.

6. "Factors Influencing Dispersion of Cobalt oxide Nanoparticles in Mesoporous Silica SBA-15", Aysen Yilmaz, Ersin Yildiz, Seyyidoglu S., Ebubekir Sen, Poster Presentation at the *Fifth International Conference on Inorganic Materials*, Ljubljana, Slovenia, September , 2006.

7. "Factors Influencing Dispersion of Cobalt oxide Nanoparticles in Mesoporous Silica SBA-15", Aysen Yilmaz, Ersin Yildiz, Seyyidoglu S., Ebubekir Sen, Oral Presentation at the *International Workshop on Nanostructured Materials*, Antalya, Turkey, June , 2006.

8. "Solid State Synthesis and Characterization of Some Novel Sodium Rare Earth Phosphates", Seyyidoglu S., Macit Ozenbas, Meral Kizilyalli, Aysen Yilmaz, Poster Presentation at the *XX Congress of International Union of Crystallography*, Florence, Italy, August, 2005.

9. "Synthesis and Characterization of Some Novel Borate Phosphates", Seyyidoglu S., Meral Kizilyalli, Poster Presentation at the 14th *International Symposium on Boron, Borides and Related Compound*, St.Petersburg, Russian Federation, June, 2002.

National Conference Presentations

1. "Tailoring the morphology and particle size of BPO_4 by solvothermal and microwave assisted synthesis methods", Mehmet Kayhan, Semih Seyyidoglu, Ayşen Yılmaz, Nano-Tr-5, Ulusal Nano Teknoloji Kongresi, Eshişehir, Haziran, 2009.

2. "Katı Hal Yöntemiyle Üretilen $LnBO_3$ (Ln= Y, La, Nd, Sm, Eu, Gd, Dy, Ho, Er, Tm, Yb, Lu) Serisinin Rietveld Analizi İle Yapısının İncelenmesi", Semih Seyyidoğlu, Ayşen Yılmaz, Oral Presentation at XXII. Ulusal Kimya Kongresi, Northern Cyprus, October, 2008.

3. "Pb^{2+} Katkılı $SrAl_2B_2O_7$ Bileşiğinin Fotoluminesans Özelliklerinin İncelenmesi", İlhan Pekgözlü, Semih Seyyidoğlu, Sülin Taşcıoğlu, Poster Presentation at X. Ulusal Spektroskopi Kongresi, İzmir, July, 2007.

4. "Pb^{2+} Katkılı $CaAl_2B_2O_7$ Bileşiğinin Fotoluminesans Özelliklerinin İncelenmesi", İlhan Pekgözlü, Semih Seyyidoğlu, Sülin Taşcıoğlu, Oral Presentation at Ulusal Teknik Eğitim, Mühendislik ve Eğitim Bilimleri Genç Araştırmacılar Sempozyumu(UMES 2007), Kocaeli, June, 2007.

5. "Nadir Toprak Elementi Katkılanmış $Sr_2P_2O_7$ Bileşiklerinin Sentezi, Karakterizasyonu ve Termolüminesan Özellikleri", Seyyidoglu S., Necmeddin Yazici, Aysen Yilmaz, Poster Presentation at the *1st National Inorganic Chemistry Days*, Adana, Turkey, April, 2007.

6. "Single-step Direct Synthesis of Cobalt Incorporated Mesoporous Silica SBA-15", Aysen Yilmaz , Ebubekir Sen, Seyyidoglu S., and Jie Fan, Oral Presentation at the *1st National Catalysis Conference*, Northern Cyprus, January, 2007.

7. "Nadir Toprak Elementi İçeren Boratların Mikrodalga ve Katı-Hal Yöntemiyle Sentezinin ve Karakterizasyonun İncelenmesi", Seyyidoglu S., Macit Ozenbas, Aysen Yilmaz, Poster Presentation at the *XIX. National Chemistry Congress*, Kusadası, Turkey, September, 2005.

8. "Borfosfatlı Bileşikler: Sentez ve Yapı Çalışmaları", Seyyidoglu S., Aysen Yilmaz, Meral Kizilyalli, Oral Presantation at the *2nd Boron Symposium*, Zonguldak, Turkey, May, 2004.

9. "Bazı Yeni Zr ve Mo Borofosfatların Katı-Hal Yöntemiyle Eldesi ve Tanımlanması", Seyyidoglu S., Meral Kizilyalli, Poster Presentation at the *1st Boron Symposium*, Balikesir, Turkey, June, 2002.